

UNIVERSITY OF OKLAHOMA
GRADUATE COLLEGE

THE WOODFOORD SHALE IN THE MARIETTA BASIN
(OKLAHOMA AND NORTH TEXAS)

A DISSERTATION
SUBMITTED TO THE GRADUATE FACULTY
in partial fulfillment of the requirements for the
Degree of
DOCTOR OF PHILOSOPHY

By
RICHARD JESUS BRITO LEONET
Norman, Oklahoma
2019

THE WOODFORD SHALE IN THE MARIETTA BASIN
(OKLAHOMA AND NORTH TEXAS)

A THESIS APPROVED FOR THE
CONOCOPHILLIPS SCHOOL OF GEOLOGY AND GEOPHYSICS

BY

Dr. Roger Slatt, Chair

Dr. Deepak Devegowda

Dr. R. Douglas Elmore

Dr. Kurt Marfurt

Dr. R. Paul Philp

© Copyright by RICHARD JESUS BRITO LEONET 2019
All Rights Reserved.

To my wife, Gabriela

Acknowledgements

I would like to start by thanking God, I am where I am because of you. Thanks for being there during every long night and every time I thought I could not move forward anymore. Everything with God, nothing without him.

To Dr. Roger Slatt, my academic adviser. I could not write enough words to thank you for this opportunity you gave me many years ago to work with you at The University of Oklahoma. I learned so much from you and I think you still have so much to teach me. I will miss working with you, but I know that now it is time for somebody else to learn from you. Thank Boss! You are amazing.

My most sincere acknowledgments to my committee members. I do have so much respect for each of you. Being a professor must be one of the most amazing things in life because you have the chance to share your knowledge with so many people, and I feel grateful to be one of those persons learning from you. I apologize if at any time I did not meet your expectation and please know I will do my best to deserve being a graduate student under your advising.

To the University of Oklahoma and the School of Geology and Geophysics, for being my alma mater, and home for so long. I will miss every person I have met here and always will have this place in my heart.

I would like to thank the oil and gas company that provided us the access to the Marietta Basin Woodford Core. I believe that without this core, we would have never committed to understanding the Woodford Shale in this basin.

Also, I would like to thank Luis A. Castillo and Jorge Quintero for their exceptional technical support since the start of this project. There were times where I lost the sight of where to move forward in this research, and you helped me to stay in track. I learned so much from both of you, in particular, those that were out of my comfort zone. I own you so much and writing you name here is the least I could do. Luis, you have done for me more than a brother would, we might not have the same blood but if God allows me, will be always there for you. Gracias Hermano.

To David Duarte, Any Ordonez, and Andrea Miceli, the final manuscript was able to get on time in the hands of my committee thanks to you and your help with the writing, figures, and references. Thanks!

To Delcio, Dalila, Henry, Bryan, Naya, and Daniela. Each of you helped me to acquire and process a big part of the data that is included in this dissertation, and I always will be grateful for that help.

To Amelia Morales and Luis A. Castillo, for allowing me to stay at your home during the last stages of this dissertation and encourage me every morning in Norman to keep working hard

to reach my goal and to never lose the faith in God. You are my parents in the USA and I always going to be grateful for that. Thanks for letting me be part of your family.

To my wife Gabriela Lugo, the love you showed me during the time I was working in this dissertation is the biggest somebody have shown me. Chuche, I love you so much and that is the reason why I dedicate this work to you. Now it is my turn to be there for you.

Finally, to my parents, who prayed every day for me to reach my goal of being the first Ph.D. in our family and hometown. I know you just want happiness for me, and this is part of it. I miss you every day of my life.

Table of Contents

Acknowledgements.....	v
List of Figures.....	x
Abstract.....	xxv
Chapter 1: Introduction.....	1
1.1 Problem Statement and Significance of this Study.....	5
1.2 Scope of Study.....	7
1.3 Structure of Dissertation.....	8
1.4 Previous Work.....	9
Chapter 2: Geologic Setting.....	12
2.1 Oklahoma Geology.....	13
2.2 Marietta Basin Geology.....	26
2.3 Woodford Shale Geology.....	29
Chapter 3: Lithofacies and Stratigraphy.....	37
3.1 Available Data.....	38
3.2 Methodology.....	40
3.3 Facies Description.....	45
3.4 Stratigraphy.....	62
3.5 Interpretation of Unofficial Members of the Woodford Shale.....	71
Chapter 4: Diagenesis.....	81
4.1 Data and Methods.....	82
4.2 Diagenesis of the Matrix and Allochems.....	85
4.3 Diagenesis of Phosphate Nodules.....	93

4.4 Fracture Diagenesis.....	96
4.5 Paragenetic Sequence.....	100
Chapter 5: Geochemistry and Geomechanics	103
5.1 Data and Methods	104
5.2 Organic Richness	108
5.3 Kerogen Type.....	111
5.4 Thermal Maturity	114
5.5 Rebound Hardness	119
Chapter 6: Subsurface Mapping.....	126
6.1 Data and Methods	126
6.2 Regional Structural Model.....	129
6.3 Type Log.....	132
6.4 Cross Sections.....	134
6.5 Subsurface Maps.....	137
Chapter 7: Production and Performance	144
7.1 Decline Curve Analysis (DCA) Theory.....	147
7.2 Data Available	150
7.3 Methods.....	151
7.4 Decline Curve Analysis (DCA) Results	153
7.5 Integration with Geology	160
Chapter 8: Conclusions and Recommendations	164
References.....	174

List of Figures

Figure 1. Ranking of states in the US by monthly crude oil production. The state of Oklahoma is ranked number 4 with a production of 18.1 million of barrels of crude oil per month. Source: EIA, 2019 1

Figure 2 Ranking of states in the US by monthly natural gas production. Oklahoma is ranked number 3 with a production of 15,513,897 million cubic feet of natural gas per month. Source: EIA, 2019 2

Figure 3 Current location of the Unconventional Resource Plays in the United States (modified from EIA, 2016). The Woodford Shale is one of the main resource shales in the Country. 2

Figure 4 Regional thickness map of the Woodford Shale by Comer, 2003 across the states of Oklahoma and Arkansas. 3

Figure 5 Location of Woodford Shale oil (green) and gas (red) wells in the state of Oklahoma. Blue oval shows the approximate location of the Marietta Basin as part of the South-Central Oklahoma Oil Play (SCOOP) area. No production data is available from North Texas..... 4

Figure 6 Location of the Marietta Basin (bright green area) overlaid on the Geologic Map of Oklahoma (Northcutt and Campbell, 1995). Colored circles represent the locations of the outcrop (type section) and core. 8

Figure 7 Schematic cross-section view of Oklahoma from Middle Cambrian time to Permian time (Modified from Hoffman et al., 1974). 13

Figure 8 Paleotectonic map of South-Eastern United States and the relative location of the Southern Oklahoma Aulacogen (SOA) and other failed rift arms in the area. DA: Delaware Aulacogen; RFR: Reelfoot Rift; RCG: Rough Creek Graben; RT: Rome Trough. Figure from Keller (1983) and modified by Becerra (2017). 14

Figure 9 shows rift axis (red) and failed arms (green) forming aulacogens in Texas, Oklahoma, and Arkansas; due to the creation of the Proto-Atlantic Ocean. Modified from Suneson, (1996) and Ataman (2008) by Ekwunife 2017)..... 14

Figure 10 Sub-Sea Depth Map of the Precambrian and Early Cambrian basement in Oklahoma and North Texas (Modified from Johnson, 2008). Numbers represent the TVD depth of the Basement in thousands of feet. 15

Figure 11 Map of the Greater Oklahoma Basin area from Late Cambrian until the Late Mississippian. Modified from Johnson et al. (1989) by Gaswirth and Higley (2014). 16

Figure 12 Reconstruction of the Late Cambrian and Early Ordovician by Johnson (2008). Deposition of the Arbuckle Group..... 17

Figure 13 Reconstruction of the Middle to Late Ordovician by Johnson (2008). Deposition of the Simpson Group. 17

Figure 14 Reconstruction of Silurian and Early Devonian rocks by Johnson (2008). Deposition of the Hunton Group. 18

Figure 15 Generalized stratigraphic section for the pre-Pennsylvanian of southern Oklahoma showing periods of non-deposition (black) and extent of the pre-Woodford unconformity (Kirkland et al., 1992)..... 18

Figure 16 “Pre-Woodford Unconformity” Sub-crop Reconstruction (above) modified from Kuykendall and Fritz, 2001. Karsted surface reconstruction (below); modified from Grotzinger and Jordan (2010). 19

Figure 17 Paleogeographic reconstruction of south United States from Late Devonian (A) to Early Mississippian (B). Figure modified from Blakey (2012). 19

Figure 18 Cross-sections showing restored Silurian, Devonian and Mississippian strata in Oklahoma (modified from Johnson and Cardott, 1990 by Miceli 2010).....	20
Figure 19 Reconstruction of dominant lithologies during most of the Mississippian period. Modified from Johnson (2008).....	21
Figure 20 Reconstruction of Pennsylvanian time, modified from Johnson (2008).....	22
Figure 21 Reconstruction of the Permian Period. Modified from Johnson (2008).	23
Figure 22 Major rivers and streams, as well as, Mountains in Oklahoma during the Quaternary Age. Modified from Johnson (2008).	24
Figure 23 Set of cross-sections along the state showing the structural setting and distribution of deposits in the state of Oklahoma.	25
Figure 24 Map of tectonic domains in South-Central Oklahoma. Red star shows the Marietta Basin. Figure modified from Cook (2010).	26
Figure 25 Generalized structural trends in Love County and Carter County in South Central Oklahoma (Westheimer, 1965).....	27
Figure 26 Stratigraphic units of the Marietta Basin (Love County) and some correlations with those of adjoining areas. Modified from Westheimer (2008).....	28
Figure 27 Facies distribution during the Late Devonian in the Southern US Mid-continent. Modified from Blakey (2012) and Comer (2008) by Miceli (2010).	30
Figure 28 Inter-Basin Correlative Stratigraphic chart of South Oklahoma Geology from Ordovician to Mississippian. Modified from Johnson and Cardott (1990).	32
Figure 29 Generalized Thickness Map of the Woodford Shale in Oklahoma and Arkansas (Comer, 2008).....	32

Figure 30 Generalized stratigraphic section of Speake Ranch Shale Pit in the Southern Limb of the Arbuckle Mountains. Modified from Galvis (2017)..... 33

Figure 31 Characteristic well log signatures of lower, middle and upper members of the Woodford Shale in the Anadarko Basin (modified from Hester et al., 1990 by Miceli 2010)..... 34

Figure 32 Gamma-Ray Parasequence subdivisions of the Woodford Shale. On the left in the subsurface of the Potawatomi County by McCullough (2014). On the right side, Galvis (2017) developed a sequence stratigraphy based on outcrop Gamma log and description..... 35

Figure 33 Map showing TOC distribution in Oklahoma and northeastern Arkansas (modified from Comer, 2005 in Comer, 2008)..... 35

Figure 34 Sequence Stratigraphic model of the Woodford Shale with examples of thin sections of key facies within the Woodford interval. Model by Slatt (2017) and kindly provided by Ruppel (pers. comm.), then later modified by Galvis (2017)..... 36

Figure 35 Map with the relative location of the cored well (magenta dot). Dash line shows the generalized outline of the Marietta Basin. Tadpoles are Woodford Shale horizontal wells drilled in the basin. 37

Figure 36 Generalized diagram of whole core slabbing viewed from the top. This process results in two core parts: a) the “Slab” side (in light blue) which has the less volume of rock; and b) the “butt” side (in yellow) which has the largest part of the volume of rock. 39

Figure 37 Red arrow shows the Brucker Tracer IV-SD Hand Held X-ray Fluorescence Spectrometer (HHXRF). Samples are placed at the top front of the gun and covered by a lead cap to prevent any X-Ray exposure to the user. Examples of resulting XRF profiles are shown in the blue box in the upper left corner. Picture provided by Turner (2016)..... 42

Figure 38 Equipment settings for Major Element Scanning and Trace Elements Scanning using the Bruker Tracer IV-SD Hand Held X-ray Fluorescence Spectrometer (HHXRF) equipment. Scanning for Major elements does not use a filter to minimize signal attenuation of lighter elements such as Ca, Si, and Al. Scanning for Trace Elements does not need vacuum because heavier elements do not attenuate the signal in the short distance to the detector..... 43

Figure 39 Elemental (Geochemical) Proxies usually used to aid the interpretation of the depositional environment of the organic-rich Woodford Shale. Figure modified from Ekwunife (2017) and Turner (2016)..... 44

Figure 40 Field-based lithofacies classification of Woodford Shale mudrocks by Galvis (2017). The asterisk denotes the most common lithofacies present in the Speake Ranch Woodford Section (considered nowadays one of the best type sections of the Woodford Shale exposed on outcrops). The classification was primarily done by describing hand size rock samples..... 46

Figure 41 Pie chart showing the distribution of each major lithofacies within the Marietta Basin Woodford Core. Siliceous Mudstone (SM) is the most common one with 28%; followed closely by Siliceous Shale (SS) and Argillaceous Shale (AS) with 25% and 22% respectively. Black Chert (BC) is fourth in the distribution with 17%. Green Claystone (GC) with 5% and Dolomitic Mudstone (DM) with 3% are the least common in the section..... 48

Figure 42 Example of Siliceous Mudstone (SM) facies. White arrows intervals show facies SM interbedded between Argillaceous Shale (AG) facies. 50

Figure 43 Example of Siliceous Shale (SS) facies (white arrow interval). Notice the better-defined laminations compared to the Siliceous Mudstones..... 51

Figure 44 Example of thick-bedded Argillaceous Shale (AS). They have very fine laminations, and horizontal fractures break along these planes. 53

Figure 45 Example of the Black Chert (BC) facies within the white arrow interval. In this picture, partially open vertical fractures are present. This facies reflects direct white light because of the high content of biogenic quartz. It can be slightly laminated, but most of the cases are massive beds. 55

Figure 46 Example of Green Claystone (GC) interbedded with Argillaceous Shale (AS). They show mottled texture like in the lower bed implying bioturbation activity during or after deposition. These GC beds tend to thin upward in the section. They are located in the lowermost part of the core. 57

Figure 47 Example of Dolomitic Mudstone (DM) facies. They are lighter in color than the rest of the lithofacies. They are faintly laminated, and normally the content of dolomite decreases upward transitioning to Siliceous Shale or Siliceous Mudstone facies. 59

Figure 48 Example of Phosphate Nodules (PN). They are variable in size (this example is 1 inch in diameter). They are very common (but not unique) in the uppermost section of the Woodford Shale. They can be embedded inside Black Chert beds, Siliceous Mudstone bed, and Siliceous Shale beds. They are not present in the rest of the facies. 60

Figure 49 Example of Mineralized Vertical Fractures. In the core, they are mostly convoluted due to compaction (therefore their interpretative name: Pre-Compaction fractures). These fractures are usually found within the Siliceous Mudstone (SM) facies and the thin Black Chert (BC) beds. 61

Figure 50 Example of Horizontal Fractures. They are usually open or partially open and are not mineralized. The break along the lamination plain in the Argillaceous Shales (AS) are less planar in the more massive Argillaceous Mudstones (AM). These fracture were probably induced during coring or when the core dried up. 62

Figure 51 Generalized description of the Marietta Basin Woodford Core. Pie charts represent the mineralogy of each dominant facies (arrows are color-coded by facies). 63

Figure 52 View of the lowermost part of the Marietta Basin Woodford Core. The red arrow shows the unconformable contact between the Woodford Shale and the Sylvan Shale. The Sylvan Shale is a clay-rich, non-organic mudstone deposited in the Ordovician Period. Notice the presence of the thin beds of the Green Claystone (GC) interbedded with the Argillaceous Shale (AS) in the Basal section of the Woodford. Next figure shows more of this section. 64

Figure 53 Core View of transition from Green Claystone (GC) dominated section at the base of this interval to Siliceous Shale (SS). Notice the thinning upward pattern of GC facies..... 65

Figure 54 Third cored interval dominated by Siliceous Mudstone (SM) facies interbedded with Siliceous Shale (SS) facies. Mineralized Vertical fractures (Fv) are present as well in this section and always bounded within Siliceous Mudstone (SM) facies. 66

Figure 55 Fourth cored intervals dominated by the Siliceous Shale (SS) facies. At the base, Dolomitic Mudstone (DM) is present (light gray) and thins upward. Fractures are mostly vertical within Siliceous Mudstone (SM) beds. Magenta arrows show the location of calcareous nodules and small phosphate nodules. They are less concentric and more crystalline than the well-known Phosphate Nodules (PN) in the upper Woodford interval. 67

Figure 56 Fifth cored interval dominated by the Argillaceous Shale (AS) facies. Many horizontal fractures that are partially open within the AS facies. Pyrite is very common as well in this section. The red box shows a diagenetically-altered bed that will be discussed in chapter 4 (Diagenesis). Vertical fractures are restricted to Siliceous Mudstone (SM) facies. 68

Figure 57 Sixth cored interval in the Marietta Basin Woodford Core. Interbedded Siliceous Shale (SS) and Siliceous (SM) at a 1:1 ratio (50% and 50%). This section is thin-bedded with many

vertical and horizontal fractures. There are no Phosphate Nodules (PN) present or Dolomitic Mudstones (DM) beds..... 69

Figure 58 Seventh cored interval dominated by Black Chert (BC) facies and many Phosphate Nodules (PN) marked with magenta arrows. Highly fractured beds are within BC and SM facies. Dolomitic beds are a light gray color..... 70

Figure 59 Uppermost Section of the core. Black Chert (BC) is the dominant facies. BC is interbedded with Siliceous Mudstones (SM). Beds are thicker (2-4 inches) compared to the rest of the core. Magenta arrows show the location of the Phosphate Nodules (PN). Green Box shows the location of the thick Dolomitic Mudstone (DM) bed. Vertical fractures are common but mostly coring induced and not natural..... 71

Figure 60 Informal Members of the Woodford Shale from Hester et al. (1990)..... 72

Figure 61 Correlation between the Speake Ranch Woodford Section and the Marietta section. Notice how the section is condensed from the NW to the SE. Gamma Ray responses are very similar to each other even within 55mi of separation between locations. 74

Figure 62 Chemostratigraphic Profiles of the Marietta Basin Core. Black arrows show major increasing-decreasing trends. The blue line represents the Maximum Flooding Surface (mfs), and red line represent the Sequence Boundary at the base of the section. The Upper Sequence Boundary was not cored..... 77

Figure 63 Depositional Model of the Woodford Shale from Slatt 2013 (modified by Galvis, 2017). The Woodford Shale sequence is composed by an early Transgressive Systems Tracts (TST) and a later Highstand Systems Tract (HST). Highest GR surface represents the Maximum Flooding Surface (mfs). 78

Figure 64 Sequence Stratigraphic correlation between the Woodford Shale exposed in the Speake Ranch outcrop and the Woodford Shale section in the southeastern part of the Marietta Basin (North Texas). Speake Ranch section modified from Galvis (2017)..... 80

Figure 65 Location of the Samples taken for thin sections in the Marietta Basin Woodford Core. 82

Figure 66 Picture of graduate student (Antonio Cervantes) looking in the Carl Zeiss AX10 Imager Z1 petrographic microscope. It has the capability of using 1) transmitted plain-polarized light (PPL), 2) transmitted cross-polarized light (XPL), and 3) reflected light (RL). This instrument is property of ConocoPhillips School of Geology and Geophysics (CPSGG) at The University of Oklahoma (OU). 84

Figure 67 Picture of the Scanning Electron Microscope (SEM) ThermoFischer FEI Quanta 250 with an attached Energy-Dispersive X-Ray Analyzer (EDX) This instrument is property of ConocoPhillips School of Geology and Geophysics (CPSGG) at The University of Oklahoma (OU). 85

Figure 68 Example of the texture of the three main matrix in the mudstones facies of the Woodford Shale. On the left (PPL): Matrix A (red arrow), Matrix B (blue arrow), and Matrix C (yellow arrow). On the center image (XPL), magnesite flowering (purple circle). On the right picture (RL), pyrite filled radiolarians (green arrows)..... 87

Figure 69 Microscopic picture of the Woodford Shale allochems. On PPL (1), Tasmanites (yellow/green arrows), Large crystals [originally Gypsum (?)] (blue arrow), and Magnesite flowering (purple circle). On XPL (2), current composition of the large crystals are small crystals of calcite and dolomite. On RL (3), Tasmanites that are dark in PPL are not reflective in RL (therefore no pyrite). 88

Figure 70 Picture of the core section that contains the large crystals (yellow arrows) in proximity to the potential flooding surface (blue arrow). Relatively distal facies overlaying relatively proximal facies. Green arrows show bitumen filled Tasmanites..... 89

Figure 71 Tasmanites from Figure 9 under Scanning Electron Microscope (SEM). Composition was obtained using the EDS. Line scan using the EDS. Observe the distribution of different minerals interpreted from the elemental composition on top of the figure..... 92

Figure 72 Mechanisms of early cementation of Tasmanites and Phosphate Nodules. Schieber (1996)..... 92

Figure 73 SEM picture of Tasmanites inside a phosphate nodule. A) Map view of location of radiolarian (1mm scale); B) Closer view (50µm scale); C) Carbon map; D) Calcium map; E) Phosphorus map; and F) Silicon map. 94

Figure 74 Contact between phosphate (upper) and matrix (lower). White color in the left image is barite. It has a yellowish-orange color in the element composition map; a combination of sulfur (yellow) and Barium (Red). 95

Figure 75 Contact between phosphate nodule and matrix. Observe the presence of Magnesite flowers in the matrix (red square), and Barite within the phosphate (yellow square). 96

Figure 76 Petrographic Microscope image (1-PPL, 2-XPL), SEM image (3), and composition from EDS (4) of the end tip of a pre-compaction fracture (Colors represent elements identified by EDX). 97

Figure 77 Relatively Straight Fracture. Observe Calcite in XPL and presence of Magnesite on the side of fracture. Not as extensive as in the convoluted fractures. 98

Figure 78 Relatively straight fracture filled with calcite and dolomite. Chalcedony is overprinted in the fracture texture (red arrow). 98

Figure 79 Shear texture (red arrows) inside a mineralized fracture. Image from Petrographic microscope.	99
Figure 80 Shear texture (red arrows) under SEM and composition obtained from EDS. Fracture core is made of calcite. Shear is made of magnesite and dolomite. Flowering is also present on the sides of the fracture.	100
Figure 81 Proposed Paragenetic Sequence of the diagenetic events and features present in the Marietta Basin Core.	101
Figure 82 showing the locations of the samples taken for RockEval Pyrolysis and Vitrinite Reflectance analysis in the Woodford Shale Core.	105
Figure 83 showing an example of a RockEval Pyrogram. S1, S2, S3, and Tmax values are interpreted from the peaks of the pyrogram and the temperature at which they reach those peaks.	106
Figure 84 Operation mechanism of the Rebound Hardness equipment (modified from Becerra, 2017)	107
Figure 85 Depth plots of the geochemical parameters. Log 1 is Organic Richness and represents the Total Organic Carbon content of the rock. Log 2 show the Hydrocarbon Potential of the rock. Log 3 and 4 are Hydrogen Index and Normalized oil content logs.	110
Figure 86 Cross-plot between Remaining Hydrocarbon Potential (S2) and TOC. All the Woodford Shale samples plot within the Type II kerogen (oil prone- marine).	113
Figure 87 Pseudo Van-Krevelen diagram (Hydrogen Index vs. Oxygen Index).	114
Figure 88 Depth plot of Vitrinite Reflectance along the Marietta Basin Woodford Core. Measured vitrinite reflectance is in black, red is calculated, green is bitumen. Bitumen	

reflectance is usually suppressed in comparison to vitrinite reflectance. VRO% average is 0.79 (oil window)..... 116

Figure 89 Cross-plot between Hydrogen Index and Tmax. Most of the samples plot within the oil window area and close to the Type II (oil-prone / marine) kerogen..... 117

Figure 90 Stratigraphic correlation between Rebound Hardness (RH) data, facies vertical distribution, and sequence stratigraphy. TST is a softer interval than the HST. Condensed section is the most ductile. Red arrows show soft sections, green hard sections, and yellow very hard sections. Black arrows show the main trends in RH data. 120

Figure 91 Cross-plot between Rebound Hardness and Quartz content (XRD). There is an inverse relationship between these clay content and rebound hardness data. 121

Figure 92 Cross-plot between Rebound Hardness and Quartz content (XRD). There is a positive relationship between these two variables. Facies color-coded. 122

Figure 93 Cross-plot between Rebound Hardness and Mineralogical Brittleness Index (using Wang and Gale’s equation). High Rebound Hardness correlates with high Brittleness Index. Facies color-coded. 123

Figure 94 Best target zone (light blue box) in the Marietta Basin Woodford Core with an ideal combination of ductile/brittle couplet (Siliceous Shale/ Siliceous Mudstone couplet) 125

Figure 95 Base map with the locations of the available well data and seismic lines. Green dots correspond to available raster logs. Red dots have digital logs. Red stars represent the location of the type logs. Purple lines represent the location and relative length of the 2D seismic lines. 127

Figure 96 Dip Line Structural Model across the Marietta Basin. Location of the line B-B’ is shown in the map for reference. Notice the presence of the Woodford Shale in the center of the

Marietta Basin Syncline. The Woodford Shale is missing in the SW edge as well as the NE edge of the basin..... 130

Figure 97 Strike Line Structural Model parallel to the syncline axis of the Marietta Basin. Location of the line A-A' is shown in the map for reference. The Woodford Shale is thinner towards the NW area of the basin where the Hunton Group is present. As the Hunton Group pinches out towards the SE the Woodford/Sycamore section becomes thicker. 131

Figure 98 Type Log of the Woodford Shale Formation in the Marietta Basin. The name of each log is displayed at the top of each track. The key interpretative surfaces are shown as horizontal lines. HST: Highstand Systems Tract. TST: Transgressive Systems Tract. MFS: Maximum Flooding Surface. SB: Sequence Boundary..... 133

Figure 99 Stratigraphic Cross-Section of the Marietta Basin. Orientation is NW-SE. The three main intervals are the Upper Woodford (U-WDFD), the Target Interval, and the Transgressive Systems Tract (TST). 135

Figure 100 Structural Cross-Section of the Marietta Basin. Orientation is NW-SE. The Woodford Shale is shown in dark colors..... 136

Figure 101 Structure (True Vertical Depth) Map of the Top of the Woodford Shale in the Marietta Basin. Contour Intervals are spaced every 1,000 feet. Basin is shallower toward the SW side and deeper in the central area of the basin. 140

Figure 102 Gross Thickness (Isochore) of the whole section of the Woodford Shale in the Marietta Basin. Contour Interval is 50 feet..... 141

Figure 103 Thickness (Isochore) Map of the Hunton Group (Limestones) in the Marietta Basin. Hunton Limestones are mostly absent in the SE area, and it is thickest in the NW area closer to the edge of the basin. 142

Figure 104 Thickness Map (Isochore) of the Target Interval which is the section between the Maximum Flooding Surface (mfs) and the Base of the Chert. Contour Intervals are every 20 feet. Green area represent thickness greater than 100 feet..... 143

Figure 105 Map with the location of Woodford Shale horizontal wells in the Marietta Basin. They are color-coded by well operator (the legend is in the upper left). Dash line represents the Marietta Basin outline..... 145

Figure 106 Histogram of Woodford Shale horizontal wells drilled and in production by year. 2019 number represents the number of Woodford wells with permits approved to drill. The peak of drilling activity was reached in 2015 with 19 wells. 146

Figure 107 Graphic representation of Arp’s Decline Models. Hyperbolic curve varies between harmonic and exponential by changing the b factor value of the equation between 0 (exponential) and 1 (harmonic). Figure modified from Odagme (2016). 150

Figure 108 Decline Curve Analysis of the well XTO MCKAY 1-22H15. Green line represents oil. Red line represents gas. Hyperbolic Model was used with a “b” factor of 1. 154

Figure 109 Decline Curve Analysis of the well XTO MANNING 1-3H. Green line represent soil. Red line represents gas. Hyperbolic Model was used with a “b” factor of 1. 155

Figure 110 Decline Curve Analysis of the well XTO ROBERTS 1-19H. 156

Figure 111 Initial Production Rates (Qi) per month for all the analyzed Woodford horizontal wells in the Marietta Basin. Green histogram represents oil, and red represents gas. 157

Figure 112 Initial Decline Rates (Di) per month for all the analyzed Woodford horizontal wells in the Marietta Basin. Green histogram represents oil, and red represents gas. 158

Figure 113 Histogram of the Estimated Ultimate Recovery (EUR) for all the analyzed Woodford horizontal wells in the Marietta Basin. Green histogram represents oil, and red represents gas. 159

Figure 114 Histogram of the Estimated Ultimate Recovery (EUR) for all the analyzed Woodford horizontal wells in the Marietta Basin normalized per 1000 feet of the lateral well. Green histogram represents oil, and red represents gas..... 159

Figure 115 Woodford Shale-Top Structure Map (TVD). Contour Interval: 1000 feet. Pie chart size represents the Estimated Ultimate Recovery. Green represents oil and Red represents Gas. Larger EURs are located in deeper areas (>10,000 feet). 161

Figure 116 Target zone between mfs and base of the Chert beds with Phosphate Nodules..... 162

Figure 117 Thickness Map of the Target Interval (between mfs and base of the Chert section – See Figure 7.13). Green areas have a thickness larger than 100 feet. Yellow areas represent a thickness between 60 and 100 feet. Red areas have thickness lower than 60 feet. Notice that the wells with larger EURs correlate with areas with thicker target intervals (in green). 163

Abstract

A geologic characterization of the Woodford Shale in the Marietta Basin has never been published due to the very limited data in the basin. The primary goal of this dissertation is to identify, analyze and interpret the characteristics of the Woodford Shale formation in the Marietta Basin in southern Oklahoma and northern Texas using recent available core data, in conjunction with well logs and production data. A second related goal is to apply the knowledge and methods from Woodford Outcrops to identify ideal target intervals in the subsurface. The applied methodology includes the description of the cored section to set the stratigraphic framework for the integration of several type of data (XRD, XRF, SEM, EDX, RockEval, VRo, and Rebound Hardness), correlation of the key stratigraphic sections across the basin using well log data to generate structure and thickness maps of the most significant intervals, followed by estimating ultimate recovery (EUR) in the Woodford producing wells in the basin. Core analysis allowed the identification six significant lithofacies: Siliceous Mudstone (SM), Siliceous Shale (SS), Black Chert (BC), Argillaceous Shale (AS), Green Claystone (GC), and Dolomitic Mudstone (DM). Combining facies associations with core gamma-ray log, and X-Ray Fluorescence profiles provided evidence to interpret a stratigraphic sequence. The Maximum Flooding Surface (MFS) of the section corresponds to the middle of the stratigraphic section with the highest gamma-ray peak and it is linked to the condensed section dominated by the AS facies. This surface separates two primary systems tracts in the Marietta Basin: The Transgressive Systems Tract (TST) in the lower and middle section and the Highstand Systems Tract (HST) in the upper section. These two system tracts correlate to outcrop sections in the Arbuckle Mountains. Based on RockEval, TOC in the section ranges from 2.93% to 9.75%, dominated by Kerogen Type II. The average thermal maturity based on Vitrinite Reflectance is

0.79% Vro. Rebound Hardness data show that the high quartz content BC and SM facies are harder rocks than the quartz-poor AS and SS facies. Vertical Mineralized Fractures are bed bounded by clay-rich beds and only present within the SM beds. The paragenetic sequence of this Woodford section is very complex, with several diagenetic alterations in fractures and matrix. The top of the Woodford Shale ranges from as shallow as 5000 feet in the NW side of the basin, to as deep as 17000 feet in the SE. Gross Woodford Shale thickness ranges from 50 feet to 300 feet. Combining good Reservoir Quality (RC) properties like organic richness (TOC) and good Completion Quality (QC) properties like thin interbedded hard/soft beds to improve high fracture density generation helps map the preferred target interval. This "target interval" was correlated from outcrops and core into the basin, is stratigraphically placed above the MFS and below the base of the Chert-dominated interval in the Marietta Basin Woodford section. The Decline Curve Analysis shows average EUR of 90,000 bbl./1000ft lateral; therefore a 5000-foot lateral unbounded well (one section) could produce an average 450,000 bbl. of oil and 1 Bcf of gas. I show that EUR directly correlates with thicker "target intervals" (>80 feet) in the Woodford section and with deeper depth due to higher reservoir pressure support. I believe this dissertation provides the first published comprehensive study of the Woodford Shale in the Marietta Basin and hope it will guide not only scientific research but also future exploration and development of this play the Marietta Basin.

Chapter 1: Introduction

The Woodford Shale is considered to be the primary source rock for most of the hydrocarbons in the state of Oklahoma and the main reason why Oklahoma is one of the largest producers of oil and gas in the United States today (**Figure 1** and **Figure 2**). The Woodford Shale plays two roles in Oklahoma and the United States: 1) a world-class source rock for conventional reservoirs, and 2) one of the best unconventional resource plays in the country (**Figure 3**). Its exceptional performance as a source rock is related to the high Total Organic Content (TOC) in the formation. Its excellent performance as a reservoir rock is related to its brittleness is due to the low clay and high biogenic quartz content (Slatt, 2018).











Rank	State	Crude Oil Production (thousand barrels)	
1	Texas	151,198	
2	North Dakota	42,574	
3	New Mexico	25,294	
4	Oklahoma	18,107	
5	Colorado	16,017	
6	Alaska	15,366	
7	California	14,384	
8	Wyoming	8,087	
9	Louisiana	3,735	
10	Utah	3,147	

Figure 1. Ranking of states in the US by monthly crude oil production. The state of Oklahoma is ranked number 4 with a production of 18.1 million of barrels of crude oil per month. Source: EIA, 2019

Rank	State	Natural Gas Marketed Production (million cu ft)
1	Texas	7,135,494
2	Pennsylvania	5,463,888
3	Oklahoma	2,513,897
4	Louisiana	2,138,918
5	Ohio	1,772,932
6	Colorado	1,683,388
7	West Virginia	1,601,047
8	Wyoming	1,585,486
9	New Mexico	1,293,040
10	Arkansas	707,292

Figure 2 Ranking of states in the US by monthly natural gas production. Oklahoma is ranked number 3 with a production of 15,513,897 million cubic feet of natural gas per month. Source: EIA, 2019

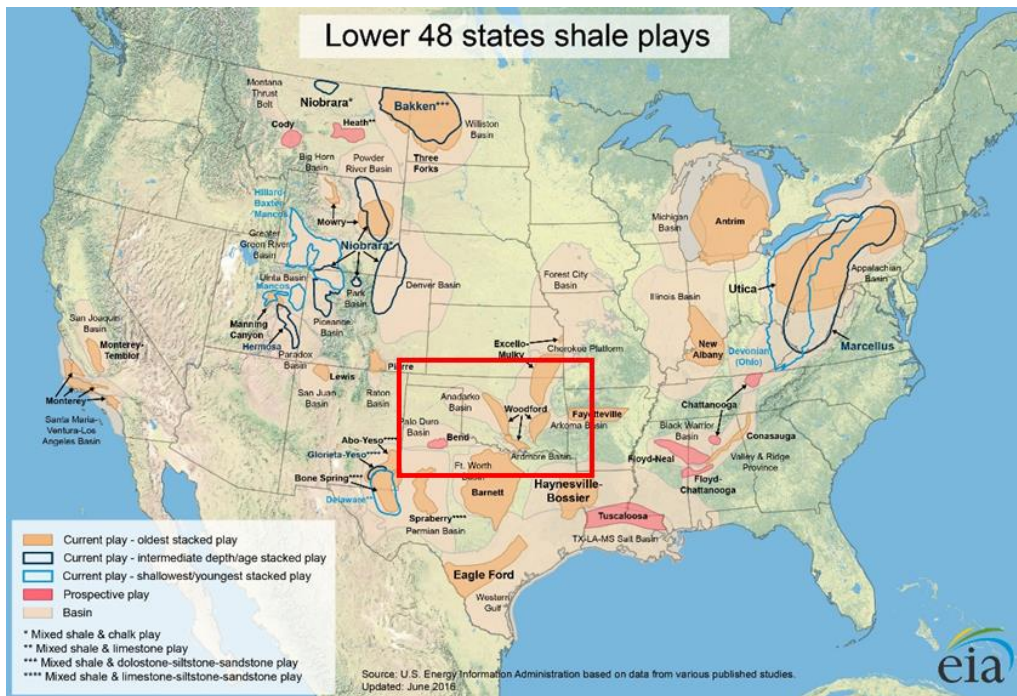


Figure 3 Current location of the Unconventional Resource Plays in the United States (modified from EIA, 2016). The Woodford Shale is one of the main resource shales in the Country.

The Woodford Shale is the main resource shale in the state of Oklahoma as well as in several areas of the state of Texas and Arkansas (**Figure 4**) with the same or similar name (Woodford Shale or Woodford Chert) and characteristics (Cardott et al., 2013; Comer et al., 2008)

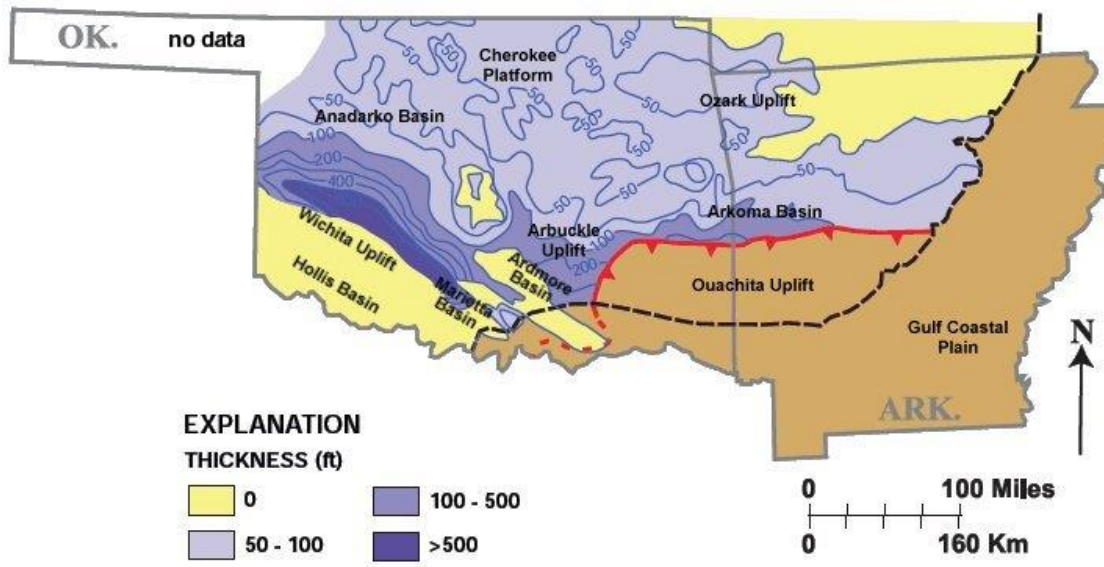


Figure 4 Regional thickness map of the Woodford Shale by Comer, 2003 across the states of Oklahoma and Arkansas.

The current activity of the Woodford Shale play is concentrated in the Anadarko and Ardmore basins (**Figure 5**) in contrast, the Woodford Shale contained within the Marietta Basin is a frontier basin in Oklahoma with very limited well data available and with unknown potential as an unconventional resource.

The Woodford Shale in the Marietta Basin has been drilled and completed by Continental Resources, JMA Energy, Walter O&G; and Jetta Operating in Grayson County, Texas. However, the only operator that has successfully taken the play into development in the basin (particularly in Love County) is XTO Energy (a subsidiary of ExxonMobil Corporation). This dissertation

integrates the reported production of XTO Energy and other operators in the basin and combines it not only with well top maps, but also to outcrop sections in southern Oklahoma to identify the best performing target zones within the Woodford Shale formation.

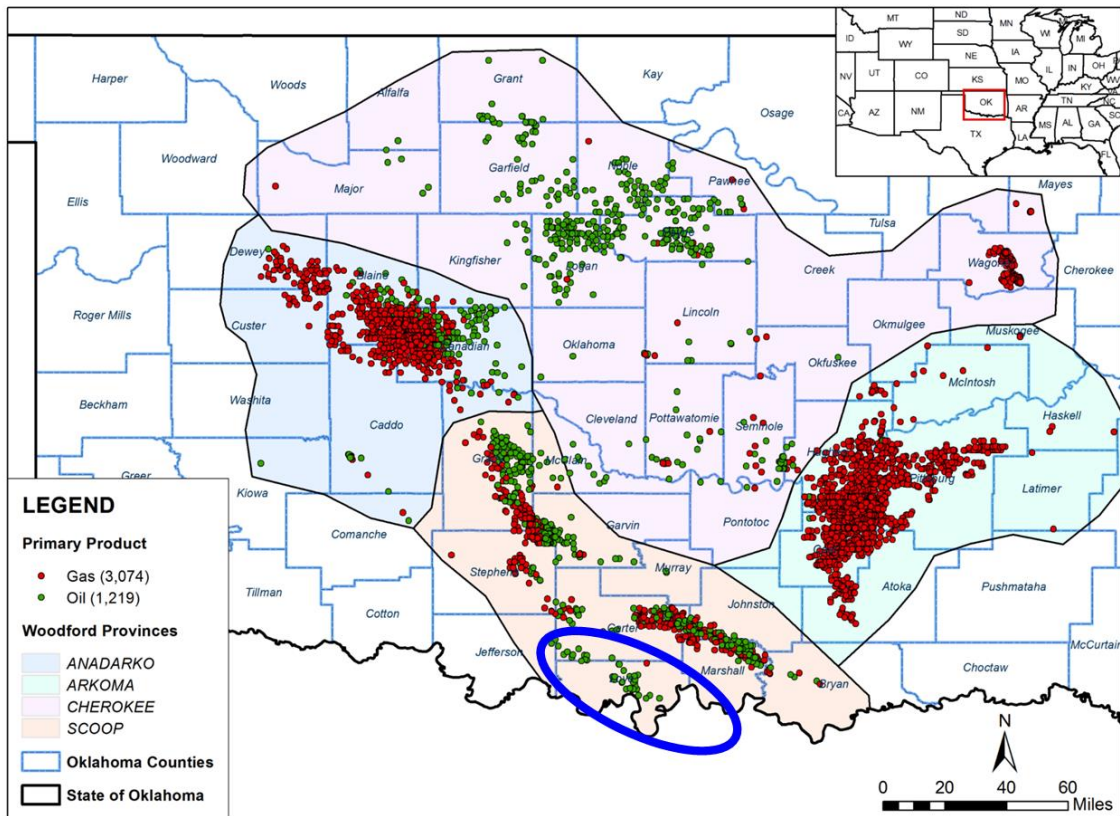


Figure 5 Location of Woodford Shale oil (green) and gas (red) wells in the state of Oklahoma. Blue oval shows the approximate location of the Marietta Basin as part of the South-Central Oklahoma Oil Play (SCOOP) area. No production data is available from North Texas.

1.1 Problem Statement and Significance of this Study

The development of the Woodford Shale as an unconventional resource play in the last ten years produced a large supply of Woodford Shale subsurface data, resulting an increase in research and publications. The bulk of publications focus on the most actively developing areas within the Arkoma Basin, the Anadarko Basin, and the Ardmore Basin (**Figure 5**), with only a few publications related to the geology of the Marietta basin (Cardott, 2018). The Woodford Shale in the Marietta Basin is less well-understood due to the minimal well data available with several operators regarding it as a “frontier” basin.

The Institute of Reservoir Characterization (IRC) in the School of Geology and Geophysics at The University of Oklahoma (OU) has obtained access to core and well data from one of the very few operators in the Marietta basin allowing the start of this dissertation project in 2014. The overarching goal of the dissertation was -and still is- to understand the geology of the basin as a guide to future expansion and successful exploration. A second, related -but more general goal- is to determine whether outcrops can be applied from one region to another over a long distance, even across basins, to successfully predict production potential.

Building on previous IRC work, this dissertation focuses on six main questions:

1. Which facies and units/intervals of the Woodford Shale are present in the Marietta Basin compared to outcrop Woodford sections in southern Oklahoma?
2. Does the Woodford Shale in the Marietta basin exhibit similar stratigraphy as the Woodford Shale in other locations in Oklahoma (such as outcrops)? Are the target zones on outcrops

correlative to target zones in the subsurface and can outcrops even be used to evaluate equivalent subsurface strata?

3. What kind of diagenetic alterations are present in the Woodford Shale of the Marietta Basin? Are there any similarities to the diagenesis at other locations?
4. How is the Woodford Shale geochemically and geomechanically characterized in the Marietta Basin, and is there any difference with other Woodford sections elsewhere?
5. How laterally extensive is the Woodford Shale across the Marietta basin? How does its thickness vary laterally? (this is a key, but currently unknown parameter that will affect exploration)
6. How do the Woodford Shale horizontal wells perform in the Marietta Basin? What is the most significant variable that affects hydrocarbon production and EURs on those wells?

In the next two subchapters, there is a list of specific objectives or steps focused on addressing the above questions as well as the definition of the geographic scope of this research study. Also, by answering these questions, this dissertation will infuse a wealth of new knowledge and understanding of the Woodford Shale in the Marietta basin into both the academic community and the oil and gas industry. Furthermore, this dissertation is looking to test the methods, concepts, and approaches used by the IRC research group in outcrops to identify target intervals for horizontal drilling and artificial fracturing. Specifically, I apply concepts and information from other areas to build a realistic geologic model, then make production predictions from that model to a real-life producing area with limited data, as is the case with this Marietta Basin Woodford Play.

1.2 Scope of Study

The geographic extent of this research includes Love, Carter, and Jefferson counties in Oklahoma; as well as Grayson and Cook counties in Texas (**Figure 6**). Grayson and Love are the most critical counties because they are where most of the well/core data and production of the Woodford Shale are located. This dissertation also reaches out in scope to include for comparison the Woodford outcrop stratigraphic work done by Galvis (2017) in the Arbuckle Mountains Speake Ranch Shale Pit.

The analytic scope of this study includes: geologic description of rock/core samples and thin sections; acquisition and analysis of SEM images (Scanning Electron Microscope); generation of X-Ray Fluorescence profiles, mineralogy from X-Ray diffraction, acquisition and processing of Rebound Hammer data; analysis of RockEval and Vitrinite Reflectance data; geologic interpretation and correlation of well logs; geologic mapping and; analysis of production maps and decline curves. The purpose of these analyses is to generate a comprehensive geologic characterization of this formation to meet the above goals and to predict future possible trends.

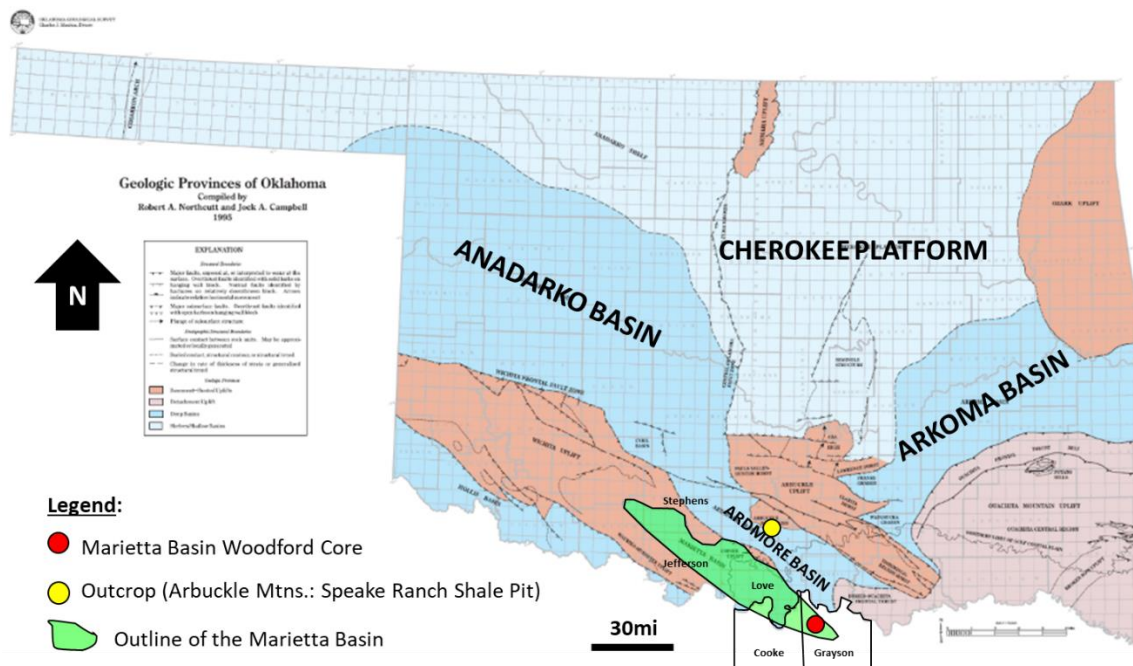


Figure 6 Location of the Marietta Basin (bright green area) overlaid on the Geologic Map of Oklahoma (Northcutt and Campbell, 1995). Colored circles represent the locations of the outcrop (type section) and core.

1.3 Structure of Dissertation

The organization of this dissertation follows the objectives described above and are broken down into chapters as follows:

- Chapter 2: Geologic Setting
- Chapter 3: Lithology, Facies and Stratigraphy
- Chapter 4: Diagenesis
- Chapter 5: Geochemistry and Geomechanics
- Chapter 6: Subsurface Mapping
- Chapter 7: Production and Well Performance.
- Chapter 8: Conclusions and Recommendations

1.4 Previous Work

There are many journal articles and conference proceedings associated with the Woodford Shale in other basins in Oklahoma like the Anadarko Basin and Arkoma Basin, but not in the Marietta Basin due to the limited amount of data. Below are the most significant Woodford Shale publications from other basins and outcrops that serve as guide and correlation to the work done in this dissertation:

The name “Woodford” was first connected to this rock formation by Taff in 1902 as "Woodford Chert" because of the location of this type of rock nearby the town of Woodford south of the Arbuckle Mountains (Cardott, 2014). The definition of "Woodford" as a formal Formation was consolidated by Morgan (1924).

Several authors have studied the regional stratigraphy of The Woodford Shale formation in the Anadarko Basin: Tarr (1955), Ham (1973), Lambert (1993), Paxton et al. (2006), Comer (2008), Chain (2012), Slatt (2013), and Slatt et al. (2017) and found the Woodford Shale has three lithostratigraphic units (Upper, Middle, and Lower) and extend across most of Oklahoma and part of Texas and Arkansas.

Urban (1960), Hass and Huddle (1965), Von Almen (1970), and Molinares (2013) studied the chronostratigraphic setup in geologic time of the Woodford Shale in the Anadarko Basin and Arkoma Basin using palynomorphs and other biostratigraphic methods and found the Woodford Shale was deposited during the Late Devonian and Early Mississippian.

Kirkland et al. (1992) Miller (2007), Serna (2013), Paxton et al. (2015), Bontempi (2015), Ekwunife (2017), Becerra (2017) and Galvis (2017) represent the most critical publications and theses related to integrated outcrop work and their correlation to subsurface data and found the properties and units present in the outcrop sections can be correlated to the subsurface and can be used to better understand the lateral changes in facies and stratigraphy across Oklahoma.

Hester et al. (1988), Johnson et al. (1989), Hester et al. (1990), Althoff (2012), Killian (2012), McCullough (2014) and many other authors have done significant subsurface mapping of the Woodford Shale in many areas of Oklahoma from the Deep Anadarko Basin to Shallower Cherokee Platform and found the Woodford Shale is thicker in areas where the Hunton Group is highly eroded, as well as, the Lower Woodford section is the less aerially correlative unit of the Woodford Shale.

Treanton (2014), Turner (2016), and Ekwunife (2017) Theses are the most in-depth research done related to Chemostratigraphy as a tool to improve the understanding of the deposition of this formation.

O'Brien and Slatt (1990), Slatt and O'Brien (2011), and Curtis et al. (2012) provide an excellent analysis of the Woodford Shale pore structure and classification.

Publications from Sanchez (2012), Cardona (2014), Verma (2014), Infante (2016), and Torres et al. (2017) used seismic amplitude, attribute, and inversion volumes to map the different members and its characteristics (TOC and Brittleness) within the Woodford Shale.

Sullivan (1985), Comer (1987), Johnson and Cardott (1992), Comer (1992) Kirkland et al. (1992), Lambert (1993), Miceli (2010), Miceli and Philp (2012), Connock (2015), Wang (2016), and Jones (2017) conducted geochemistry analyses in the Woodford Shale in Central and North Oklahoma and found the organic richness and biomarkers varies vertically and laterally along the Anadarko, Arkoma, and Ardmore basins.

Cardott, (1989, 2009a, 2009b; 2014) provides a comprehensive analysis of the Woodford Shale thermal maturity lateral variability in Oklahoma.

Slatt and Abousleiman (2011), Becerra (2017) and Becerra et al. (2018) describe the mechanostratigraphic characteristics of the Woodford Formation in outcrops located in the Arbuckle Mountains. Sierra et al. (2011) conducted lab geomechanics of the Woodford Shale, while Portas (2009), Badra (2011), Ghosh (2017), Ghosh et al. (2018a), and Ghosh et al. (2018) mapped fracture networks from Woodford Shale core and outcrop data.

Although Westheimer (1965), Frederickson and Redman (1965) and Bradfield (1968) studied the Marietta Basin, they focus on the underlying Viola Limestone conventional reservoir.

Chapter 2: Geologic Setting

This chapter covers the geologic background used as the baseline for this dissertation. It includes a comprehensive but concise summary of research work done by other authors in previous publications with the aim to provide a foundation for the interpretations, correlations, and discussions in the next five chapters.

The first part comprises the regional geology of Oklahoma, the formation of the geologic provinces in the state as they are defined today with paleogeographic location. It summarizes the main depositional sequences, groups and formations within the major basins in the state, and how they correlate in time. It also has a synopsis of the main tectonic events in the geologic history of Oklahoma.

The second part covers the local geology of the Marietta Basin in South Oklahoma and North Texas. This geologic review is probably the least complete or comprehensive due to the limited number of publications about the area. It is one of the main reasons for the making of this dissertation; to provide additional information to the academic community about the basin and the Devonian Woodford Shale section.

The third and last part of this chapter corresponds to the regional stratigraphic framework in place for the Woodford Shale in Oklahoma based upon publications from Slatt et al. (2011, 2012, 2013, 2016, 2018) and Comer (2005, 2008). There is a particular emphasis on work done on outcrops by Galvis (2017) in the Arbuckle Mountains (Speake Ranch Shale Pit) because it is

the most complete and detailed data set available of any Woodford Shale outcrop in South Oklahoma. Additionally, the mapping research work written by McCullough (2014, 2017) covered the subsurface.

2.1 Oklahoma Geology

Three main episodes can summarize (Figure 7) the tectonostratigraphic history of Oklahoma and North Texas: 1) extension tectonics during the Late Proterozoic and Early Cambrian; 2) quiet subsidence from the Late Cambrian to the Mississippian Period; and finally, 3) the orogenic episodes during the Pennsylvanian to Permian Periods.

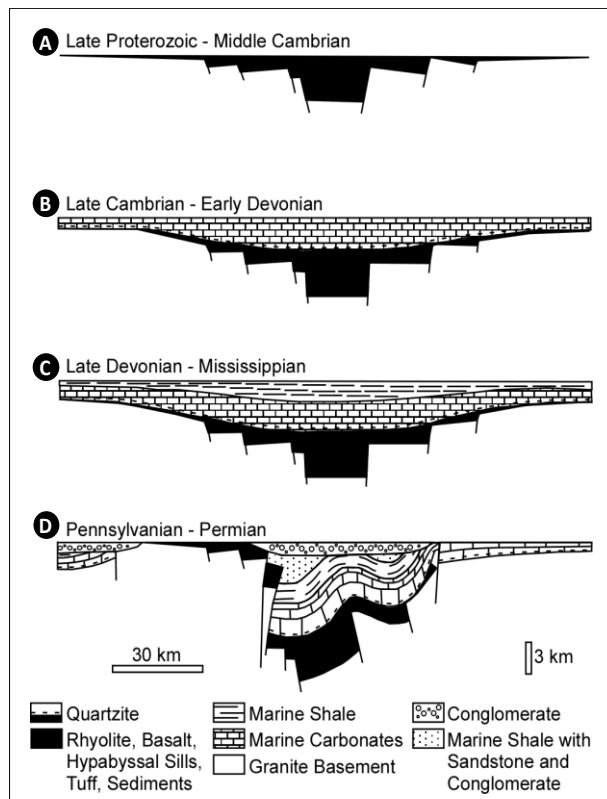


Figure 7 Schematic cross-section view of Oklahoma from Middle Cambrian time to Permian time (Modified from Hoffman et al., 1974).

The Late Precambrian to Cambrian time interval was an interval of extensional and rifting pulses that resulted in the creation of the failed arm of a triple-junction rift called the Southern Oklahoma Aulacogen (SOA) (**Figure 8**).

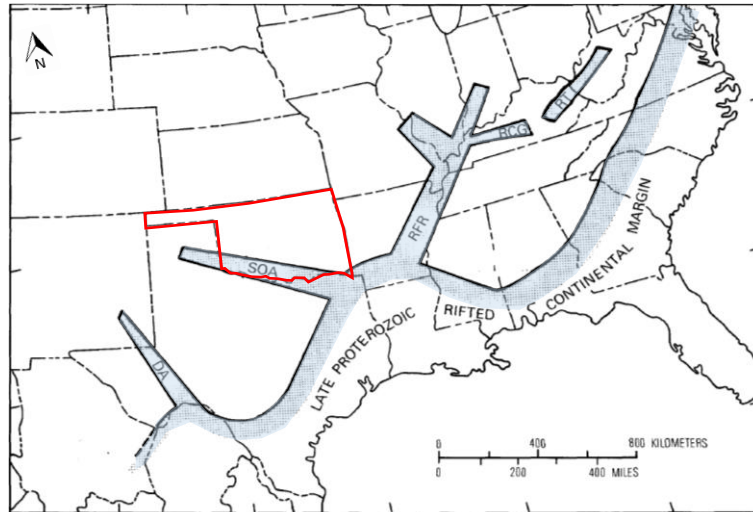


Figure 8 Paleotectonic map of South-Eastern United States and the relative location of the Southern Oklahoma Aulacogen (SOA) and other failed rift arms in the area. DA: Delaware Aulacogen; RFR: Reelfoot Rift; RCG: Rough Creek Graben; RT: Rome Trough. Figure from Keller (1983) and modified by Becerra (2017).

The separation between the North America plate and the Proto-South American plate and creation of the Proto-Atlantic Ocean is the reason for the extensional forces that created the SOA (**Figure 9**) (Wickman, 1978; Ataman, 2008).

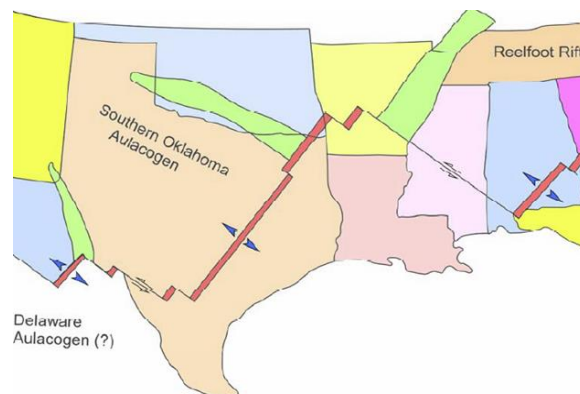


Figure 9 shows rift axis (red) and failed arms (green) forming aulacogens in Texas, Oklahoma, and Arkansas; due to the creation of the Proto-Atlantic Ocean. Modified from Suneson, (1996) and Ataman (2008) by Ekwunife 2017).

The rift formed the oldest rocks in Oklahoma: Precambrian igneous and metamorphic rocks dating from 1.4 billion years ago that include granites, rhyolites, gabbros, and basalts (Johnson, 2008). These rocks form what is considered today the basement of the current basins and platforms within Oklahoma and North Texas. **Figure 10** is a map that shows the current sub-sea depth of this basement in Oklahoma's subsurface. Basement is located as deep as 30,000-40,000 feet in the Anadarko basin and exposed in the subsurface in the Wichita and Arbuckle Uplifts.

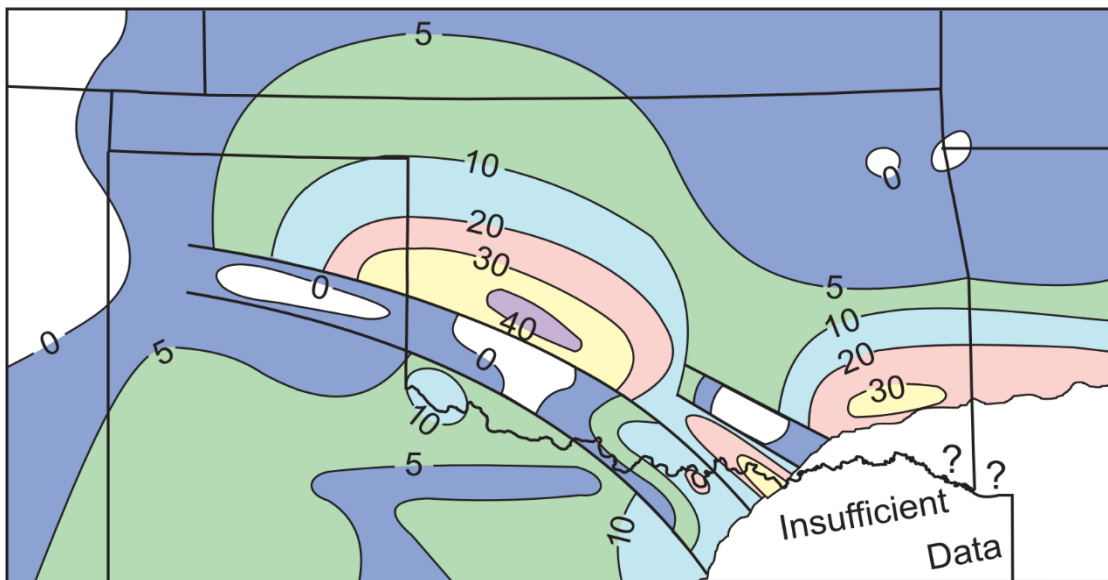


Figure 10 Sub-Sea Depth Map of the Precambrian and Early Cambrian basement in Oklahoma and North Texas (Modified from Johnson, 2008). Numbers represent the TVD depth of the Basement in thousands of feet.

When the igneous and volcanic rocks started to cool during the late Cambrian, the subsidence of denser rocks created a depocenter named the Proto-Anadarko Basin. In a larger scale, this depocenter and surrounding shallower areas formed the Greater Oklahoma Basin that fully covered Oklahoma and large areas of Kansas, Arkansas, North Texas, and Southeast

Colorado. **Figure 11** shows the extent of the Oklahoma Basin and the relative location of the Southern Oklahoma Aulacogen.

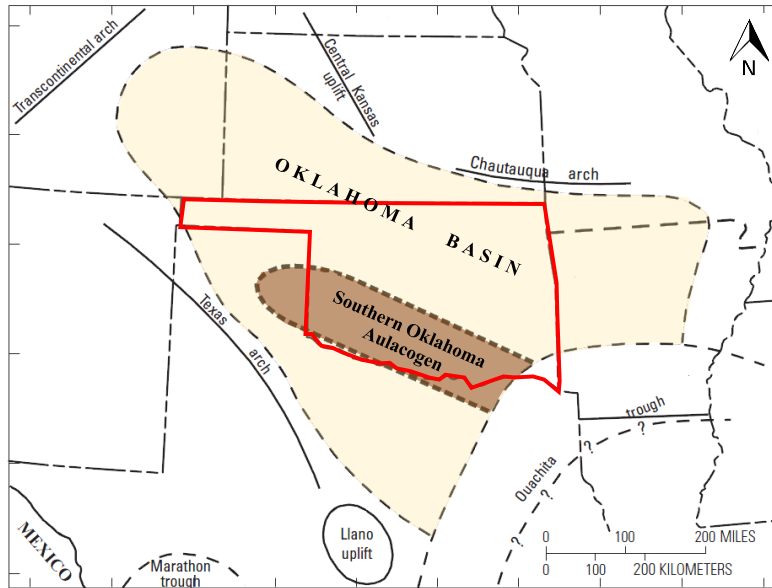


Figure 11 Map of the Greater Oklahoma Basin area from Late Cambrian until the Late Mississippian. Modified from Johnson et al. (1989) by Gaswirth and Higley (2014).

A stage of relative quiet tectonics followed the Late Cambrian, where the Oklahoma basin was entirely flooded by the sea and a deep-water environment was dominant along the Southern Oklahoma Aulacogen axis and shallow water environment in the surrounding areas and platforms. The Reagan sandstones within the Timbered Hills Group represent detrital sediments eroded from the basement, followed by the deposition of the thick (1,000 - 7,000 feet) limestones and dolomites of the Arbuckle Group (**Figure 12**).

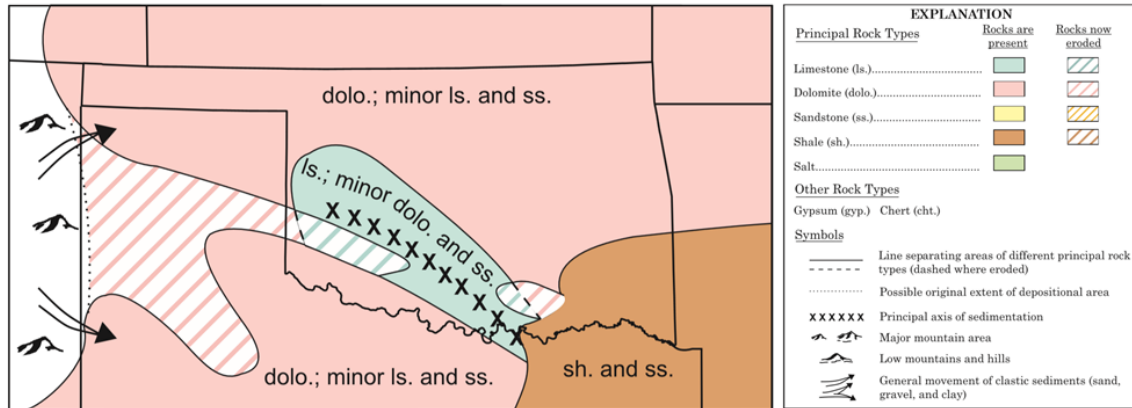


Figure 12 Reconstruction of the Late Cambrian and Early Ordovician by Johnson (2008). Deposition of the Arbuckle Group.

After the carbonate sequence of the Arbuckle Limestones the siliciclastic dominated (Figure 13) Simpson Group was deposited during the Middle and Late Ordovician, capped by the thick Viola Limestone and Sylvan Shale with a combined thickness up to 2,500 feet.

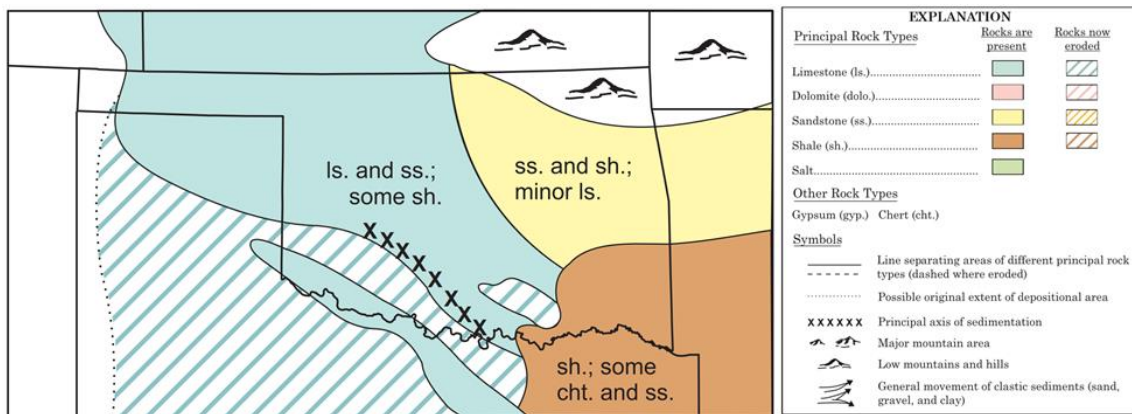


Figure 13 Reconstruction of the Middle to Late Ordovician by Johnson (2008). Deposition of the Simpson Group.

The Silurian and Early Devonian Periods led to deposition of limestone and dolomite of the Hunton Group (Figure 14). A combination of a eustatic drop of sea level and uplift from local tectonics exposed the Hunton Group (and older formations) to erosion in the northern part

of Oklahoma resulting in the first significant unconformity in the area called "Pre-Woodford Unconformity".

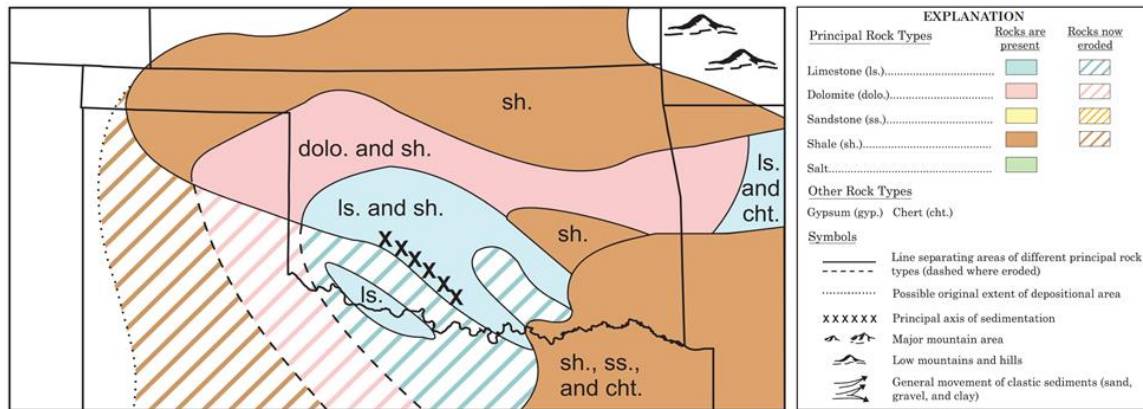


Figure 14 Reconstruction of Silurian and Early Devonian rocks by Johnson (2008). Deposition of the Hunton Group.

Figure 15 shows a representation of the general stratigraphy of the Oklahoma Basin. This unconformity shaped the paleotopography of Oklahoma resulting in the formation of incised valleys and karsts (**Figure 16**).

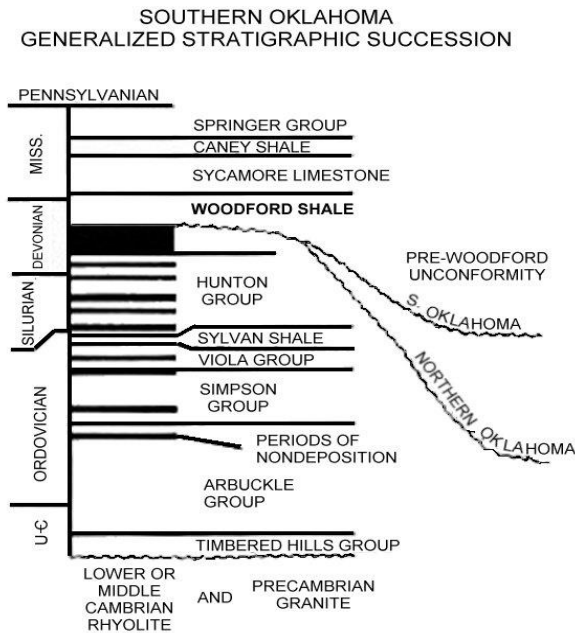


Figure 15 Generalized stratigraphic section for the pre-Pennsylvanian of southern Oklahoma showing periods of non-deposition (black) and extent of the pre-Woodford unconformity (Kirkland et al., 1992).

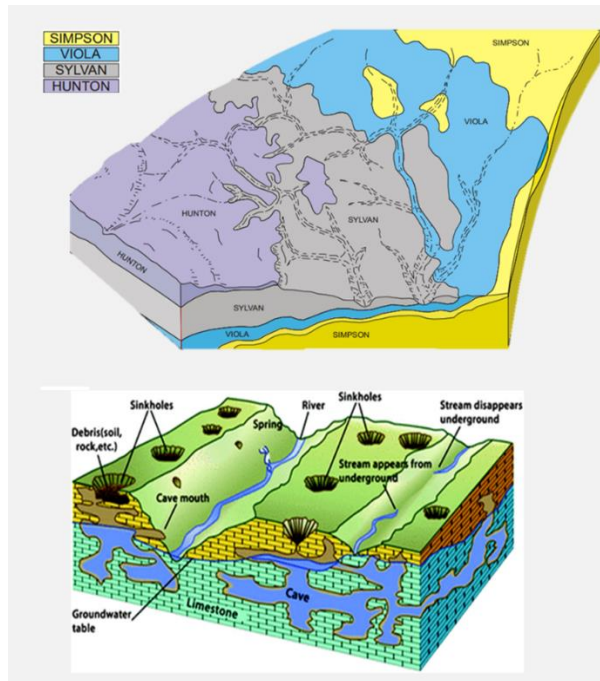


Figure 16 “Pre-Woodford Unconformity” Sub-crop Reconstruction (above) modified from Kuykendall and Fritz, 2001. Karsted surface reconstruction (below); modified from Grotzinger and Jordan (2010).

After a period of lowered relative sea level, there was a major transgression that covered most of North America and formed many epicontinental seas. This transgression lasted into the Early Mississippian Period (Figure 17).

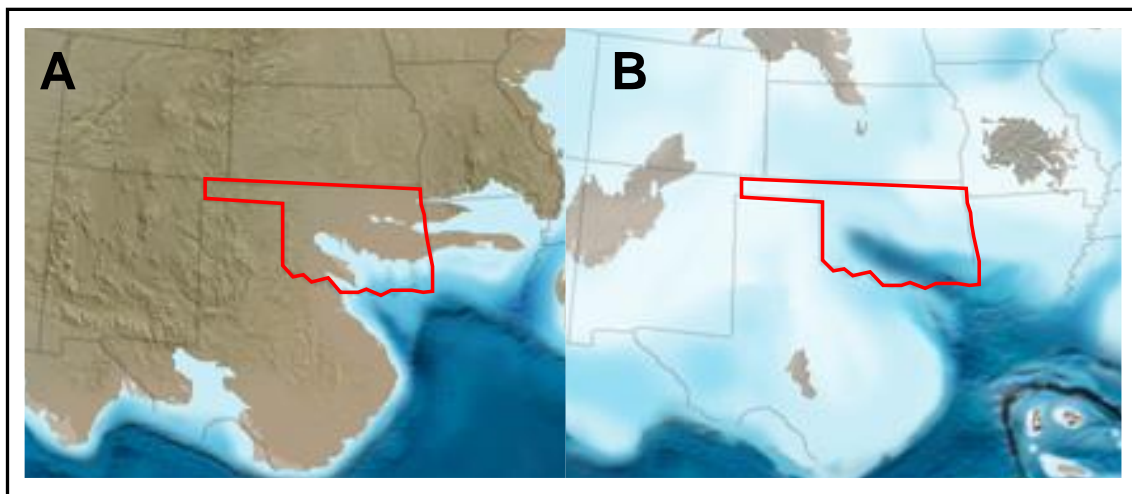


Figure 17 Paleogeographic reconstruction of south United States from Late Devonian (A) to Early Mississippian (B). Figure modified from Blakey (2012).

The early transgression deposited the basal Misener Sandstone. The Woodford Shale formation and correlative formations (Arkansas Novaculite, Chattanooga) in Arkansas were deposited during the onset of this transgression (**Figure 18**). The lateral distribution and thickness of the Woodford Shale in Oklahoma and North Texas were shaped by the paleotopographic relief created during the Post-Hunton/Pre-Woodford Unconformity (Slatt et al., 2016; McCullough, 2017).

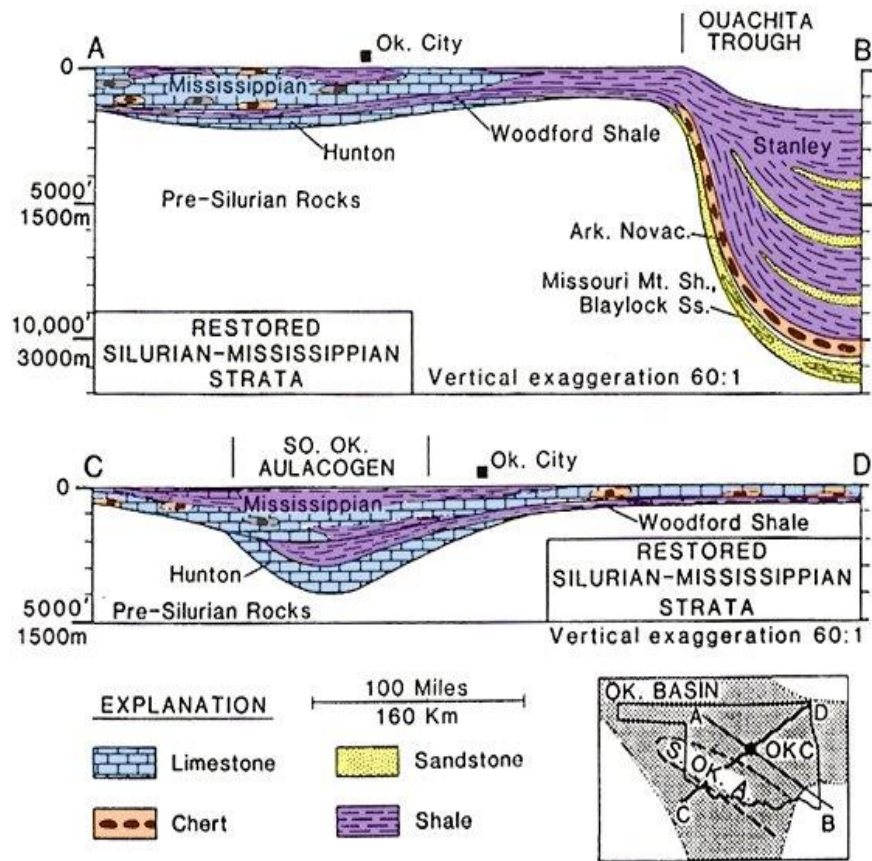


Figure 18 Cross-sections showing restored Silurian, Devonian and Mississippian strata in Oklahoma (modified from Johnson and Cardott, 1990 by Miceli 2010).

The Mississippian was a time of relative quiet dominated in Oklahoma by deposition of the Sycamore Limestone, Caney Shale, and Goddard/Springer formations in southern Oklahoma

and the Mississippian strata (Osage, Meramec, and Chester formations) in northern Oklahoma (Figure 19).

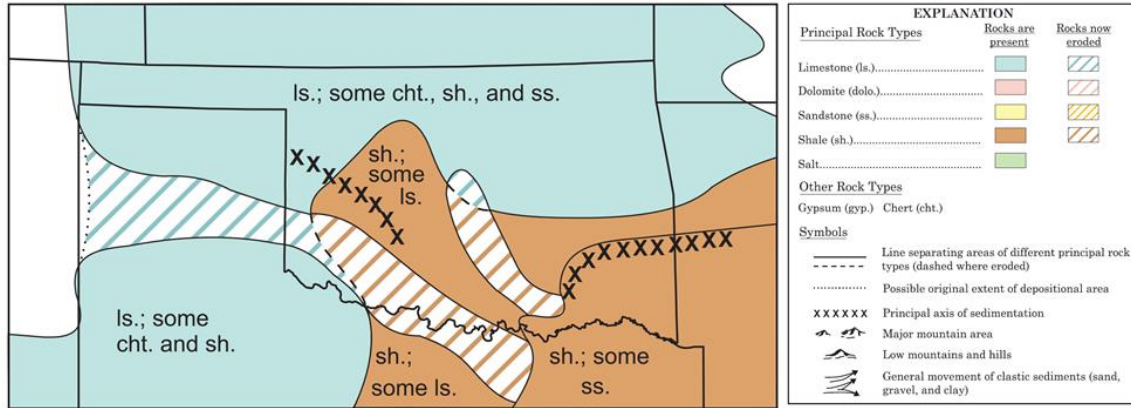


Figure 19 Reconstruction of dominant lithologies during most of the Mississippian period. Modified from Johnson (2008)

The Pennsylvanian Period represents a drastic change in the environments in Oklahoma and North Texas due to the formation of mountains during the Morrowan Orogeny and the later Desmoinesian Orogeny. A large area of the Midcontinent was uplifted, forming the Wichita, Arbuckle, Ouachita, and Ozark uplifts, as well as areas like the Criner Hills. **Figure 20** shows a reconstruction of Early to Late Pennsylvanian time.

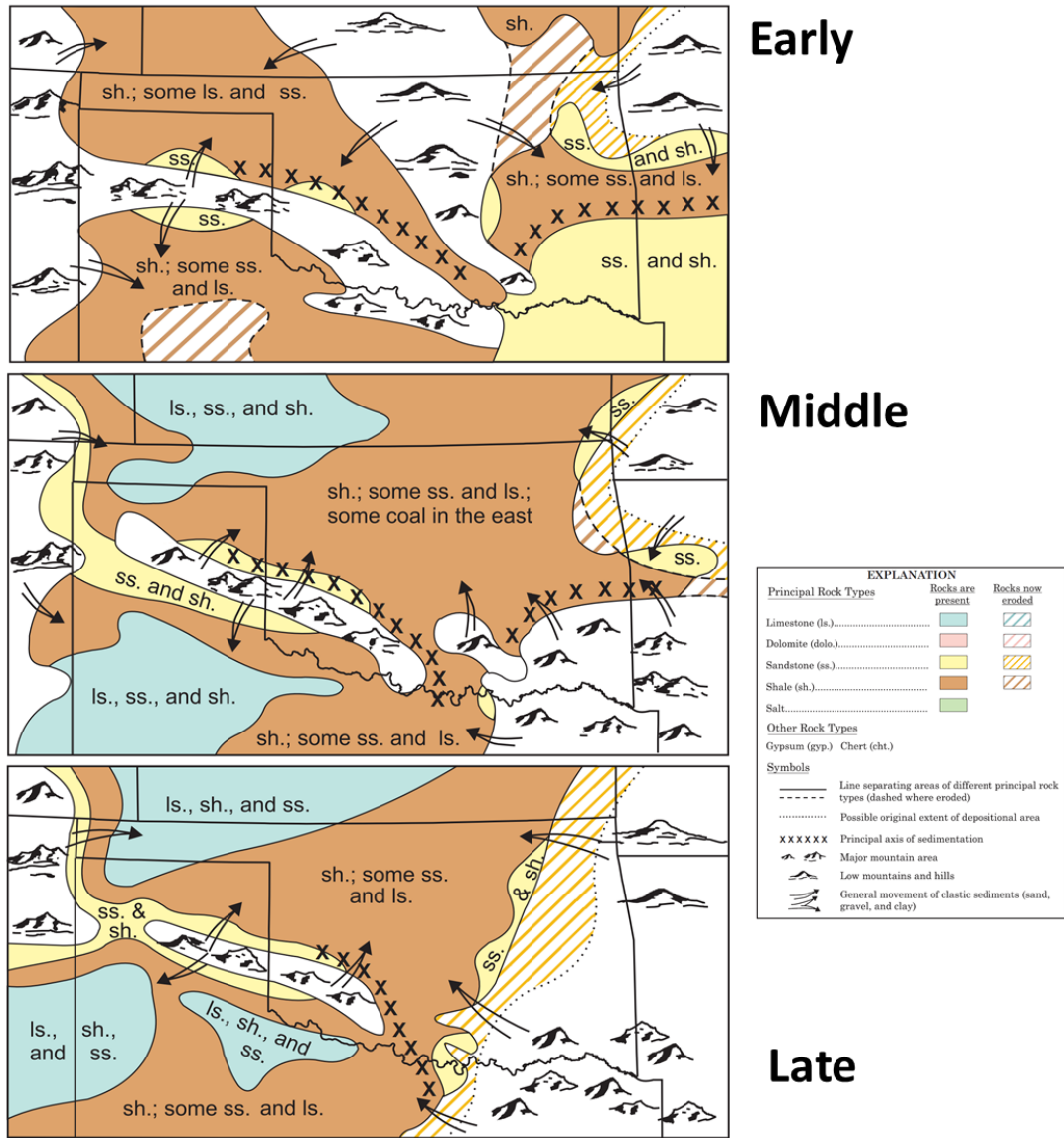


Figure 20 Reconstruction of Pennsylvanian time, modified from Johnson (2008).

The Pennsylvanian Strata in Oklahoma is dominated by siliciclastic deposits (conglomerates, sandstones, and shales) which are 2,000 to 5,000 feet thick in Northern Oklahoma and can have thicknesses up to 18,000 feet in the Arkoma Basin, 16,000 feet in the Anadarko Basin, 15,000 feet in the Ardmore Basin, and 13,000 feet in the Marietta Basin.

After the active time of the Pennsylvanian, shallow areas were flooded in western Oklahoma during the Permian Period and exposed in the eastern side of the state, Arkansas, and

parts of northeastern Texas. The Western area deposition was dominated by shales, sandstones, and evaporites (**Figure 21**)

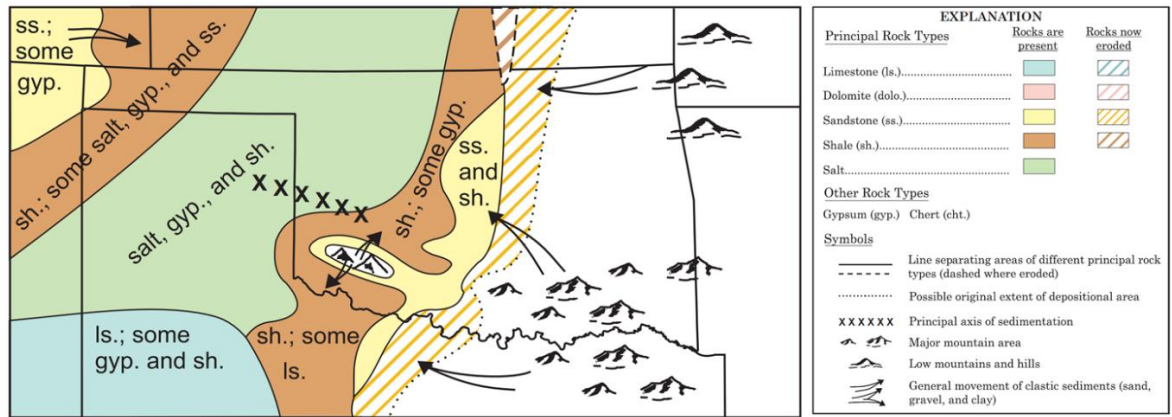


Figure 21 Reconstruction of the Permian Period. Modified from Johnson (2008).

During most of Triassic and Jurassic time, Oklahoma’s surface was exposed with low deposition rates. The Cretaceous led to a large-scale transgression the flooded most of western Oklahoma, but most of the rock record of this time was eroded during the uplift of the Rocky Mountains in Late Cretaceous and Early Tertiary time. The Late Tertiary and Quaternary Periods were characterized by the formation of the soil we see today in Oklahoma, and the only deposition is happening along streams and rivers as fluvial banks (**Figure 22**).

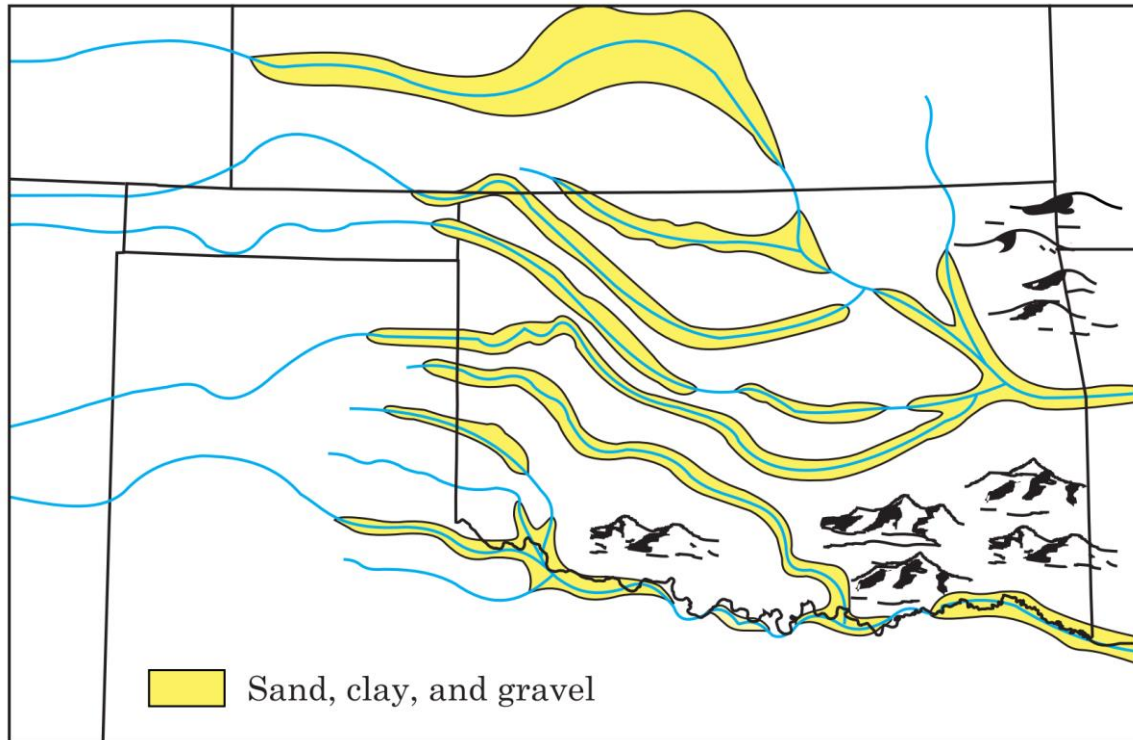


Figure 22 Major rivers and streams, as well as, Mountains in Oklahoma during the Quaternary Age. Modified from Johnson (2008).

The current arrangement of basins, platforms, and uplifts also known as the Geologic Provinces of Oklahoma are the result of the previously described tectonostratigraphic history of Oklahoma. The OGS Educational Publication #9 by Johnson (2008) shows a set of cross-sections (**Figure 23:** next Page) along the state showing the structural setting and distribution of deposits in the state:

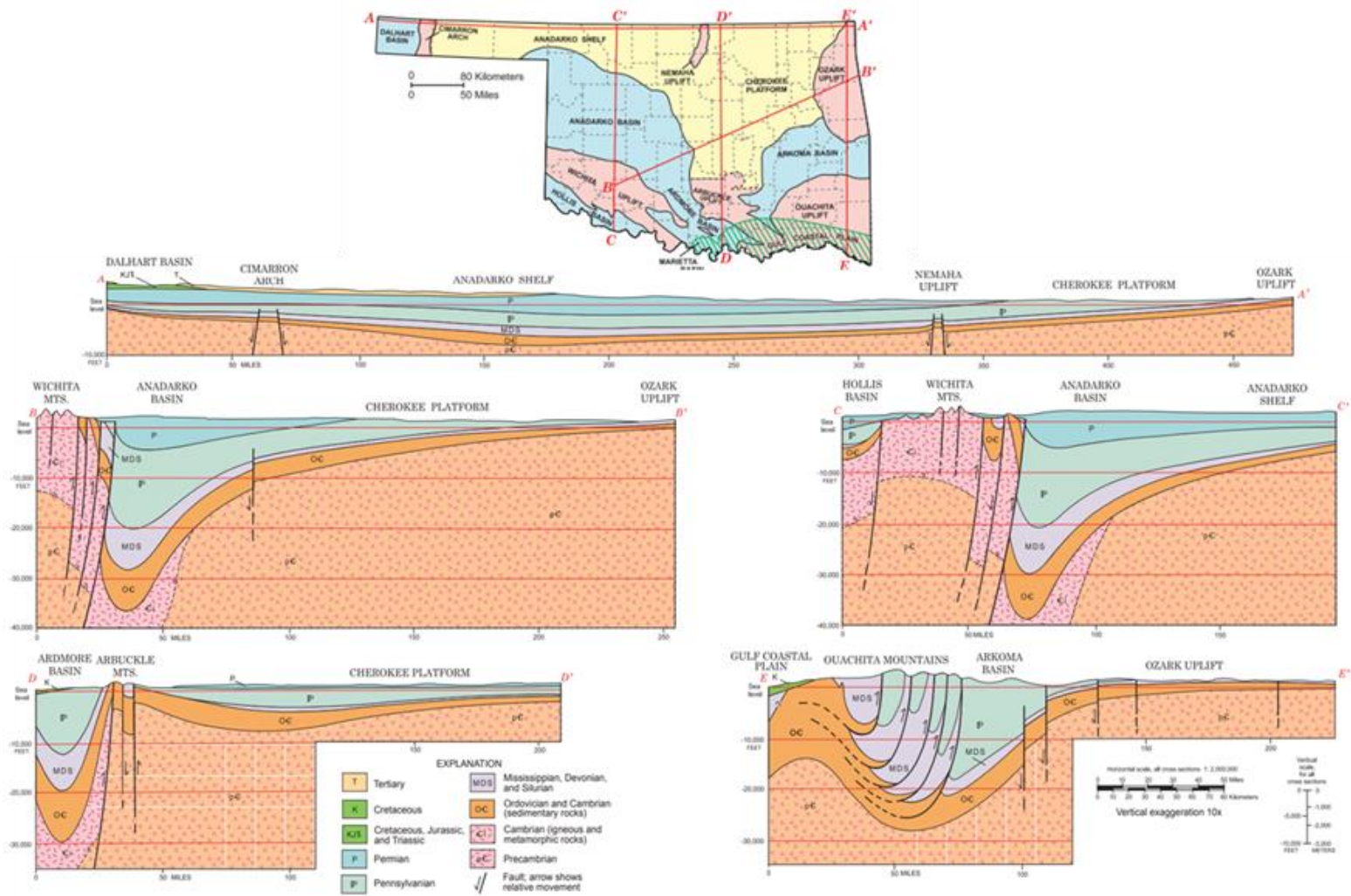


Figure 23 Set of cross-sections along the state showing the structural setting and distribution of deposits in the state of Oklahoma.

2.2 Marietta Basin Geology

The Marietta Basin is the smallest and least known of the basins that are part of the Geologic Provinces of Oklahoma. It is located in the south-central border between Oklahoma and Texas. It covers a large area of Love County (OK) and Grayson County (TX) with partial areas of Jefferson County (OK) and Cooke County (TX). Its limits are: a) in the north with the Criner Hills and Wichita Mountain Uplift; b) in the south and west with the Waurika-Muenster Arch; c) and in the east with the Ouachita Mountains Foldbelt (**Figure 24**).

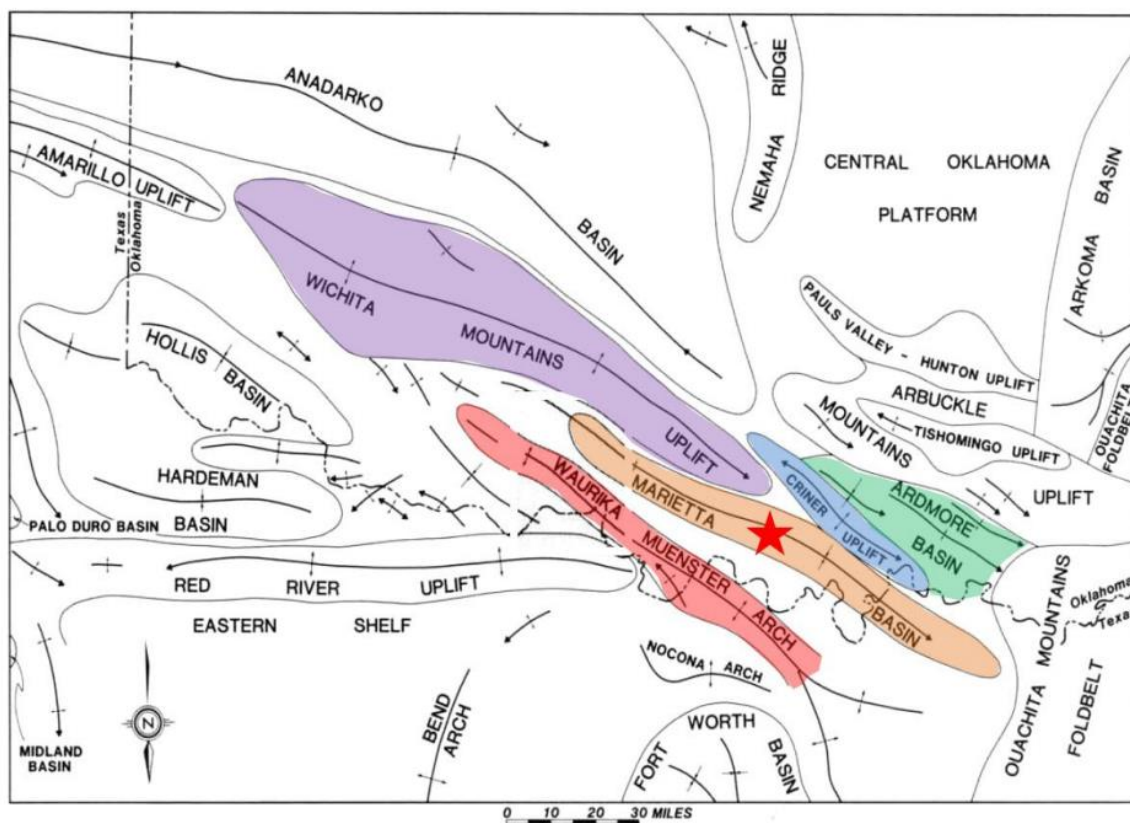


Figure 24 Map of tectonic domains in South-Central Oklahoma. Red star shows the Marietta Basin. Figure modified from Cook (2010).

The Marietta Basin is also called The Marietta Syncline (**Figure 25**), and it was part of the Greater Oklahoma Basin from the Late Cambrian until the beginning of the Pennsylvanian Period. The formation of the basin started with the Southern Oklahoma Aulacogen (SOA); therefore, sharing the same basement with the Ardmore Basin and Anadarko Basin.

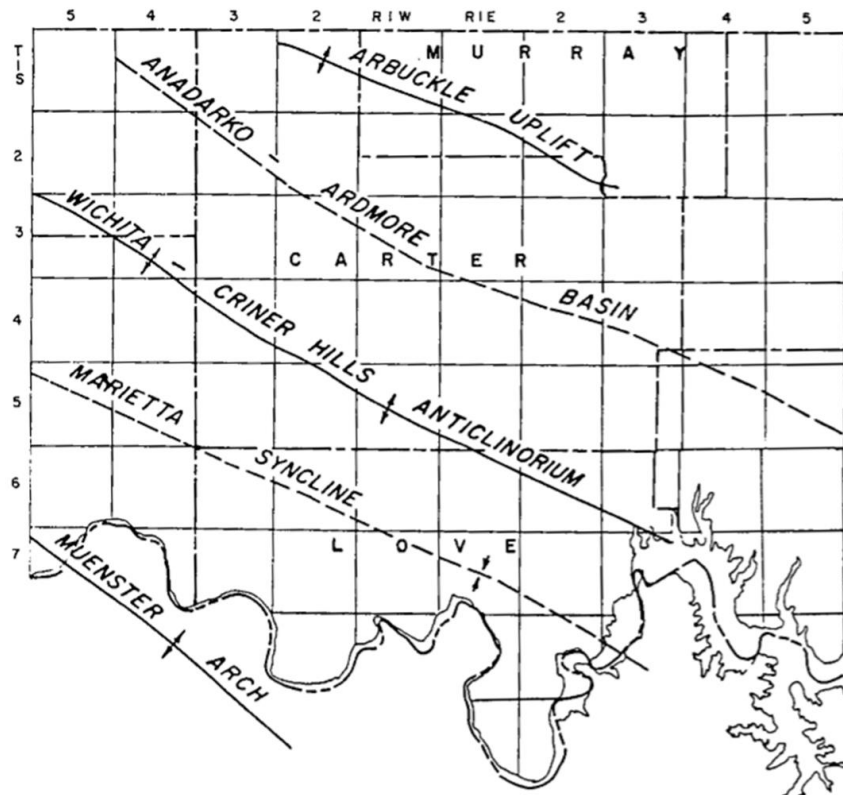


Figure 25 Generalized structural trends in Love County and Carter County in South Central Oklahoma (Westheimer, 1965)

According to Westheimer (1965), the general stratigraphy of the Marietta Basin includes the Pre-Pennsylvanian strata, which correlate to the stratigraphy of the Ardmore Basin (**Figure 26**). The sequence of formations from older to younger in Love County (OK) are: Arbuckle Group (Ordovician), Simpson Group (Ordovician), Viola Group (Ordovician), Sylvan Formation (Ordovician), Hunton Group (Silurian-Devonian), Woodford Formation (Devonian- Early Mississippian), Sycamore Formation (Early Osagean), Caney Group (Late Meramecian),

Goddard Formation (Late Mississippian), Dornick Hills (Early Mississippian), Deese Group (Early Mississippian), and Hoxbar and Cisco Groups (Late Mississippian).

SYSTEM	SERIES	GROUP	FORMATION	MEMBERS AND LOCAL NAMES	
CRETACEOUS	Comanchean				
	Virgilian	Cisco	Pontotoc terrane	Shale, sandstone, and arkosic conglomerate Shale, sandstone, and nonarkosic conglomerate	
PENNSYLVANIAN	Missourian	Hoxbar		Home Creek Ls. Zuckermann Ls. Ranger Ls. Daube Ls. Anadarche Ls. Twin lime Crinerville Ls. Hoosier lime Confederate Ls.	
			West Arm Fm.	Natsy Ls. Williams Ls.	Chubbee sand Cox sand Lonc Grove zone
	Desmoinesian	Deese	?	Rucky Point Cgl.	Bruhlmeyer zone
			Millsap Lake Fm.	Arnold Ls. lower "Fusulina" sand Devils Kitchen Cgl.	Ryan sand Hudspeth zone Snuggs sand Ramsey sand Best sand Peabody sand
					Beasley sand Morris sand Dillard sand Stockton sand Winger sand
	Atokan	Dornick Hills	Big Branch Fm.	Pumpkin Creek Ls. Frensey Ls. Lester Ls. Davis sand	Micaceous sand Hartshorne Ss. ? Hefner sand
			Lake Murray Fm.	Shale above Bostwick Member Bostwick Cgl.	
	Morrowan		Golf Course Fm.	Otterville Ls. Jolliff Ls. Primrose Ss.	Wapanucka Ls. Union Valley Ls.
	MISSISSIPPIAN			Springer Fm.	Lake Ardmore Ss. Overbrook Ss. Hod Club Ss. Markham sand Aldridge sand
		Chesterian		Goddard Fm.	Redoak Hollow Ss.
Meramecian			Caney Sh. (conglomeratic) Caney Sh.		
Osagean			Sycamore Ls.		
DEVONIAN	Helderbergian	Hunton	Bois d'Arc Ls.		
			Haragan Fm.		
			Henryhouse Fm. Chimneyhill Ls.		
SILURIAN	Niagaran		Sylvan Sh.		
	Alexandrian		Fernvale ls.		
ORDOVICIAN	Mohawkian	"Viola"	Trenton ls.		
			Bromide Fm.		
	Chazyan	Simpson	McLish Fm. Oil Creek Fm. Joins Fm.	Joins dolomite "Wade zone"	
	Canadian	Arbuckle	West Spring Creek Fm.	"Gray zone"	
			Knoxlake Fm.	"Brown zone"	

Figure 26 Stratigraphic units of the Marietta Basin (Love County) and some correlations with those of adjoining areas. Modified from Westheimer (2008).

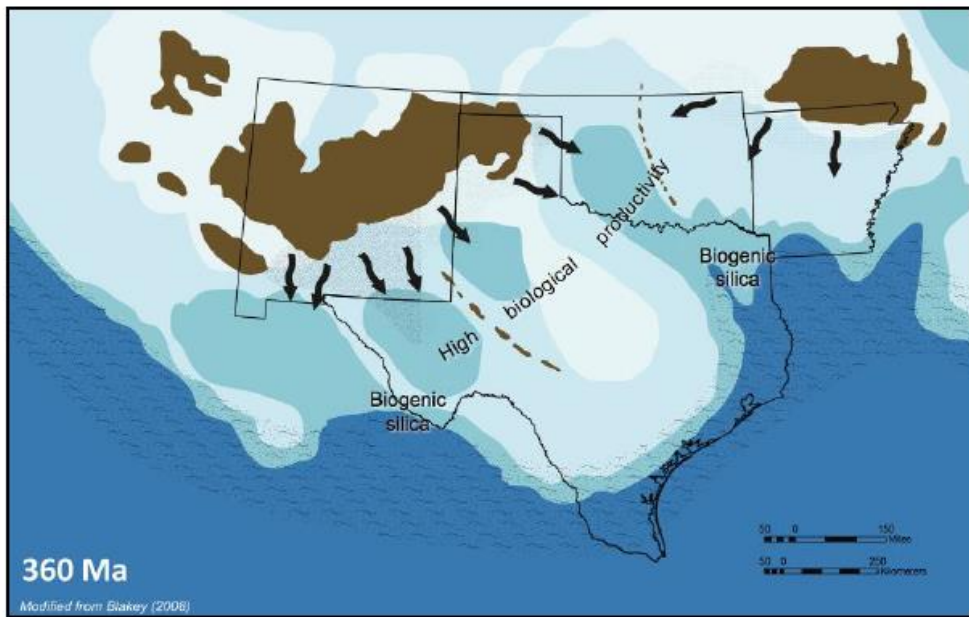
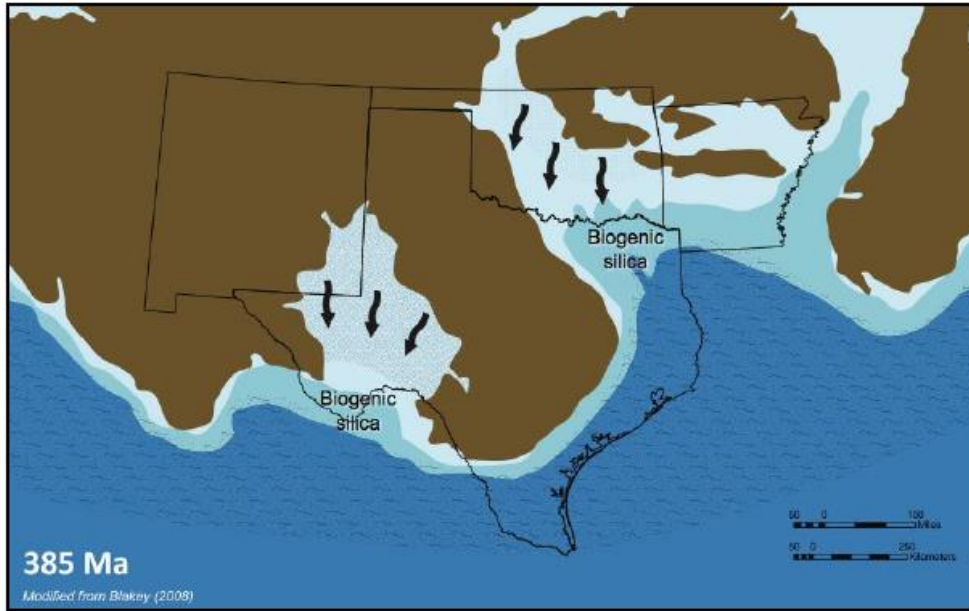
Every formation from the Arbuckle until the Sylvan is present in most of the basin.

However, the Hunton Group is present only on the western side of the basin, and it is eroded in

the central part of the basin, and either missing or not deposited in the eastern part of the basin (Westheimer (1965)). The erosion is related to the Pre-Woodford Unconformity formed because of a period of uplift and erosion as discussed in the previous sub-chapter. After the uplifting episode, the Woodford Shale was deposited during the onset of the Late Devonian- Early Mississippian transgression. The later deposits of the Sycamore and Caney were partially eroded during the Pennsylvanian orogeny that resulted in the formation of the Criner Hills and the Muenster Arch. Even though the Ardmore basin had renewed deposition and subsidence during the Late Mississippian, the Marietta Basin remained relative stable since the Middle Meramecian time (Westheimer, 1965). This resulted in the main difference between the stratigraphy of the Ardmore Basin and the Marietta Basin.

2.3 Woodford Shale Geology

The Woodford Shale (also called in earlier publication the Woodford Chert) is a formation deposited during the Late Devonian and Earlier Mississippian during a massive transgressive episode that covered a large area of what is today the U.S. Midcontinent: Oklahoma, North Texas and West Texas, Arkansas, Kansas, and New Mexico (**Figure 27**).



- | | |
|--|------------------------------|
| Land | Zone of coastal upwelling |
| Deep ocean | Source of silt |
| Epeiric Sea
(darker shade = deeper depth) | Source of sand |
| Cratonic basins | Sediment transport direction |

Figure 27 Facies distribution during the Late Devonian in the Southern US Mid-continent. Modified from Blakey (2012) and Comer (2008) by Miceli (2010).

The underlying and overlying units associated with the Woodford Shale varies in names and characteristics depending on its location. Pre-Woodford strata is variable due to the unconformity that occurred during the Middle Devonian. In Northern Oklahoma and Eastern Oklahoma, the Woodford Shale can directly the Sylvan Shale and the Viola Limestone where incision from erosional valleys cut down deeper into the section eroding the Hunton Group (**Figure 28**). In the Ardmore Basin, the Woodford Shale overlies the Hunton Formation in most of the area, however, in the Marietta Basin the Hunton is either eroded or simply not deposited because of distal and deeper water in that area during the Silurian Period. Regarding the overlying strata, in the Anadarko basin, the Woodford is covered by the Mississippian Osage and Meramec, which are laterally correlative to the Sycamore Formation and Lower Caney Group in the Ardmore Basin. In the Marietta Basin, towards the west, the Woodford is overlain by the Sycamore, but the Mississippian strata are eroded in the southeast area by the Pennsylvanian detrital sandstones.

The thickness of the Woodford Shale is controlled in large part by the available accommodation space in the paleogeography left after the Pre-Woodford/Post-Hunton Unconformity and the high subsidence during the Late Devonian in the Proto-Anadarko Basin area. Woodford Shale thickness ranges from 50 feet in the Northern Oklahoma platforms (Anadarko and Cherokee) to 900 feet in the Deeper Anadarko Basin (**Figure 29**) (Hester et al. 1990; Comer, 2005; Comer, 2008). The thickness in the Arbuckle Mountains and Criner Hills outcrops ranges from 300 to 350 feet (Ekwunife, 2017; Galvis, 2017; Becerra, 2017).

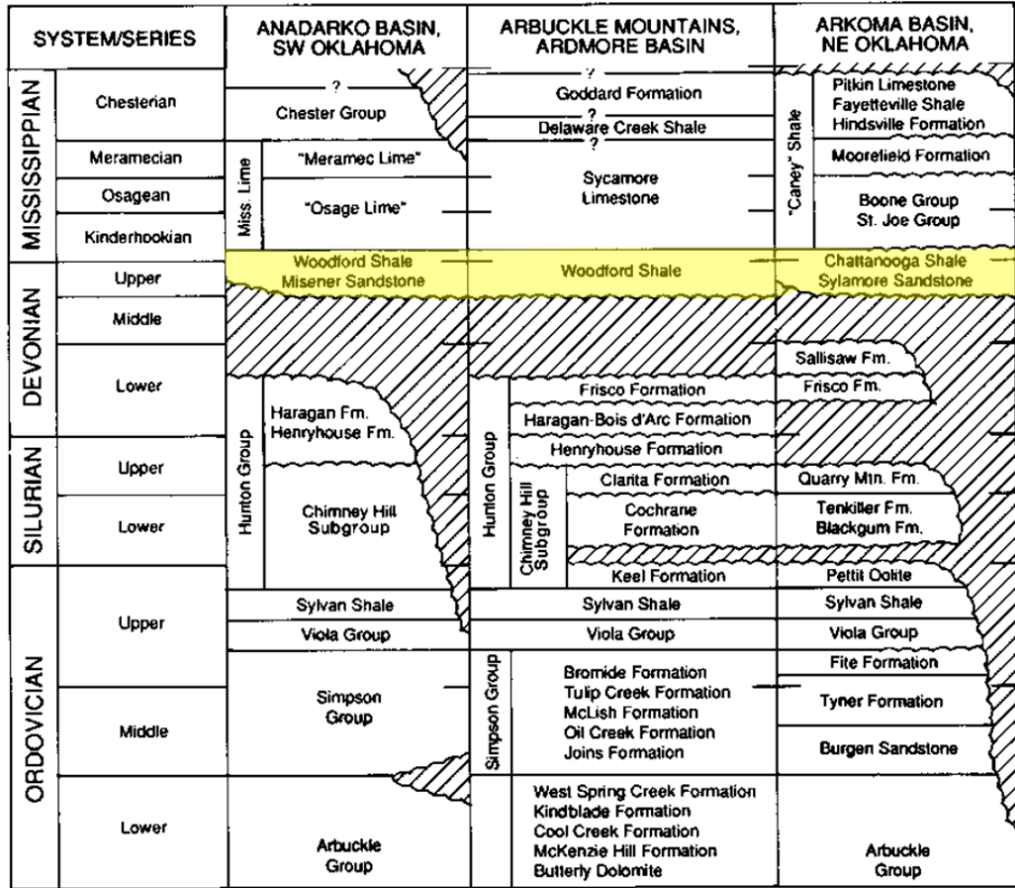


Figure 28 Inter-Basin Correlative Stratigraphic chart of South Oklahoma Geology from Ordovician to Mississippian. Modified from Johnson and Cardott (1990).

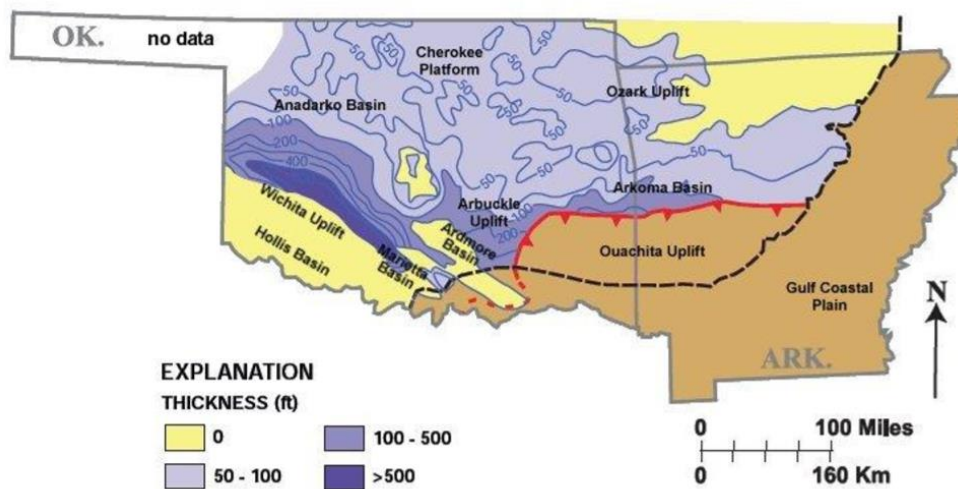


Figure 29 Generalized Thickness Map of the Woodford Shale in Oklahoma and Arkansas (Comer, 2008)

The Woodford Shale is characterized by siliceous and argillaceous shales interbedded with blocky siliceous mudstones and chert; with beds of glauconitic sandstones interbedded with green mudstones at the base, and green mudstones at the top where the contact with the Mississippian Sycamore or Osage is located stratigraphically (**Figure 30**).

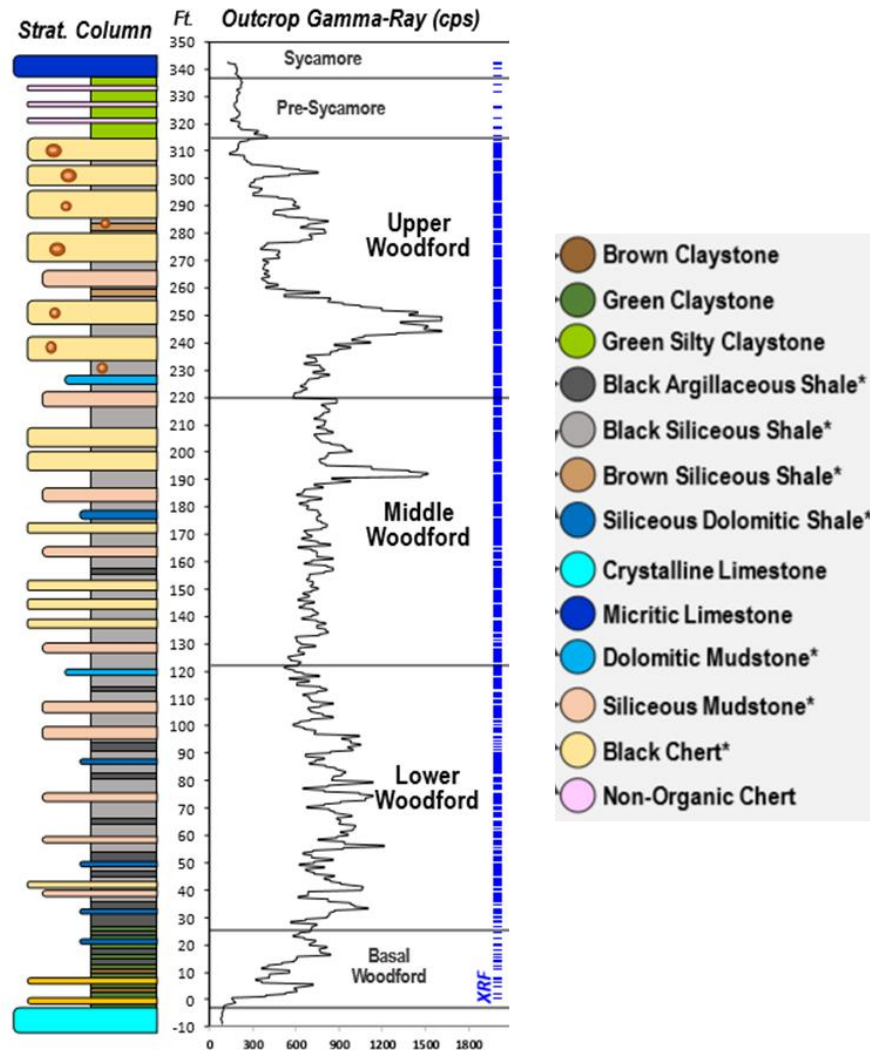


Figure 30 Generalized stratigraphic section of Speake Ranch Shale Pit in the Southern Limb of the Arbuckle Mountains. Modified from Galvis (2017).

Hester et al. (1990) split the Woodford Shale into three informal members: Lower Woodford, Middle Woodford, and Upper Woodford based on Well Logs (Gamma-Ray, Density, and Resistivity) (**Figure 31**). However, later work done by McCullough (2014) in the Cherokee

platform (**Figure 32**), and work done by Galvis (2017) in the Speake Ranch Outcrop (**Figure 30**) have divided the Woodford into several correlative Gamma-Ray Parasequences.

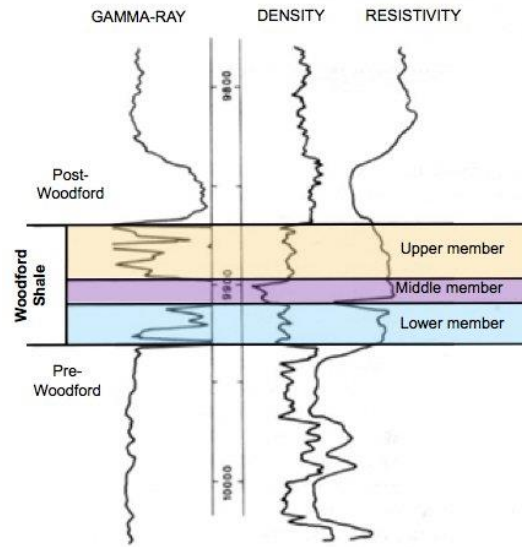


Figure 31 Characteristic well log signatures of lower, middle and upper members of the Woodford Shale in the Anadarko Basin (modified from Hester et al., 1990 by Miceli 2010).

The Woodford Shale is a world-class source rock thanks to its very high percent of Total Organic Content (TOC). A map (**Figure 33**) modified from Comer (2005 and 2008) shows the distribution of average TOC in Oklahoma. The highest TOC areas are in the deeper depocenter in the Anadarko Basin, Ardmore Basin, Arkoma Basin, and Marietta Basin. These variations of TOC have been studied by many authors (Johnson and Cardott, 1990; Comer, 2005; Miceli, 2010; Wang, 2016; Slatt et al., 2016; and Slatt, 2018) concluding that the main reason for the high TOC within the Woodford Shale is related to poorly oxygenated water columns (anoxia) during the Late Devonian-Early Mississippian and restriction of water circulation due to paleotopographic control of the Post-Hunton/Pre-Woodford unconformity.

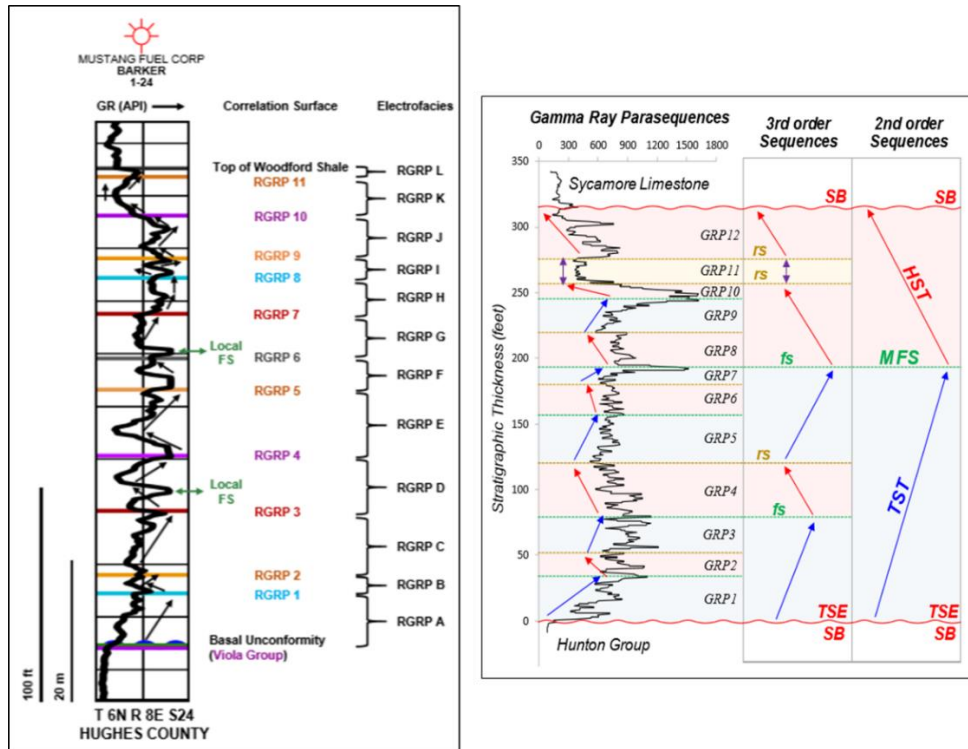


Figure 32 Gamma-Ray Parasequence subdivisions of the Woodford Shale. On the left in the subsurface of the Potawatomi County by McCullough (2014). On the right side, Galvis (2017) developed a sequence stratigraphy based on outcrop Gamma log and description.

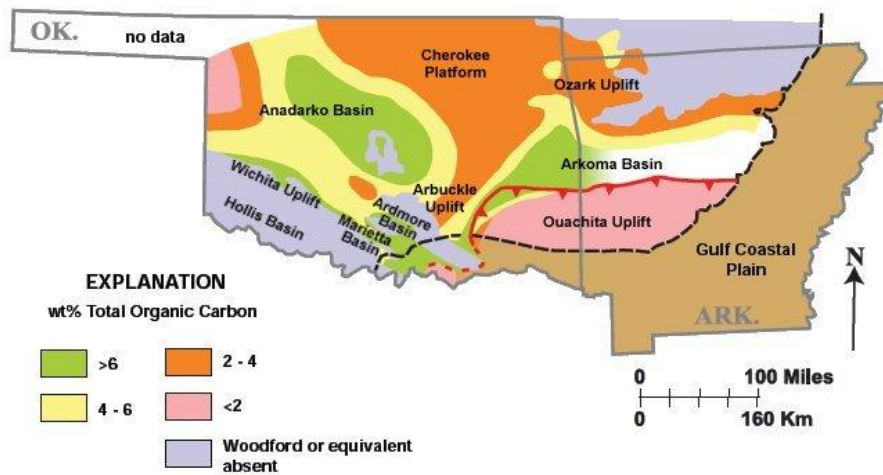


Figure 33 Map showing TOC distribution in Oklahoma and northeastern Arkansas (modified from Comer, 2005 in Comer, 2008).

The current depositional model proposed by Slatt and Rodriguez (2012) and refined by Slatt (2017) consists in dividing the Woodford Shale into a Lower Transgressive Systems Tract interval comprising of the Lower Woodford and Middle Woodford; reaching maximum flooding

surface at the top of the Middle Woodford. Then, a prograding Highstand Systems Tract representing the deposition of the Upper Woodford. The basal Sequence Boundary or Transgressive Surface of Erosion is represented by the Post-Hunton/Pre-Woodford Unconformity (**Figure 34**)

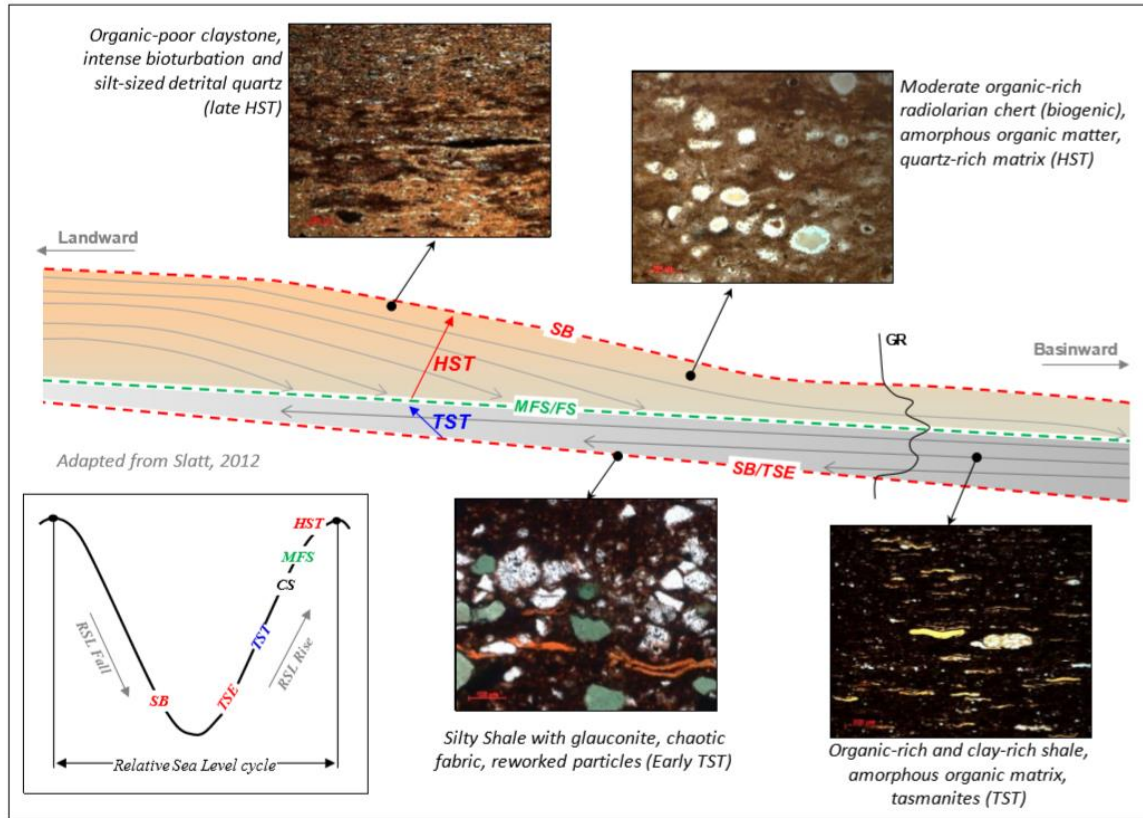


Figure 34 Sequence Stratigraphic model of the Woodford Shale with examples of thin sections of key facies within the Woodford interval. Model by Slatt (2017) and kindly provided by Ruppel (pers. comm.), then later modified by Galvis (2017).

Chapter 3: Lithofacies and Stratigraphy

This section comprises the description and interpretation of the available Woodford Shale core data in the Marietta Basin. One of the active oil and gas operators in the basin provided this core to the Woodford Shale Consortium (which is part of the Institute of Reservoir Characterization within the ConocoPhillips School of Geology and Geophysics at The University of Oklahoma) for research and academic purposes. To preserve the confidentiality of this data; the name and depth intervals of this well have been removed from the data published in this dissertation book. Henceforth, this research will refer to this core as the "Marietta Basin Woodford Core" instead of displaying the name of the well. **Figure 35** shows the relative location of the core in the Marietta Basin.

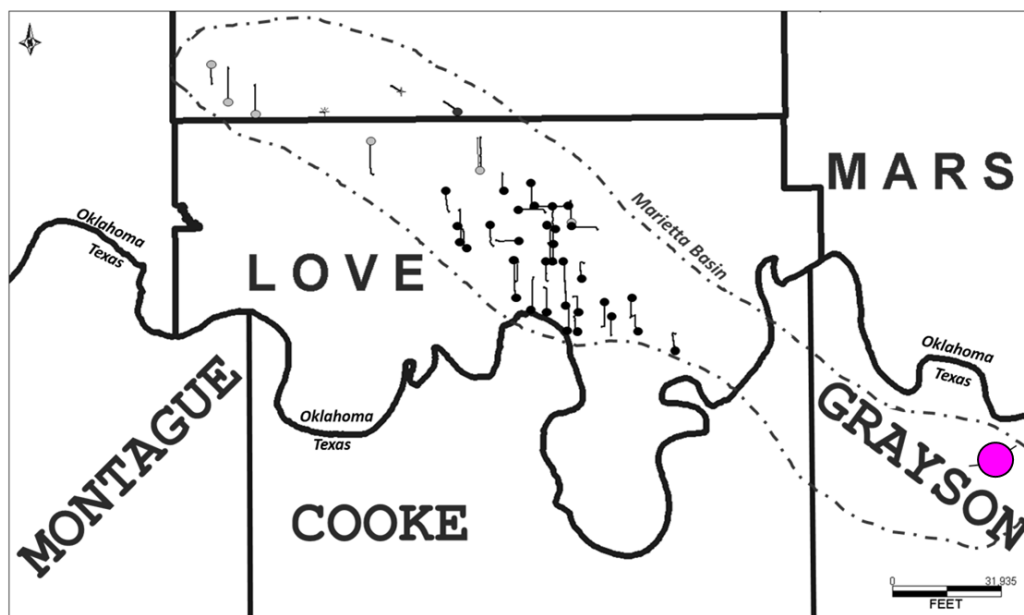


Figure 35 Map with the relative location of the cored well (magenta dot). Dash line shows the generalized outline of the Marietta Basin. Tadpoles are Woodford Shale horizontal wells drilled in the basin.

Subchapter 3.1 covers the data available from the core used in this study and the relative location of the core within the basin. Subchapter 3.2 describes the methodology to process the data. Subchapter 3.3 shows the description and mineralogy composition of the lithofacies present in this section of the Woodford Shale. Finally, subchapter 3.4 and subchapter 3.5 cover the relationship between lithofacies and the stratigraphy of the Woodford Shale in this area and how it ties to the general depositional model of this formation.

The primary goal of this section of the dissertation is to tie the actual hard data from the rock record available to other Woodford Shale characteristics described and interpreted in the following chapters. In other words, set the foundation and framework to place other data like geochemistry and geomechanics within the formation and how it relates to the lithofacies.

3.1 Available Data

The data from the Marietta Basin Woodford Core includes approximately 145 feet of core which includes 127 feet of Woodford Shale rock and the remaining of Sylvan Shale rock. The Woodford Shale section is not complete because the core does not include the upper contact of the Woodford Shale with the overlying formation (Detrital Pennsylvanian Sands). The core is mostly complete from top to bottom, and it has been slabbed in 1/3 called "slab" section and 2/3 called "butt" section. **Figure 36** shows a visual representation of the two parts of the core (slab and butt). The "Butt" side is ideal for performing destructive analysis like RockEval, Leco TOC, X-Ray Diffraction, and geomechanics tests. On the other hand, the "Slab" side should be preserved for future description and references. If the "butt" side is not complete after samples

are taken for destructive analysis, the “slab” can be used to perform non-destructive analyses like X-Ray Fluorescence or Rebound Hammer tests.

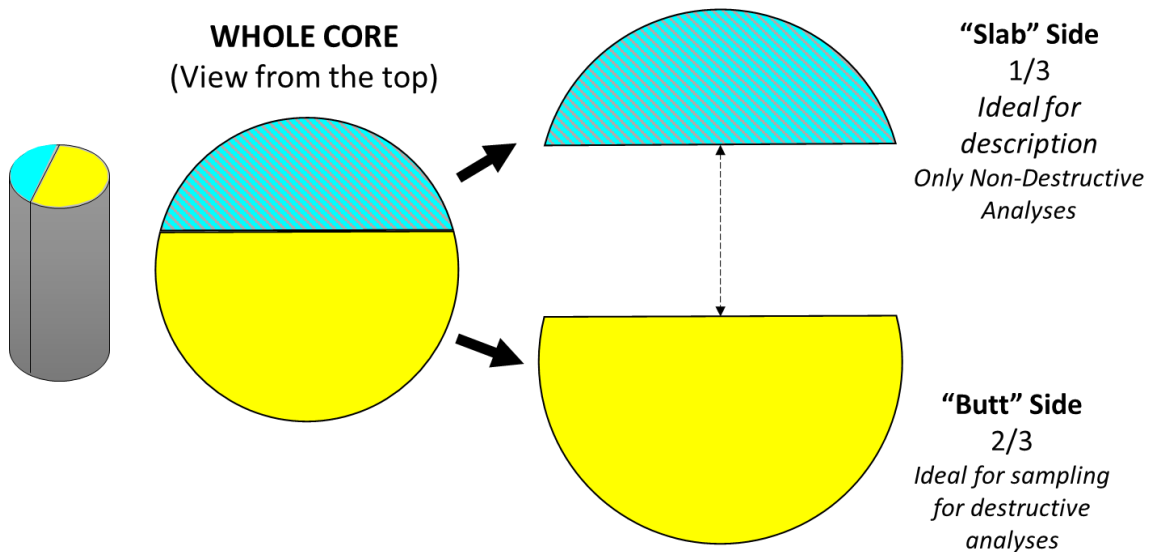


Figure 36 Generalized diagram of whole core slabbing viewed from the top. This process results in two core parts: a) the “Slab” side (in light blue) which has the less volume of rock; and b) the “butt” side (in yellow) which has the largest part of the volume of rock.

In addition to the rock itself, the operator provided lab data performed by Weatherford Labs after the core was extracted. This lab data includes core spectral gamma-ray log data, selected borehole logging data, core photographs, X-Ray Diffraction (XRD) data, and RockEval/Vitrinite Reflectance data (which are discussed in depth in the next couple of chapters).

To complement the data provided by the operator, Dr. Brian Turner acquired X-Ray Fluorescence (XRF) data every 2 inches along the core (in some sections data was acquired every 1 inch or less to capture the thin-bedded variability within the rock). XRF data allows the

analysis of the elemental composition of the rock throughout the core and how it changes from the bottom of the sections (older rock) to the top of the core (younger rock).

Furthermore, ten thin sections were made to perform petrographic description and SEM/EDX imaging to key lithofacies and sedimentary/diagenetic features in the core like mineralized fractures and phosphate nodules. SEM stands for Scanning Electron Microscope and EDX for Energy-Dispersive X-Ray Analyzer. SEM helps to capture the nanoscale features in fine-grained mudrocks like the Woodford Shale. EDX provides maps of the elemental composition of the rock on the thin section slides.

Finally, the last data acquired in the core is the Rebound Hammer (Bambino) Data. The Rebound Hammer data provides geomechanical information of the rock samples in the core.

3.2 Methodology

The core comes in two assemblies of boxes. The "slab" section includes clean-surface rock pieces. This set is ideal for the visual description of the rock. The "butt" section which is dirty and has missing pieces includes the most significant volume of rock from the core, and it is ideal for getting plugs or smaller samples for lab analysis (like thin sections or geochemistry).

The first step was to describe the core. Each hand-size piece of the core in the "slab" section was described by visual inspection with and without hand lens (10x zoom) and binocular microscope (20x to 30x zoom). The description was from the base of the core (including the

Sylvan Shale interval) to the top of the core. The properties described include color (using the Rock-Color Chart), bed thickness, texture, grain size (if visible), sedimentary structures (if present), mineralized and open fractures, reaction to hydrochloric acid (HCl 10%), white light reflection, ultraviolet ("black") light reflection, hydrocarbon presence, and texture of the rock at the back of the core (which is an excellent indicator of the response of the rock to the core drilling bit). The visual description was done to dry and wet samples, just in case the water in the surface of the rock could enhance the sedimentary features of the core.

After the description of the whole core, the X-Ray Fluorescence was acquired using the Bruker Tracer IV-SD Hand Held X-ray Fluorescence Spectrometer (HHXRF) tool owned by the Institute of Reservoir Characterization at the ConocoPhillips School of Geology and Geophysics. This equipment (**Figure 37**) is a handheld device that emits low doses of X-rays to the rock to measure the concentration of elements in each sample. The release of X-rays displaces electrons in the orbit of the atoms in the rock resulting in the release of energy that the instrument captures, then the software with input from the user categorizes the resulting diffractogram and outputs the elemental composition of the sample. This same process must be done twice for each sample: 1) for Major Elements like Silicon (Si), Aluminum (Al), and Calcium (Ca); and 2) for Trace Elements like Zirconium (Zr), Titanium (Ti), Uranium (U), Vanadium (V) and Molybdenum (Mo). **Figure 38** shows the equipment settings for each process (Major and Trace).

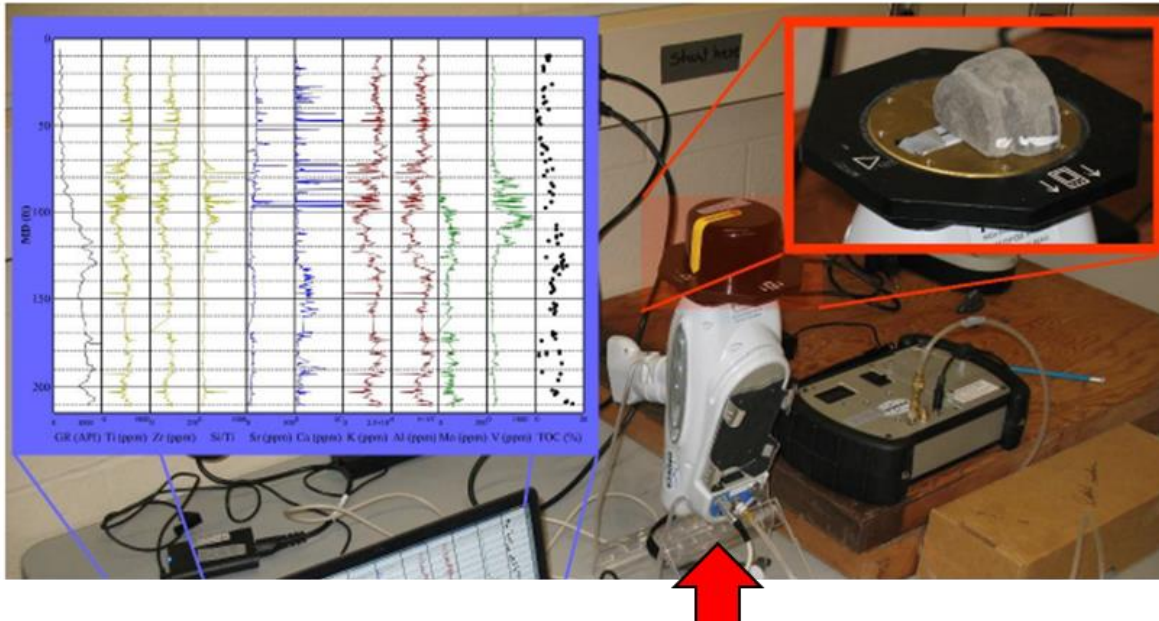


Figure 37 Red arrow shows the Brucker Tracer IV-SD Hand Held X-ray Fluorescence Spectrometer (HHXRF). Samples are placed at the top front of the gun and covered by a lead cap to prevent any X-Ray exposure to the user. Examples of resulting XRF profiles are shown in the blue box in the upper left corner. Picture provided by Turner (2016).

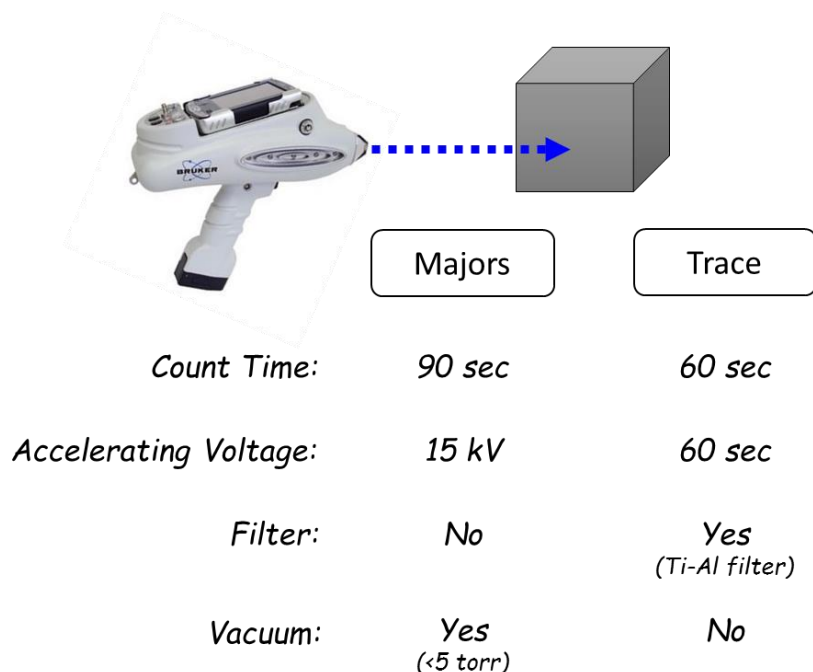
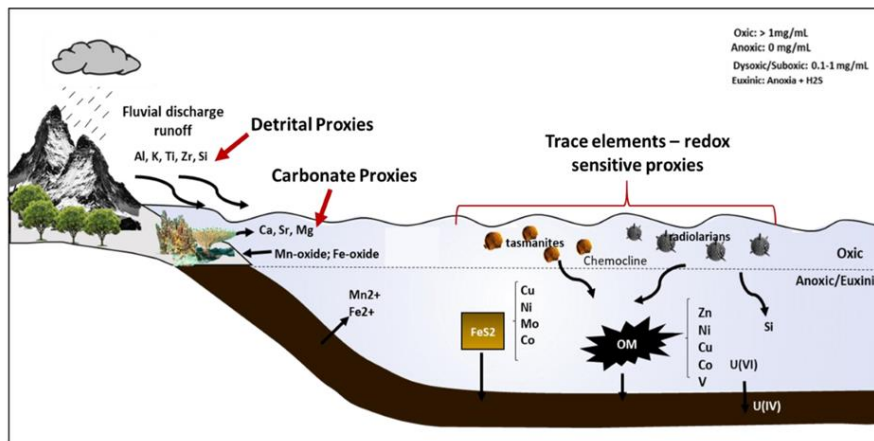


Figure 38 Equipment settings for Major Element Scanning and Trace Elements Scanning using the Brucker Tracer IV-SD Hand Held X-ray Fluorescence Spectrometer (HHXRF) equipment. Scanning for Major elements does not use a filter to minimize signal attenuation of lighter elements such as Ca, Si, and Al. Scanning for Trace Elements does not need vacuum because heavier elements do not attenuate the signal in the short distance to the detector.

The results from the X-ray Fluorescence (XRF) analysis were combined with the facies description to build a stratigraphic framework. The XRF were plotted on a depth track as curves (like borehole or petrophysical logs). These XRF curves were compared to the core description profile and the Core Gamma-Ray profile to interpret key sequence stratigraphic surfaces that represent changes in original depositional conditions like redox (oxic-anoxic) conditions, sediment source (detrital vs. biogenic quartz), organic productivity, and water chemistry. A set of elements are the most significant to make these interpretations, and because of that, they are considered Geochemical Proxies (Ekwunife, 2017). **Figure 39** shows a list of elements used as proxies in the analysis of mudrocks and how it does relate to the Woodford Shale depositional environment.



Element	Indication	References
Titanium (Ti), Zirconium (Zr), Aluminum (Al), Potassium (K)	Indicator of continentally derived sediments	Sageman and Lyons, 2004; Tribovillard et al., 2006
Silicon/Aluminum (Si/Al)	Indicator of detrital, and biogenic quartz.	Pearce and Jarvis, 1992; Pearce et al., 1999; Tribovillard et al., 2006.
Phosphorus (P)	Phosphate accumulation	Tribovillard et al., 2006
Calcium (Ca), Magnesium (Mg), Strontium (Sr)	Carbonates	Banner, 1995; Tribovillard et al., 2006.
Molybdenum (Mo), Vanadium (V), Uranium (U), Nickel (Ni), Cobalt (Co), Copper (Cu), Chromium (Cr), Zinc (Zn)	Redox-sensitive elements	Tribovillard et al., 2006

Figure 39 Elemental (Geochemical) Proxies usually used to aid the interpretation of the depositional environment of the organic-rich Woodford Shale. Figure modified from Ekwunife (2017) and Turner (2016).

Finally, the sequence stratigraphic surfaces that resulted from the integration of all the data in this chapter served to interpret the parasequences and systems tracts of the Woodford Shale section in the Marietta Basin and were tied back to the depositional model proposed by Slatt (2017) for Oklahoma resources like the Woodford Shale.

3.3 Facies Description

Galvis (2017) generated the most comprehensive lithofacies classification done in the Woodford Shale. His classification (**Figure 40**) describes the facies present in the Woodford Shale outcrop located in the Speake Ranch Shale Pit in the southern limb of the Arbuckle Mountains, which is considered today one of the most significant type sections of this formation. Galvis (2017) described thirteen lithofacies as shown in Figure 3.6; based on weathering response and geomechanical response (hard vs. soft beds) as well as the texture of the rock and composition of each lithofacies. He used a combination between X-Ray Diffraction (XRD), X-Ray Fluorescence (XRF), petrography and SEM imaging to support his classification.

Galvis (2017) is the foundation for the facies description classification used in this chapter. However, some of the facies that are present in the Speake Ranch Woodford Section are not present in the Marietta Basin Woodford Core. Additionally, Galvis (2017) described mainly outcrop rock samples that are relatively weathered compared to subsurface core samples which are as "fresh" (unweathered) rock samples as can be. Therefore, any of the criteria enhanced by weathering like for example the degree of fissility cannot be assessed adequately in core samples, but they can be interpreted from thin sections (thin, well-defined laminations under thin sections of core samples are expected to weather into fissile thin shales with time under outdoor conditions).

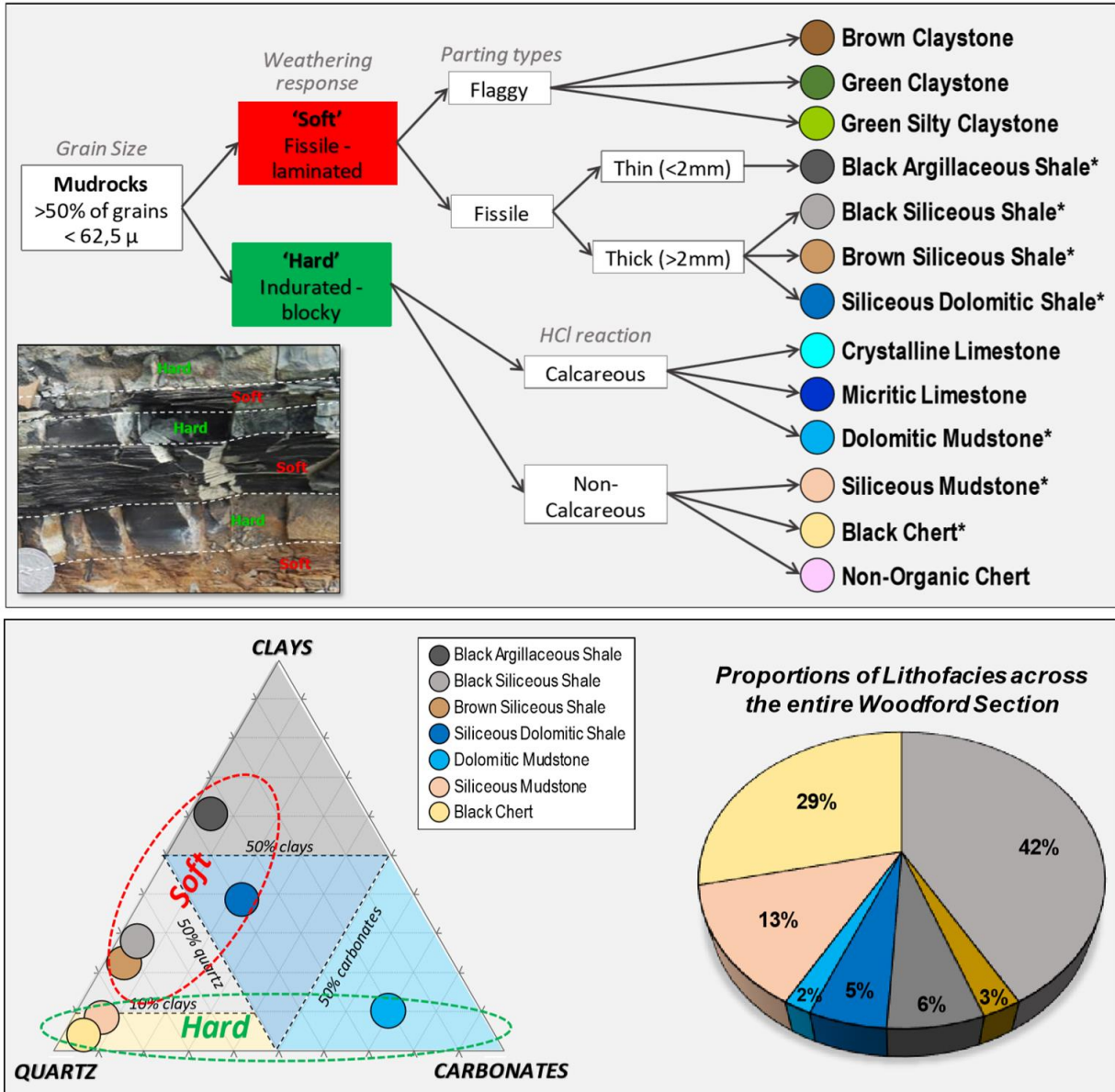


Figure 40 Field-based lithofacies classification of Woodford Shale mudrocks by Galvis (2017). The asterisk denotes the most common lithofacies present in the Speake Ranch Woodford Section (considered nowadays one of the best type sections of the Woodford Shale exposed on outcrops). The classification was primarily done by describing hand size rock samples.

After modifying Galvis (2017) classification based on the limitations of describing core versus outcrop samples, the lithofacies present in the Woodford Shale core in the Marietta Basin are:

1. Siliceous Mudstone (SM)
2. Siliceous Shale (SS)
3. Argillaceous Shale (AS)
4. Black Chert (BC)
5. Green Claystone (GC)
6. Dolomitic Mudstones (DM)

Additionally, there are significant features present in the core that are not lithofacies (*sensu stricto*) but are pivotal in the interpretation of critical intervals within the Woodford Stratigraphy or have implications for horizontal drilling and hydraulic fracturing. These are:

- A. Phosphate Nodules (PN)
- B. Fractures (F): Vertical (Fv) and Horizontal (Fh)

The proportion of each lithofacies (**Figure 41**) in the Woodford Shale cored section are:
a) 28% Siliceous Mudstone (SM); b) 25% Siliceous Shale (SS); c) 22% Argillaceous Mudstone (AM); d) 17% Black Chert (BC); e) 5% Green Claystone (GC); f) 3% Dolomitic Mudstone (DM).

Lithofacies Proportions in the *Marietta Basin Woodford Core*

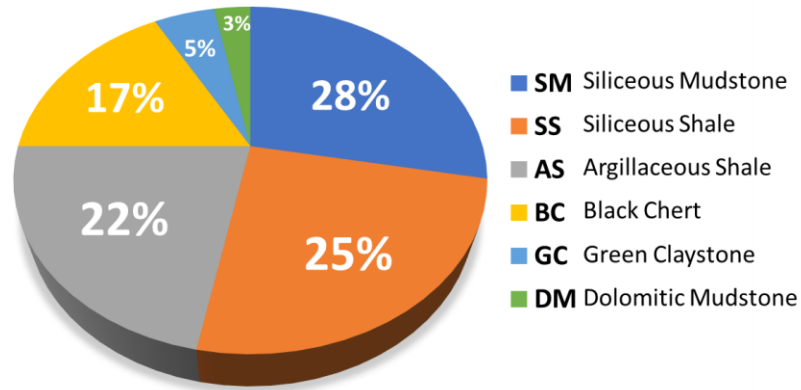


Figure 41 Pie chart showing the distribution of each major lithofacies within the **Marietta Basin Woodford Core**. **Siliceous Mudstone (SM)** is the most common one with **28%**; followed closely by **Siliceous Shale (SS)** and **Argillaceous Shale (AS)** with **25%** and **22%** respectively. **Black Chert (BC)** is fourth in the distribution with **17%**. **Green Claystone (GC)** with **5%** and **Dolomitic Mudstone (DM)** with **3%** are the least common in the section.

The lithofacies present in the Marietta Basin Woodford Core are described in detail next.

Siliceous Mudstone (SM)

The Siliceous Mudstone (**Figure 42**) is the most representative lithofacies in the Marietta Basin Woodford Core throughout most of the section, and it is particularly dominant in some intervals. Bed thickness varies significantly from less than half of an inch up to 2-3 inches. Color ranges from Dark gray (N3) to Grayish Black (N2). When exposed to direct white light, it reflects the light in a glossy/glass style. Laminations are present but slightly visible in hand sample and are not very well-defined under thin sections. It does not react to Hydrochloric Acid (HCl 10%) except when acid is dropped directly on the sample. The back side of the core along this lithofacies is rough and irregular (not a smooth surface). The mineralogic composition from

X-Ray Diffraction is 60% quartz, 20% clays, 10% feldspars, 5% dolomite, and 5% pyrite. TOC% ranges from 4% to 6%. Vertical mineralized fractures are most common bounded within this lithofacies compared to any other lithofacies in the core. Phosphate nodules can be present in this lithofacies particularly in the uppermost interval of the core. This facies shows pyrite like dust imprinted on the matrix.

Siliceous Shale (SS)

Siliceous Shale (**Figure 43**) is the second most common lithofacies in the Marietta Basin Woodford Core. Bed thickness varies from half of an inch to 2 inches. This lithofacies is very common in the lower and middle section of the core and scattered in the upper section of the core. Color ranges from Brownish Black (5YR 2/1) to Grayish Black (N2). This facies does not react to Hydrochloric Acid (HCl 10%). The backside of the core is smoother than siliceous mudstones and have tiny ridges along the laminations. The mineralogic composition from X-Ray Diffraction is 50% quartz, 30% clays, 11% feldspars, 6% pyrite, and 3% dolomite. TOC% ranges from 6% to 8%. This lithofacies does not glow under ultraviolet (black) light. It has a medium reflection to direct white light; neither matte nor glossy. Laminations are typical in this lithofacies and are relatively continuous laterally.

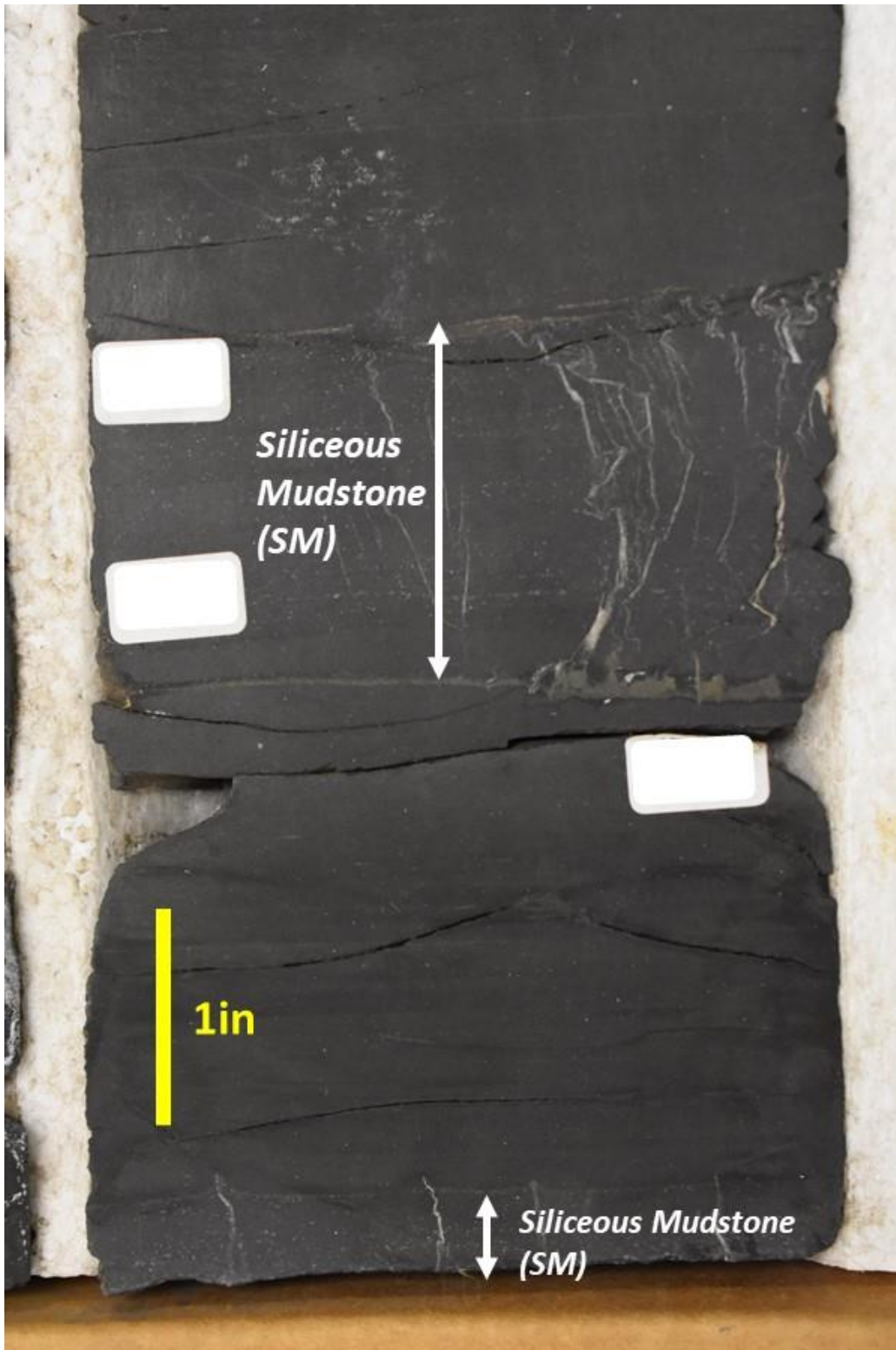


Figure 42 Example of Siliceous Mudstone (SM) facies. White arrows intervals show facies SM interbedded between Argillaceous Shale (AG) facies.

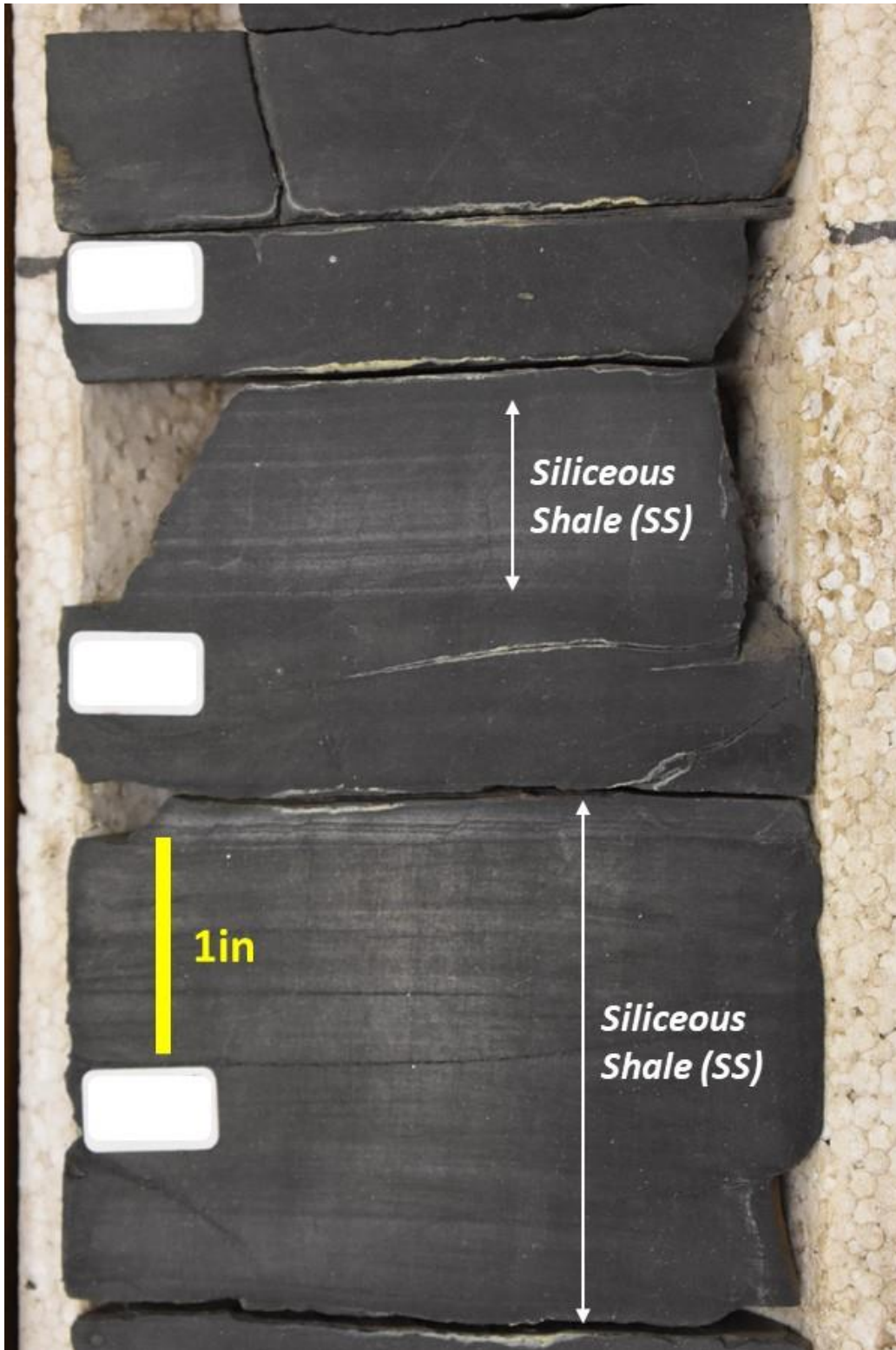


Figure 43 Example of Siliceous Shale (SS) facies (white arrow interval). Notice the better-defined laminations compared to the Siliceous Mudstones.

Argillaceous Shale (AS)

Argillaceous Mudstone (**Figure 44**) is the third most common lithofacies in the Marietta Basin Woodford Core. Beds are relatively thick compared to other lithofacies present in the core and can range from two inches to six inches. This lithofacies is dominating in the middle section of the core as thick beds, and in some cases interbedded with other lithofacies as thinner beds in the lower and upper part of the core. Color is the darkest in the section: Black (N1). This facies does not react to Hydrochloric Acid (HCl 10%). The backside of the core has a very smooth surface, flat and cleaner than any other lithofacies texture. The mineralogic composition from X-Ray Diffraction is 40% clays, 30% quartz, 15% pyrite, 10% feldspars, and 5% dolomite. TOC% ranges from 7% to 10%. This lithofacies does not glow under ultraviolet (black) light. Under direct white light, it reflects poorly the direct white light and has a very matte texture. This facies is very well laminated, and laminations are very continuous.

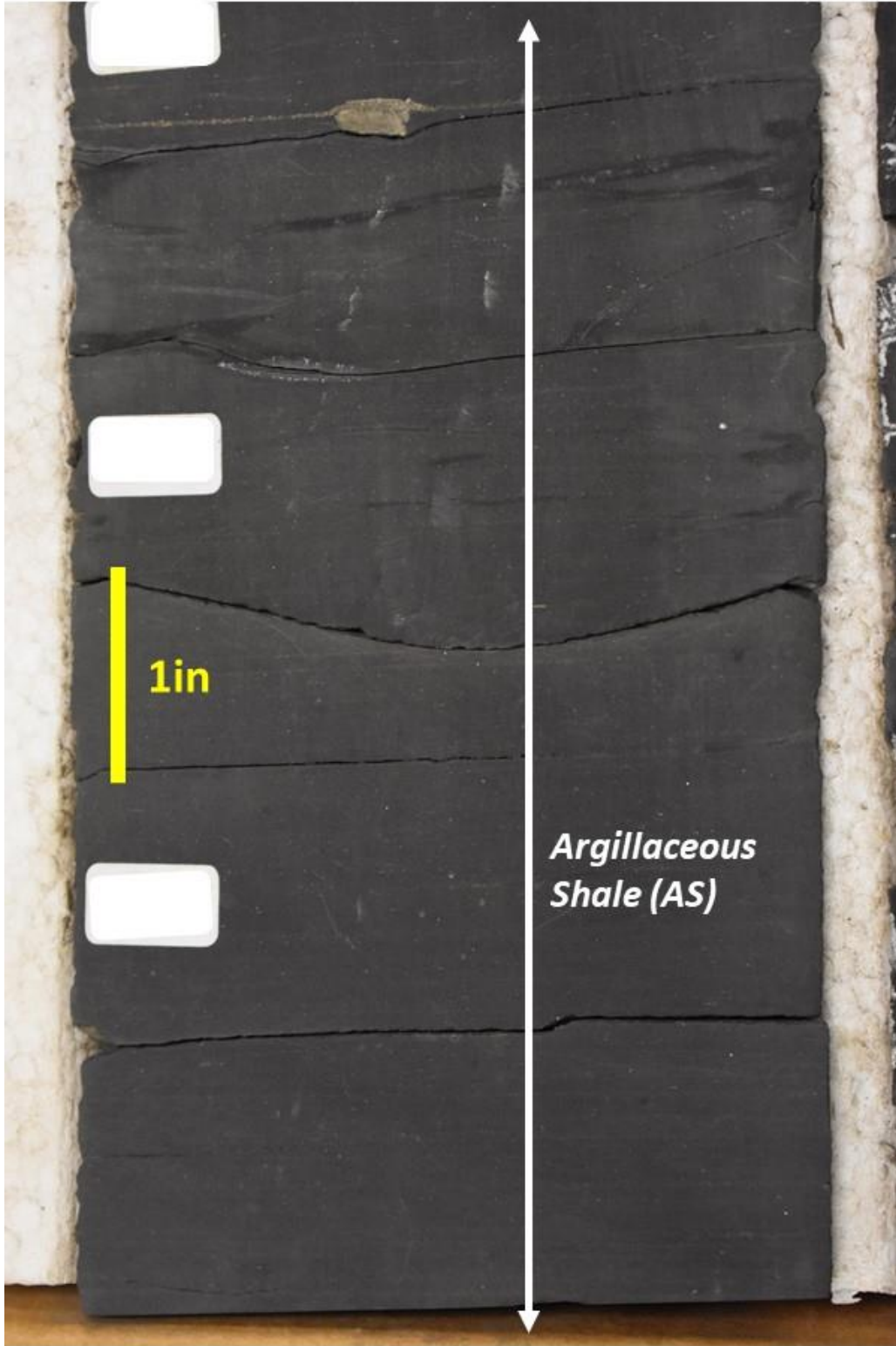


Figure 44 Example of thick-bedded Argillaceous Shale (AS). They have very fine laminations, and horizontal fractures break along these planes.

Black Chert (BC)

Black Chert (**Figure 45**) is the fourth most common lithofacies in the Marietta Basin Woodford Core. Beds are thicker than the Siliceous Shale (SS) and Siliceous Mudstone (SM) but not as thick as the Argillaceous Shale (AS); they range from two to four inches. Black Chert (BC) lithofacies is unique of the uppermost part of the core and is usually interbedded with siliceous mudstones and siliceous shales. Color ranges from Dark Gray (N3) to Black (N1). This facies does not react to Hydrochloric Acid (HCl 10%). The backside of the core is very irregular and with angular holes on it; it shows the most irregular surfaces of all lithofacies. The mineralogic composition from X-Ray Diffraction is 90% quartz, 7% clays, 1% feldspars, and 2% pyrite. TOC% ranges from 2% to 4%. This lithofacies does not glow under ultraviolet (black) light. However, it does reflect direct white light in a glossy texture, even more than the Siliceous Mudstone facies. Laminations are very rare to non-existent.

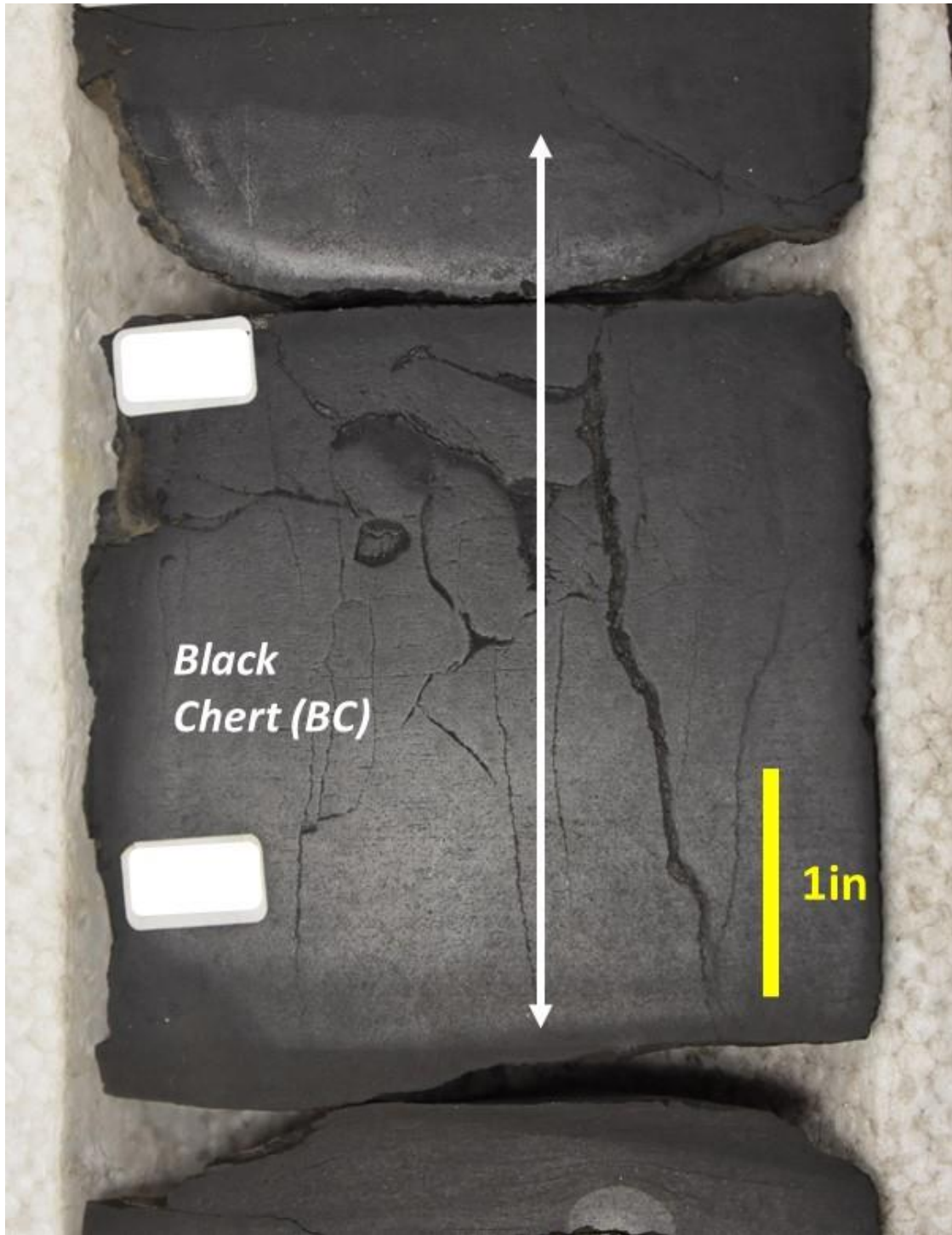


Figure 45 Example of the Black Chert (BC) facies within the white arrow interval. In this picture, partially open vertical fractures are present. This facies reflects direct white light because of the high content of biogenic quartz. It can be slightly laminated, but most of the cases are massive beds.

Green Claystone (GC)

Green Claystone (**Figure 46**) is the fifth most common lithofacies in the Marietta Basin Woodford Core. Bed thickness is very variable and tends to thin-upward along the core section. Beds are unique to the lowermost section of the core at the base of the Woodford Shale and interbedded with Siliceous Shale facies (SS). Color ranges from Greenish Gray (5GY 6/1) to Dark Greenish Gray (5G 4/1). This facies does not react to Hydrochloric Acid (HCl 10%). The backside of the core is caved into the core slab and forms deep ridges aligned with hardened laminations within the bed. The mineralogic composition from X-Ray Diffraction is 66% clays, 22% quartz, 5% feldspars, 5% dolomite, and 2% pyrite. This lithofacies glows under ultraviolet (black) light. Laminations are rare and very disrupted. The texture of this rock is mottled which is very common in bioturbated sediments.



Figure 46 Example of Green Claystone (GC) interbedded with Argillaceous Shale (AS). They show mottled texture like in the lower bed implying bioturbation activity during or after deposition. These GC beds tend to thin upward in the section. They are located in the lowermost part of the core.

Dolomitic Mudstones (DM)

Dolomitic Mudstone (**Figure 47**) is the sixth most common lithofacies in the Marietta Basin Woodford Core. Beds are either thick (two to three inches) or very thin (less than half of an inch). This lithofacies is common in the middle (as thin beds) and the upper section (as thick beds). This facies usually is not interbedded with other facies, but instead, it is present as just one bed within other facies. Color ranges from Medium Gray (N5) to Medium Bluish Gray (5B 5/1); and grades upwards to darker colors. This facies has a faint reaction to Hydrochloric Acid (HCl 10%) at room temperature, but when acid is slightly heated, these dolomitic beds react more vigorously. The backside of the core is irregularly similar to the Siliceous Mudstone (SM). The mineralogic composition from X-Ray Diffraction is 50% dolomite, 35% quartz, 10% clays, and 5% pyrite. The Dolomitic Mudstone lithofacies glows under ultraviolet (black) light. Laminations are present, but they are dull.

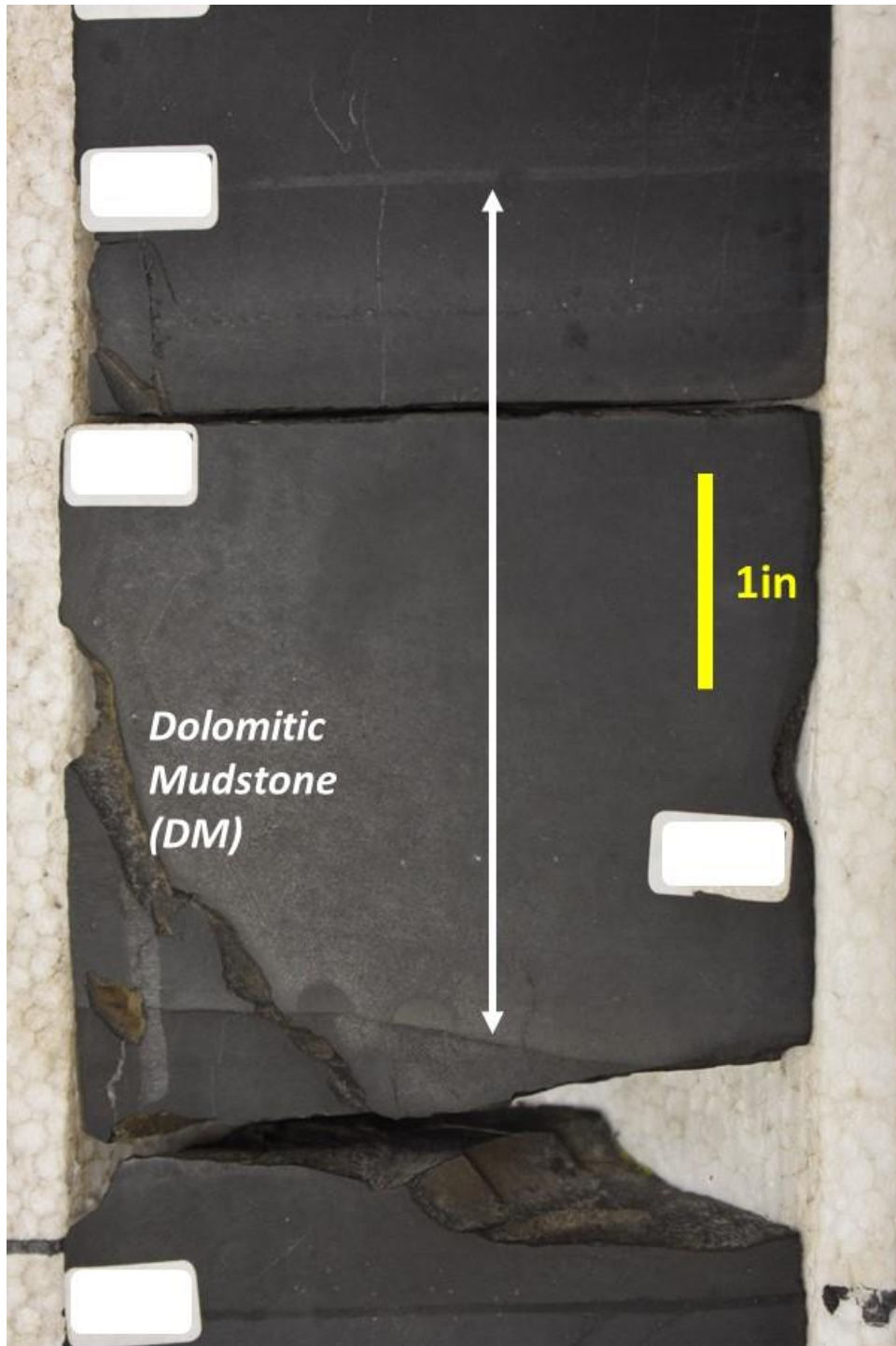


Figure 47 Example of Dolomitic Mudstone (DM) facies. They are lighter in color than the rest of the lithofacies. They are faintly laminated, and normally the content of dolomite decreases upward transitioning to Siliceous Shale or Siliceous Mudstone facies.

Examples of Phosphate Nodules (**Figure 48**), Vertical Fractures (**Figure 49**) and Horizontal Fractures (**Figure 50**) are shown below and are discussed more in depth in Chapter 4 (Diagenesis):

Phosphate Nodules (PN)

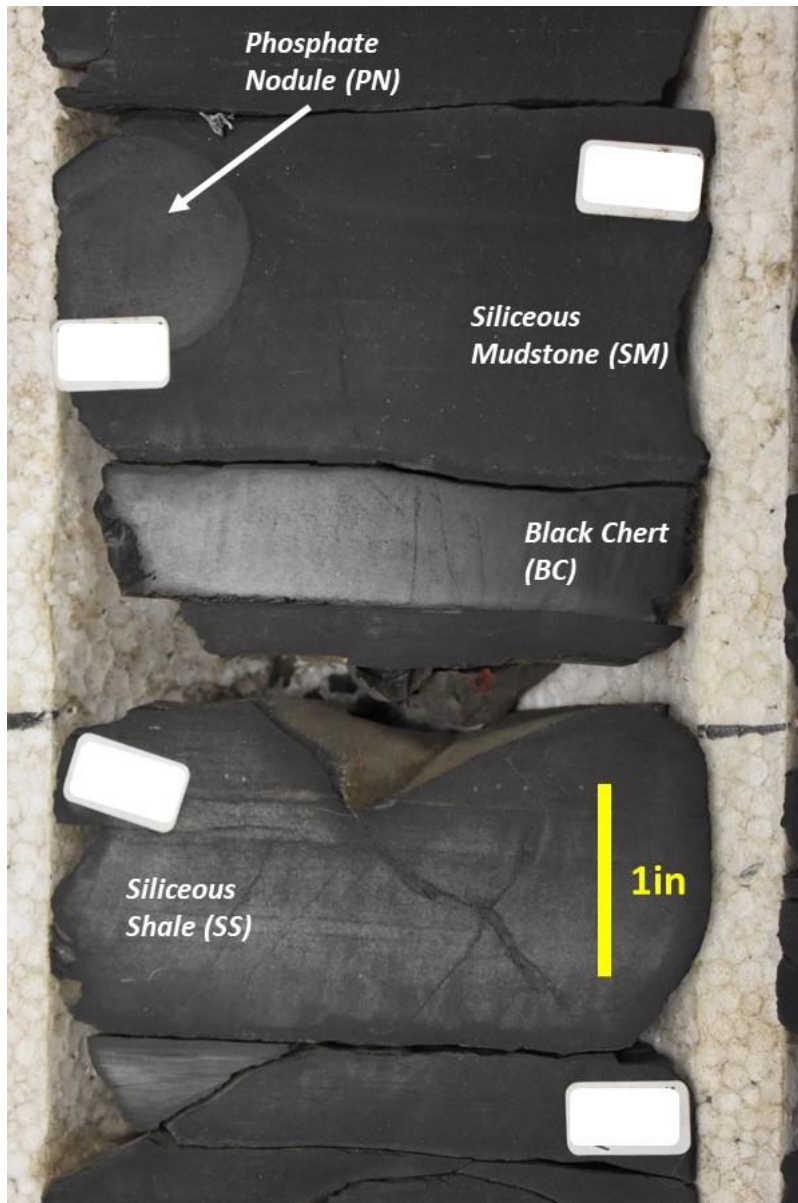


Figure 48 Example of Phosphate Nodules (PN). They are variable in size (this example is 1 inch in diameter). They are very common (but not unique) in the uppermost section of the Woodford Shale. They can be embedded inside Black Chert beds, Siliceous Mudstone bed, and Siliceous Shale beds. They are not present in the rest of the facies.

Fractures (F)

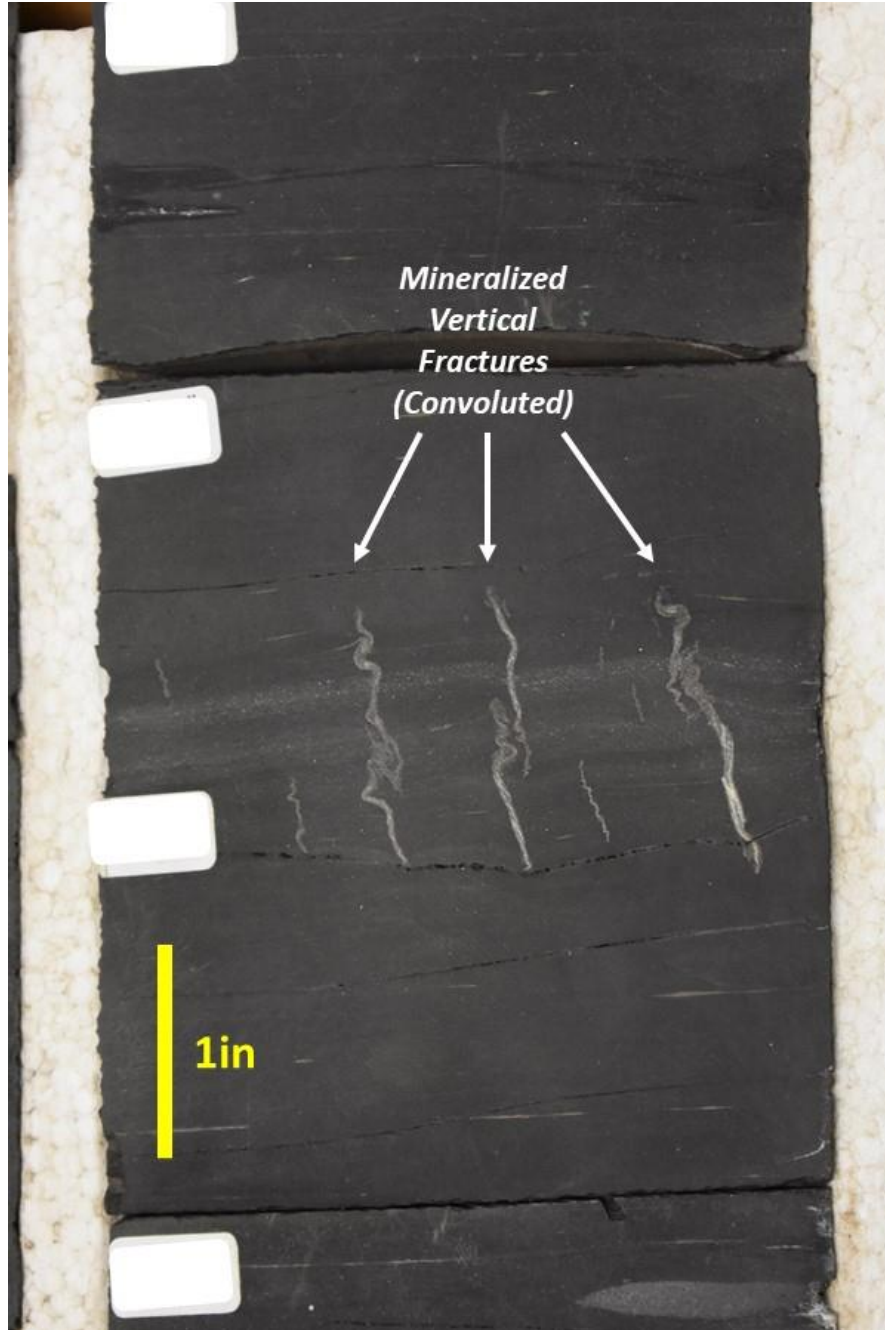


Figure 49 Example of Mineralized Vertical Fractures. In the core, they are mostly convoluted due to compaction (therefore their interpretative name: Pre-Compaction fractures). These fractures are usually found within the Siliceous Mudstone (SM) facies and the thin Black Chert (BC) beds.

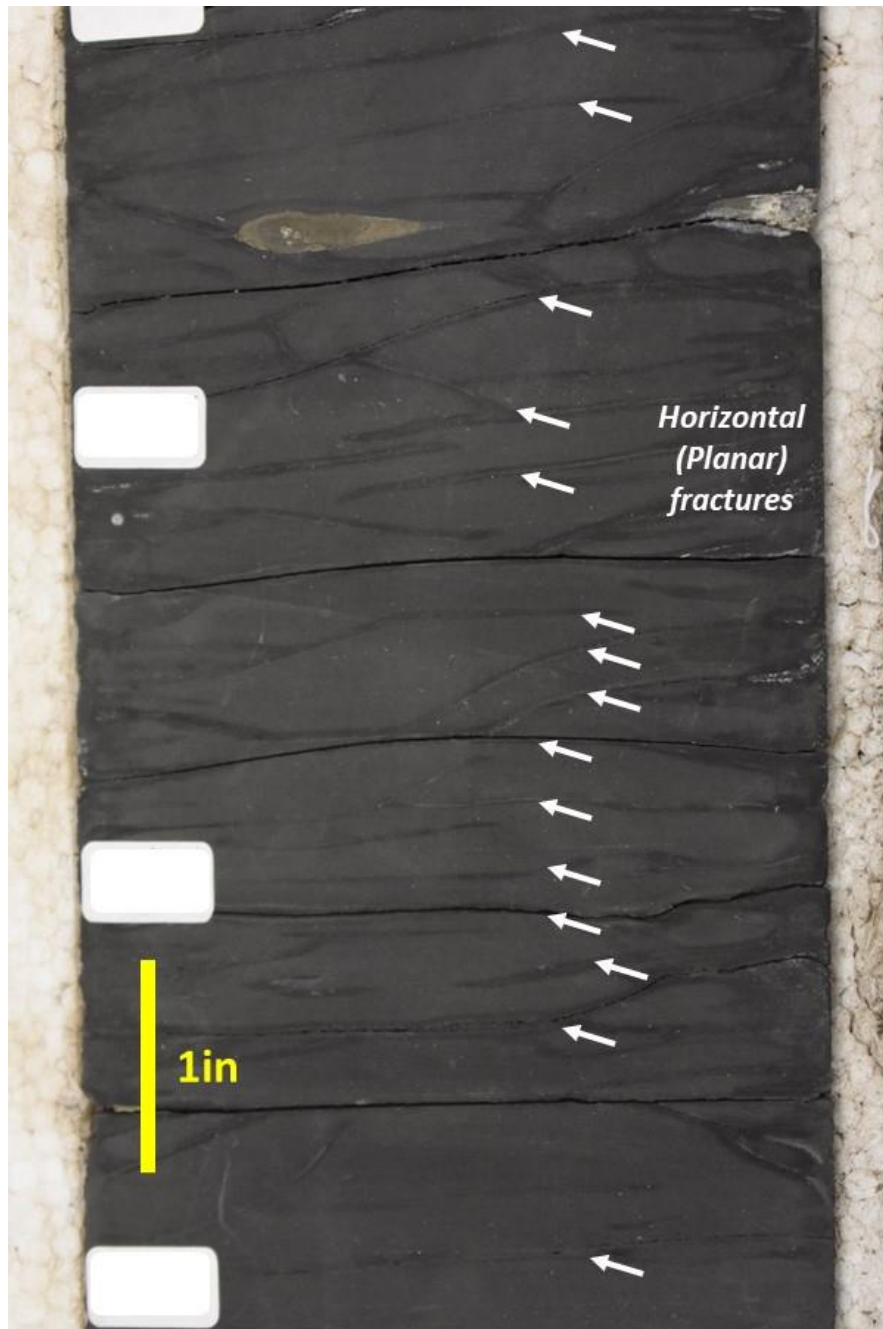


Figure 50 Example of Horizontal Fractures. They are usually open or partially open and are not mineralized. The break along the lamination plain in the Argillaceous Shales (AS) are less planar in the more massive Argillaceous Mudstones (AM). These fracture were probably induced during coring or when the core dried up.

3.4 Stratigraphy

The lithofacies described in the last subchapter are for the block of the stratigraphic framework of the Woodford Shale. These lithofacies are present in sections of the Woodford

Shale all around the state of Oklahoma and North Texas. In this subchapter, the goal is to describe how these lithofacies stack together, understand their relationship, and how they fit into the regional depositional model for the Woodford Shale published by Slatt (2013).

Figure 51 shows the result of the geologic characterization in a generalized stratigraphic column with the most dominant lithofacies in each section of the core.

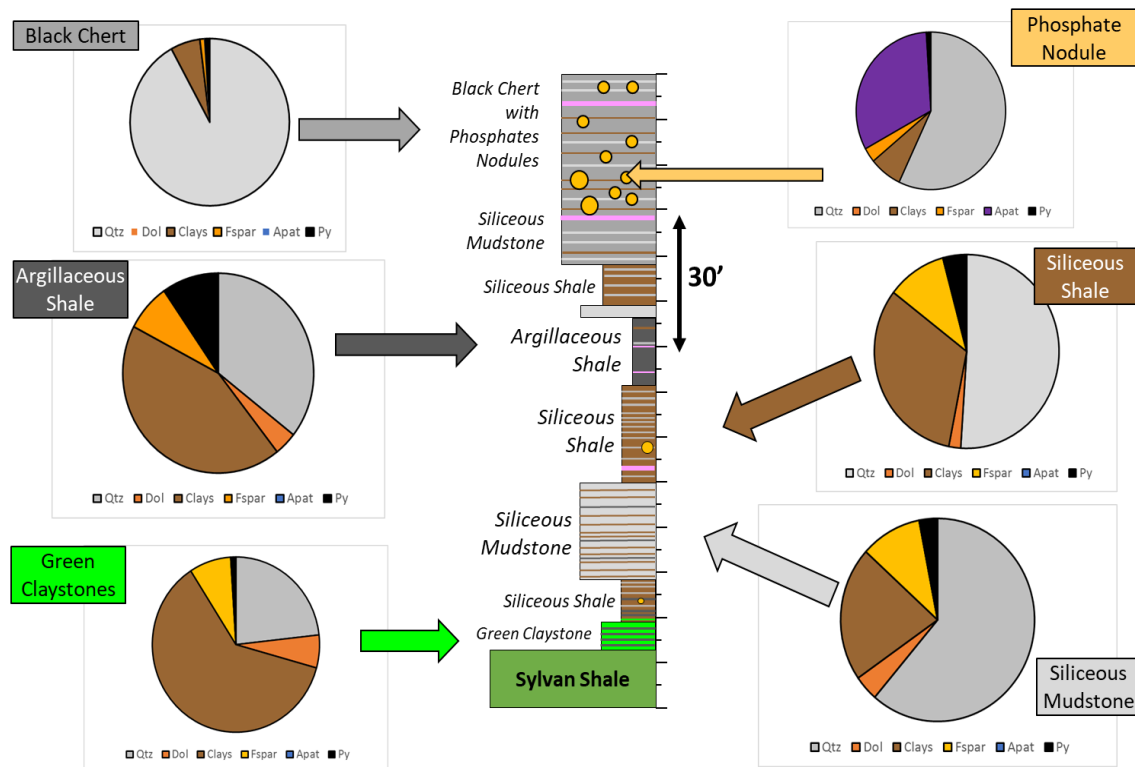


Figure 51 Generalized description of the Marietta Basin Woodford Core. Pie charts represent the mineralogy of each dominant facies (arrows are color-coded by facies).

The Woodford Shale in this location (North Texas) overlays the Sylvan Shale. The contact between the Sylvan Shale and the Woodford Shale is unconformable (**Figure 52**). The surface does not look erosional (*sensu stricto*) but instead represents a hiatus of non-deposition time. The missing rock is the Hunton Group. The hypothesis is the carbonate factory of the

Hunton Limestone did not deposit this rock in the southeastern side of the basin. Chapter 6 includes isochore maps of the Hunton Limestone supporting this hypothesis.

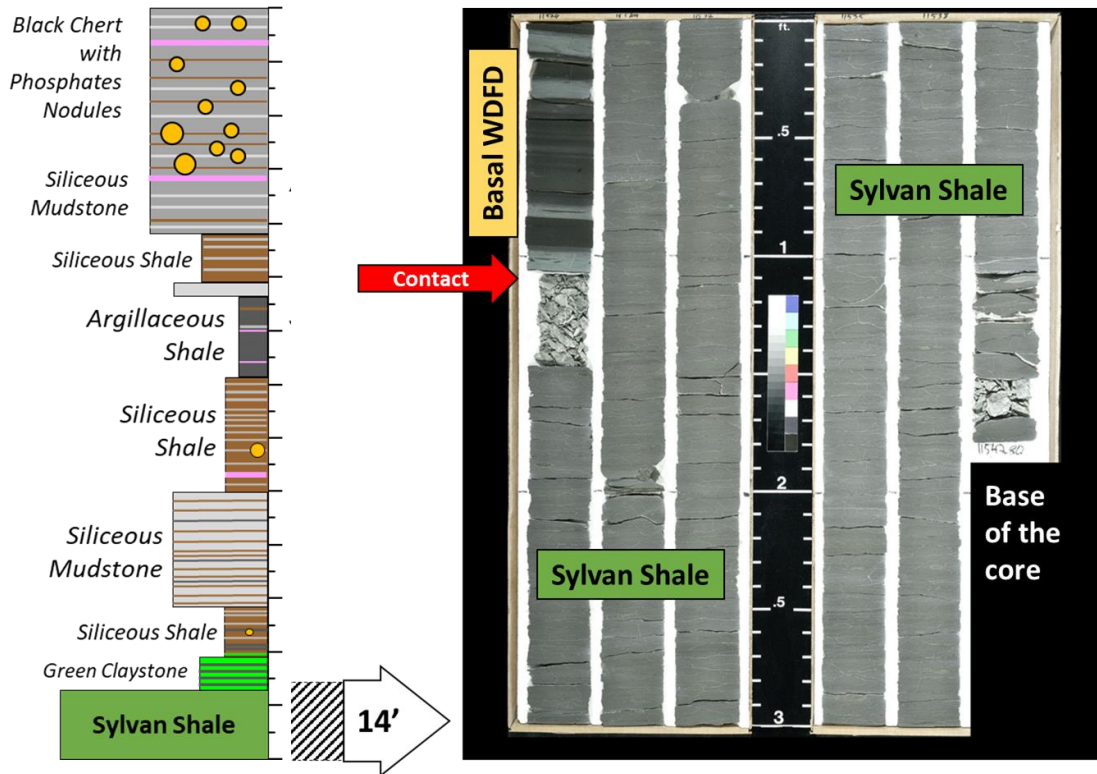


Figure 52 View of the lowermost part of the Marietta Basin Woodford Core. The red arrow shows the unconformable contact between the Woodford Shale and the Sylvan Shale. The Sylvan Shale is a clay-rich, non-organic mudstone deposited in the Ordovician Period. Notice the presence of the thin beds of the Green Claystone (GC) interbedded with the Argillaceous Shale (AS) in the Basal section of the Woodford. Next figure shows more of this section.

The "Basal Woodford" is the lowermost part of the Woodford Shale in this core. Intercalations of Green Claystone (GC) facies with Argillaceous Shales (AS) and Siliceous Shales (SS) dominates this "Basal Woodford" section. **Figure 53** shows how the Green Claystone facies thins upward in the Basal Woodford section and transitions to a Siliceous Shale, and Siliceous Mudstone dominated interval. The Green Claystone is interpreted to be deposited

in a low energy environment in shallow waters. The presence of mottled texture is evidence of bioturbation, which combined with low present-day measured TOC% support the interpretation of oxygenated shallow water depth. The shoreline probably moved back and forth with a general landward trend which resulted in the interbedded fining upward stacking pattern transitioning to deeper water facies like the Siliceous Shale and Siliceous Mudstones.

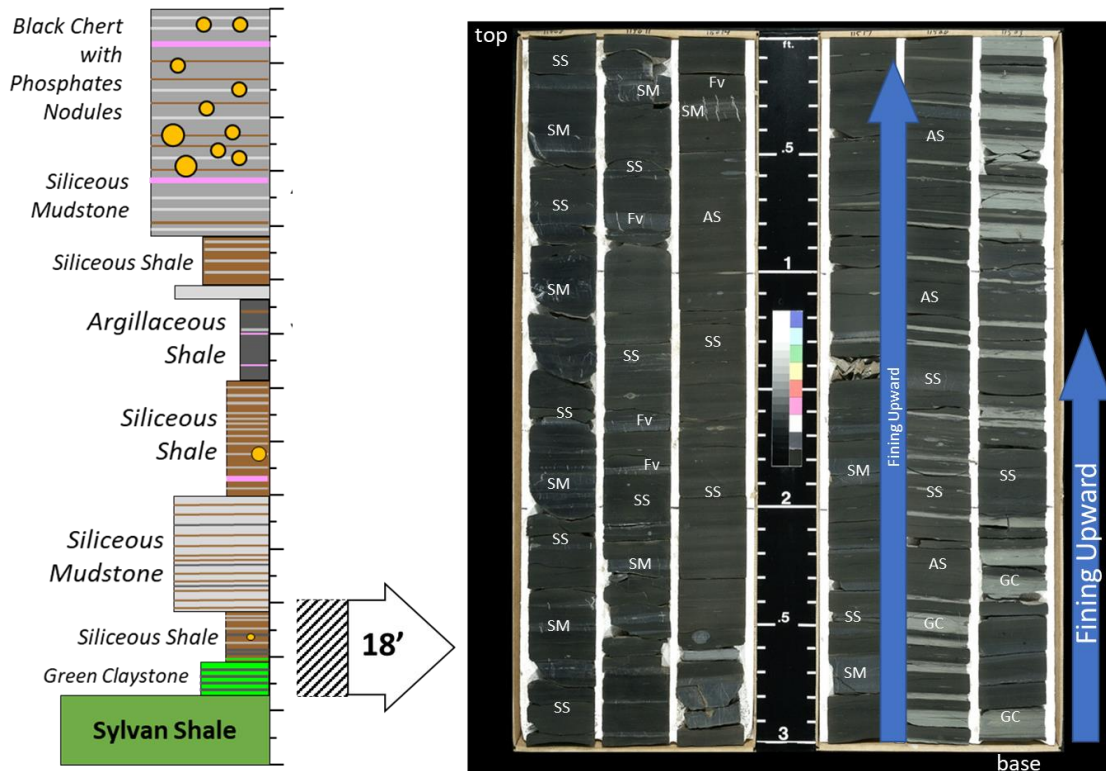


Figure 53 Core View of transition from Green Claystone (GC) dominated section at the base of this interval to Siliceous Shale (SS). Notice the thinning upward pattern of GC facies.

Siliceous Mudstone (SM) facies dominates the following cored section (**Figure 54**). Most of the Siliceous Mudstones intercalates with Siliceous Shale (SS) facies and a few beds of Argillaceous Shale (AS). Like the previous section on Figure 53, the Siliceous Mudstone facies usually have mineralized vertical fractures (Fv) with white or light beige color that rarely extends out to other facies in this section.

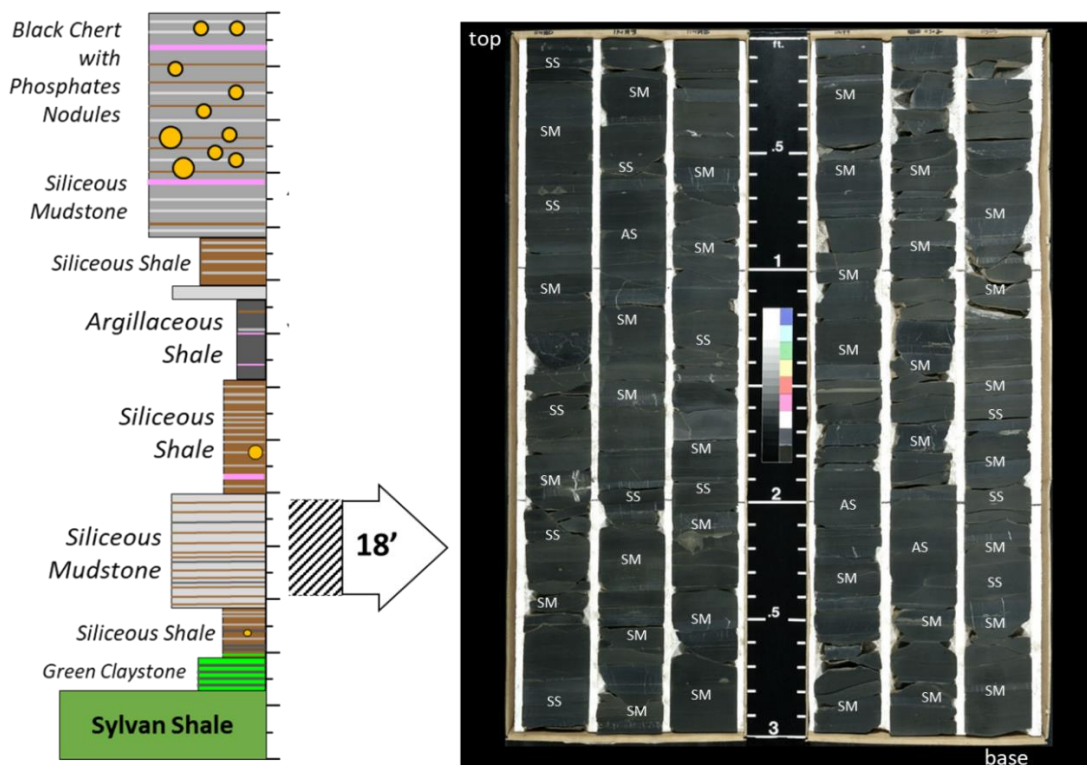


Figure 54 Third cored interval dominated by Siliceous Mudstone (SM) facies interbedded with Siliceous Shale (SS) facies. Mineralized Vertical fractures (Fv) are present as well in this section and always bounded within Siliceous Mudstone (SM) facies.

Moving upward in these cored sections of the Woodford Shale, the Siliceous Mudstone (SM) dominated interval transitions to Siliceous Shale (SS) dominated intervals (**Figure 55**). Noticing the presence of light gray color beds is important. These beds are made of Dolomitic Mudstones (DM) facies. They thin-upward until there are no more such beds present. These facies are also common in outcrop exposures like the McAlister Cemetery quarry and Speake Ranch. They can also serve as marker beds when correlating across the basin. Once again, vertical fractures are present in the thin-bedded Siliceous Mudstones (SM) facies of this interval. A few phosphate and calcareous nodules are present in this section. One key element to see in this interval is how the lighter colored beds transition upward to darker color; beds which correspond with changes in TOC from 4% to 7%.

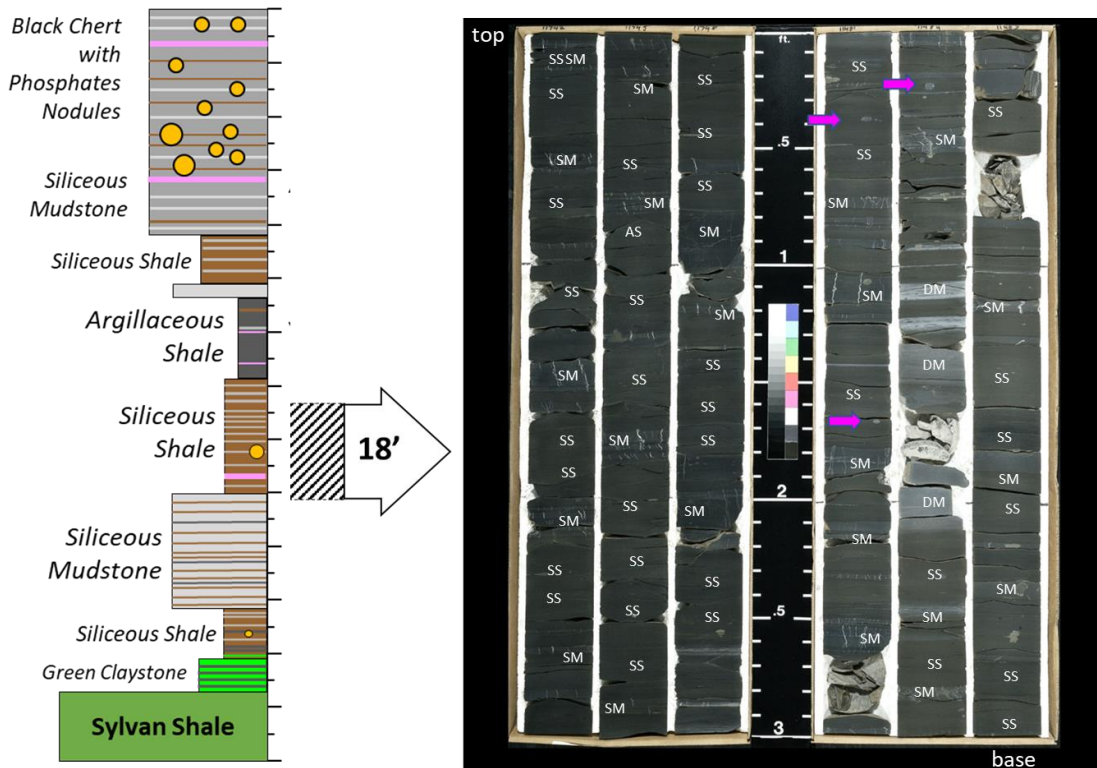


Figure 55 Fourth cored intervals dominated by the Siliceous Shale (SS) facies. At the base, Dolomitic Mudstone (DM) is present (light gray) and thins upward. Fractures are mostly vertical within Siliceous Mudstone (SM) beds. Magenta arrows show the location of calcareous nodules and small phosphate nodules. They are less concentric and more crystalline than the well-known Phosphate Nodules (PN) in the upper Woodford interval.

The fifth cored section is shown in **Figure 56**. Argillaceous Shale (AS) is the most dominant facies in this stratigraphic interval. This facies has a higher clay content compared to the other interbedded facies (Siliceous Mudstone and Siliceous Shale) resulting in a matte texture (very silky and smooth). TOC% is very high in the AS dominated interval, ranging from 6% to 9%. Vertical fractures are limited to the Siliceous Mudstone (SM) facies; however, there are several horizontal or planar fractures within the Argillaceous Shale (AS) facies. These fractures are partially open, and many of them have remaining bitumen inside. Additional to the features described above, there is one bed (red box in Figure 3.22) that will be discussed in detail in the next chapter because it contains large replaced crystals and radiolarians with bitumen inside.

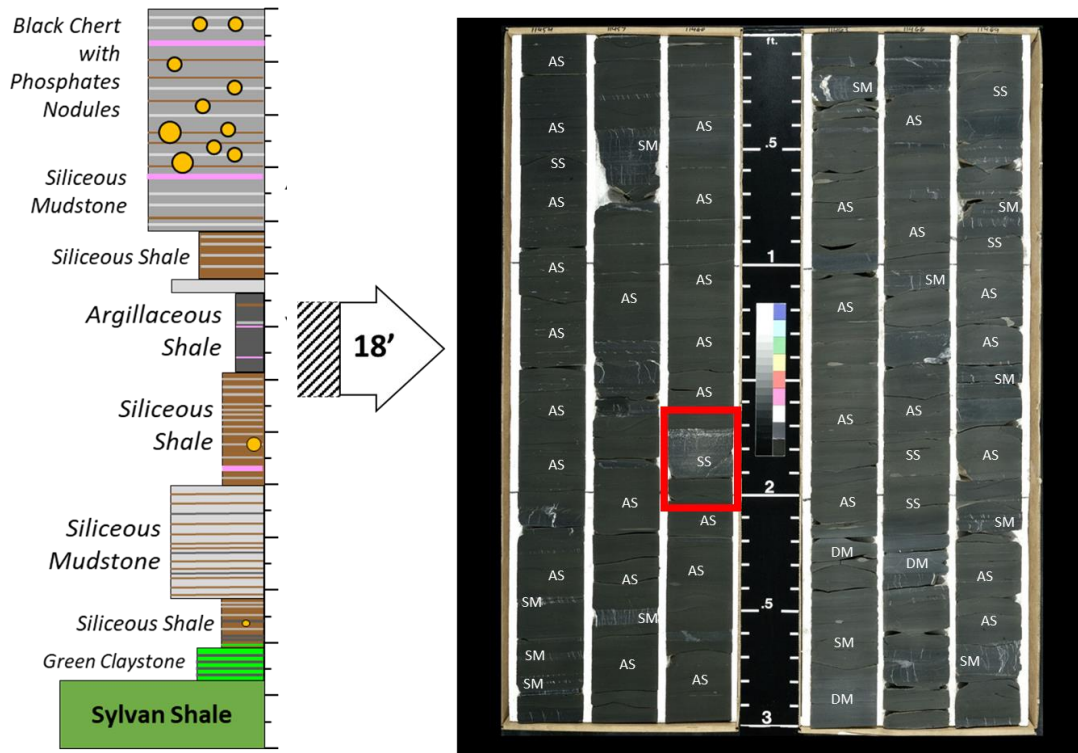


Figure 56 Fifth cored interval dominated by the Argillaceous Shale (AS) facies. Many horizontal fractures that are partially open within the AS facies. Pyrite is very common as well in this section. The red box shows a diagenetically-altered bed that will be discussed in chapter 4 (Diagenesis). Vertical fractures are restricted to Siliceous Mudstone (SM) facies.

The sixth cored interval (**Figure 57**) is dominated by 1-inch beds of interbedded Siliceous Mudstone (SM) and Siliceous Shale (SS) with relatively good TOC (4% to 8%). Some Argillaceous Shale (AS) is also present in this section. Fracture density is higher in thinner beds as described by Ghosh (2018) in outcrops. The upper part of this section starts transitioning to Black Chert (BC) facies, but they are still thin compared to the uppermost part of the core. Horizontal fractures are frequent in softer beds (AS, SS) and Vertical fractures are frequent in harder beds (SM, BC).

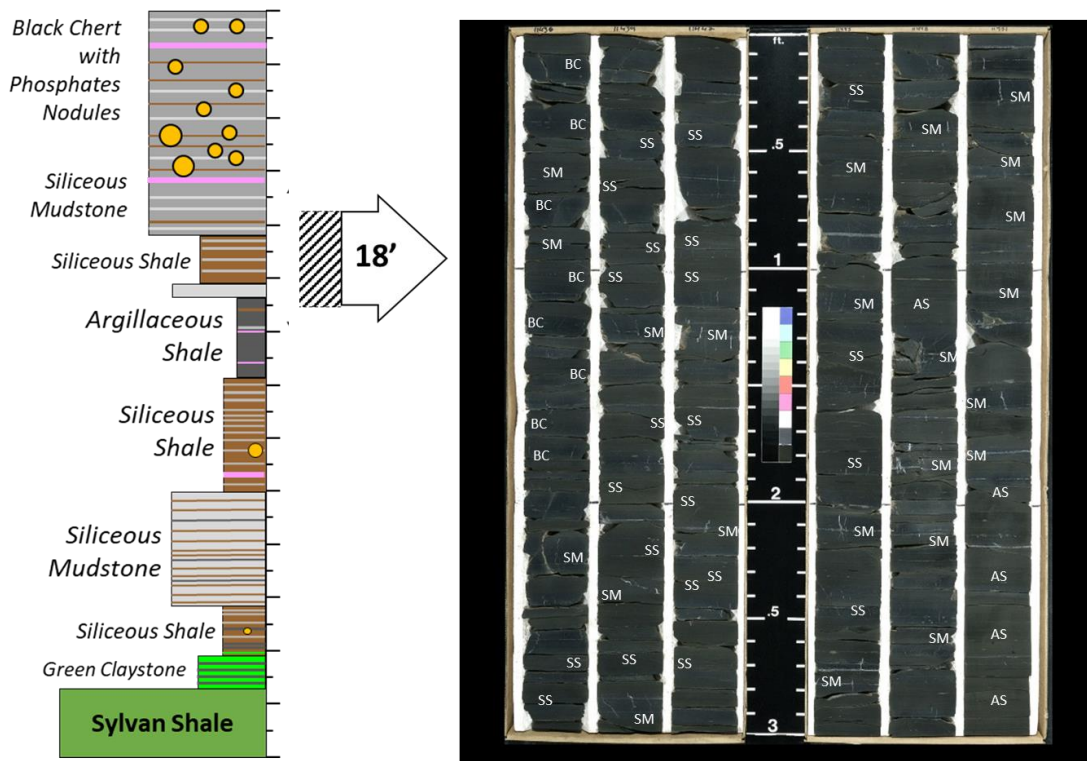


Figure 57 Sixth cored interval in the Marietta Basin Woodford Core. Interbedded Siliceous Shale (SS) and Siliceous (SM) at a 1:1 ratio (50% and 50%). This section is thin-bedded with many vertical and horizontal fractures. There are no Phosphate Nodules (PN) present or Dolomitic Mudstones (DM) beds.

The second to last cored interval contains many Phosphate Nodules (PN) shown in magenta arrows in **Figure 3.58**. This interval is mainly dominated by Black Chert (BC) beds interbedded with some Siliceous Mudstones (SM). There are a few Dolomitic Mudstone (DM) beds at the lower half of this interval. Some of these Dolomitic beds have very well-defined laminations. They are a lighter color than the black chert beds. Vertically open and partially open fractures are very common in the Black Chert (BC) beds as well as in the interbedded Siliceous Mudstones (SM). This interval has a lower TOC% than the previous sections. The few high TOC beds are mostly Siliceous Shale beds within the section.

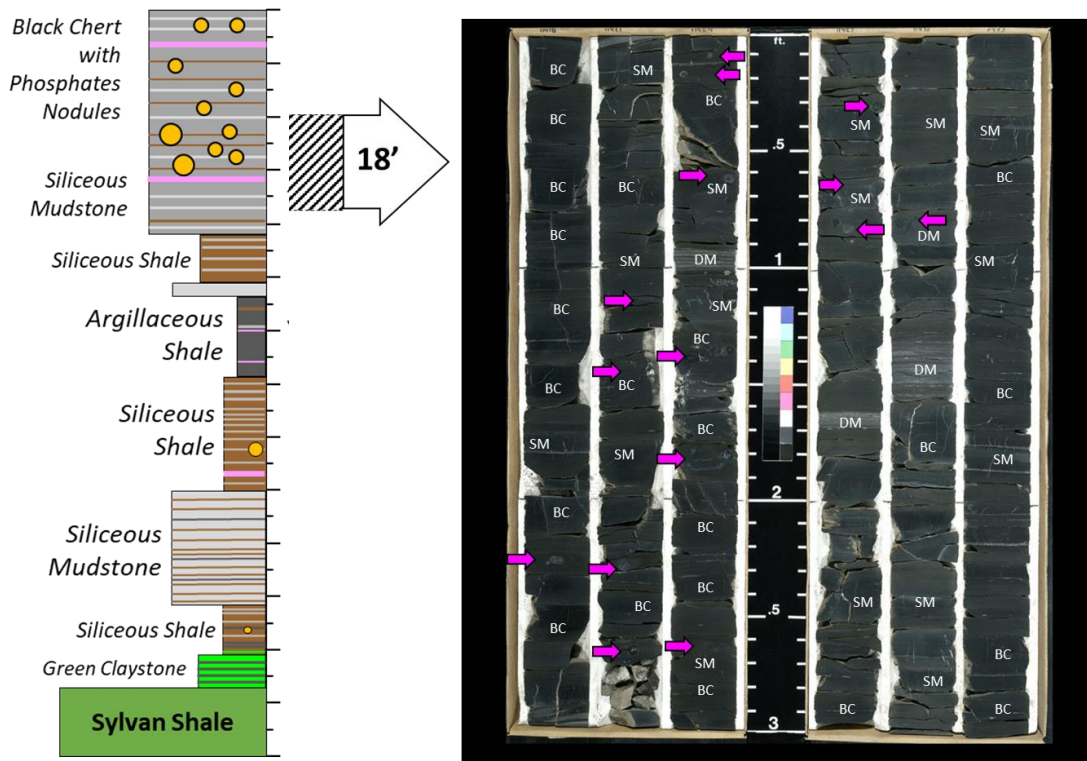


Figure 58 Seventh cored interval dominated by Black Chert (BC) facies and many Phosphate Nodules (PN) marked with magenta arrows. Highly fractured beds are within BC and SM facies. Dolomitic beds are a light gray color.

The uppermost part of the core (**Figure 59**) continues with intervals of Black Chert (BC) interbedded with Siliceous Mudstones (SM). The difference with the previous cored section is the thickness of the beds; these are thicker than any other beds in the core except for the Argillaceous Shale (AS) beds in the middle of the core. There are mostly vertical fractures, partially open, and not mineralized. Some of these fractures are probably induced when these rocks were cored but some others are mineralized and closed which means they are natural. TOC in this interval is the lowest in the core (from 2% to 4%). Phosphate nodules are less common in the section but still present. There is one thick dolomitic bed (DM) that has a sharp contact at the base with Siliceous Mudstone beds, and it transitions upward to laminated Dolomitic Mudstones and back to Black Chert. This facies does not have any vertical fractures and acts as a fracture-boundary for the mineralized fractures in the bed below.

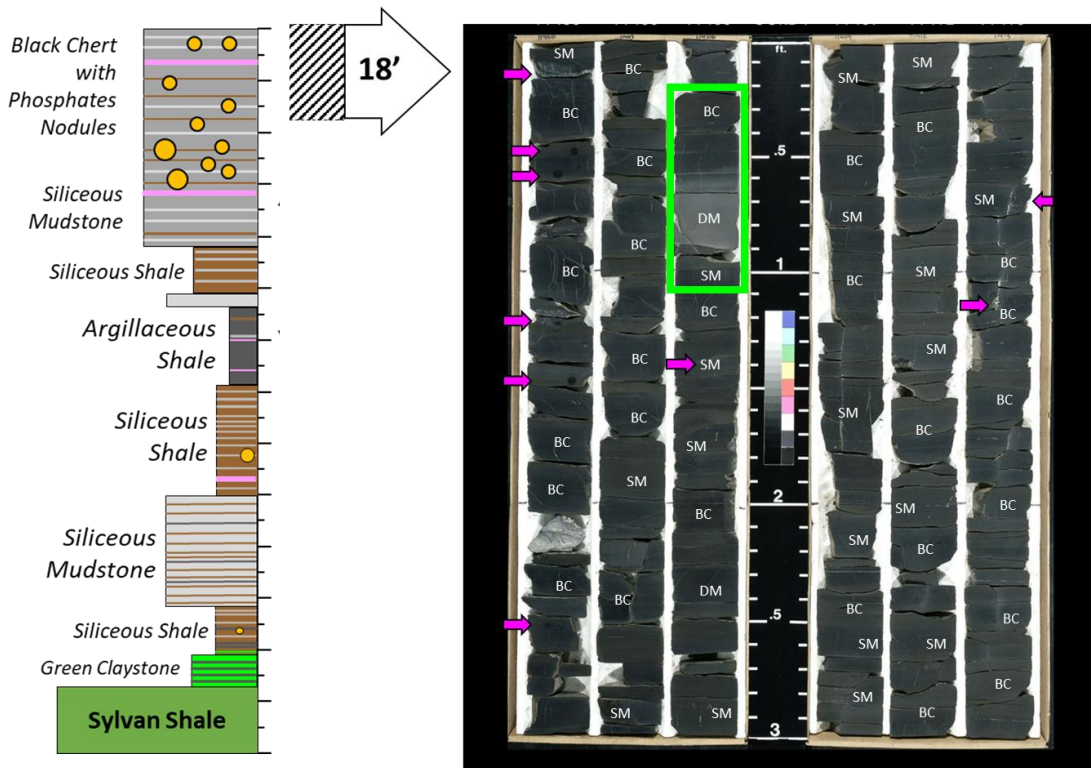


Figure 59 Uppermost Section of the core. Black Chert (BC) is the dominant facies. BC is interbedded with Siliceous Mudstones (SM). Beds are thicker (2-4 inches) compared to the rest of the core. Magenta arrows show the location of the Phosphate Nodules (PN). Green Box shows the location of the thick Dolomitic Mudstone (DM) bed. Vertical fractures are common but mostly coring induced and not natural.

3.5 Interpretation of Unofficial Members of the Woodford Shale

The Oklahoma Geological Survey (OGS) has not defined official members for the Woodford Shale Formation. However, Sullivan (1985) originally proposed to break down the Woodford Shale into several units. Later, Hester et al. (1990) proposed the 3-member subdivision of the Woodford Shale denoted as Lower Woodford, Middle Woodford, and Upper Woodford. These subdivisions are based on log responses like Gamma-Ray log, Resistivity Log, and Density log. Some lithofacies or sedimentary/diagenetic features are unique to some member

allowing the differentiation between these informal members. **Figure 60** shows the subdivision proposed by Hester et al. (1990).

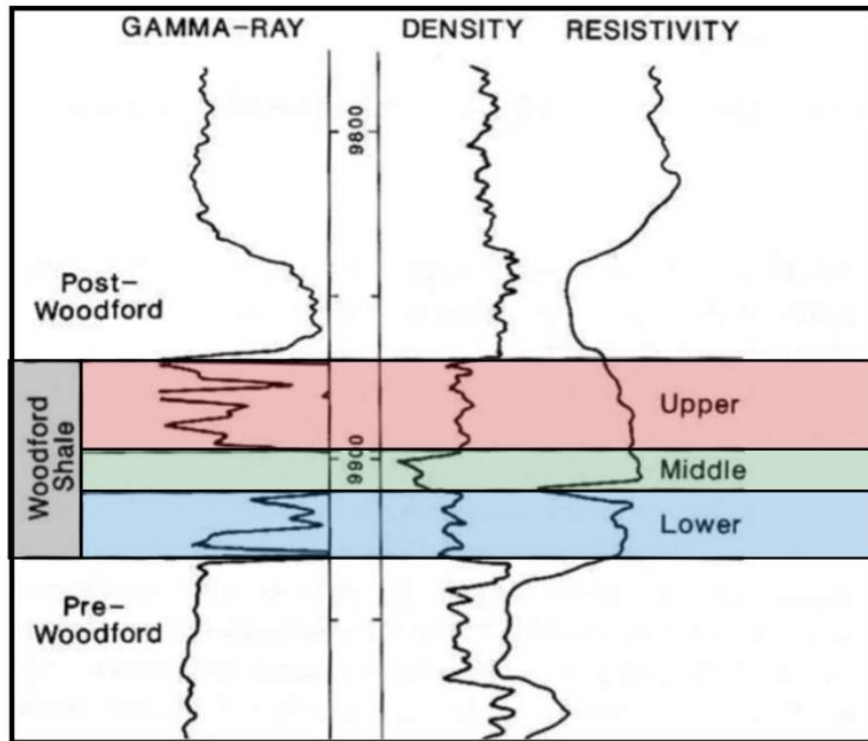


Figure 60 Informal Members of the Woodford Shale from Hester et al. (1990).

The Middle Woodford Shale usually has the highest Gamma-Ray values of the section. Because of the higher content of detrital clays and Argillaceous Shale facies, the Middle Woodford shows lower density and lower resistivity on borehole logs. In contrast, the Upper Woodford has the lowest Gamma-Ray profile within the Woodford due to the high content of biogenic silica within the chert beds. Density in the Upper Woodford is higher than the Middle Woodford due to the lower clay content and lower TOC%, making the rock heavier. The Lower Woodford is the most laterally variable of the informal members because it does have a combination of many lithofacies. Density tends to be in between the Middle Woodford, and the Upper Woodford and resistivity tends to do the same trend. Finally, there is a "fourth" member which is ubiquitous in thick Woodford Sections in southern Oklahoma (Ardmore and Marietta),

which is called "Basal Woodford". It contains the Green Claystone (GC) facies interbedded with glauconitic sandstones. In northern Oklahoma, and contains a dolomitic sandstone called the Misener Sand. This unit is restricted to some locations and is not laterally continuous.

Galvis (2017) identified these 3+1 members in one of the most complete sections of the Woodford Shale in the Arbuckle Uplift called Speake Ranch Woodford Outcrop. **Figure 61** shows Galvis' outcrop description correlated to the Marietta Basin Woodford core of this dissertation and the correlative contacts between Upper, Middle, Lower, and Basal Woodford members. The Marietta Basin Section is a condensed section of the Speake Ranch section. Thickness varies from 315 feet in Speake Ranch to 175 feet in the Marietta Basin section. Every unofficial member can be identified in both sections; the difference in thickness is probably due to the difference in paleotopography and accommodation space between both places; as well as differences in sediment supply.

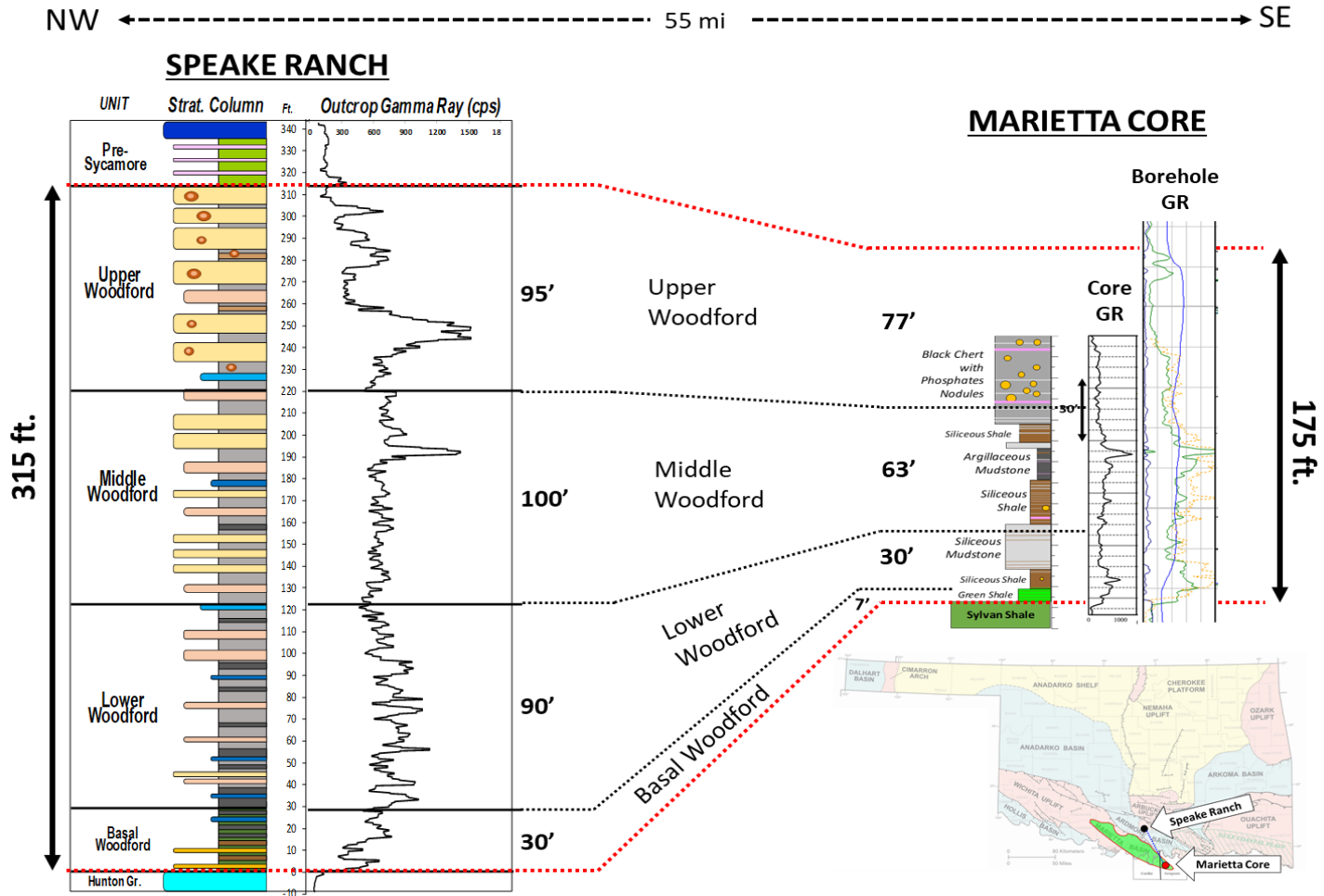


Figure 61 Correlation between the Speake Ranch Woodford Section and the Marietta section. Notice how the section is condensed from the NW to the SE. Gamma Ray responses are very similar to each other even within 55mi of separation between locations.

Using the X-Ray Fluorescence data acquired in the core, depositional environment or conditions can be inferred from the geochemical (elemental) proxy curves. From all the elements, Treanton (2014), Turner (2016) and Ekwunife (2017) identified the most important proxies shown in **Figure 39** of this chapter and discussed below:

- Silicon (Si), Aluminum (Al), Potassium (K), Titanium (Ti), and Zirconium (Zr) are the most detrital sensitive elements. Si, Al, and K are very common in clays. Silicon (Si) is also common in quartz, but the caveat is XRF cannot differentiate between Si in clays and Si in quartz. Therefore, the use of the Si/Al ratio is a key indicator of quartz-associated Silicon when the Si/Al is high, and Clay-associated Silicon when Si/Al is low. The second limitation, which is very important to the Woodford Shale, is to know what the source of quartz-associated Silicon is. It could either be detrital- or biogenic- sourced. To solve this limitation, the Si/Al ratio should be compared to Titanium (Ti) and Zirconium (Zr) content in the rock because these are unique to detrital deposits and are normally in very low concentration in biogenic-quartz dominated rocks.
- Calcium (Ca) and Strontium (Sr) elements are usually found in carbonate rocks. Therefore, they are considered Carbonate Proxies. It is very important to notice that the fractures can contain minerals like Calcite and Dolomite.
- Finally, Molybdenum (Mo) and Vanadium (V), are proxies for Redox conditions. They are elements that normally become fixed in anoxic environments, such that the higher their concentration the lower the oxygen content in the water column. The only limitation is with Vanadium (V) content that can have high nutrient content in the water column as well.

Figure 62 shows the chemostratigraphic profile of the Marietta Basin Woodford Core. The key elements discussed before were plotted with depth and correlated to the core depth and

core gamma-ray log. Black arrows show the major decreasing-increasing trends for each curve. The Detrital Sensitive Proxies (Si, Al, K, Ti, and Zr) show a general decreasing upward trend from the base to the top of the core. This effect is interpreted as a shift from detrital dominated environments to a biogenic dominated environment during the deposition of this Woodford Shale. By looking at the Si/Al ratio (red curve), this trend can be confirmed by the high increase of Si/Al in the upper section. Carbonate Sensitive Proxies like Calcium (Ca) and Strontium (Sr) are relatively low in the Upper Woodford Section and are variable in the Middle and Lower section. Ca and Sr show that the Carbonate Sensitive Proxies are capturing the Dolomitic Mudstone (DM) facies and calcite-rich nodules across the section. Phosphorus (P) peaks corresponds to measurements on the phosphate nodules. Finally, the Vanadium (V) curve supports the high bionutrient conditions when the Upper Woodford section was deposited.

Using the combination between the gamma-ray log response, and the X-Ray Fluorescence profile, I interpret the Maximum Flooding Surface (mfs) at the top of the Argillaceous Shale (AS) dominated interval, where Si/Al ratios are the lowest and turn around to an increasing upward trend, where Mo and V curves start to increase upward, and where the highest gamma-ray of the section is located. This “mfs” surface is the separation between the Transgressive Systems Tract (TST) in the lower and middle Section and the Highstand Systems Tract (HST) in the upper section.

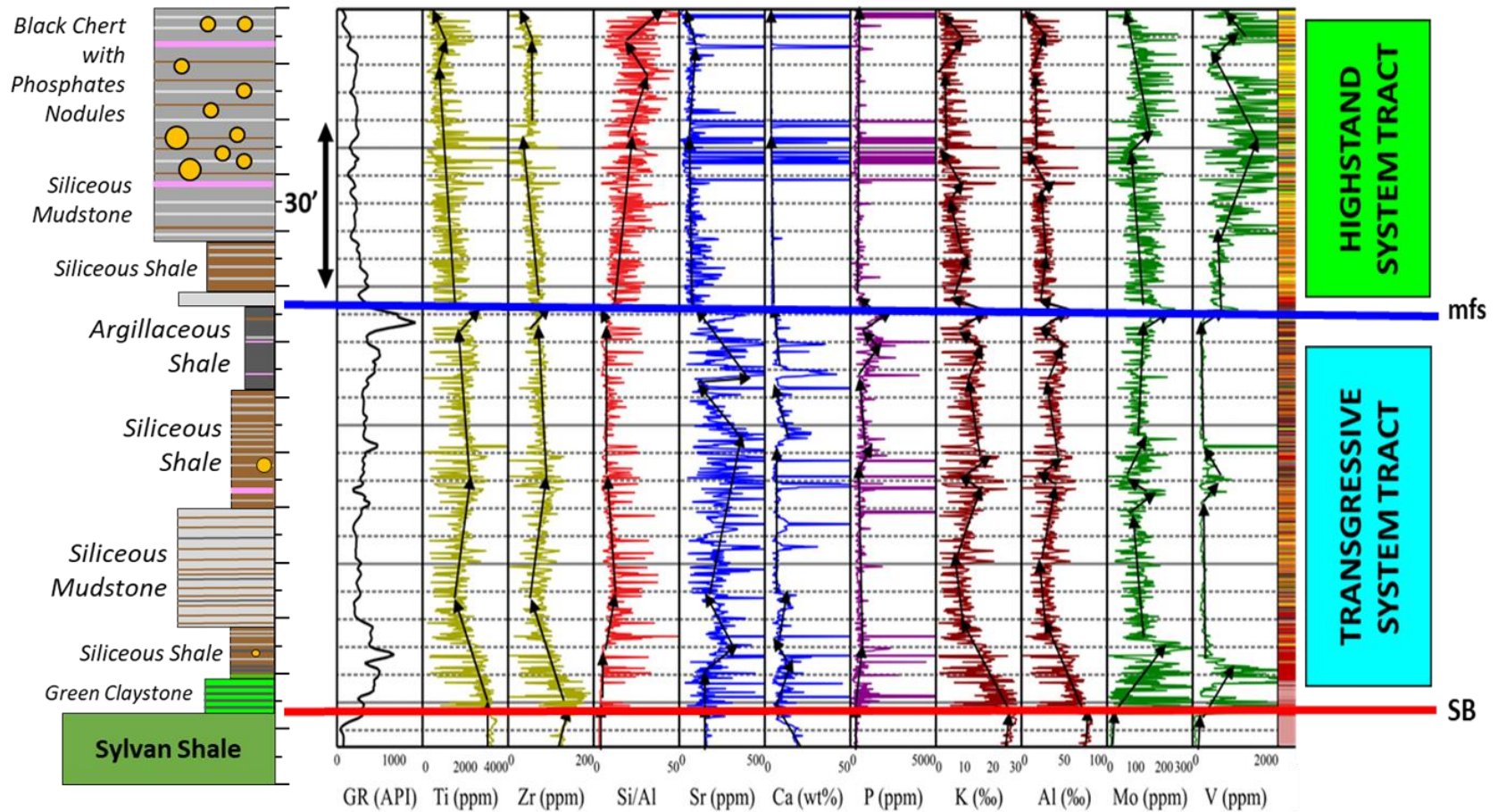


Figure 62 Chemostratigraphic Profiles of the Marietta Basin Core. Black arrows show major increasing-decreasing trends. The blue line represents the Maximum Flooding Surface (mfs), and red line represent the Sequence Boundary at the base of the section. The Upper Sequence Boundary was not cored.

The previously described interpretation correlated well with the depositional model proposed by Slatt (2013), shown in **Figure 63**. From bottom to top of the core, the Basal Woodford shows evidence of shallow water facies (Green Claystone, detrital) correlative to the glauconitic detrital deposits in the basal interval of Speake Ranch Woodford Section. These deposits represented the early transgression deposits when the shoreline started moving landward after the Pre-Woodford Unconformity time. The transition from the Green Claystones to Siliceous Shales represents the deepening of the water column in the basin due to rising of the relative sea level during the TST.

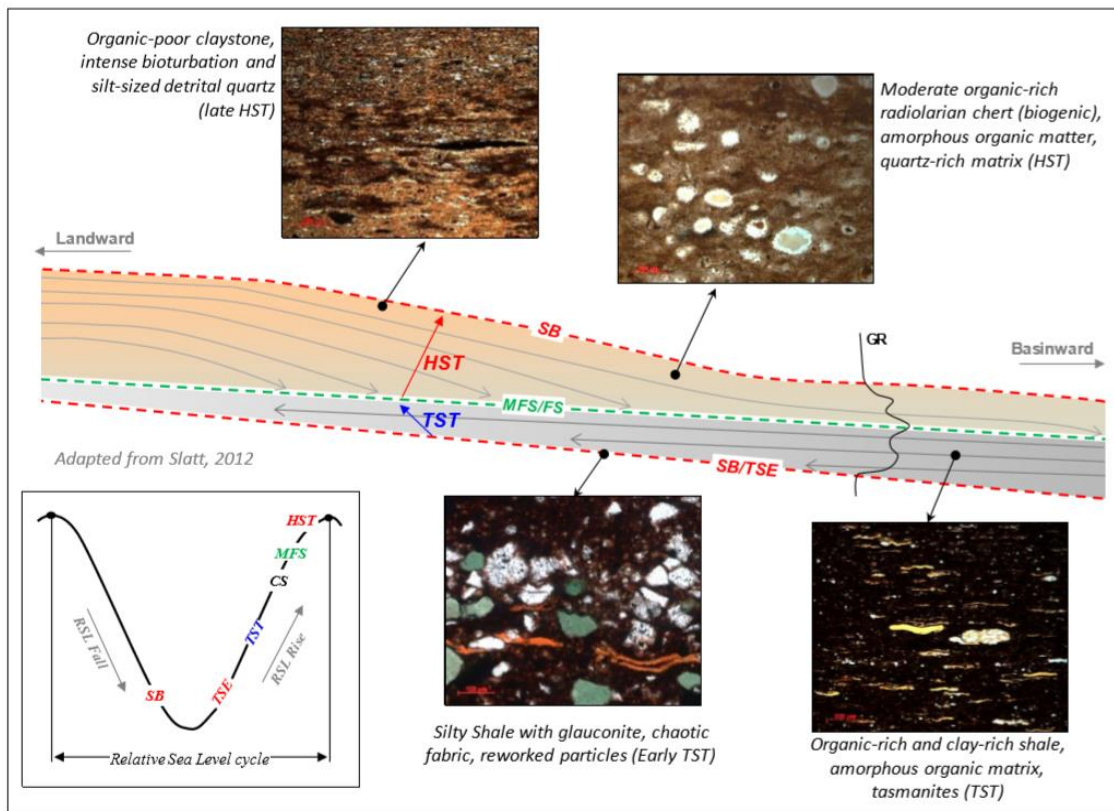


Figure 63 Depositional Model of the Woodford Shale from Slatt 2013 (modified by Galvis, 2017). The Woodford Shale sequence is composed by an early Transgressive Systems Tracts (TST) and a later Highstand Systems Tract (HST). Highest GR surface represents the Maximum Flooding Surface (mfs).

The onset of transgression is reached at the Maximum Flooding Surface (mfs) where the Argillaceous Shale (AS) facies dominates, and later changes to a biogenic dominated section with many thick chert beds. During the HST, the relative sea level was high, waters were well oxygenated, and most of the area of Oklahoma and Texas was flooded, resulting in higher water circulation in the basin, better distribution of nutrients and silica-rich biotas like radiolarians and lower preservation of organic matter because water columns were better oxygenated.

Figure 64 shows the final correlation between the Speake Ranch Woodford Section and the Marietta Basin Woodford Section. The Maximum Flooding Surface (mfs) represented by the high gamma-ray peak can be easily identified in Speake Ranch and the Marietta Basin Core. It is, by definition, the most laterally continuous marker across the area where the Woodford Shale was deposited because it represents the onset of transgression in the basin. Finally, it is important to notice that the upper sequence boundary was not identified in the cored section. However it was identified using the borehole gamma ray log of the well and correlated to the upper sequence boundary identified by Galvis (2017) in Speake Ranch, forming a complete Woodford Shale Sequence.

Chapter 6 (Mapping) and Chapter 7 (Production Performance) will utilize this model to identify the most prolific intervals of the Woodford Shale for horizontal drilling and hydraulic fracturing and correlate them to the current production and estimated ultimate recovery (EUR) of Woodford Shale wells in the Marietta Basin.

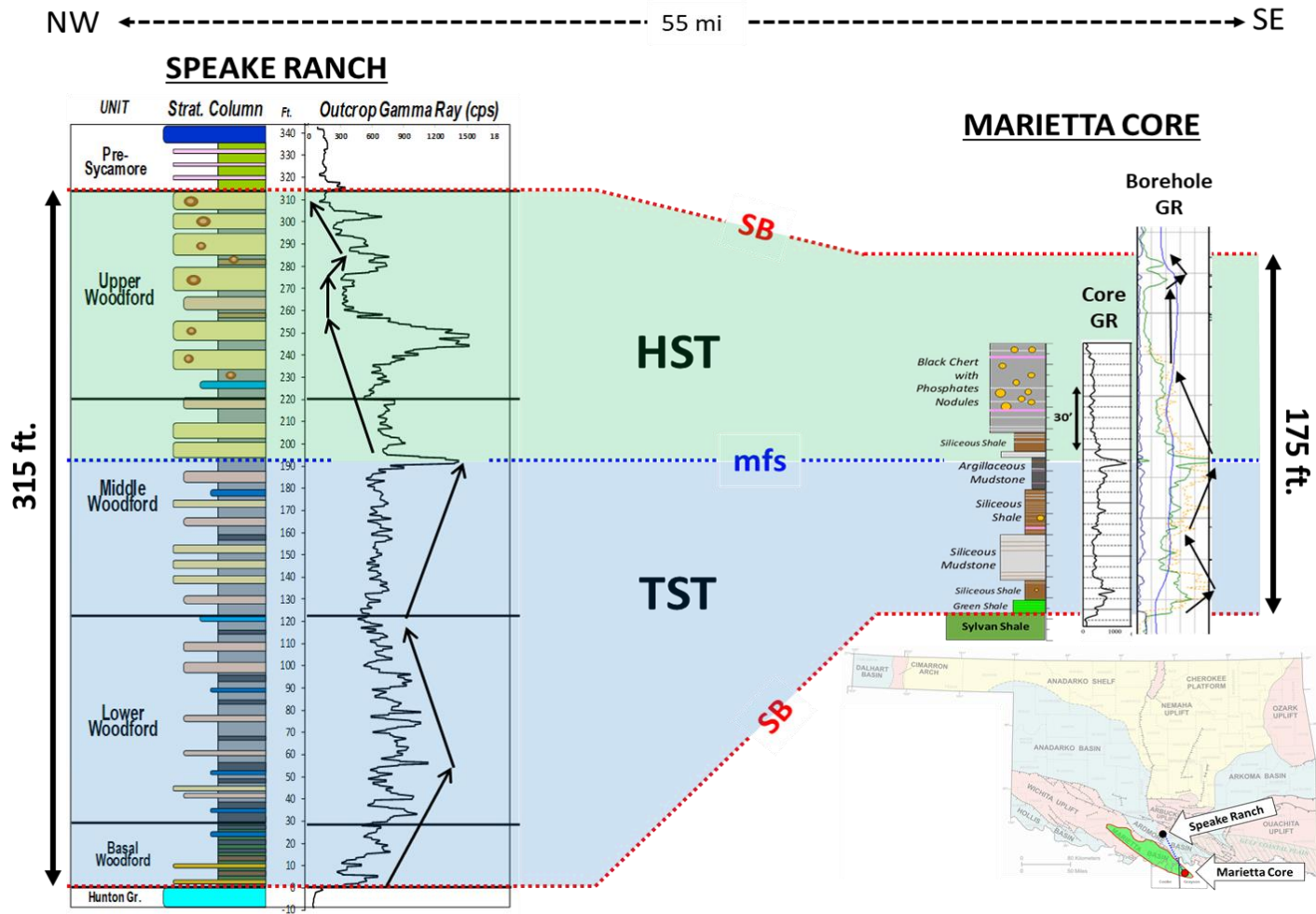


Figure 64 Sequence Stratigraphic correlation between the Woodford Shale exposed in the Speake Ranch outcrop and the Woodford Shale section in the southeastern part of the Marietta Basin (North Texas). Speake Ranch section modified from Galvis (2017).

Chapter 4: Diagenesis

The depositional processes, composition, sedimentary facies, stratigraphy, seismic character, well log patterns, paleomagnetism, geochemistry, geomechanics, and petrophysics are some of the most critical aspects recently studied about organic-rich shales, and particularly, the Woodford Shale in Oklahoma. However, the diagenesis of the Woodford Shale is one of these aspects that is not entirely understood. The most significant publications are Berryman (2013) who studied the timing and paragenesis of the calcite-filled fractures in the Woodford Shale, and Roberts and Elmore (2017) who did a diagenetic study of the Woodford Shale in the southeastern Anadarko Basin in Oklahoma. Hence, there is motivation to understand the diagenetic history of the Woodford Shale in a new unstudied location like the Marietta Basin in North Texas.

One additional significance of this project is grounded on the idea of Elmore et al. (2016) that diagenetic alterations of these organic-rich shales affect the geomechanics properties of the rock (brittleness or frackability) and are an essential variable in the characterization of an unconventional resource shale for horizontal drilling and artificial fracking to produce hydrocarbons.

The primary objective of this part of the dissertation is to describe the main diagenetic features present in polished thin section samples from the Marietta Basin Woodford Shale core and generate a paragenetic sequence of the diagenetic events. The results of the diagenetic analysis are divided into 1) diagenesis of the Matrix and Allochems, 2) diagenesis of phosphate

nodules, and 3) diagenesis of mineralized fractures; to conclude with the proposal of a paragenetic sequence for this Woodford Shale cored section.

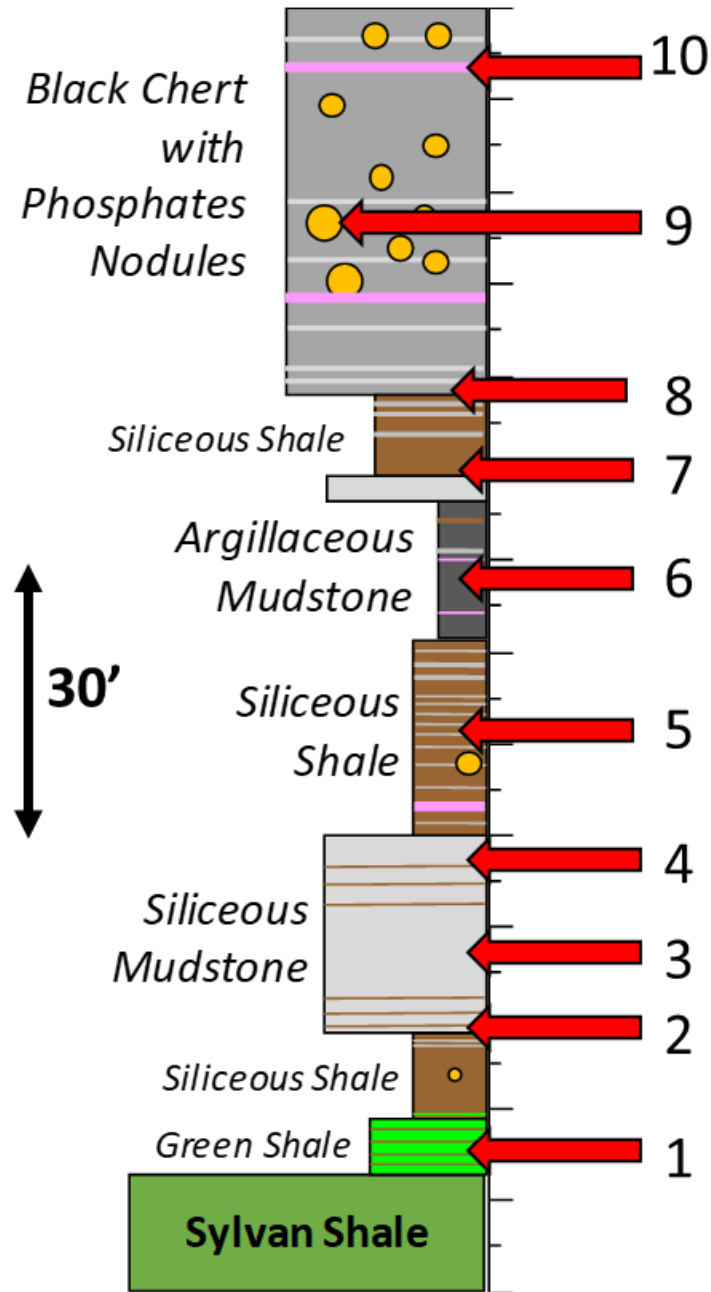


Figure 65 Location of the Samples taken for thin sections in the Marietta Basin Woodford Core.

4.1 Data and Methods

The data to perform the diagenetic study of this dissertation consisted of 10 petrographic thin sections from the Marietta Basin Woodford Core. These thin sections were microprobe polished slides without cover glass embedded with blue resin suitable for SEM and EDX analysis. Spectrum Petrographic was the lab that made the thin sections.

The stratigraphic locations of the samples to make the thin sections were chosen based on facies and presence of significant diagenetic features like phosphate nodules, bed contacts, facies interface, and mineralized fractures. Furthermore, the samples were taken from different stratigraphic depths within the core. **Figure 65** shows the relative location of samples in the core.

The methodology of this diagenetic analysis consists of direct observation and description of the available thin sections under a petrographic microscope (PM) (**Figure 66**) and a Scanning Electron Microscope (SEM) (**Figure 67**). Composition, texture, and cross-cutting relationships between minerals are the most decisive aspects to understand the paragenetic sequence of this rock. The thin sections were described in three stages: 1) transmitted plain-polarized light (PPL), 2) transmitted cross-polarized light (XPL), and 3) reflected light (RL). In transmitted plain-polarized light (PPL) translucent minerals (for example, quartz, calcite, and dolomite) allow light to pass through them. Slides were rotated along the axis of crystals to find angles of extinction position. The transmitted cross-polarized light (XPL) helped to discern between refractive minerals that show color bi-refraction (calcite and dolomite) from those that do not (quartz). The reflected light was necessary to identify reflective minerals like pyrite from other dark non-reflective materials in PPL and XPL like bitumen (in this case). Finally,

elemental composition maps and cross-sections were done using the Energy-Dispersive X-Ray analyzer (EDS) to validate mineral composition and scan for rare elements in the samples.



Figure 66 Picture of graduate student (Antonio Cervantes) looking in the Carl Zeiss AX10 Imager Z1 petrographic microscope. It has the capability of using 1) transmitted plain-polarized light (PPL), 2) transmitted cross-polarized light (XPL), and 3) reflected light (RL). This instrument is property of ConocoPhillips School of Geology and Geophysics (CPSGG) at The University of Oklahoma (OU).

The petrographic microscope is a Carl Zeiss AX10 Imager Z1 microscope with camera capabilities. The Scanning Electron Microscope (SEM) is a ThermoFischer FEI Quanta 250 with an attached Energy-Dispersive X-Ray Analyzer (EDX) for elemental composition. These devices are property of the ConocoPhillips School of Geology and Geophysics at The University of Oklahoma.

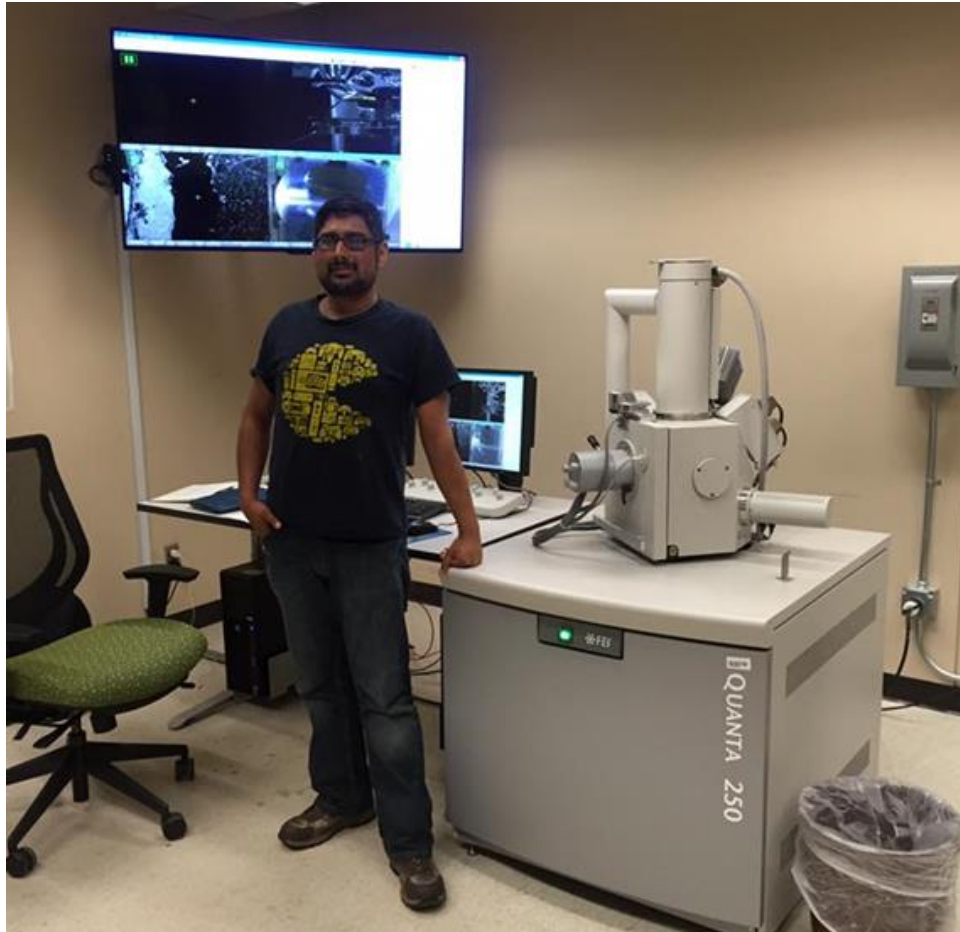


Figure 67 Picture of the Scanning Electron Microscope (SEM) ThermoFischer FEI Quanta 250 with an attached Energy-Dispersive X-Ray Analyzer (EDX) This instrument is property of ConocoPhillips School of Geology and Geophysics (CPSGG) at The University of Oklahoma (OU).

4.2 Diagenesis of the Matrix and Allochems

The matrix of the Woodford Shale in the Marietta Basin core has three primary types based on rock texture and present diagenetic features:

- Matrix A (red arrow in **Figure 68**): is clay-rich matrix within the well-laminated Argillaceous shales (AS). This matrix has a high content of clays (up to 35%) and low content of biogenic quartz and diagenetic pyrite. It looks dark without allochems under transmitted plain-polarized light (PPL), transmitted cross-polarized light (XPL), and reflected light (RL).
- Matrix B (blue arrow in **Figure 68**): is a silica-rich matrix within the Siliceous Mudstones (SM). This matrix has a high content of crystallized Radiolarians and Tasmanites (usually filled with quartz, and rarely with calcite or dolomite). Clay content is lower than Matrix A (around 20%)
- Matrix C (yellow arrow in **Figure 68**): is an organic-rich matrix within the Siliceous Shales (SS). It contains Radiolarians and Tasmanites as Matrix B, filled with organic matter and pyrite instead of quartz and has similar clay content than Matrix B but lower than Matrix A.

One key observation of **Figure 68** is the fracture extension across the matrixes. This fracture propagates through Matrix B (yellow arrow) and C (blue arrow); however, it does not propagate across Matrix A. It appears the matrix is a mechanical barrier for the fracture probably due to the high clay content that makes Matrix A more ductile. The radiolarian rich matrixes (cemented with quartz and pyrite) are brittle enough to let fractures be created and mineralized before compaction. These convoluted or deformed fractures are often called Ptygmatic fractures or pre-compaction fractures (Caldwell (2012), Kennedy et al. (2016), Roberts and Elmore, 2017).

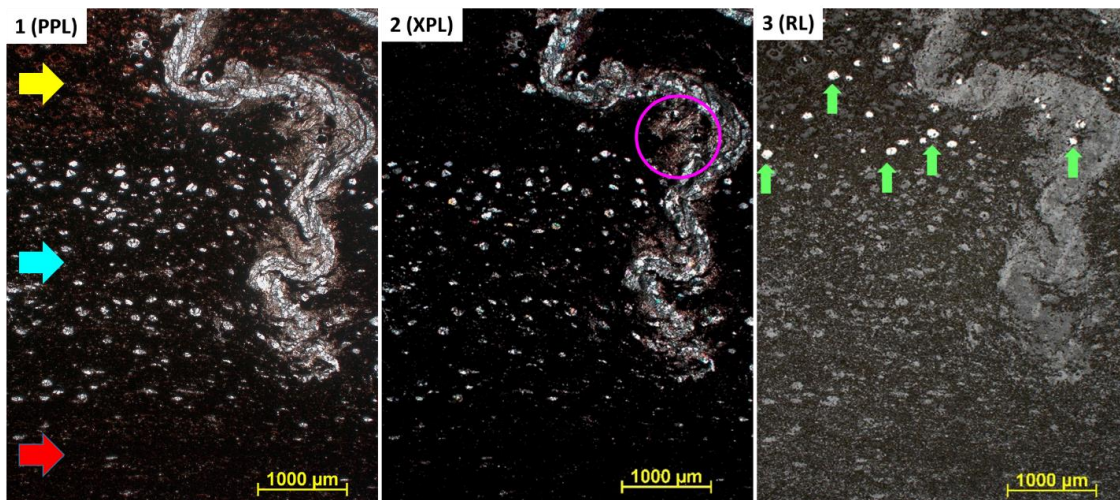


Figure 68 Example of the texture of the three main matrix in the mudstones facies of the Woodford Shale. On the left (PPL): Matrix A (red arrow), Matrix B (blue arrow), and Matrix C (yellow arrow). On the center image (XPL), magnesite flowering (purple circle). On the right picture (RL), pyrite filled radiolarians (green arrows).

In **Figure 68**, the magenta circle shows a texture described by Roberts et al. (2017) as Flowering Texture. This light brown texture is color birefringent in XPL and is composed of Magnesite (MgCO_3 - Magnesium Carbonate). This texture is usually associated with fractures. EDX analysis validated that this Flowering feature replaces the silica-rich matrix with magnesium-rich calcite-less carbonate (Magnesite).

Another example of Magnesite Flowering as described before can be seen in **Figure 69** in the purple circle. All the light brown matrix is replaced by Magnesite, very similar to the texture shown next to the fracture on **Figure 68**, with the difference being that in the sample of Figure 9 there are no associated large fractures to the Magnesite. Instead, there are large crystals (in PPL), which are interpreted as Gypsum pseudomorphs because of their peculiar habit, size, and shape. They are filled with dolomite crystals.

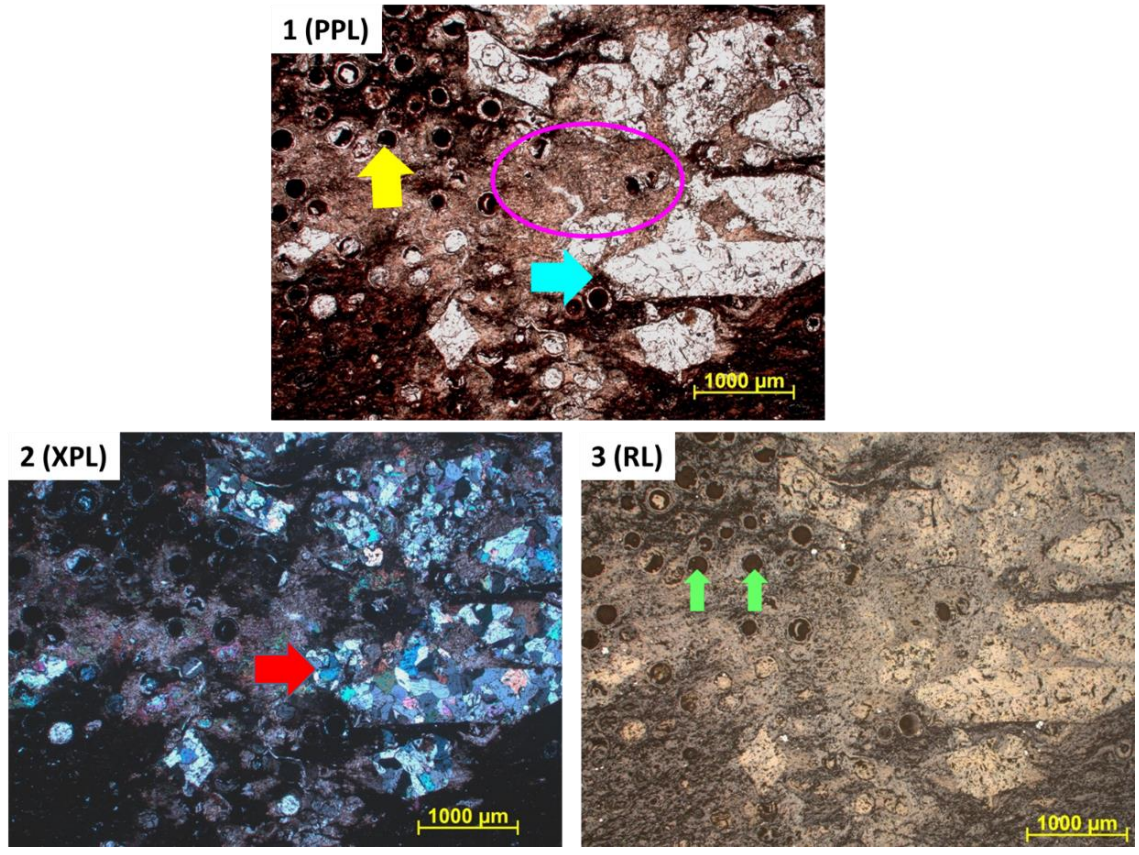


Figure 69 Microscopic picture of the Woodford Shale allochems. On PPL (1), Tasmanites (yellow/green arrows), Large crystals [originally Gypsum (?)] (blue arrow), and Magnesite flowering (purple circle). On XPL (2), current composition of the large crystals are small crystals of calcite and dolomite. On RL (3), Tasmanites that are dark in PPL are not reflective in RL (therefore no pyrite).

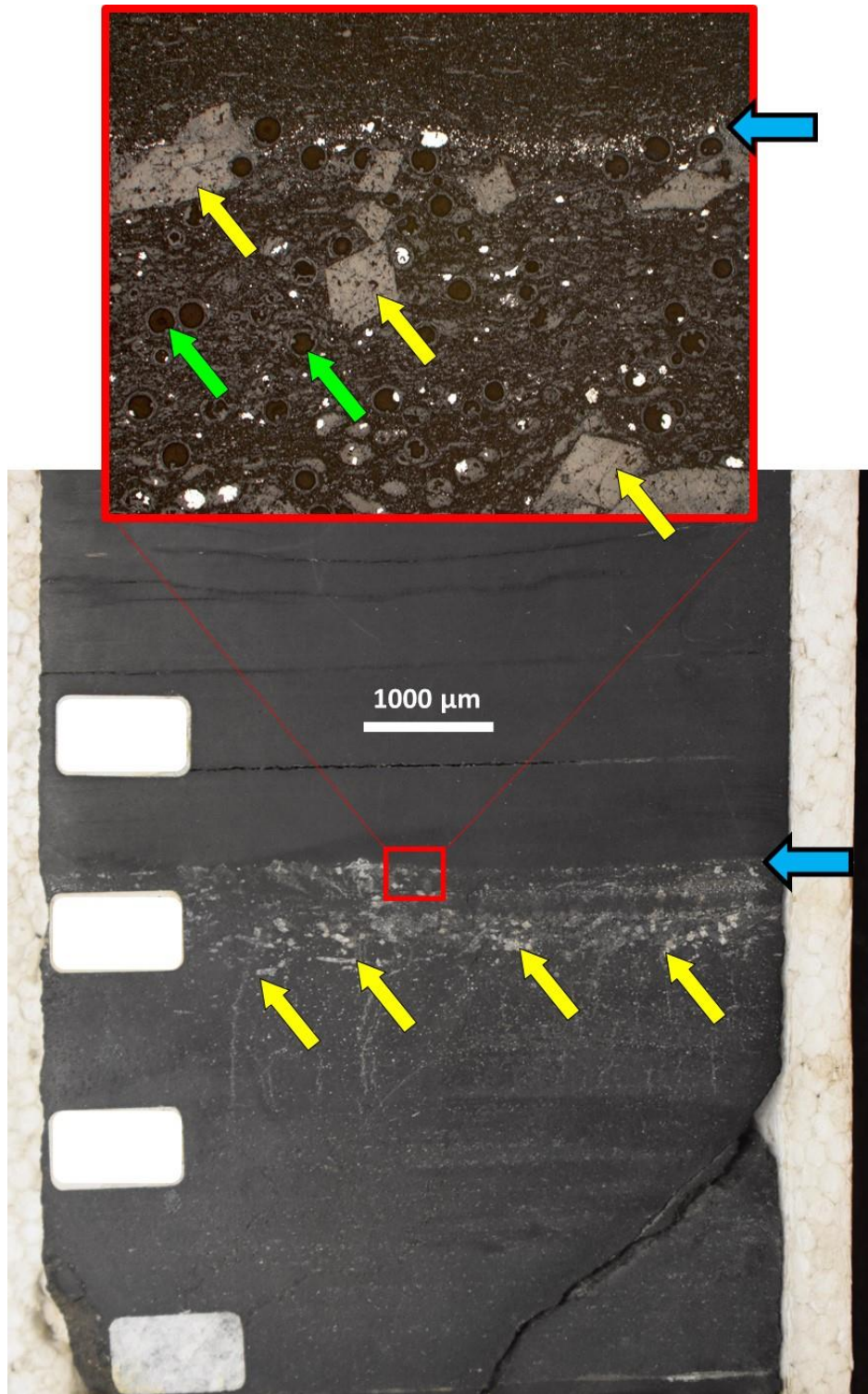


Figure 70 Picture of the core section that contains the large crystals (yellow arrows) in proximity to the potential flooding surface (blue arrow). Relatively distal facies overlaying relatively proximal facies. Green arrows show bitumen filled Tasmanites.

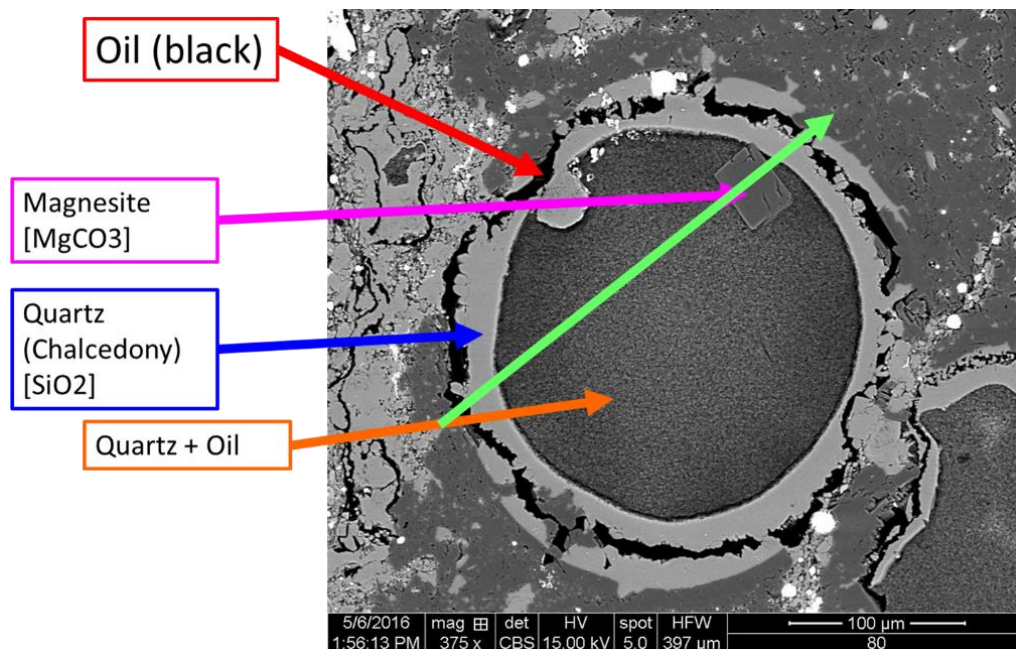
The sample is unique in the core; only one is present along all the section. It is in sharp contact between Siliceous Shale (SS) and Argillaceous Shale (AS) **Figure 70**. Gypsum pseudomorph can be identified in hand-sample. The lower bed has Tasmanites and Radiolarians cemented by quartz aligned along laminations and tiny fractures in it. The upper bed is faintly laminated, clay-rich, dark shale with horizontal open and partially open fractures.

Based on the description of the lower bed and the upper bed, this surface is interpreted as a classic flooding surface atop one parasequence. Flooding surfaces are sharp contacts where relatively distal facies overlays relatively proximal facies. Therefore, facies above the flooding surfaces have finer grain sizes than facies below the flooding surface (Catuneanu, 2011). These flooding surfaces are evidence of prolonged low sedimentation rates allowing the accumulation and precipitation of authigenic minerals and early cementation as evidenced by preservation of the full circle shape of Tasmanites and Radiolarians below the flooding surface. **Figure 70** shows how the shape of Tasmanites is preserved below the contact, therefore circular; but they are flattened by compaction in the clay-rich facies above the contact.

These cemented Radiolarians and Tasmanites are the most common allochems in the Woodford Shale all over Oklahoma and North Texas. On **Figure 69 (3-RL)** and **Figure 70**, the Tasmanites are dark color in PPL and XPL, but they are not pyrite cemented because they do not reflect light under RL (which is characteristic of metallic minerals like Pyrite). This sample was analyzed using the SEM to take a closer view of the Tasmanites, and its composition was extracted using the EDX. **Figure 71** shows one of these cemented Tasmanites from **Figure 70**.

The original shape of this Tasmanites is perfectly preserved. This effect is strong evidence the Tasmanites were cemented before compaction as proposed by Schieber (1996). The walls of the Tasmanite cyst must be crystallized before compaction to preserve the perfect rounded shape. **Figure 72** shows the mechanism of the early cementation process of these cysts.

A cross-sectional survey using Energy-Dispersive X-Ray Spectroscopy (EDX) was performed on this sample to observe the transversal composition of this Tasmanite (**Figure 72**). The compositional cross-section shows how the wall of the Tasmanite was cemented by quartz. The exterior matrix composition is Magnesite (Flowering Effect on **Figure 69**). The inside of the Tasmanites contains carbon (C), Oxygen (O) and Silicon (Si) which is interpreted to be hydrocarbons and very fine silica. This silica is microcrystalline (chalcedony). The well-shaped crystal inside the radiolarian is Magnesite (it has Mg, C, and O; but not Ca).



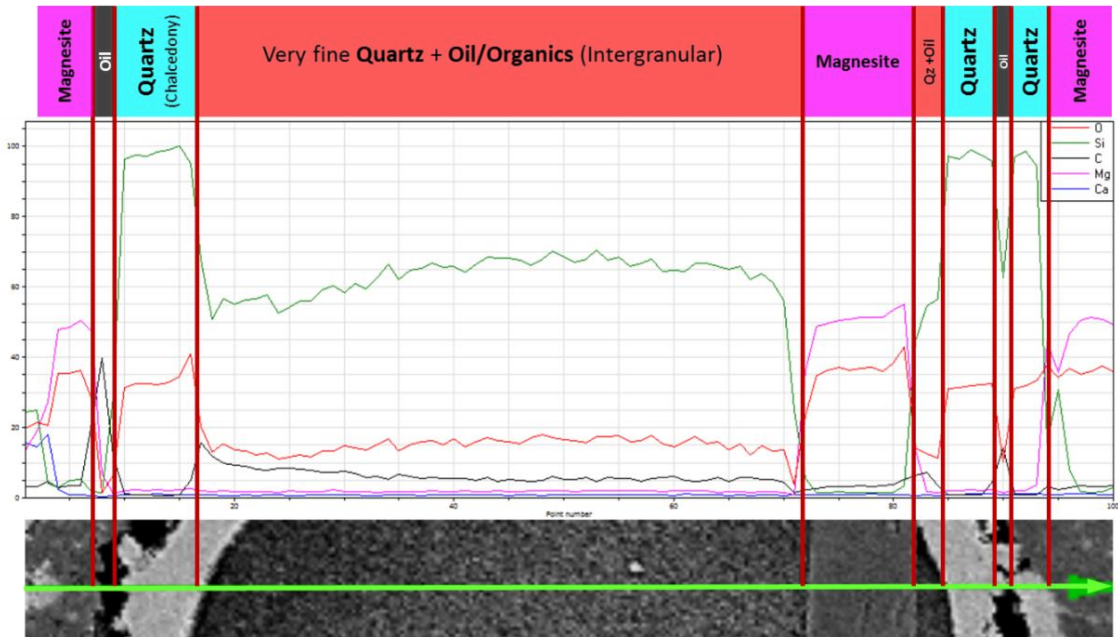


Figure 71 Tasmanites from Figure 9 under Scanning Electron Microscope (SEM). Composition was obtained using the EDS. Line scan using the EDS. Observe the distribution of different minerals interpreted from the elemental composition on top of the figure.

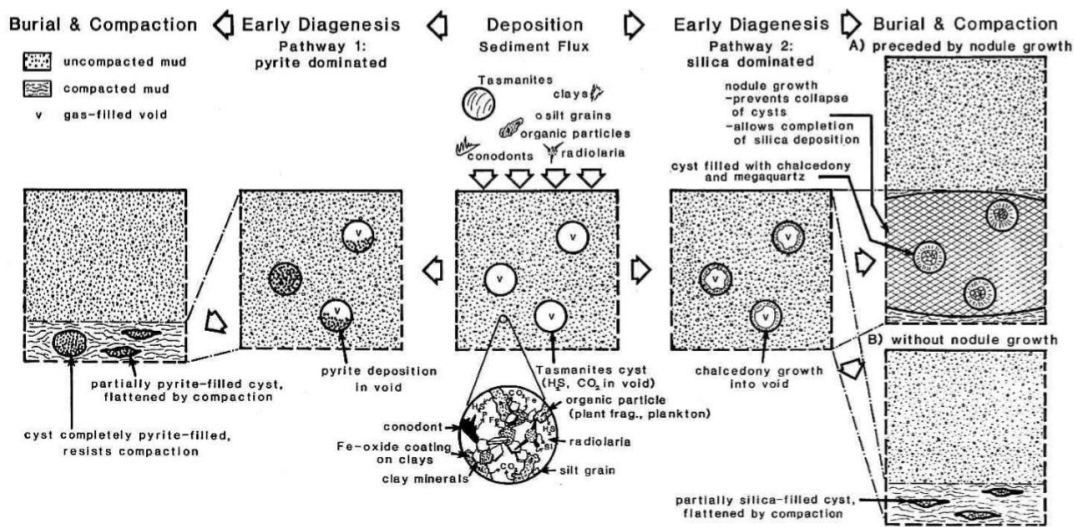


Figure 9: Schematic presentation of early diagenetic processes. Two potential pathways of mineral deposition in cysts are envisioned, one in which mainly pyrite is deposited (pathway 1), and one in which mainly silica is deposited (pathway 2). Enlarged view of initial sediment shows envisioned fabric of freshly deposited mud, and sources of early diagenetic products (CO_2 and H_2S from degradation of organic matter by sulfate reducing bacteria, silica in pore waters from dissolution of radiolarians, iron from dissolution of iron oxyhydroxides on clays, and phosphorous from dissolution of conodonts and fish debris). Which pathway is favored may depend on the initial sediment composition (few radiolaria = pathway 1; abundant radiolaria = pathway 2).

Figure 72 Mechanisms of early cementation of Tasmanites and Phosphate Nodules. Schieber (1996)

4.3 Diagenesis of Phosphate Nodules

Well-preserved Cemented Tasmanites are not uniquely present in the matrix of the mudstones but also inside the phosphate nodules. Phosphate nodules are another diagenetic feature prevalent in the Woodford Shale, particularly in the upper portion of the section along chert beds.

Phosphate Nodules in the Woodford Shale formed at the water-sediment interface within the upper few inches of sediments when the pores of newly deposited muds are saturated with organic-rich water in anoxic to suboxic environments (Siy, 1988). **Figure 73** shows one Tasmanite inside a phosphate nodule (**Figure 73 A and B**), and a composition map scan from the EDX equipment (**Figure 73 C-F**). Observe how the Tasmanites kept the perfect circular shape as in the previous example (**Figure 69**), but in this example (**Figure 73**) the Tasmanites is inside the Phosphate Nodule. The Tasmanite has been entirely replaced by apatite which is rich in calcium and phosphorus (**Figure 73 D and E**). There is still a remnant of the original cemented wall in the outside rim which is rich in Si (**Figure 73-F**) probably from the quartz cement. Finally, **Figure 73-C** shows that the inside of the Tasmanites in this example has a high content of Carbon (C) probably associated to bitumen-filled (hydrocarbon) pore space.

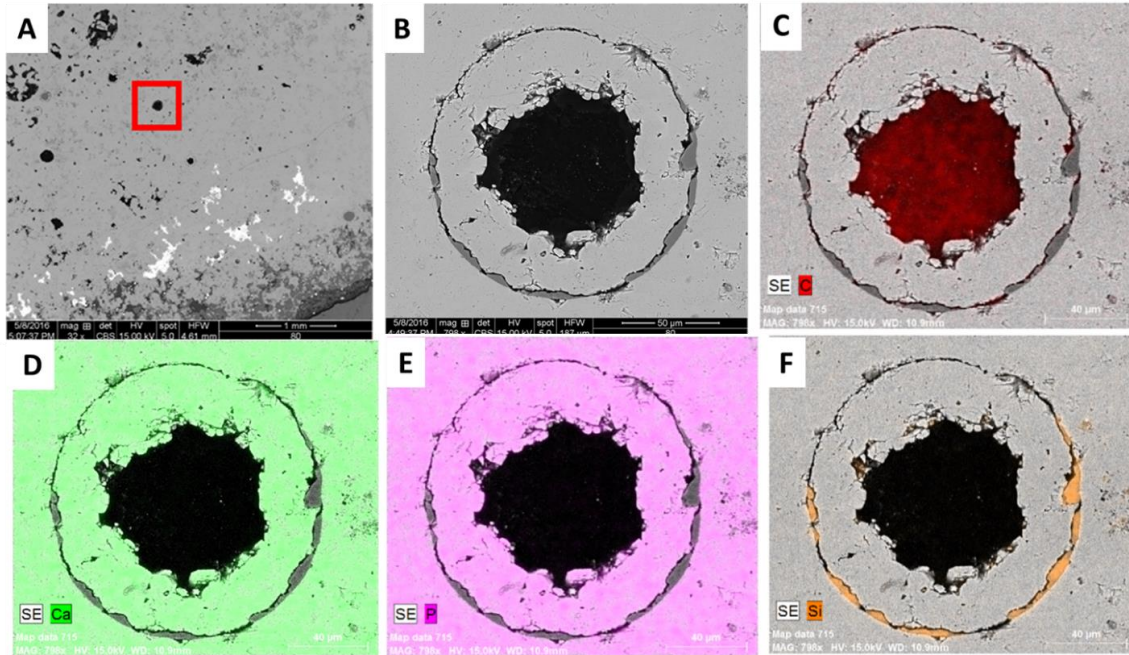


Figure 73 SEM picture of Tasmanites inside a phosphate nodule. A) Map view of location of radiolarian (1mm scale); B) Closer view (50µm scale); C) Carbon map; D) Calcium map; E) Phosphorus map; and F) Silicon map.

Looking at the other components of the phosphate nodule (**Figure 74**), there is a white color mineral. This feature was measured using EDX and shown to be Barium Sulfate (also known as Barite).

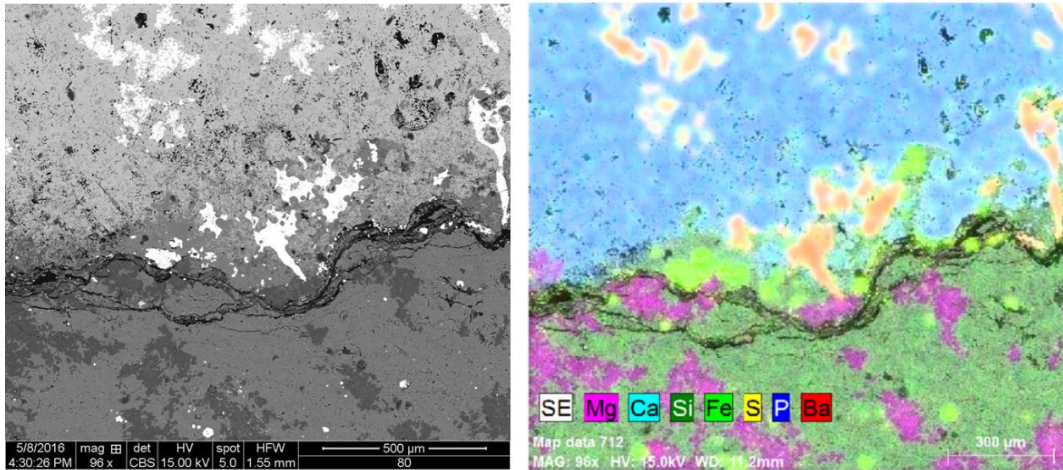


Figure 74 Contact between phosphate (upper) and matrix (lower). White color in the left image is barite. It has a yellowish-orange color in the element composition map; a combination of sulfur (yellow) and Barium (Red).

The SEM image of the sample in **Figure 74** was compared with its respective petrographic microscope image (**Figure 75**), and the Barite is highlighted in transmitted cross-polarized light (XPL). The magnesium in the matrix surrounding the Phosphate Nodule is again associated with Magnesite. This example in **Figure 75** is another case where Magnesite is not directly related to any mineralized fracture or large crystals like previously shown.

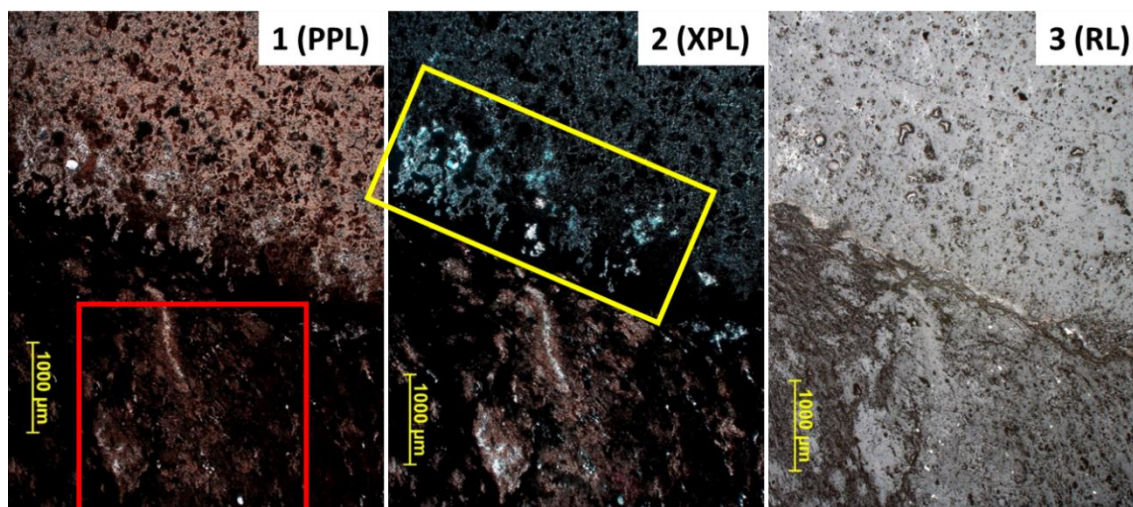


Figure 75 Contact between phosphate nodule and matrix. Observe the presence of Magnesite flowers in the matrix (red square), and Barite within the phosphate (yellow square).

4.4 Fracture Diagenesis

There are two vertical fracture groups in the Marietta Basin Woodford Core: 1) the ptygmatic (convoluted) fractures also called Pre-Compaction fractures and 2) the (relatively) straight fractures. Both show a different cross-textural relationship and characteristics.

Pre-compaction fractures (**Figure 76**) are highly convoluted or deformed, usually composed by dolomite in the core of the fracture with some well-shaped crystals of calcite. They have very extensive “flowering” texture of Magnesite propagating from the fracture towards the matrix. **Figure 4.76** (4-EDS) shows the composition of one of these convoluted fractures at the end tip. The core of the fracture has Ca and Mg (implying dolomite composition). However, the flowering texture (light brown in PPL) is composed of Mg, but without Ca (implying Magnesite composition). The matrix is mostly composed of clays with a high content of Silicon (Si) and

Aluminum (Al) elements; the ductility of this clay-rich bed is the reason why this fracture ended at that point and did not propagate any further.

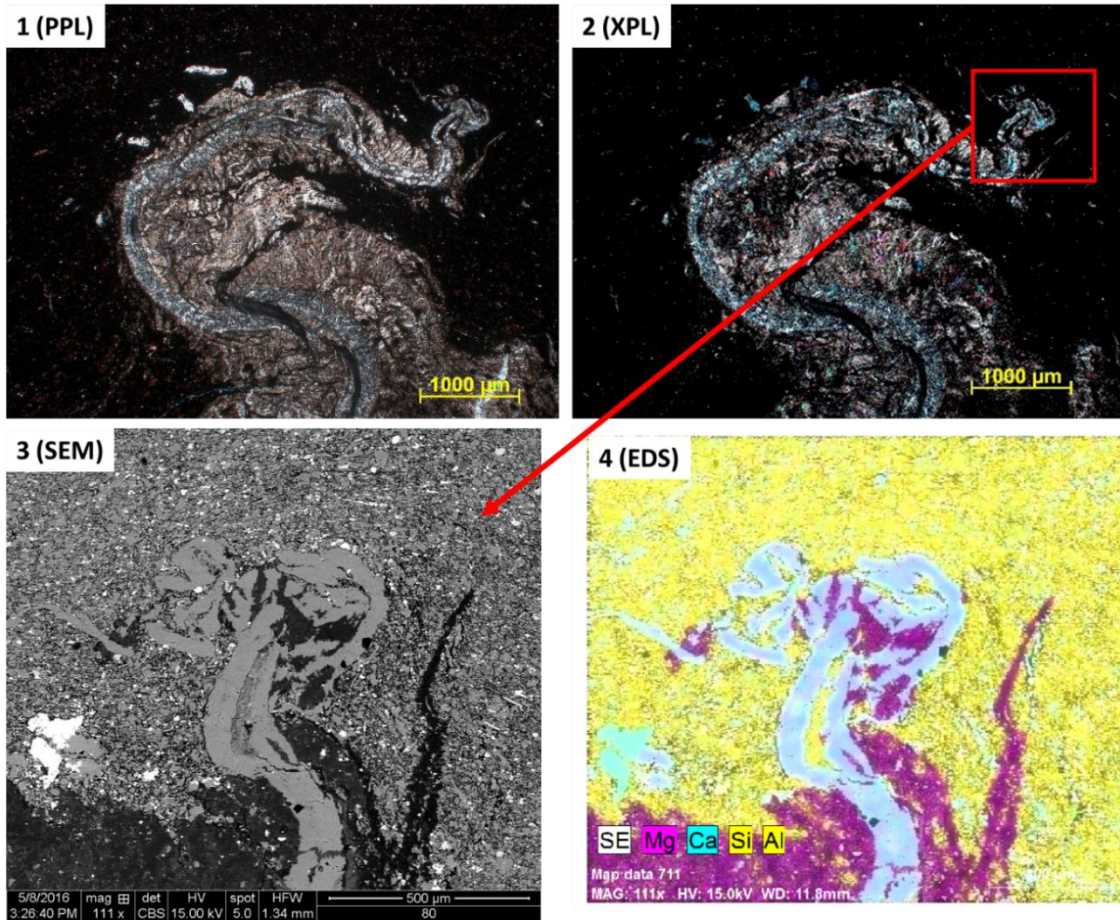


Figure 76 Petrographic Microscope image (1-PPL, 2-XPL), SEM image (3), and composition from EDS (4) of the end tip of a pre-compaction fracture (Colors represent elements identified by EDX).

In contrast, relatively straight fractures are composed in some cases by dolomite, other cases by calcite, and quartz (**Figure 77**). These “straight” fractures show less presence of Magnesite on the sides compared to the pre-compaction fractures.

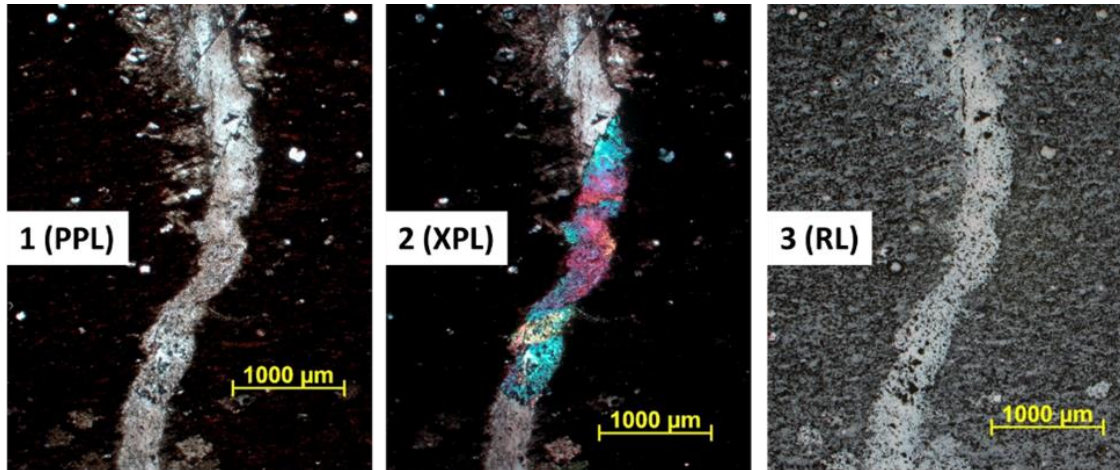


Figure 77 Relatively Straight Fracture. Observe Calcite in XPL and presence of Magnesite on the side of fracture. Not as extensive as in the convoluted fractures.

However, the chalcedony replacement is more predominant in a Straight Fracture (**Figure 78**: red arrow in XPL and RL). Chalcedony appears to be later in the fracture compared to the early diagenesis chalcedony of the Radiolarians and Tasmanites in the matrix.

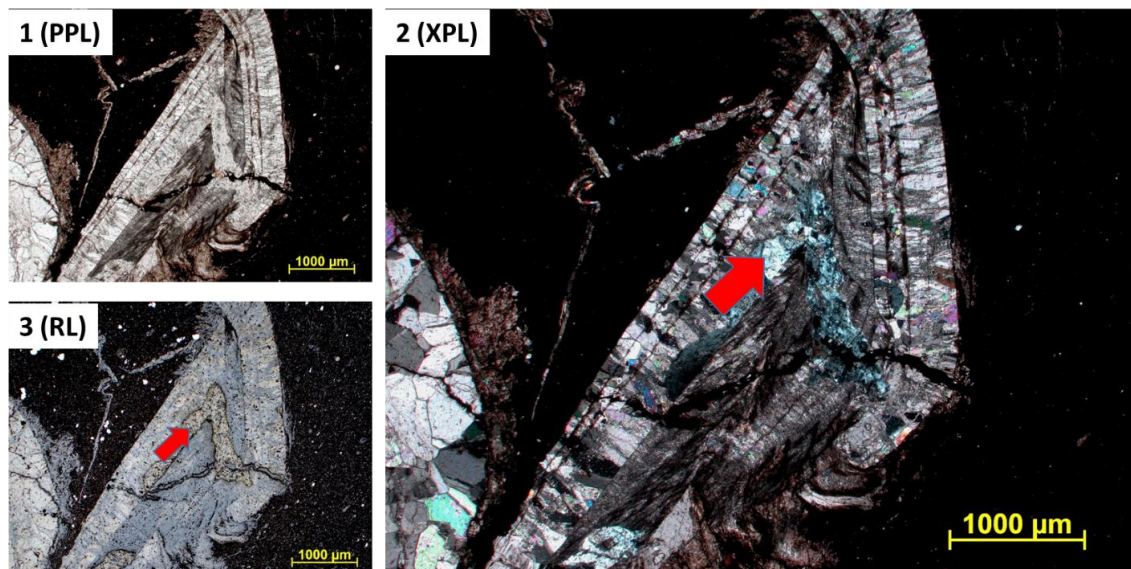


Figure 78 Relatively straight fracture filled with calcite and dolomite. Chalcedony is overprinted in the fracture texture (red arrow).

One feature present in both fractures, convoluted and straight fractures, is the “shear” texture (**Figure 79**). This texture might be related to offset of the fracture during precipitation of the minerals. When this sample is analyzed under SEM and EDX, it shows that the core of the fracture is made of calcite (blue), the "shear" texture is made of dolomite and magnesite as is observed in **Figure 4.80**.

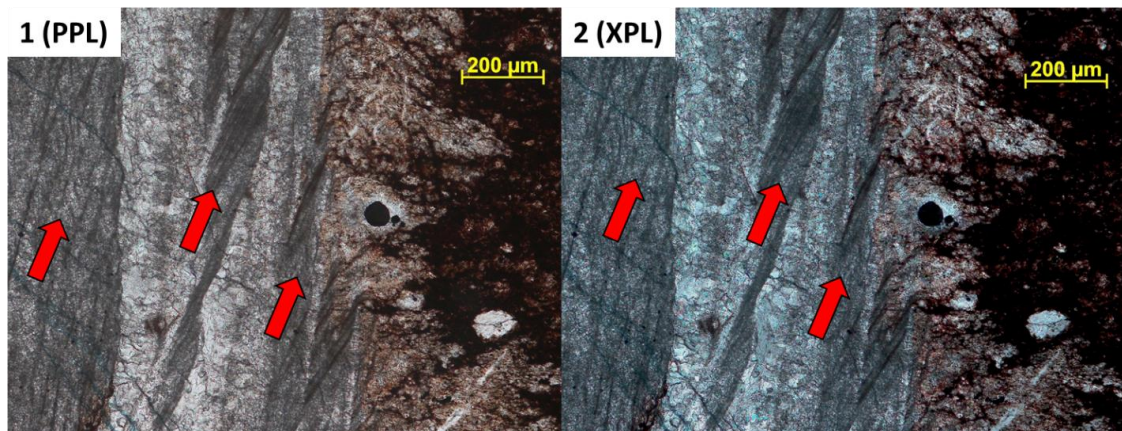


Figure 79 Shear texture (red arrows) inside a mineralized fracture. Image from Petrographic microscope.

This “Shear texture” might be drilling-induced or made when slabbing the core. However, there is not substantial evidence that supports that hypothesis because this "shear texture" is present in several of the intervals of the core including fracture surfaces that were not slabbed or in direct contact with the drilling barrel/bit.

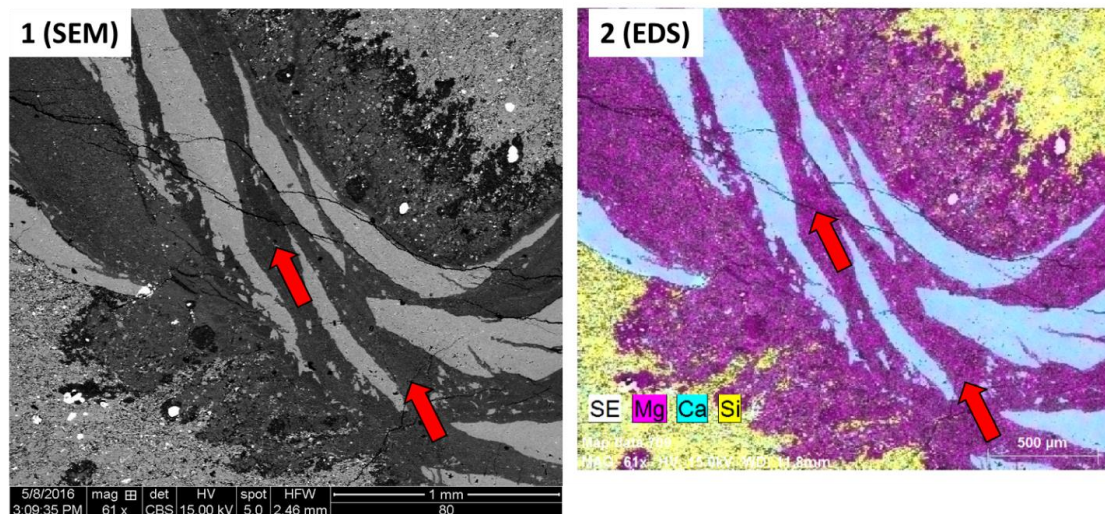


Figure 80 Shear texture (red arrows) under SEM and composition obtained from EDS. Fracture core is made of calcite. Shear is made of magnesite and dolomite. Flowering is also present on the sides of the fracture.

4.5 Paragenetic Sequence

Figure 81 shows the proposed paragenetic sequence for the Marietta Basin Woodford Core. The timing of the events is based on the cross-textural relationship of minerals, the relationship of the elemental and mineralogic composition, the characteristic of contacts between minerals, and the geometry of fractures and allochems. Ptygmatic (convoluted) fractures are very early because they are formed and mineralized (calcite and dolomite) before compaction. Pyrite and Chalcedony in the allochems (Radiolarians and Tasmanites) must be very early, also before compaction, making them resistant to fracturing during compaction, therefore, preserving their perfect circular shape after compaction. Phosphate nodules are commonly associated with early diagenesis. Shear Texture (if not induced) might be middle to late diagenesis; and vertical fractures appear to be later in the diagenetic timeline. Silica in the fractures (as chalcedony and crystals) are also middle to late diagenesis. Magnesite appears to be also middle diagenesis because of their overprint on the matrix and along the sides of the fractures. Finally, Barite

precipitation is the latest event, present mostly in the phosphate as an overprint of the other features.

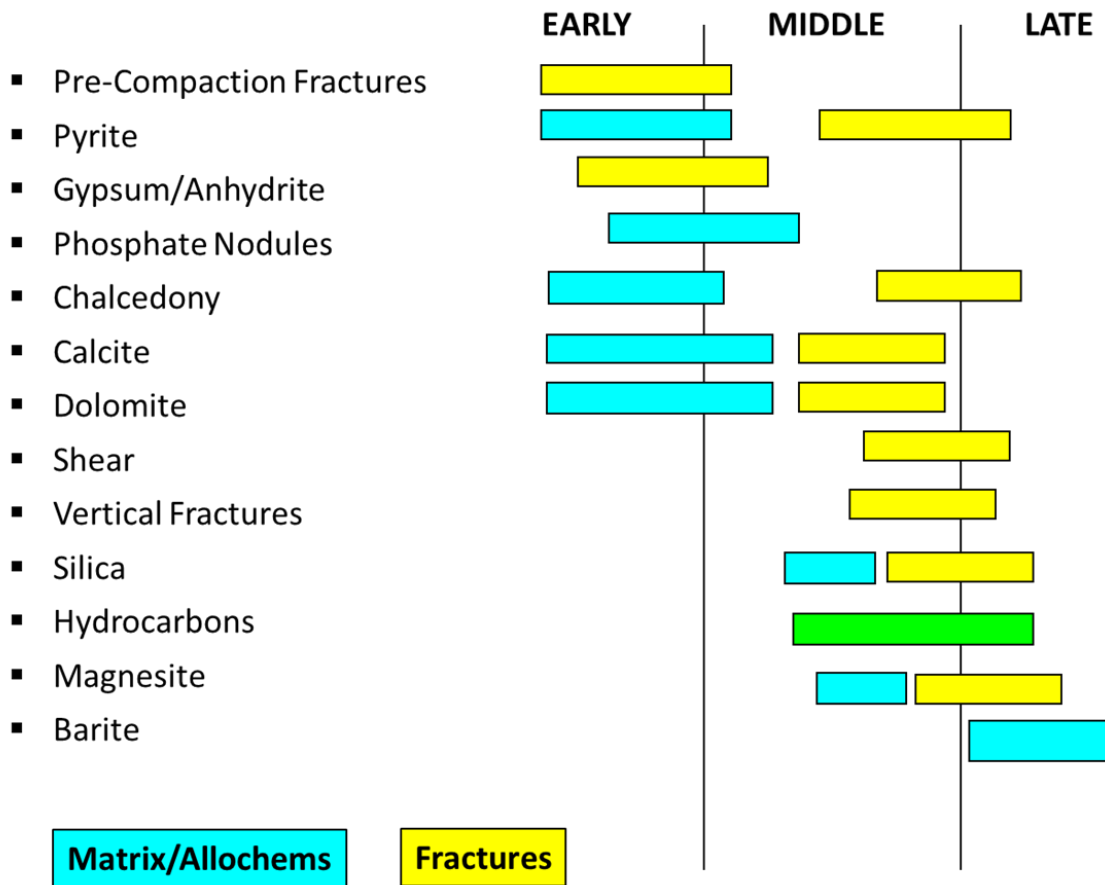


Figure 81 Proposed Paragenetic Sequence of the diagenetic events and features present in the Marietta Basin Core.

The Woodford Shale in the Marietta Basin has very complex diagenesis that includes many diagenetic alterations in the matrix and fractures that occurred before compaction and others that are after compaction.

The interaction between calcite-dolomite-magnesite in the fracture is a feature not very common in other organic-rich shales. However, these features have been found before in Woodford Shale samples in another core tens of miles north in the Anadarko Basin by Roberts et

al. (2017). This interrelation of magnesium with and without the presence of calcium is an effect that should be studied more in depth in future work.

In the case of Tasmanites, there is evidence that early silica cementation results in the preservation of their circular shape, particularly, in low sedimentation facies. However, if they are not cemented early enough, they tend to get flattened by burial and compaction. The Tasmanites and Radiolarians, which are the main allochems in the Woodford Shale, were expected to be only filled with microcrystalline quartz. However, they have many different diagenetic alterations, from those filled with bitumen bounded by silica rims and magnesite crystals inside, to the ones present inside the phosphate almost entirely replaced by apatite.

Fractures appear to be created in the siliceous rich shales, but they do not propagate through the clay-rich zones which are more ductile. This feature has an important implication on hydraulic fracking for unconventional shale because they could serve as an essential criterion to choose in which interval the horizontal well should be placed to optimize the creation of hydraulic fractures. The effect of the matrix composition in fractures propagation is one of the most significant findings of this work. It proves that the relationship of facies and stratigraphy with generation and geometry of fractures (also known as Mechanostratigraphy) is an important relationship in the Woodford Shale. This is the primary foundation used when creating 3D fracture models and it means a facies model must be generated and used as input for the artificial fracturing model.

Chapter 5: Geochemistry and Geomechanics

The Geochemical and Geomechanical properties are the most deciding factors in the assessment and characterization of unconventional resource shales to drill and complete wells to produce hydrocarbons effectively. Geochemistry affects the Reservoir Quality (RQ), and Geomechanics affect the Completion Quality (CQ) of a rock, and both are intrinsically related (Breyer et al., 2016).

Reservoir Quality (RQ) of an unconventional reservoir relates to porosity/permeability, organic richness, kerogen type, and thermal maturity of the rock; which provide information about how much hydrocarbons are in the rock formation. In contrast, Completion Quality (CQ) corresponds to how easy it is to frack the reservoir to create induced hydraulic fractures; therefore, increasing the pathways (permeability) for hydrocarbons to flow back to the wellbore.

There is previous work done regarding the Geochemistry and Geomechanics of the Woodford Shale. The research of Ghosh (2017) is the most comprehensive work done in the study of fractures sets in the Woodford Shale and how they correlate to different tectonic events and hydrocarbon expulsion. Becerra (2017, 2018) correlated Rebound Hardness data with Uniaxial Compressive Strength (UCS), and lithofacies in outcrops of the Woodford Shale in southern Oklahoma. Miceli (2010) combined source rock characterization with biomarker analysis of Woodford Shale cores in central Oklahoma. Connock (2015) studied the geochemistry of the Woodford Shale in the McAlister Cemetery Quarry Woodford Section. Wang (2016, 2019) studied the oil families tied to the Woodford Shale in the Anadarko Basin area. Finally, Cardott (1989; 2009a; 2009b);

2012, and 2014) provides the most comprehensive studies done about the thermal maturity of the Woodford Shale.

The structure of this chapter follows a similar style to the previous chapters. First, the discussion of the available data and methodology of each topic (geochemistry and geomechanics), then the results of organic richness, kerogen type, and thermal maturity are discussed, to finally close with the discussion of the fracture analysis and rebound hammer data results.

5.1 Data and Methods

The geochemistry data includes the RockEval data and the Vitrinite Reflectance data. The operator of the extracted Marietta Basin Woodford Core sent 23 samples to Weatherford Laboratories to perform RockEval Pyrolysis analysis and 14 samples to measure Vitrinite and Bitumen Reflectance. **Figure 82** shows the location of these samples in the stratigraphic profile of the core.

The RockEval pyrolysis consists of heating the pulverized rock sample in vacuum during an interval of time then analyzing the hydrocarbons (HC) and carbon dioxide (CO₂) expelled by the sample in that same interval of time. The RockEval pyrogram reflect the results in visual form (**Figure 83**). From the pyrograms, the laboratory interprets the values S1, S2, S3, and Tmax. Then, they calculate the values of Hydrogen Index (HI) and Oxygen Index (OI).

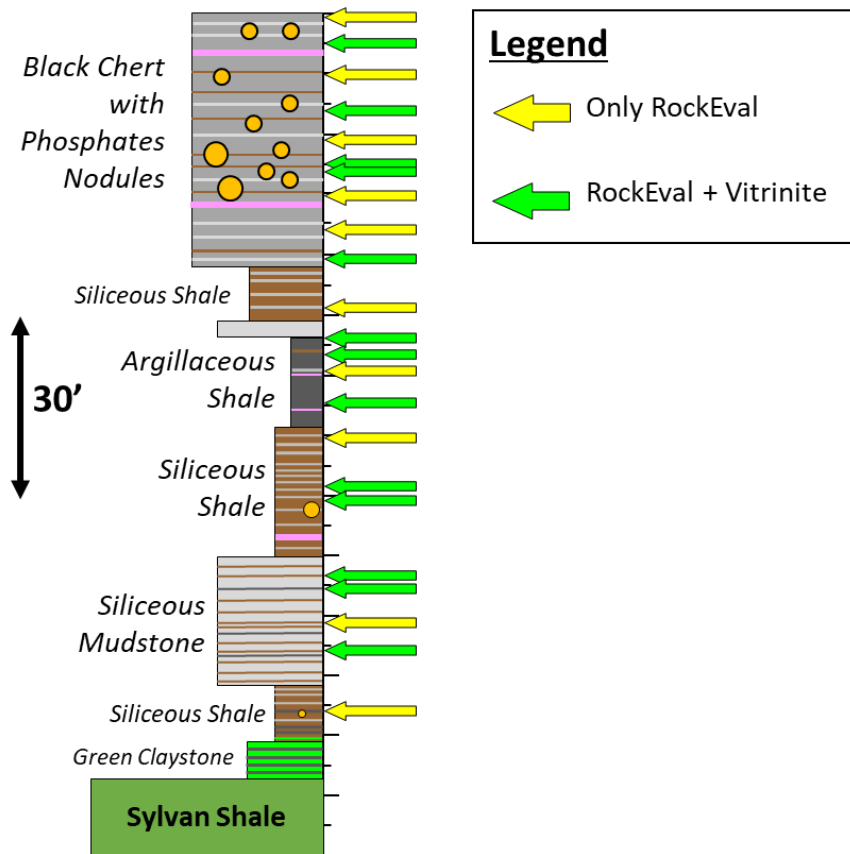


Figure 82 showing the locations of the samples taken for RockEval Pyrolysis and Vitrinite Reflectance analysis in the Woodford Shale Core.

LECO TOC measures the amount of Total Organic Carbon (TOC) similarly to RockEval Pyrolysis, although the samples need additional pre-treatment before applying heat. Samples are powdered and weighed, and then chemically treated with acid to remove inorganic carbonate material and left to dry over time to release free hydrocarbons.

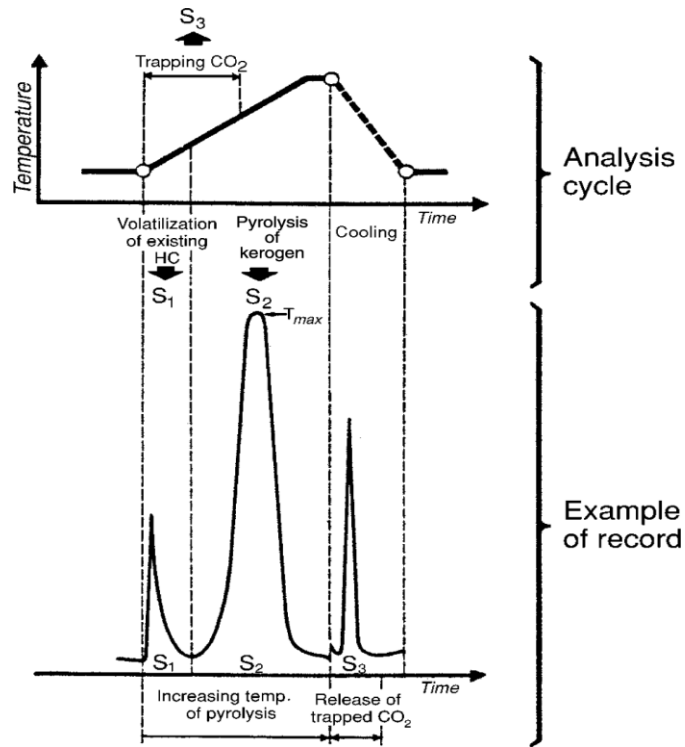
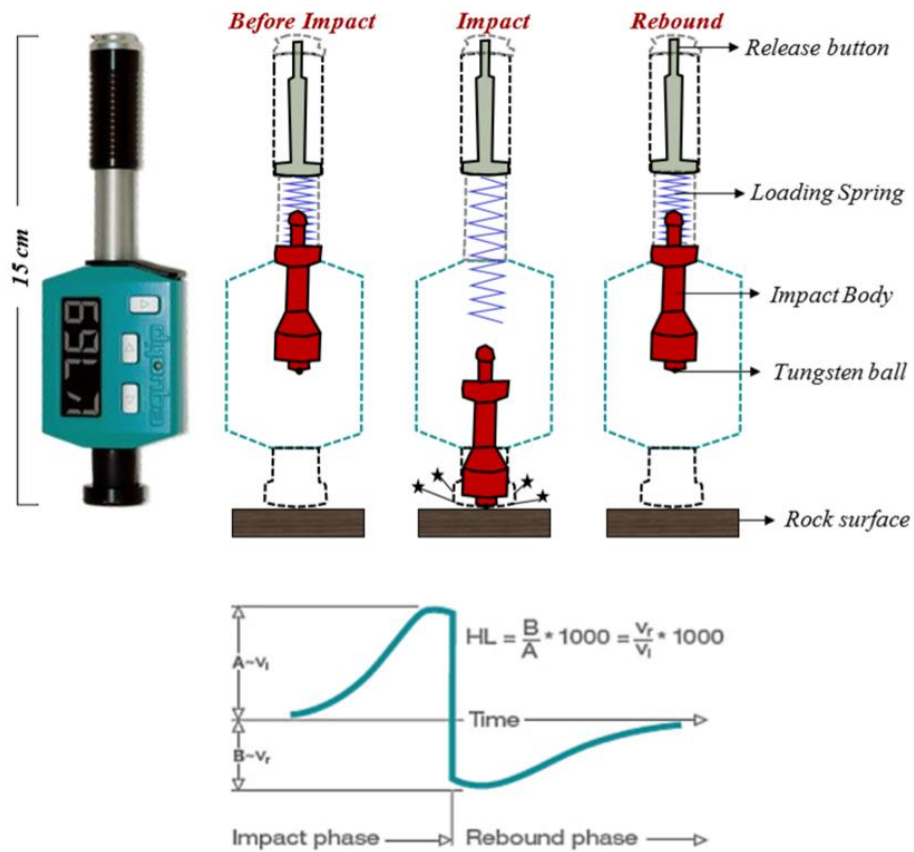


Figure 83 showing an example of a RockEval Pyrogram. S1, S2, S3, and Tmax values are interpreted from the peaks of the pyrogram and the temperature at which they reach those peaks.

For geomechanics, the equipment to measure Rebound Hardness data is the Equotip Piccolo 2 from Proceq. This tool lets a 3-millimeter tungsten carbide ball drop onto the rock sample from a spring in the upper part of the equipment and then measures the velocity of the impact, and the velocity of the rebound to calculate Rebound Hardness values (unitless). **Figure 84** shows a diagrammatic representation of the Rebound Hardness test.

Rebound Hammer data was measured perpendicular to the "slab" surface of the core in every same location where X-Ray Fluorescence data was acquired. In each location, five to ten measurements were taken, then the highest 20% and the lowest 20% (Upper/Lower 20 Filter) of the measurements were removed to eliminate spikes. The final value consists of the average of remaining measurements after applying the Upper/Lower 20 Filter from the same stratigraphic

bed. In total, there were 1536 stratigraphic locations for Rebound Hammer tests in the core. Each of the stratigraphic locations had 5 to 10 measurements. The raw total of Rebound Hammer points was 10,360 measurements.



$$\text{Hardness (LH)} = \frac{\text{Rebound velocity (Vr)}}{\text{Impact velocity (Vi)}} * 1000$$

Figure 84 Operation mechanism of the Rebound Hardness equipment (modified from Becerra, 2017)

5.2 Organic Richness

The most common measurement to study the organic richness of a source rock is Total Organic Carbon (TOC) content. TOC stands for Total Organic Carbon, and it reflects the amount of organic carbon in rocks. TOC is usually represented as weight percent (wt.%).

The TOC in the Marietta Basin Woodford Shale core ranges from 2.93 to 9.75wt.% with an average value of the 23 tested samples of 6.06wt.%. However, the average TOC differs by the lithofacies of each sample. There are some lithofacies prone to higher TOC values compared to others. For example, the TOC of the Argillaceous Shale (AS) facies ranges from 7.23 to 9.75wt.% and its average is 8.49wt.%, which is considerably higher than the average of the full dataset. In contrast, the TOC of the Black Chert (BC) facies ranges from 2.93 to 4.18wt.% with an average of 3.52 wt.%; the lowest TOC in the Woodford Shale section. The TOC of the Siliceous Mudstone (SM) facies ranges from 4.34 to 6.57wt.% with an average of 5.30wt.%. Finally, the TOC of the Siliceous Shales (SS) facies ranges from 6.21 to 8.0wt.%. No samples were taken from the Green Claystone (GC) facies by decision of the company owner of the core because TOC was expected to be negligible in the GC facies. **Figure 85** shows a series of source rock evaluation depth plots; the first track shows the distribution of TOC in the Marietta Basin Woodford Shale core.

Log 1 in **Figure 85** is called the Organic Richness, and it is the depth plot of Total Organic Content. On the left side of the figure is the stratigraphic description of the Marietta Basin Woodford Core. The color of the points represents the lithofacies. Black box represents the

Black Chert (BC) facies. Yellow box represents the Siliceous Mudstone (SM) facies. Blue circle and Red circle represent the Siliceous Shale (SS) and Argillaceous Shale (AS) facies respectively. The TOC depth plot has a decreasing upward trend. This trend reflects the control of the lithofacies on the distribution of TOC content throughout the section. For example, the TOC is lower in the upper section where the Black Chert dominates which is interpreted to be the Highstand Systems Tract of the Woodford Sequence. This relates to better circulation in the water column during deposition, thus oxidizing organic matter. On the contrary, where the Siliceous Shale and Argillaceous Shale predominate -which is in the Transgressive Systems Tract of the section- the TOC is higher; particularly closer to the maximum flooding surface (mfs). This relationship is very similar and correlates to the TOC distribution by facies in the Speake Ranch Woodford Outcrop (Galvis, 2017). Based on typical ranges of source rocks TOC values, the organic richness of the Woodford Shale in the Marietta Core is excellent and can be compared to other organic-rich source rocks like the Eagle Ford and Barnett Shales in Texas.

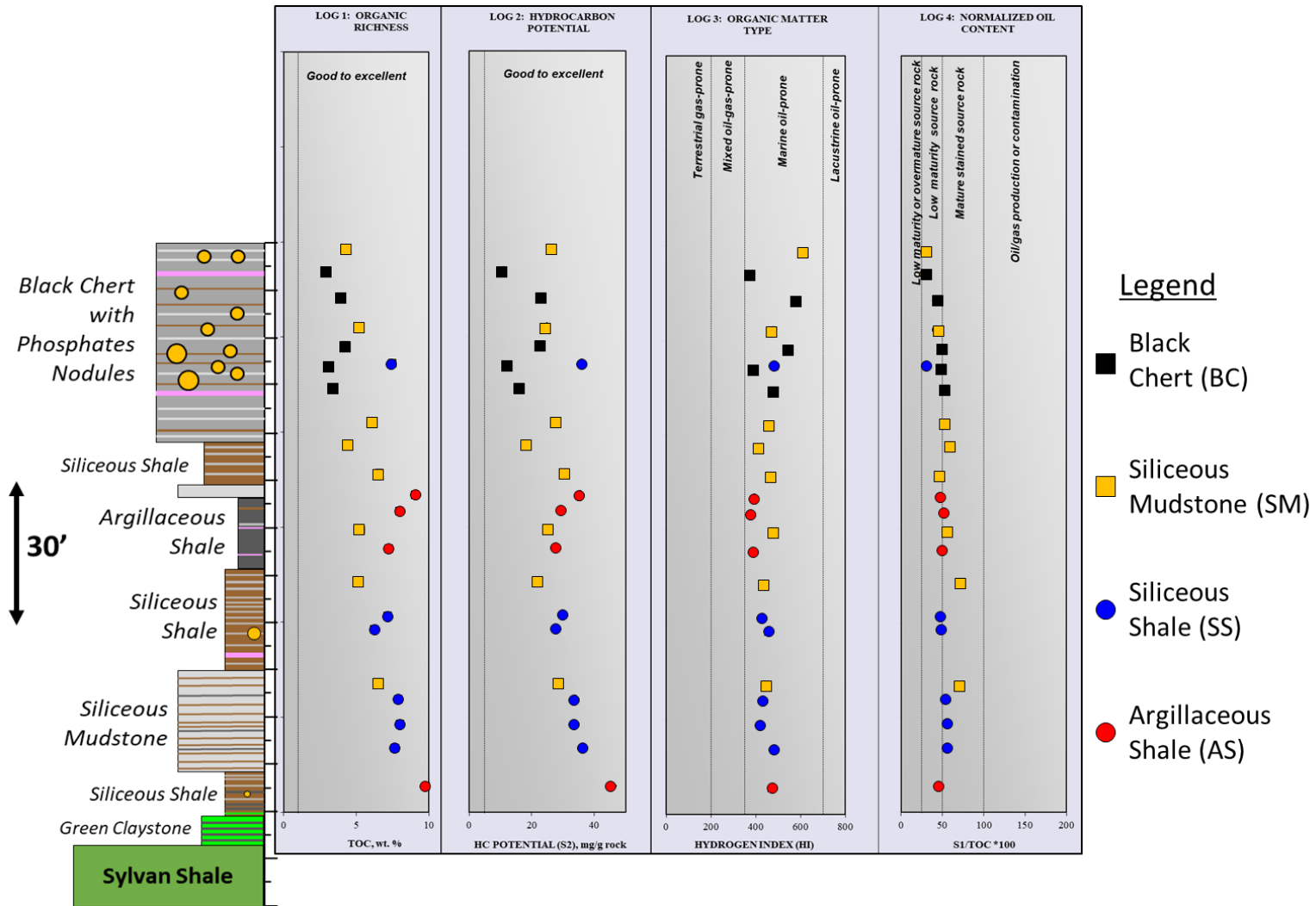


Figure 85 Depth plots of the geochemical parameters. Log 1 is Organic Richness and represents the Total Organic Carbon content of the rock. Log 2 show the Hydrocarbon Potential of the rock. Log 3 and 4 are Hydrogen Index and Normalized oil content logs.

Log 2 in **Figure 85** shows the depth plot of S2 values. S2 values represent the measurement of the second peak in the pyrogram (curve) that results from the Rock-Eval analysis. S2 measures the volume of hydrocarbons that is expelled from the rock during the thermal pyrolysis and is used to estimate the remaining generation potential of hydrocarbons of a sample. Its unit is mg of hydrocarbon per gram of rock (mgHC/g). The hydrocarbon potential (S2) for the Woodford shale section in the Marietta Basin core is very high; it ranges from 10.97 to 45.87 mgHC/gRock with an average of 28.18 mgHC/gRock. The S2 values have a decreasing trend upward similar to the trend present in the organic richness depth plot (**Figure 85**) because the samples are immature and are also controlled by the dominant lithofacies of the samples. These values of S2 for the whole section are evidence that the Hydrocarbon Potential of this Woodford Shale interval is excellent.

5.3 Kerogen Type

The type of kerogen in a source rock is related to the depositional environment and has implications in the resulting type of dominant hydrocarbon (liquid oil or dry gas) that the rock can expel (Tissot and Welte, 1978). The kerogen can be Type I which is oil-prone, and it is usually associated with lacustrine source rocks. The Type II kerogen is oil-prone as well but is associated with organic-rich marine deposits. The Type III kerogen is mainly gas-prone and is associated with terrestrial input and the Type IV is primarily inert material that does not generate hydrocarbons.

There are three standard methods to interpret kerogen type using Rock-Eval pyrolysis data (Peters, 1986; Jarvie et al., 2007): 1) the depth plot of Hydrogen Index (HI); 2) cross-plot

between Remaining Hydrocarbon Potential (S₂) and TOC; and 3) the Modified Van Krevelen diagram.

Hydrogen Index (HI) is calculated multiplying the S₂ values by one hundred and then dividing it by the TOCwt.% measured from that same sample. The unit of HI is mg HC/g TOC. **Figure 85** shows the plot of Hydrogen Index by depth. All the samples plot in the domain of Marine Oil-Prone range. The samples from the upper section of the core have higher HI because their TOC% is lower. However, the hydrocarbon potential of this section is relatively high on average.

The second method to interpret kerogen type is the cross-plot between the remaining Hydrocarbon Potential (S₂) against the TOC% of each sample. **Figure 86** corresponds to this plot. The results show all the samples fit within the area that corresponds to Type II kerogen, also known as oil-prone kerogen, usually marine. Argillaceous Shales (red circles) and Siliceous Shales (blue circles) have the highest TOC values and the highest remaining hydrocarbon potential (S₂) values of the core. Black Chert (BC) and Siliceous Mudstone (SM) have relatively lower values for both HI and TOC.

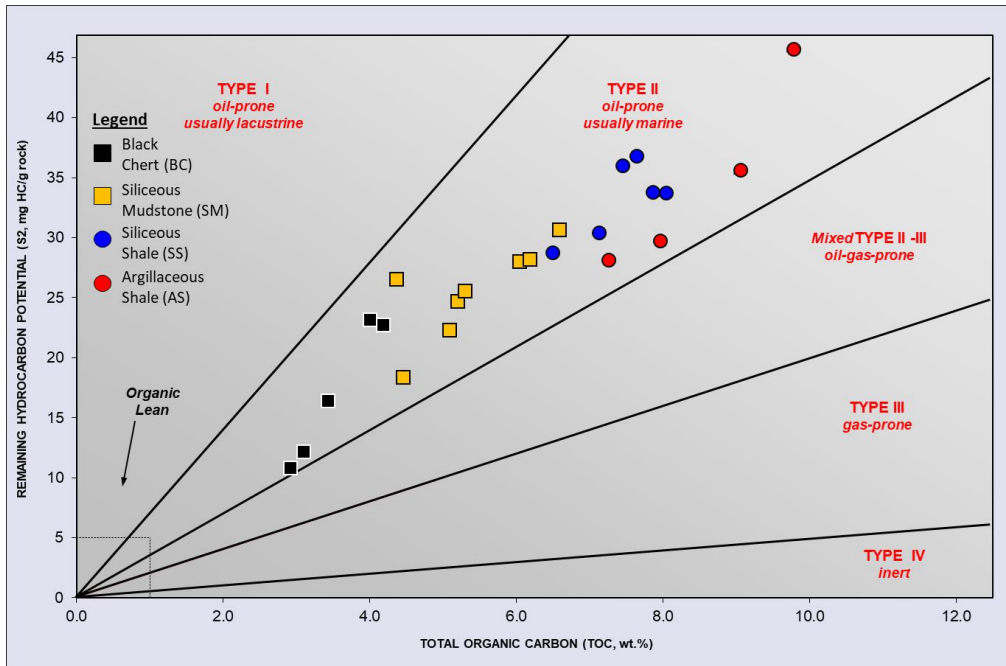


Figure 86 Cross-plot between Remaining Hydrocarbon Potential (S2) and TOC. All the Woodford Shale samples plot within the Type II kerogen (oil prone- marine).

The pseudo Van Krevelen diagram is the plot between Hydrogen Index (HI) and Oxygen Index (OI). Oxygen Index is calculated by dividing the S3 values from Rock-Eval against TOC for all the samples. S3 represents the amount of carbon dioxide (CO₂) released from the source rock sample during pyrolysis. The unit of OI is mg CO₂/g TOC. **Figure 87** shows the pseudo Van Krevelen plot. On this diagram, most of the samples are Type II kerogen. In summary, by comparing HI versus depth, TOC, and OI (**Figures 85, 86, 87**), and by integrating this information with the core description from Chapter 3, there is enough evidence to conclude that the organic matter present in the Woodford Shale in this area must be predominantly Type II kerogen, which is associated with marine depositional environments. Additional research is being conducted by Torres (2019) at the University of Oklahoma in order to verify if there is any lacustrine or hypersaline-related kerogen in the Woodford Shale.

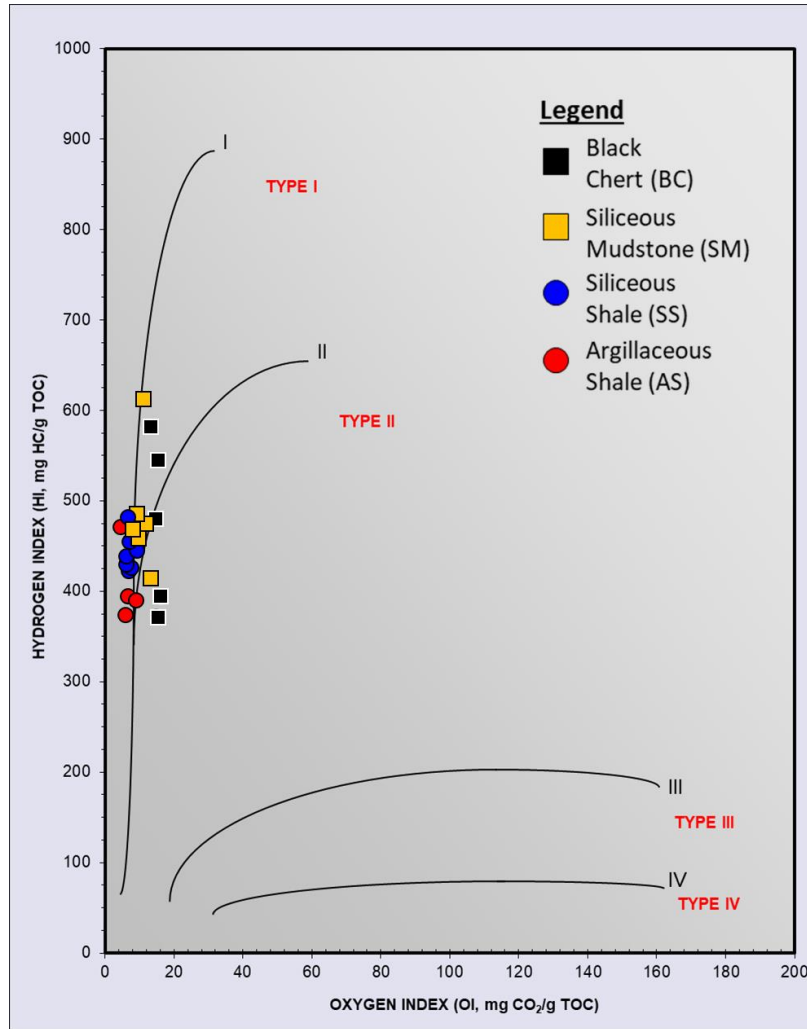


Figure 87 Pseudo Van-Krevelen diagram (Hydrogen Index vs. Oxygen Index).

5.4 Thermal Maturity

Thermal Maturity is probably one of the most critical parameters that define the capability of an unconventional resource shale to produce hydrocarbons. It is the degree of heat-controlled reactions that transform the organic matter in the rock. If the thermal maturity is too high the source rock is overmature, and it might have expelled all the possible hydrocarbons into other shallower formations. In contrast, if the thermal maturity is low, then the rock is immature, and has not being subjected to enough temperatures for a long enough time to transform the

kerogen into hydrocarbons. Furthermore, the thermal maturity defines what type of hydrocarbons an operator could mainly produce from an unconventional resource; either liquids, wet gas, or dry gas.

There are several methods to measure or calculate the thermal maturity of a source rock. The most common analyses in the oil and gas industry are the measurement of vitrinite reflectance and the measurement of Tmax from Rock-Eval Pyrolysis. Vitrinite reflectance is probably the most common method, but it has the limitation that vitrinite, a terrigenous, woody maceral is not always present in significant amounts in source rock samples of marine origin and it is an interpretative visual measurement. If vitrinite is in low amounts or not present in the sample, then solid bitumen can be used as a proxy for thermal maturity by calculating an Equivalent Vitrinite Reflectance (eVRo) using the equation proposed by Jacob et al. (1989). This calculation is used for organic-rich shales where $eVRo = 0.618 \times (Bitumen\ Reflectance) + 0.4$. **Figure 88** shows the depth plot of measured vitrinite reflectance (black data points), solid bitumen reflectance (green data points), and equivalent vitrinite reflectance (red data points). These values represent the mean value of several (20 to 50) point measurements made in the source rock samples. The measured vitrinite reflectance ranges from 0.73%VRo to 0.85%VRo with an average of 0.79%VRo. The measured bitumen reflectance ranges from 0.54%BRO to 0.61%BRO, with an average of 0.59%BRO. After using Jacob et al. (1989) equation to convert BRO to eVRo, the results range from 0.73%eVRo to 0.78%eVRo with an average of 0.76%eVRo. **Figure 88** shows how close the calculated values are from the measured values. In most of the samples, the calculated vitrinite reflectance (eVRo) is slightly lower than the

measured vitrinite reflectance (VRo). Additionally, two samples did not have enough vitrinite to provide statistically representative values for VRo; therefore, these samples only have eVRo.

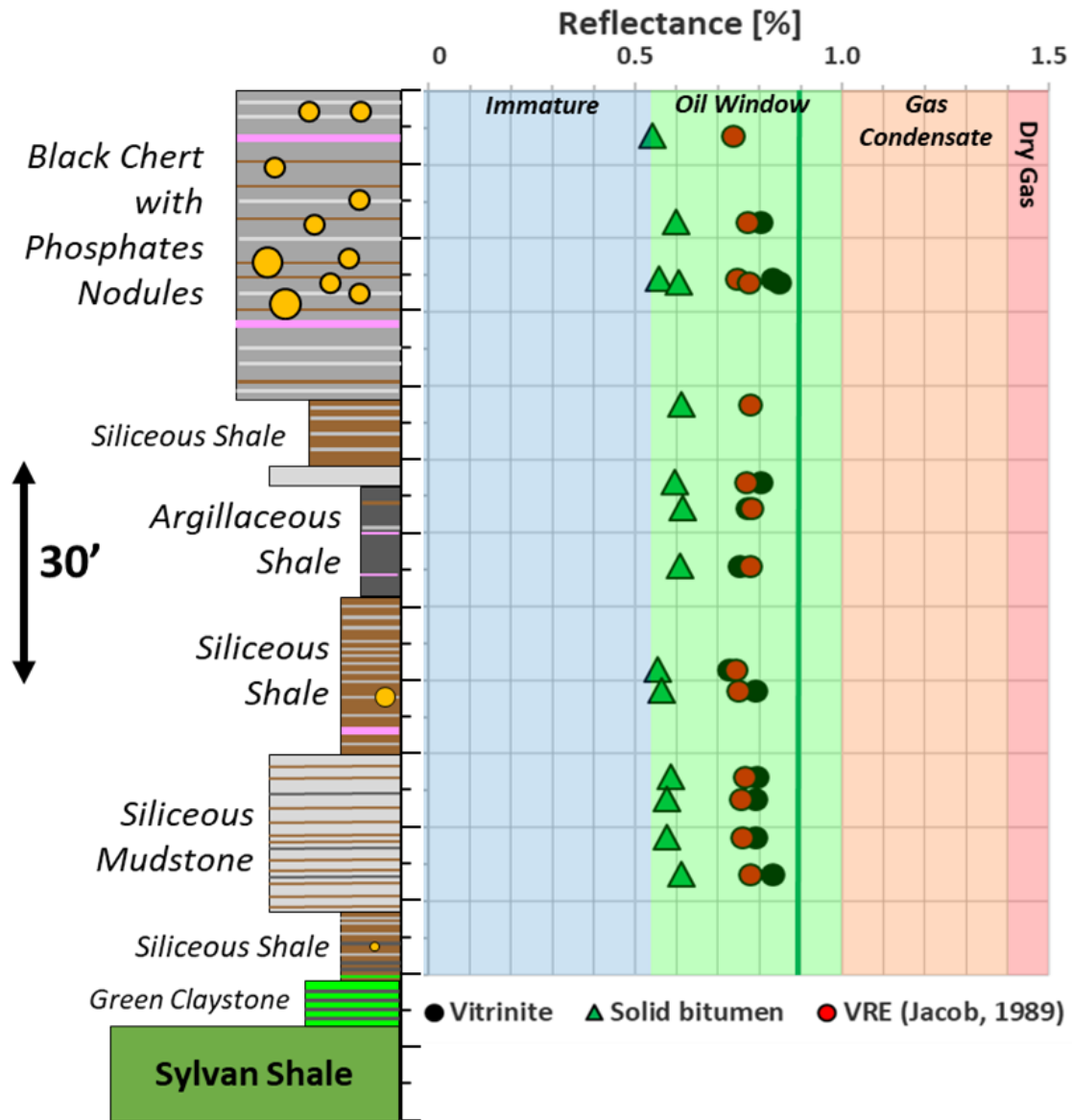


Figure 88 Depth plot of Vitrinite Reflectance along the Marietta Basin Woodford Core. Measured vitrinite reflectance is in black, red is calculated, green is bitumen. Bitumen reflectance is usually suppressed in comparison to vitrinite reflectance. VRO% average is 0.79 (oil window).

The results from the estimation of thermal maturity from the measurement of vitrinite reflectance show that every sample from the core is within the oil window (0.55% VRo to 1.10

%VRo). At present day, this section of the Woodford Shale in the Marietta Basin is prone to produce liquid oil instead of gas condensates or dry gas.

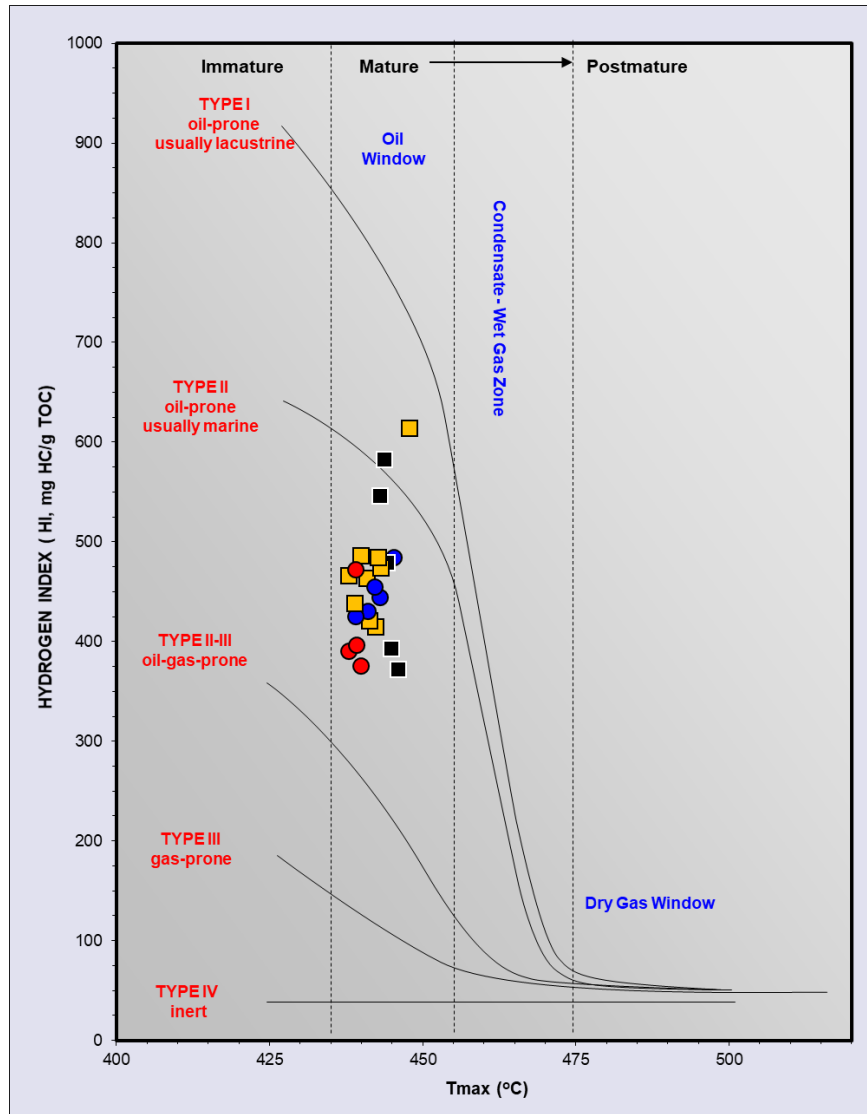


Figure 89 Cross-plot between Hydrogen Index and Tmax. Most of the samples plot within the oil window area and close to the Type II (oil-prone / marine) kerogen.

The second most used method for estimating thermal maturity is the plot of HI versus Tmax, standard output parameters from Rock-Eval pyrolysis. This method is less expensive and simpler to perform than vitrinite reflectance measurements, and it needs fewer quantities of rock

samples. Tmax is the temperature at which the S2 peak reaches its maximum height during the pyrolysis of the source rock. **Figure 89** shows the HI vs. Tmax plot, and it is color-coded by lithofacies. The values of Tmax for the Marietta Basin Woodford Core range from 438°C to 448°C, with an average of 442°C. In this graph, most of the core samples plot within the oil window and between the Type II (oil-prone) and the Type II-III (Oil-Gas prone) mixed kerogen.

In conclusion, the Woodford Shale section in the Marietta Basin core is a rock interval with excellent organic richness (high TOC), high remaining hydrocarbon potential (high S2), dominated by Type II oil-prone kerogen, and currently in the oil window based on thermal maturity estimations from vitrinite reflectance and Tmax. Hence, it has excellent characteristics for major exploration and development of this asset as an unconventional resource shale by horizontal drilling and hydraulic fracturing in the Marietta Basin.

5.5 Rebound Hardness

As explained in the introduction of this chapter, geomechanics is the other key factor to assess before and during the drilling and completion of horizontal wells in the Woodford Shale. Rebound Hardness data help to understand how hard or soft the rock is. Work done by Becerra (2017; 2018) show a strong correlation between rebound hardness and brittleness of the rocks; and the composition of the lithofacies mostly drives this correlation. This correlation is also present in this section of the Woodford Shale. **Figure 90** shows the resulting rebound hardness data in a depth plot and correlated to the respective lithofacies described in the core. The ranges are variable in each section showing the effect of highly interbedded stratigraphy of the Woodford Shale. Therefore, it is critical to observe the main trends in the data along the stratigraphy. The resulting profile shows the lower values of rebound hardness (<600) are prevailing in the intervals where the Siliceous Shale (SS) and Argillaceous Shale (AS) facies dominate (red arrows). The intervals dominated by Siliceous Mudstones have high values of hardness (>600). The uppermost section, which is dominated by black chert facies and phosphate nodules have the highest ranges of hardness in the section. Data supports the interpretation that the Highstand Systems Tract (HST) is harder than the Transgressive Systems Tract (TST), and the most ductile rocks are located within the Condensed Section (CS) of the sequence. This correlation is reasonable because the TST facies are usually dominated by higher clay content than the HST facies.

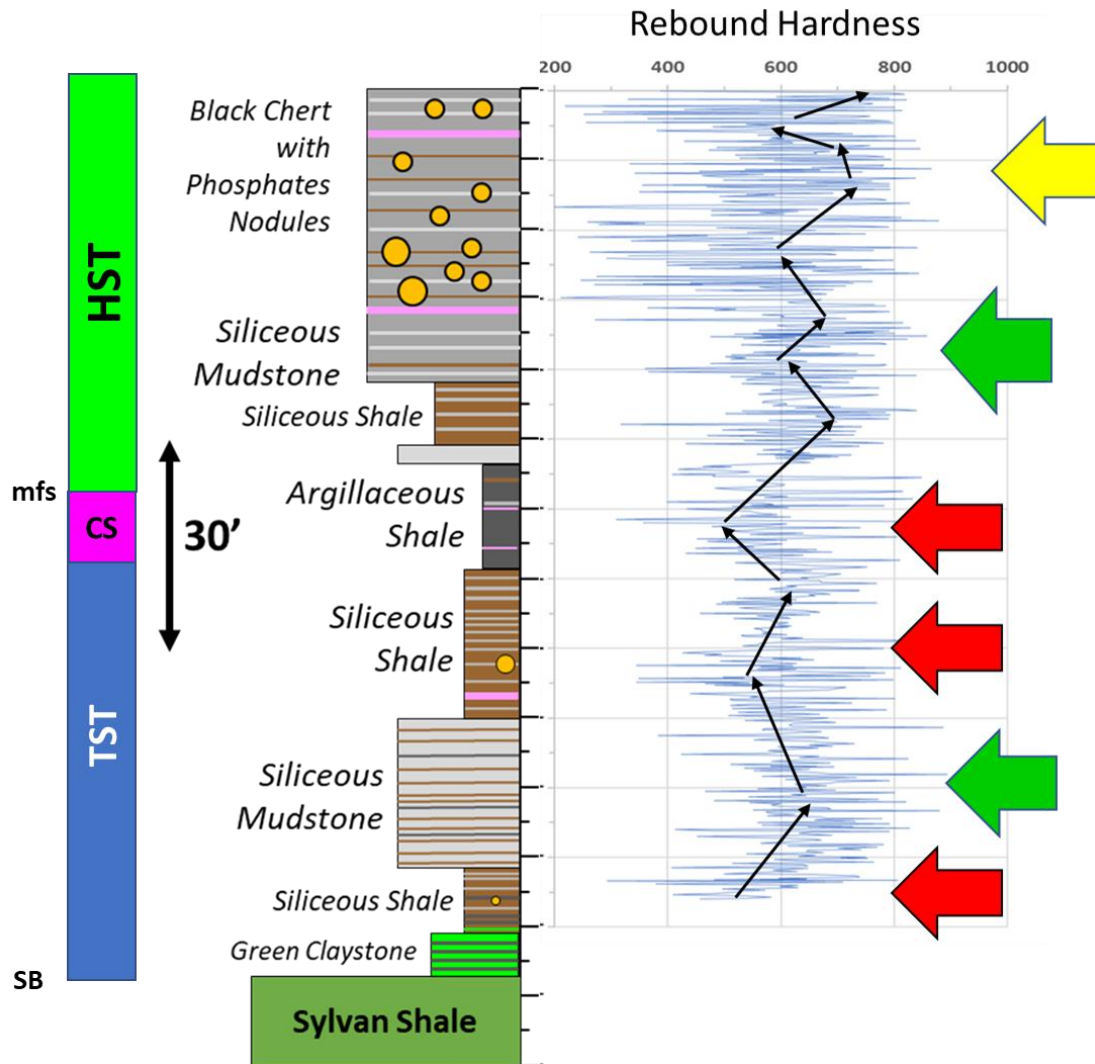


Figure 90 Stratigraphic correlation between Rebound Hardness (RH) data, facies vertical distribution, and sequence stratigraphy. TST is a softer interval than the HST. Condensed section is the most ductile. Red arrows show soft sections, green hard sections, and yellow very hard sections. Black arrows show the main trends in RH data.

The reason there is a relationship between lithofacies and rebound hardness data is due to the mineralogy of these rocks. Lithofacies like Argillaceous Shales and Siliceous Shale have a higher clay content than the Siliceous Shales and Black Chert Facies. Figure 5.10 shows a plot of rebound hardness data versus clay content; lithofacies are color-coded to observe the correlation with the data. There is an inverse relationship between rebound hardness and clay content.

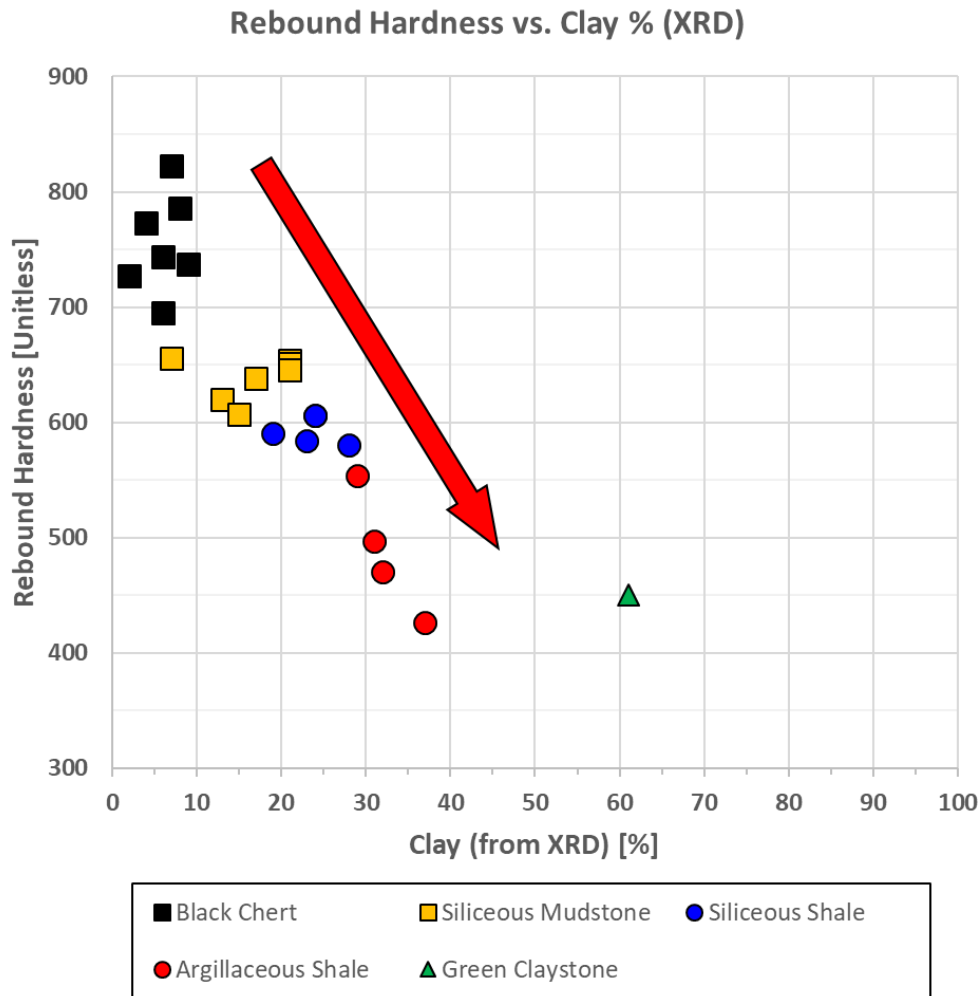


Figure 91 Cross-plot between Rebound Hardness and Quartz content (XRD). There is an inverse relationship between these clay content and rebound hardness data.

Therefore, the argillaceous shale which dominates the condensed section of the Woodford Sequence has the highest amount of clay, but also it has the lowest amount of quartz. Green Claystones also have very low quartz content and high clay content, but they are restricted to the basal section of the Woodford shale. **Figure 92** shows the direct relationship between rebound hardness and quartz content — higher quartz in the rock, the higher the rebound hardness.

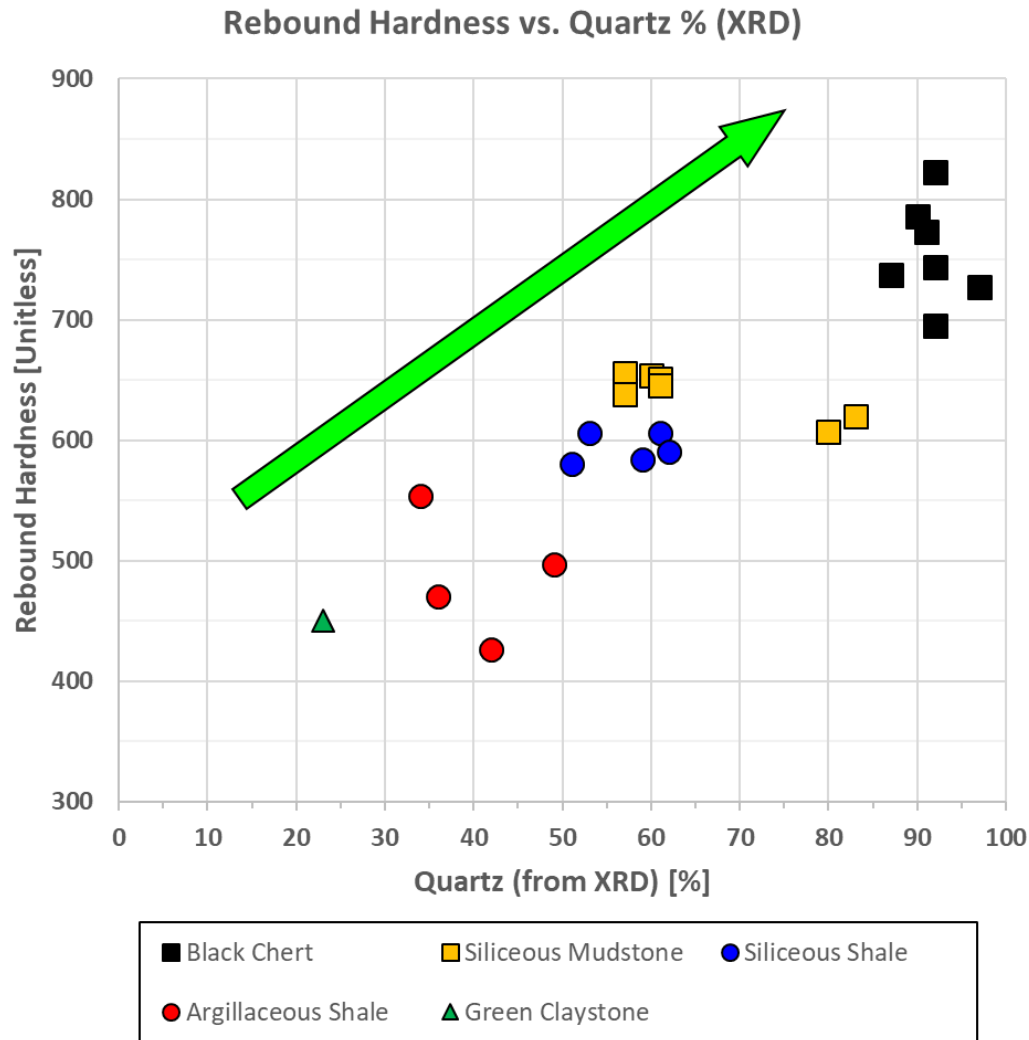


Figure 92 Cross-plot between Rebound Hardness and Quartz content (XRD). There is a positive relationship between these two variables. Facies color-coded.

Black Cherts are the hardest rocks in the Woodford Core. However, if the rocks are too hard, the drilling bit needs more effort to go through them resulting in slower drilling times and therefore higher operating costs when targeting that specific section. Additionally, as discussed earlier in this chapter, black cherts have the lowest TOC content in the section, making them lower Reservoir Quality (RQ) compared to other lithofacies.

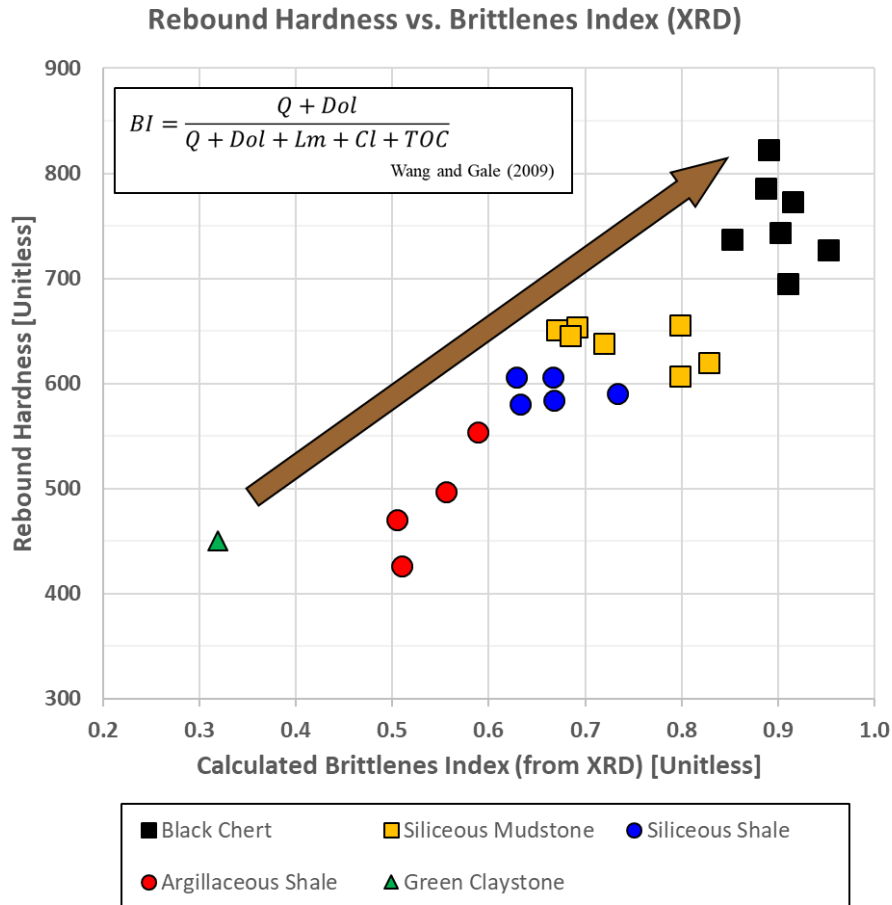


Figure 93 Cross-plot between Rebound Hardness and Mineralogical Brittleness Index (using Wang and Gale's equation). High Rebound Hardness correlates with high Brittleness Index. Facies color-coded.

Instead of analysis mineral by mineral with the rebound hardness data, a better way is to look at the Brittleness Index of the rock calculated using X-Ray Diffraction data in combination with TOC content using Wang and Gale's (2009) Brittleness relationship. TOC, as it generates a ductile material decreases the brittleness of the rock. **Figure 93** shows the plot between rebound hardness and Mineralogical Brittleness Index. According to the data, there is a direct positive correlation between hardness and brittleness. Higher the Brittleness Index due to the higher content of quartz and lower content of clay and TOC results in the higher values of rebound

hardness and vice-versa. Therefore, because lithofacies are also controlled by mineralogy, then harder lithofacies (BC and SM) are more brittle than softer/ductile lithofacies (AS, SS, and GC).

In conclusion, using the Rebound hardness data shown in **Figure 94**, the best target zones with high Completion Quality (QC) are where the Siliceous Mudstone facies dominates, and it is interbedded with organic-rich Siliceous Shales and a few Argillaceous Shales. Green arrows indicate these good target sections in Figure 94. Sections dominated by Argillaceous Shales are very organic-rich but have a higher clay content; therefore, making the rock softer and more ductile, reducing the distribution of fractures in the section and making it harder to produce hydrocarbon from the rocks effectively. These more ductile sections are shown with the red arrows. Finally, the uppermost section is very brittle because it is mainly chert beds, but they cause other issues like low drilling times and more expensive operations when being targeted. Therefore, the best target is right above the maximum flooding surface and just below the Black Chert/ Phosphate Nodules section. This target section forms an ideal brittle/ductile couplet to be drilled and completed.

The next chapter contains the thickness maps of these stratigraphic sections and the target zone, and how they correlate to the current Woodford Shale production in the active area of this asset in the Marietta Basin.

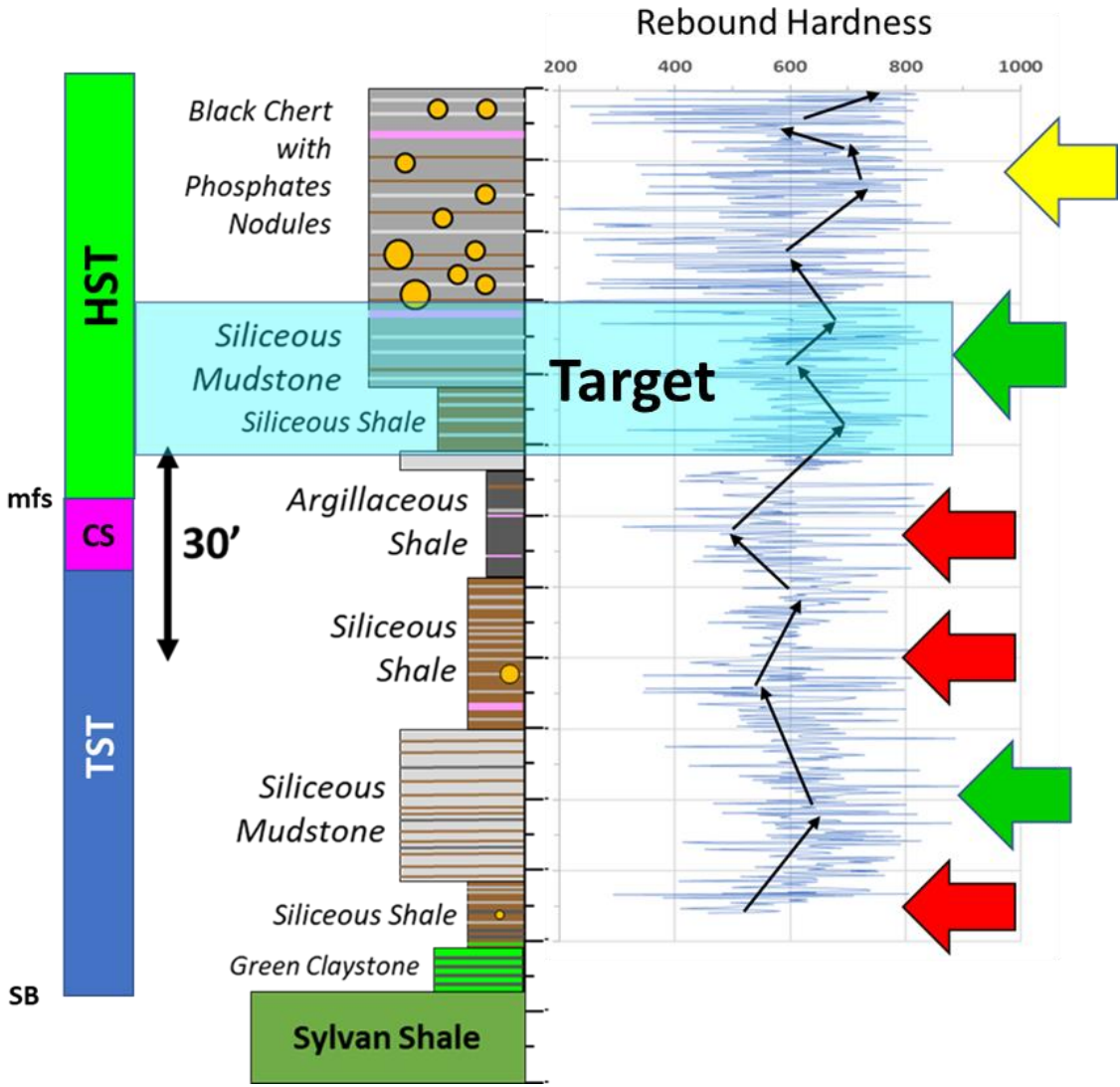


Figure 94 Best target zone (light blue box) in the Marietta Basin Woodford Core with an ideal combination of ductile/brittle couplet (Siliceous Shale/ Siliceous Mudstone couplet)

Chapter 6: Subsurface Mapping

Two of the critical questions this dissertation is trying to answer are “How laterally extensive is the Woodford Shale across the Marietta basin? How does its thickness vary laterally?”. To answer these questions, the Woodford Shale and other significant formations were mapped across the basin using mainly raster and digital well logs with the support of structural models based on seismic. These maps provide the foundation to find any correlation with the hydrocarbon production from horizontal Woodford Shale wells discussed in chapter 7 and to predict the placement of future Woodford wells in the basin.

This chapter covers the available data and methods used for the subsurface mapping, a regional structure framework based on seismic, the definition of the most important surfaces in the type log, structure and stratigraphic cross-section along the basin, and the depth and thickness maps of the Woodford Shale and other significant formations.

6.1 Data and Methods

The Well Data available in the Marietta basin is limited to a few sets of vertical wells targeting conventional reservoirs in the structural traps located close to the edge of the basin or close to faults. **Figure 95** shows the location of the wells used in the mapping process as well as the location of the seismic lines used for the regional structure models.

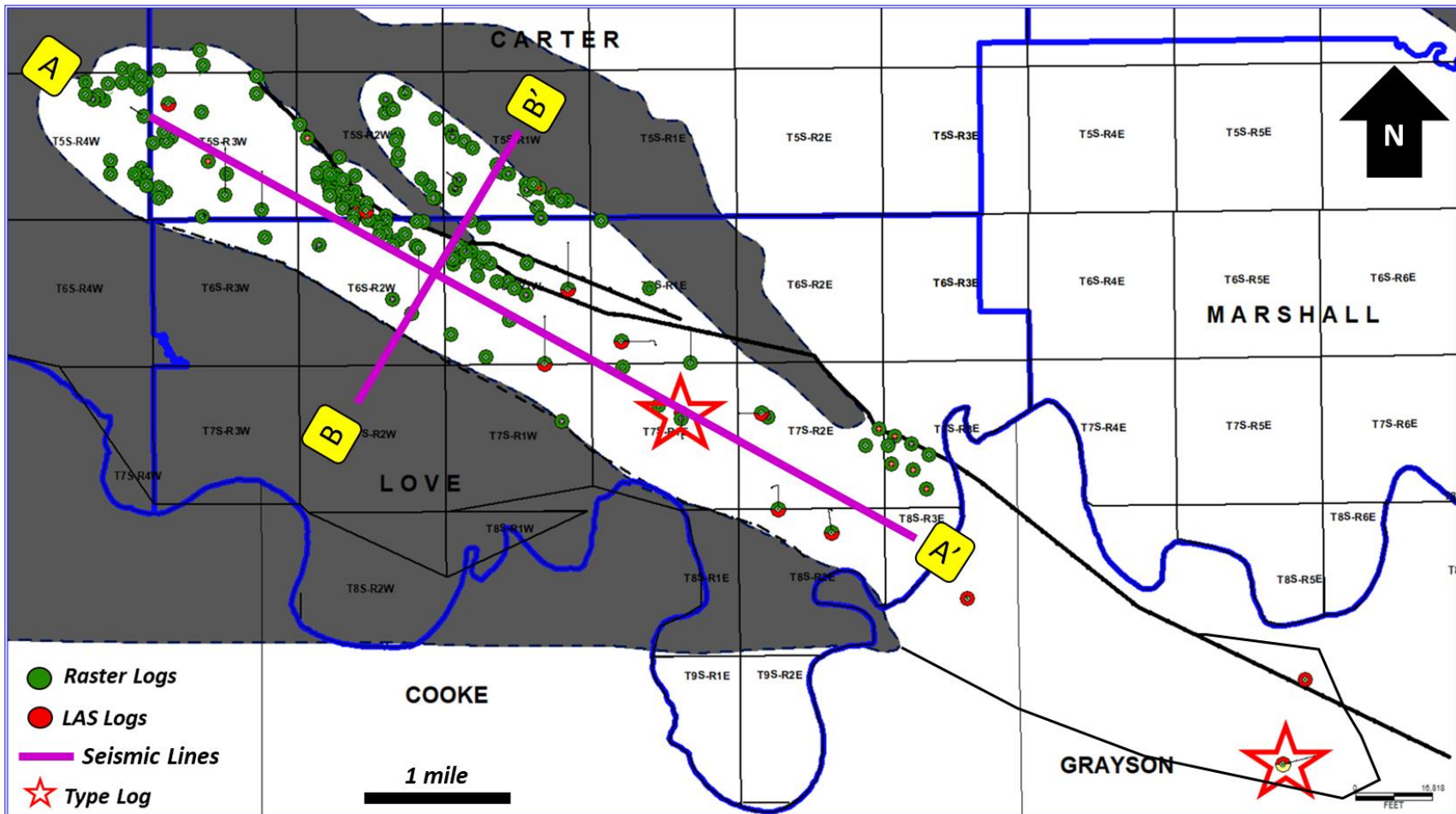


Figure 95 Base map with the locations of the available well data and seismic lines. Green dots correspond to available raster logs. Red dots have digital logs. Red stars represent the location of the type logs. Purple lines represent the location and relative length of the 2D seismic lines.

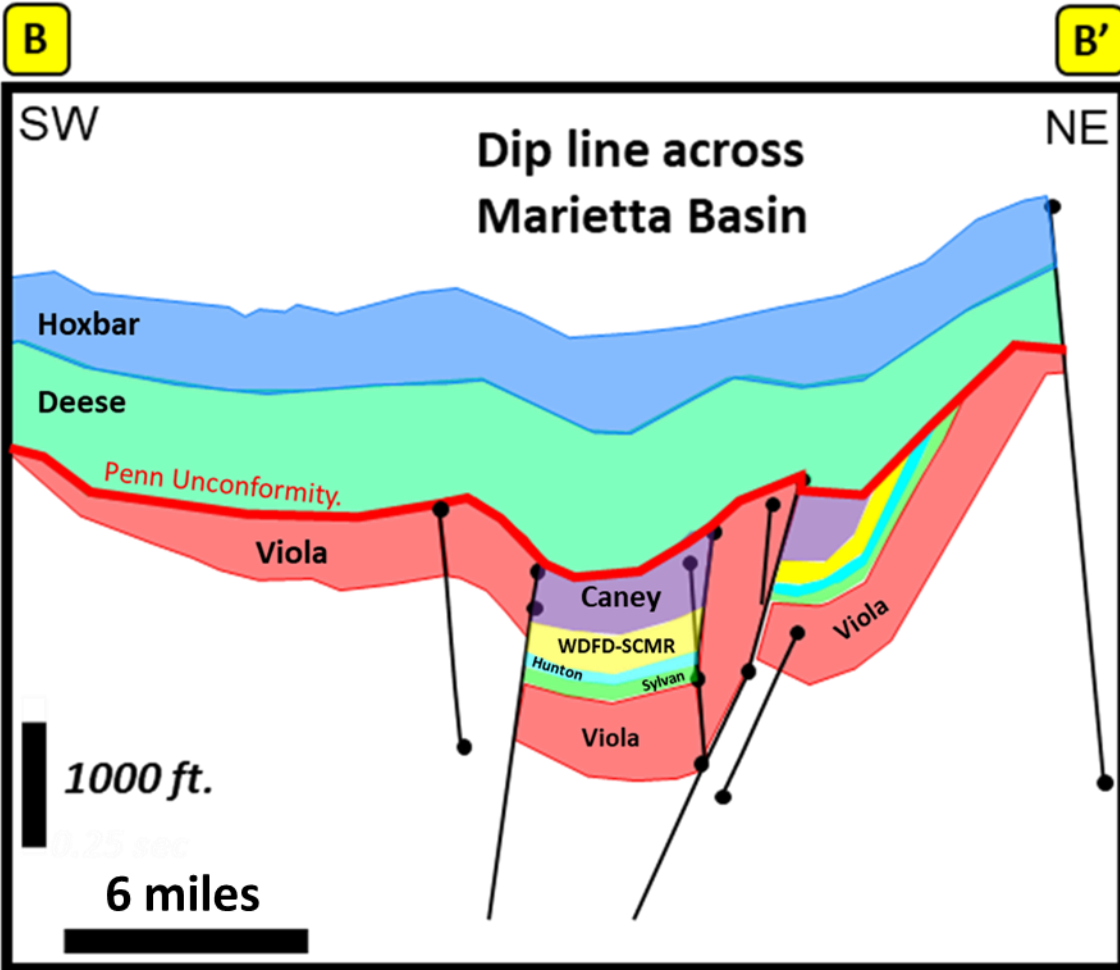
The Well Data includes 149 vertical wells and 13 horizontal wells. Most of the vertical wells were drilled before 1980 and had a limited set of logs available. 90% of the wells are in raster log format, and 10% of the wells were available either in digital version or digitized for this dissertation. Well data is concentrated in the NW side of the basin in the Oklahoma side, and it is spatially scattered in the SE area of the basin into Texas. Each well has at least resistivity (Res) and Spontaneous Potential (SP) logs, and at least 50% have Gamma-Ray (GR) logs or Bulk Density (RhoB) logs. The problem with the GR log is the Woodford Shale has a very wide GR range (from 100 to 700 API) and the old raster logs have tracks that go from 0 to 150 API; therefore, the GR logs in some wells are cut to 150 API, and the log character higher than 150 API is unavailable. The correlation between wells was done using the most significant tops and surfaces interpreted from the type logs (location in **Figure 95**). One of these surfaces is the base of the Woodford Shale which represents the Pre-Woodford Unconformity and depending on the location it could be the top of the Hunton Group or the top of the Sylvan Shale (when the Hunton Group is missing in the section). Another significant surface is the Maximum Flooding Surface (MFS) which separates the Transgressive Systems Tract (TST) in the lower half of the Woodford from the Highstand Systems Tract in the upper half of the formation. The base of the Chert-Dominated section is also an easy to pick top/surface because it has relatively lower GR values and is not affected by the 150 API cutoff from the raster logs.

The regional structural model of the basin was done based on 2D time-migrated seismic lines. One of these seismic lines is perpendicular to the basin axis or syncline; this line is oriented SW to NE. The second seismic line is parallel across the syncline axis of the basin in a NW to SE direction. The location of these seismic lines is shown in **Figure 95**. This seismic are

proprietary and confidential; therefore, they cannot be included in this dissertation book. However, the generalized structural model resulting from the interpretation of the seismic is included in this book. The next subchapter discusses the results of the regional structure model.

6.2 Regional Structural Model

The Marietta Basin is a narrow syncline with northwest-southeast axis orientation. The basin is deeper closer to the axis of the syncline and shallower on the sides. Generalized structural models of the basin were created based on proprietary 2D seismic lines. The Dip Line (**Figure 96**) shows that the presence of the Woodford Shale is principally in the center of the basin and it is controlled by the combination of faults and the erosional Pennsylvanian Unconformity (red line in the figure). On seismic lines the top of the Woodford Shale was very difficult to pick so instead the top of the Sycamore Formation was picked down to the top of the Hunton Group forming the yellow interval in Figure 96. In the SW side of the basin and the NE edge, most of the Silurian-Devonian-Mississippian section (which includes the Sylan Shale, the Hunton Limestone, the Woodford Shale, the Sycamore Limestone, and the Caney Shale) was eroded by the Pennsylvanian Unconformity. This Dip Line Structural Model was used as a guideline when correlating wells in the SW-NE direction and provided confidence in the location of the major faults.



- Hoxbar Fm.
- Deese Fm.
- Caney Gp.
- Woodford Fm. & Sycamore Fm.
- Hunton Gp.
- Sylvan Fm.
- Viola Fm.

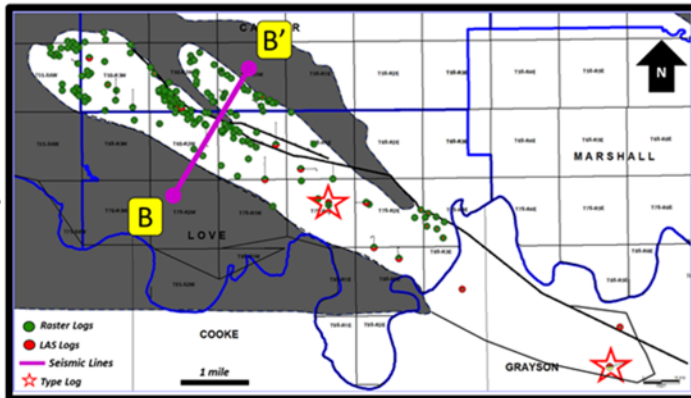


Figure 96 Dip Line Structural Model across the Marietta Basin. Location of the line B-B' is shown in the map for reference. Notice the presence of the Woodford Shale in the center of the Marietta Basin Syncline. The Woodford Shale is missing in the SW edge as well as the NE edge of the basin.

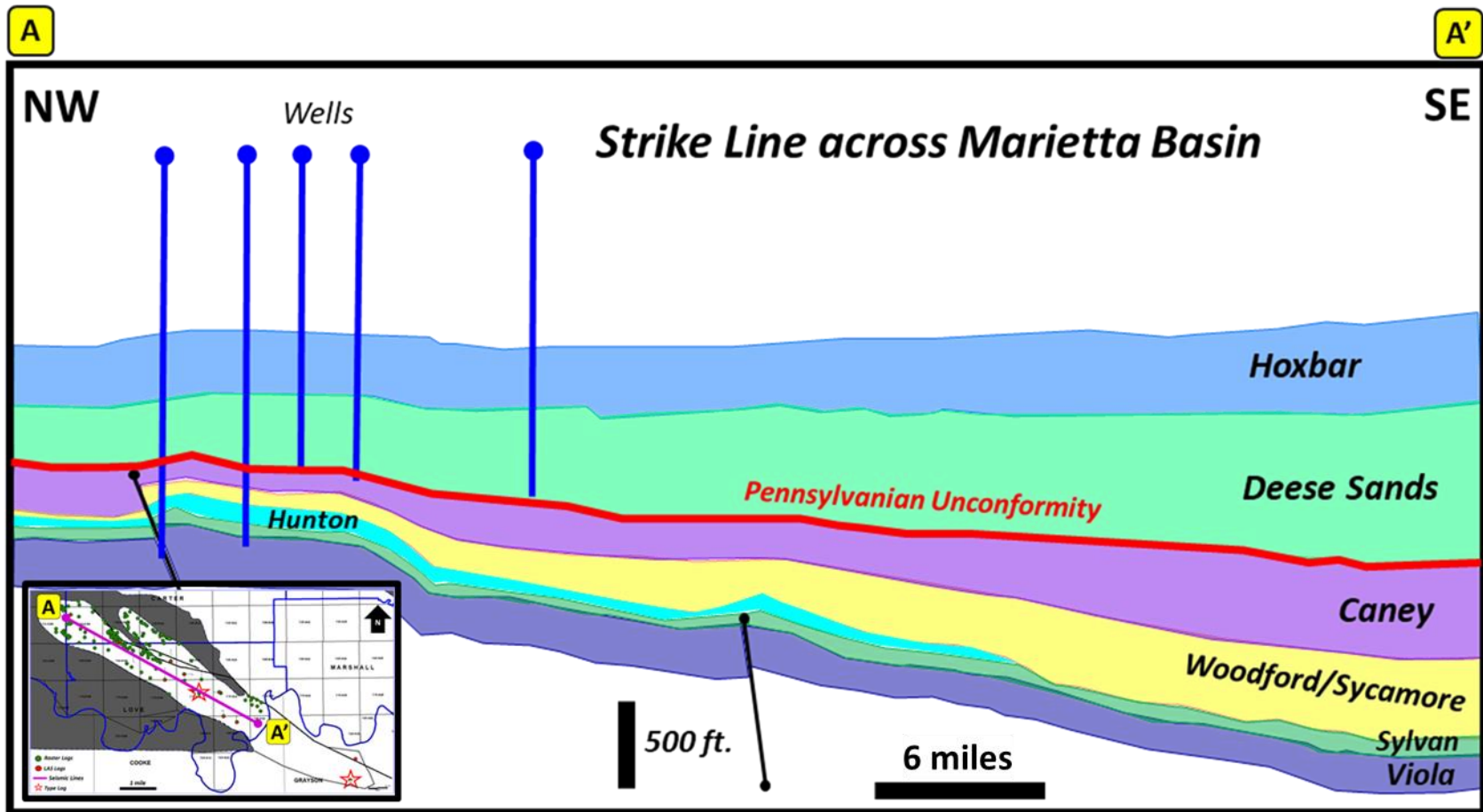


Figure 97 Strike Line Structural Model parallel to the syncline axis of the Marietta Basin. Location of the line A-A' is shown in the map for reference. The Woodford Shale is thinner towards the NW area of the basin where the Hunton Group is present. As the Hunton Group pinches out towards the SE the Woodford/Sycamore section becomes thicker.

The Strike Line Structural Model is located along the syncline axis of the Marietta Basin. The generalized cross-section is shown in **Figure 97**. The Woodford Shale is present all along the line. It is thinner in the northwest, and it is thicker towards the southeast part of the basin. Hunton Group is present only in the NW part of the basin, and it is either eroded or was not deposited towards the SE. The Pennsylvanian Unconformity is less prominent along the axis of the basin because that area was not uplifted like the edge of the basin. There are just a couple of minor faults perpendicular to the axis of the basin. The location of some of the wells used to tie the seismic to the logs are shown in this line and are located in the NW area of the basin where conventional structure traps were the target. Most of the current activity of horizontal wells in the Woodford formation is on the SE side of the basin where the Woodford Shale is thicker and deeper.

6.3 Type Log

The type log of the Woodford Shale in the Marietta Basin is shown in **Figure 98**. The Woodford Shale is characterized by very high Gamma-Ray (GR) log compared to the overlying and the underlying formations due to the higher content of clay and organics. The Woodford Shale also has a positive deflection in the Spontaneous Potential (SP) log. Resistivity is relatively high in most of the Woodford section, and both density and neutron are lower compared to formations above and below the Woodford formation. Within the Woodford interval, there are three significant surfaces that can be interpreted from the combination of GR, Density, and Resistivity. These are the Maximum Flooding Surface (mfs) just at the highest GR peak of the section, which correlates to the lower density log measurement. The other two surfaces that can

be mapped are the top of the Basal Woodford represented by the increasing upward resistivity from the base of the Woodford and decreasing upward of the Density logs. Finally, the other key surface is the Base of Chert-Dominated section in the Upper Woodford which has relatively lower GR and slightly higher Density Log.

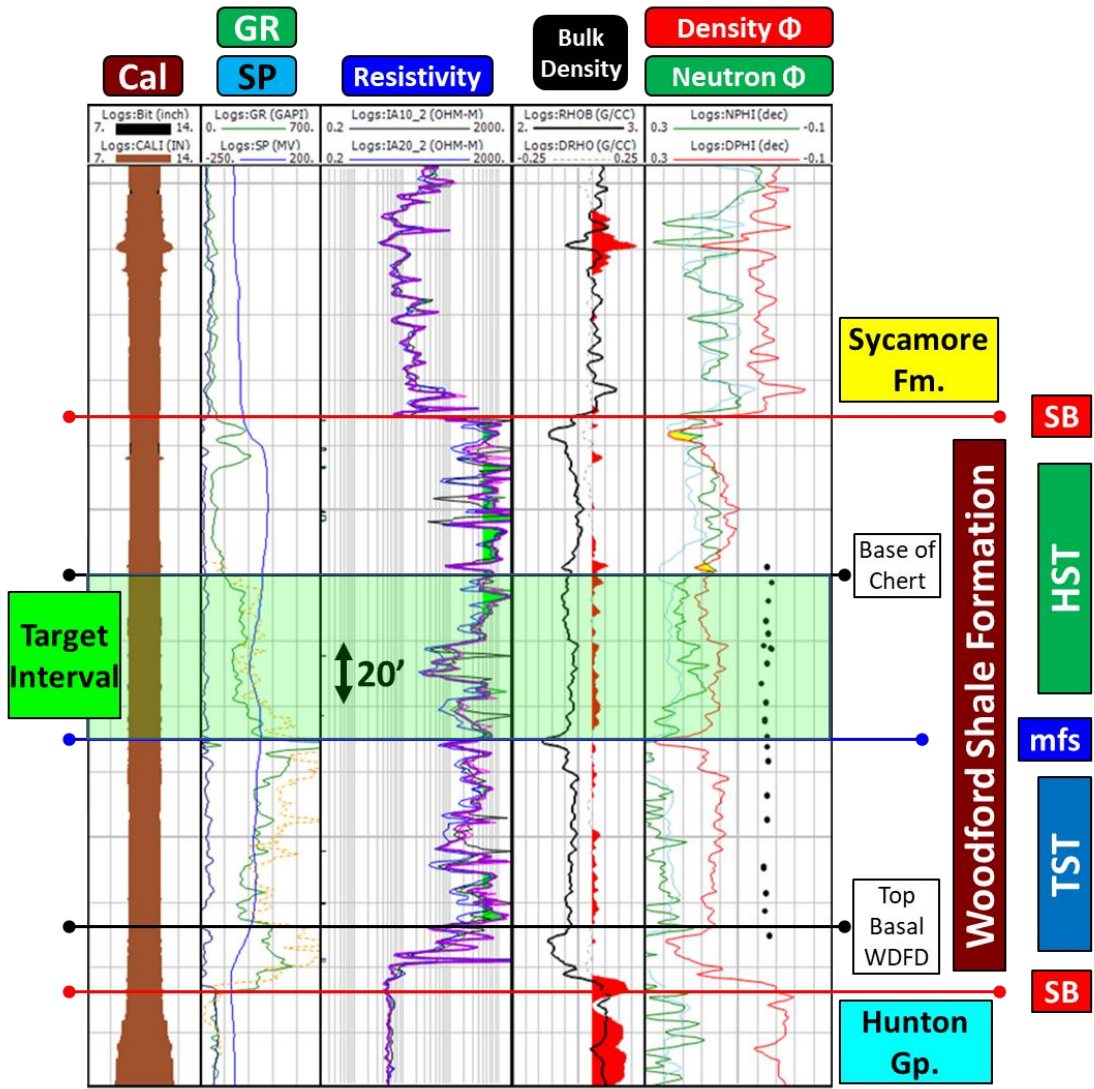


Figure 98 Type Log of the Woodford Shale Formation in the Marietta Basin. The name of each log is displayed at the top of each track. The key interpretative surfaces are shown as horizontal lines. HST: Highstand Systems Tract. TST: Transgressive Systems Tract. MFS: Maximum Flooding Surface. SB: Sequence Boundary.

6.4 Cross Sections

Structural and Stratigraphic Cross-Section were generated after the interpretation of the key surfaces and tops discussed earlier in the Type Log subchapter. The Stratigraphic Section (**Figure 99**) is flattened at the top of the Woodford Shale Formation. The thickness of the Woodford Shale varies laterally, becoming thicker in areas closer to the axis of the basin. There are three units interpreted in the cross section from bottom to top: a) Lower Transgressive Systems Tract (TST) below the MFS surface; b) the interval from the MFS to the Base of Chert-Dominated Section (which I identified as the target zone in Chapter 4); and c) the Upper Woodford Section with lower Gamma Ray log response.

The Upper Woodford Section has a relatively constant thickness across the basin. Therefore, the significant changes in the gross Woodford Thickness are due to the lateral changes of the thickness of the Lower TST interval and the Target Zone between the MFS and the Base of the Chert surface.

Figure 100 shows the Structural Cross-Section along the central axis of the basin. The Woodford Interval becomes deeper towards the southeastern area of the basin, and then it appears to have been uplifted by a set of faults in the Texas side of the Basin. Depth varies from 10,000 feet to 16,000 feet. The reason why the SE side of the basin is uplifted is that the Ouachita Thrust Belt pushed all the sediments north, creating a set of reverse and thrust faults.

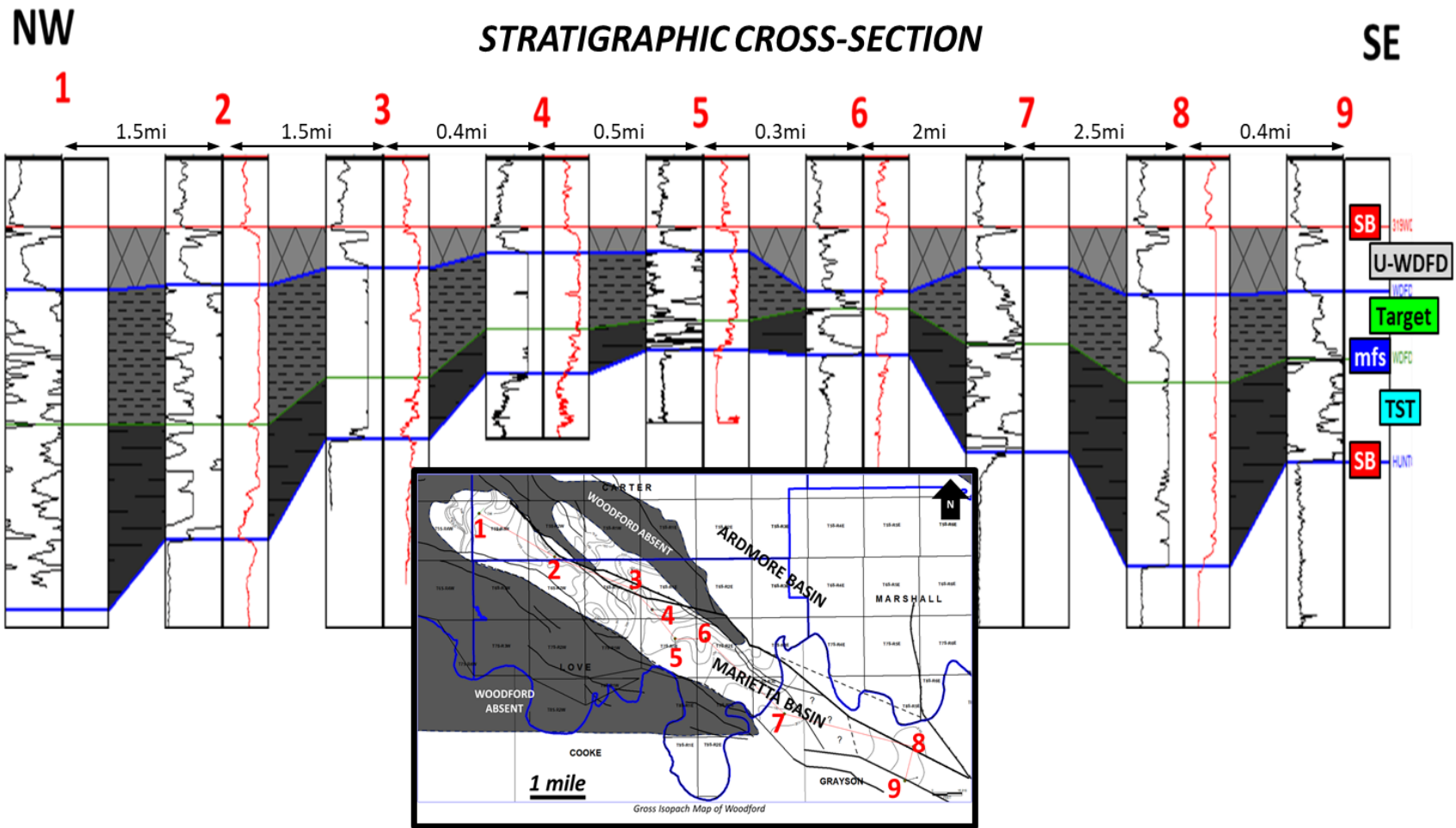


Figure 99 Stratigraphic Cross-Section of the Marietta Basin. Orientation is NW-SE. The three main intervals are the Upper Woodford (U-WDFD), the Target Interval, and the Transgressive Systems Tract (TST).

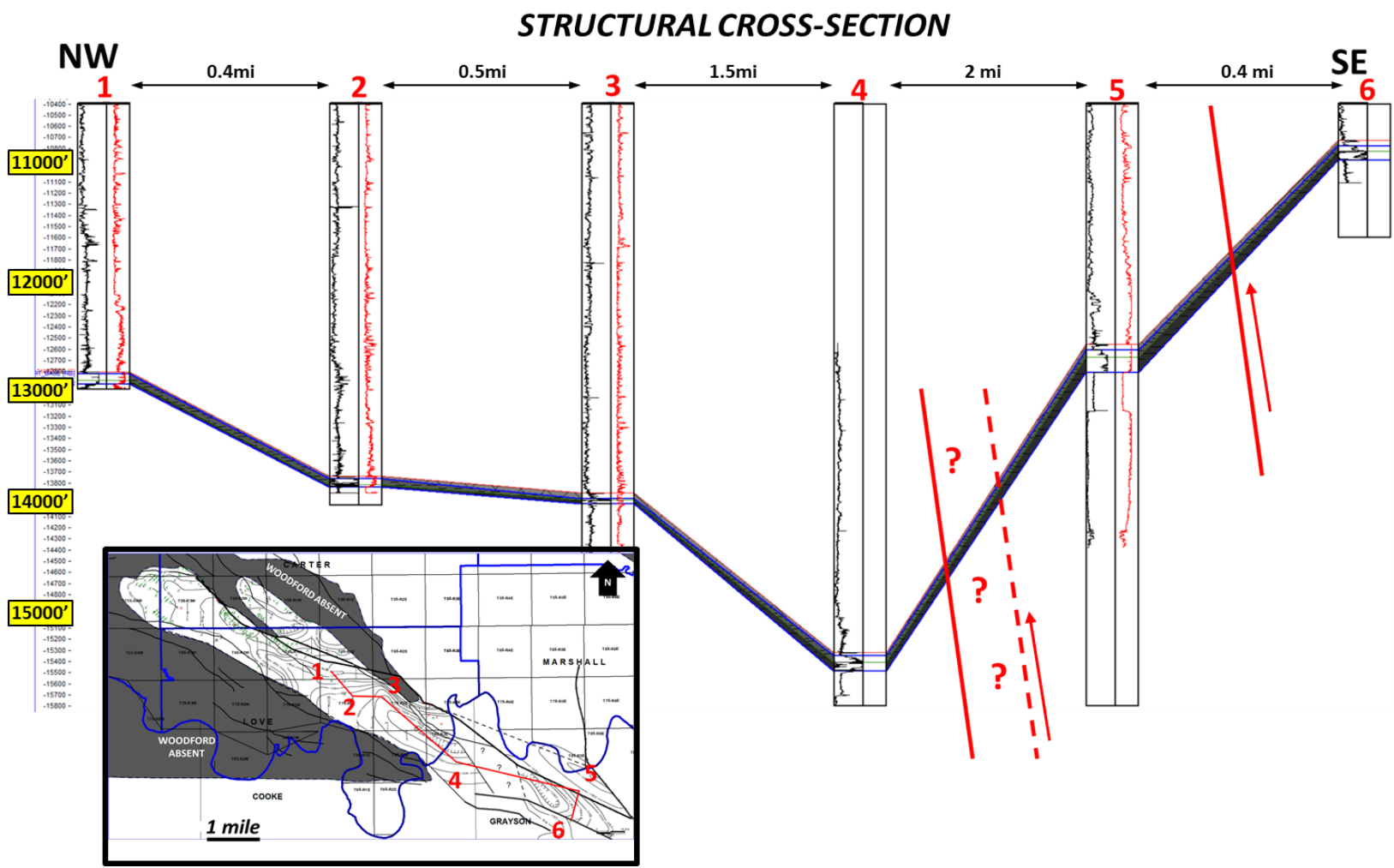


Figure 100 Structural Cross-Section of the Marietta Basin. Orientation is NW-SE. The Woodford Shale is shown in dark colors.

6.5 Subsurface Maps

After performing the well log correlations to the most significant surfaces across the basin, subsurface maps of the most important intervals were generated. **Figure 101** shows the distribution of the depth for the top of the Woodford Shale Formation in the Marietta Basin. This map, as well as the thickness maps, are the first Woodford Map ever published in this basin. The accuracy of the map is excellent in shallower areas where there is the most well control, and less accurate in the deeper areas where there is less well control. Woodford Top (True Vertical Depth: TVD) ranges from 5000 feet to 17000 feet. The Woodford Shale is shallow in the northwestern side of the basin, and it deepens gradually to the center of the basin towards the southeast, then due to the combination of reverse faults in the Texas side of the Basin, the Woodford is found at shallower depths. This observed variability of the Woodford Shale depths is very important to identify because the reservoir pressure usually varies with depth. The deeper the reservoir is placed, the higher the reservoir pressure will be. Higher reservoir pressure is needed to have an economical flow of hydrocarbons, particularly liquids, as it has been identified in chapter 5 as the main hydrocarbon phase. In the next chapter, the effect of depth/pressure with Estimated Ultimate Recovery of producing Woodford Wells is discussed.

Figure 102 shows the gross isopach (isochore) map of the Woodford in the Marietta Basin. Gross thickness varies from 100 feet to 300 feet. There are no clear trends in the gross thickness map. Most of the thicker Woodford Shale is located in the northwestern side of the basin where it reaches up to 300 feet. Previous publications (McCullough, 2014; Infante et al, 2016) have identified the Woodford Shale as tending to become thicker in areas where the

Hunton Group is thinner or absent. However, when generating a thickness map of the Hunton Group (**Figure 103**), this relationship of Thin Hunton=Thick Woodford is not visible. It appears the Hunton Group is only present in the NW side of the Basin, and absent in the SE area of the basin. My hypothesis is that the Hunton Group was not eroded in the Marietta Basin as it was in Central Oklahoma where McCullough (2014) and Infante et al. (2016) did their research. Instead, the Hunton Group in the southeastern area of the Marietta basin might be absent because it was never deposited (i.e. the carbonate factory did not extend south probably because water depth in that area was deeper. One evidence that supports this hypothesis is the contact between the Woodford Shale and the Sylvan Shale in the core described in chapter 3. This contact does not show any erosive feature, neither mud rip-up clasts or any type of erosive lag. The contact is planar without any scour. Grain size along the contact is only mud size, and there is no clast or sand, or gravel as has been identified by Galvis (2017) in the Speake Ranch outcrop in the Arbuckle Mountains. Therefore, it is most probable that the Hunton Group was just not deposited in the area where the Marietta Woodford Core was taken.

The top and base of the ideal target interval identified in the previous chapter was mapped, and a thickness map was generated. This thickness map (**Figure 104**) shows a better-defined thickness trend compared to the Gross Woodford Thickness discussed previously. Thickness values range from 40 feet to 120 feet. The Target Interval is thicker along the axis of the syncline and thinner toward the edges of the basin. I interpret the thickness variability of the Target Interval as being better defined because this interval was deposited after the onset of maximum transgression (above the Maximum Flooding Surface in the stratigraphic rock record); therefore, the whole area was completely flooded, and sediments could be evenly distributed

across the basin. The high variability without defined spatial trend in the gross Woodford thickness map is probably due to the variable thickness of the Basal Woodford, and Lower Woodford deposited during the early transgression. These sediments in the Lower Woodford are probably thicker in the depocenter areas that flooded first during the transgression.

Consequently, the thickness of the lower Woodford defines the total gross thickness of the Woodford Shale. In either case, the lower section was not identified as the better-quality rock to be considered an unconventional shale resource; instead, it is the “Target Interval” above the MFS and below the Chert bench that has the ideal combination of Reservoir Quality and Completion Quality as discussed in Chapter 5. Therefore, if the objective is to look for new locations for Woodford development wells in the basin, it is the thickness Target Interval that matters. Thicker sections of the Target Interval in combination with enough depth (>10,000 feet) to have good reservoir pressure represents the prime area for development to maximize the production of oil and gas from the formation. This relationship is proven in the next chapter when Estimated Ultimate Recovery (EUR) values from current producing Woodford Wells are calculated and plotted on the thickness map of the Target Interval and Structure Map of the Woodford Shale.

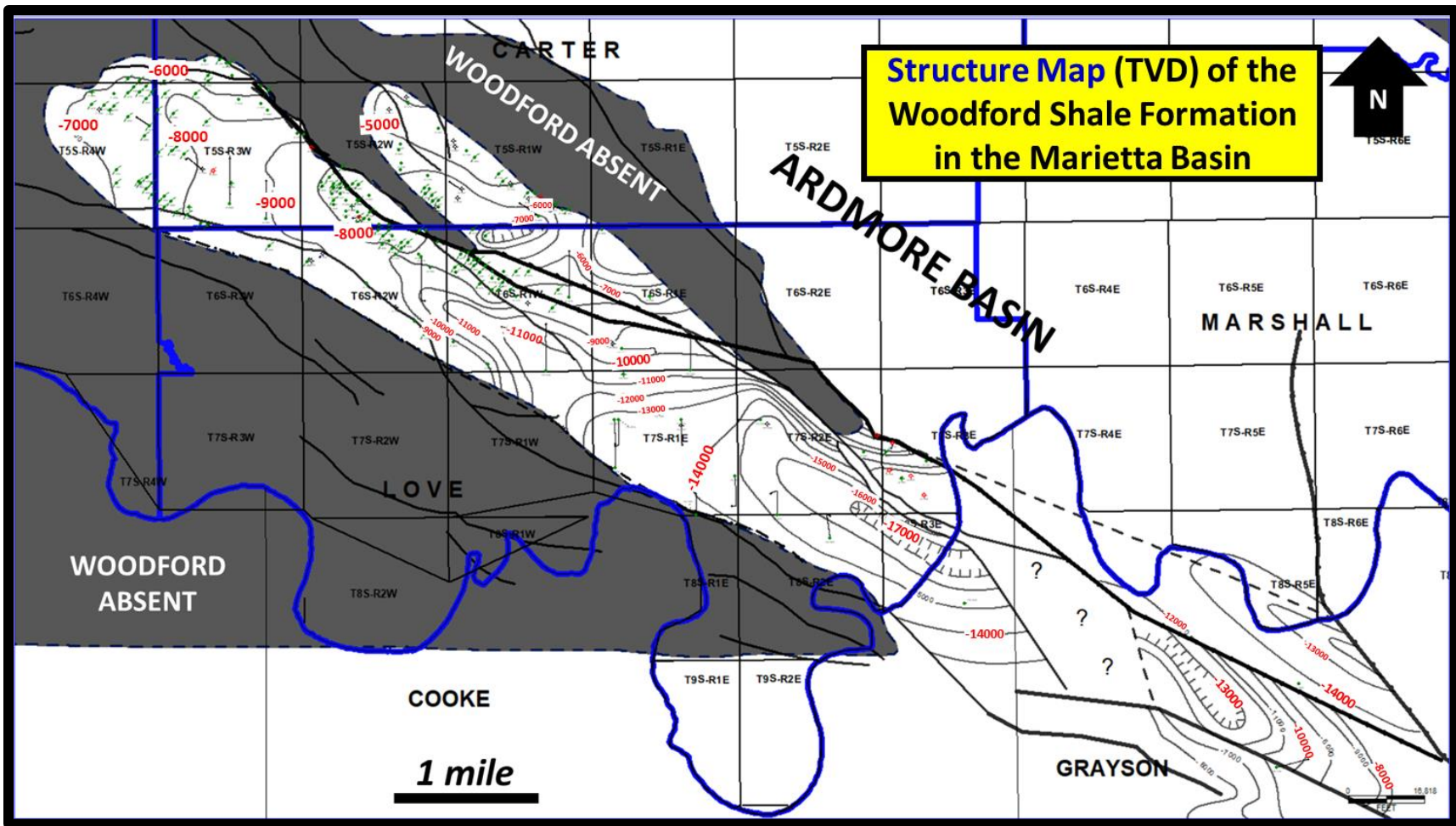


Figure 101 Structure (True Vertical Depth) Map of the Top of the Woodford Shale in the Marietta Basin. Contour Intervals are spaced every 1,000 feet. Basin is shallower toward the SW side and deeper in the central area of the basin.

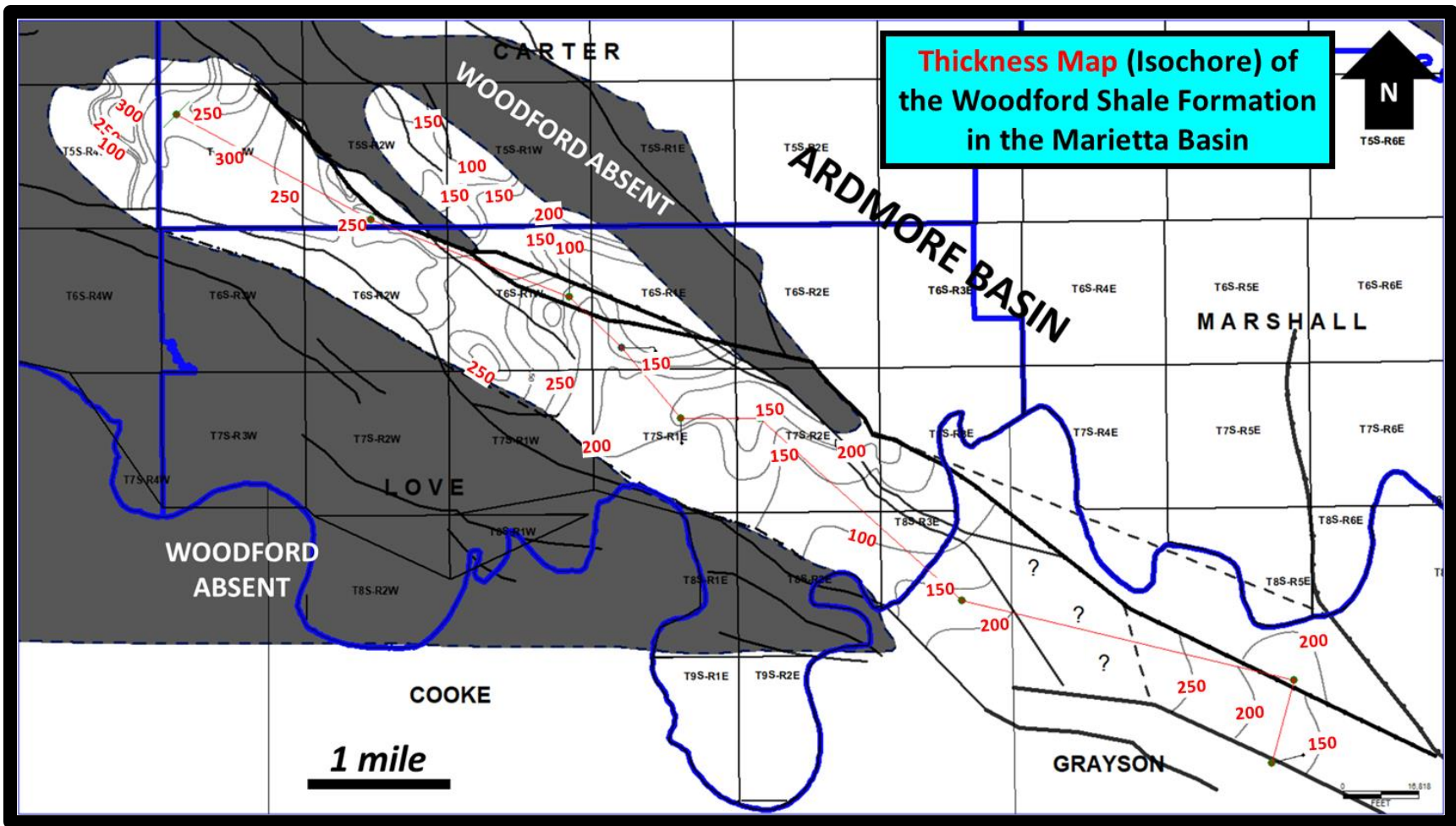


Figure 102 Gross Thickness (Isochore) of the whole section of the Woodford Shale in the Marietta Basin. Contour Interval is 50 feet.

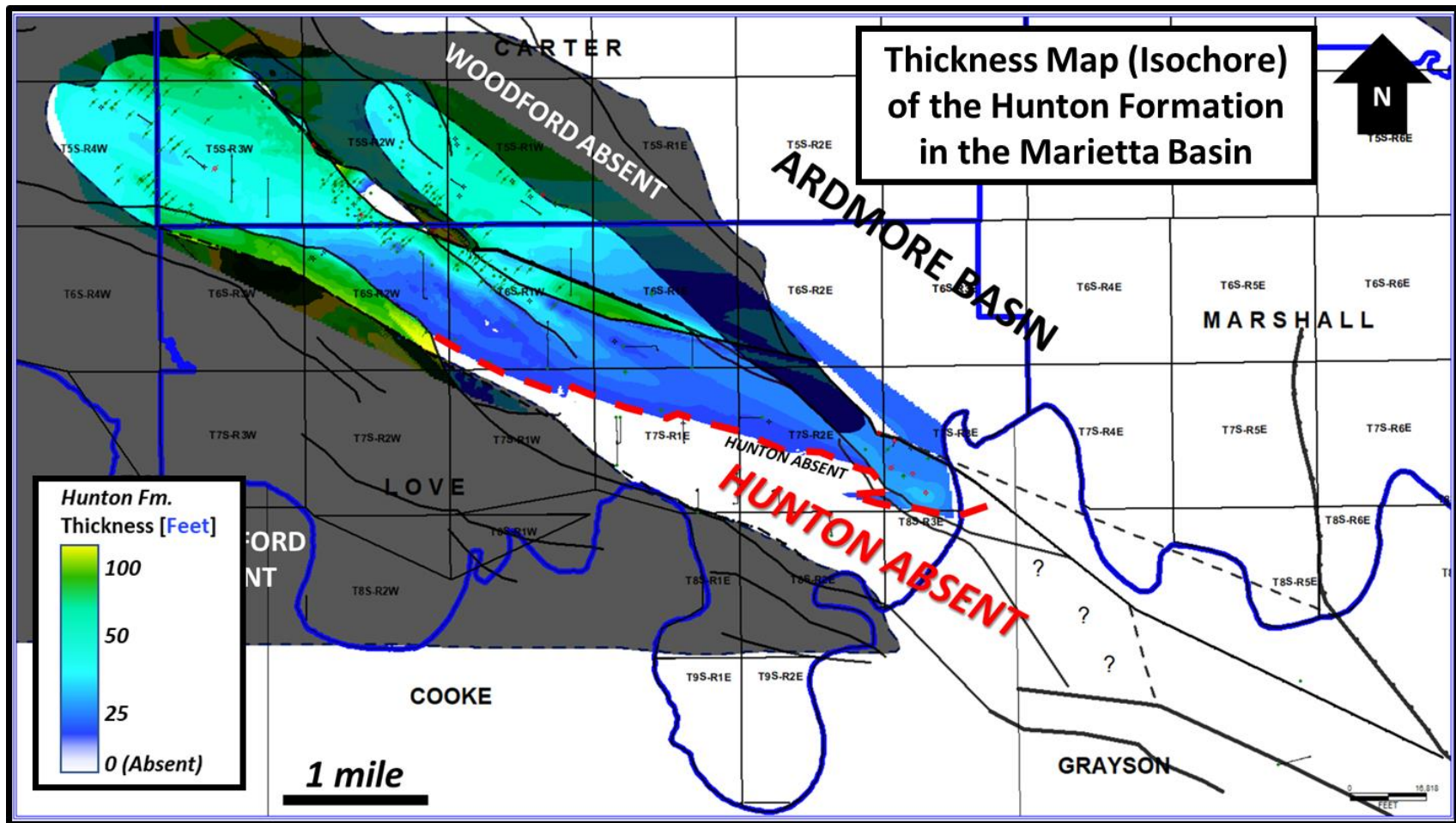


Figure 103 Thickness (Isochore) Map of the Hunton Group (Limestones) in the Marietta Basin. Hunton Limestones are mostly absent in the SE area, and it is thickest in the NW area closer to the edge of the basin.

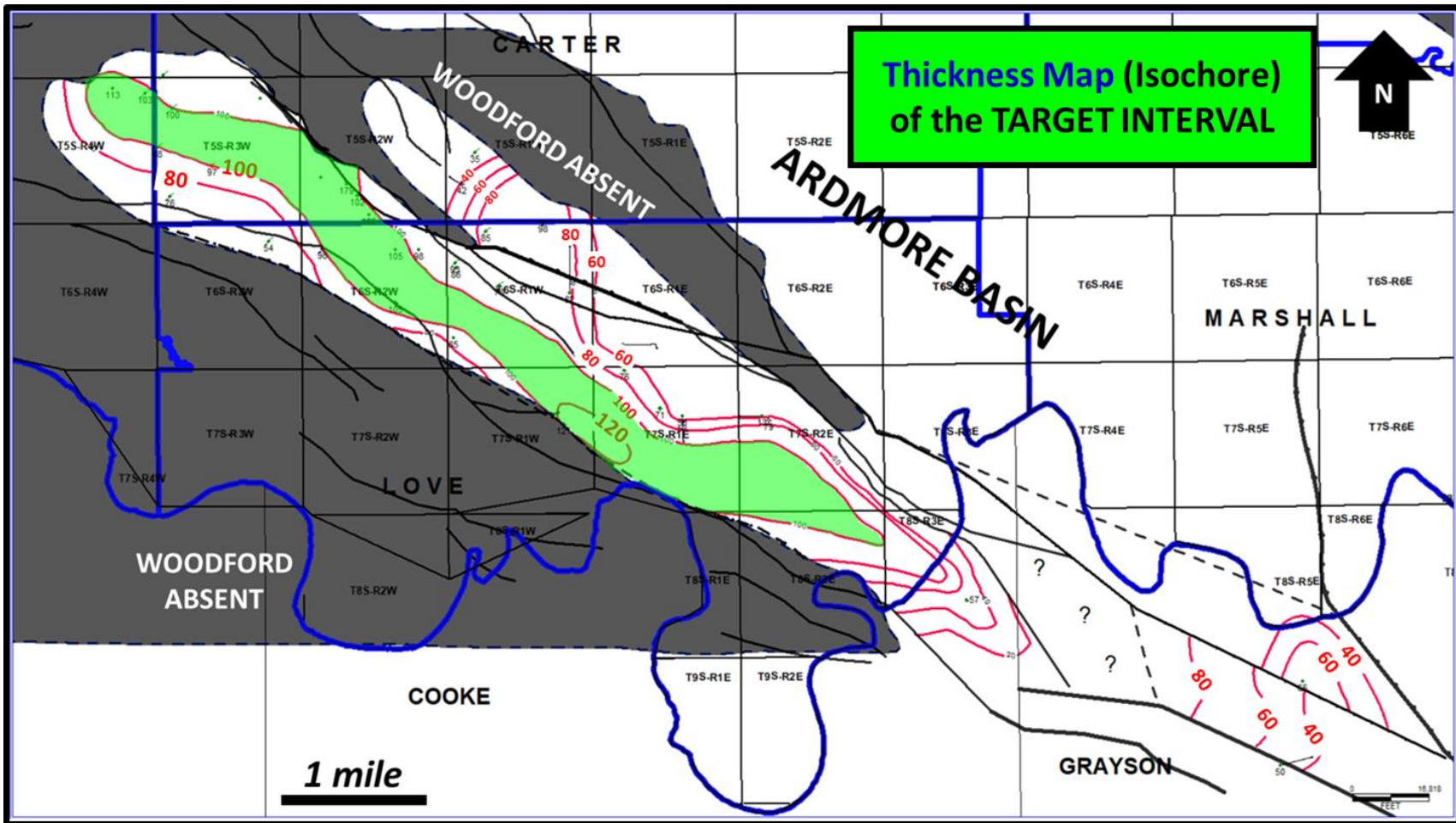


Figure 104 Thickness Map (Isochore) of the Target Interval which is the section between the Maximum Flooding Surface (mfs) and the Base of the Chert. Contour Intervals are every 20 feet. Green area represent thickness greater than 100 feet.

Chapter 7: Production and Performance

This Dissertation concludes with the analysis of the up-to-date production data of the Woodford Shale wells in the Marietta Basin, the forecasting of Estimated Ultimate Recovery (EUR) of these wells, and which geologic factors discussed in the previous chapters might be controlling EURs.

There are many reasons for forecasting future production of Woodford Shale wells in the basin. One example is to better understand the economic potential of the play or how fast wells can be Free Cash Flow (FCF). Another valid reason is to compare the Woodford-Marietta Play to the similar plays of the Woodford Shale in other locations like the Anadarko Basin, Ardmore Basin, or Arkoma Basin. Lastly, and one of the most important, is to identify the best zones or intervals within the stratigraphy of the formation as the target for future development wells.

The beginning of this chapter (Subchapter 7.1) covers a summary of the theory behind the Decline Curve Analysis (DCA) technique. Then, I show the data available for this analysis in Subchapter 7.2, as well as, the methodology (Subchapter 7.3) step by step to forecast the cumulative production of horizontal wells drilled and completed in the Woodford Shale within the Marietta Basin. It also includes the analysis of the distribution of well performance of the main development area. Finally, the results of the DCAs (Subchapter 7.4) and the discussion of the geologic controls that might be affecting the current production and the Estimated Ultimate Recovery (EUR) of these Woodford Shale wells (Subchapter 7.5) are discussed.

Currently, a few operating companies are completing wells in the Woodford Shale interval of the Marietta Basin. **Figure 105** shows a base map of the horizontal Woodford wells in the basin. The most active operator is XTO Energy Inc. (a subsidiary of ExxonMobil) with 37 wells from 2012 to 2018. The second most active operator is Continental Resources Inc. with four wells. The first Woodford Shale well drilled in the Marietta Basin was completed in 2012. Operators reached the peak of drilling activity in 2015. **Figure 106** shows a bar chart with the number of wells drilled and put into production by year since the first Woodford (horizontal) well in the basin until today. The peak of drilling activity was reached in 2015 when companies were drilling to hold acreage by production.

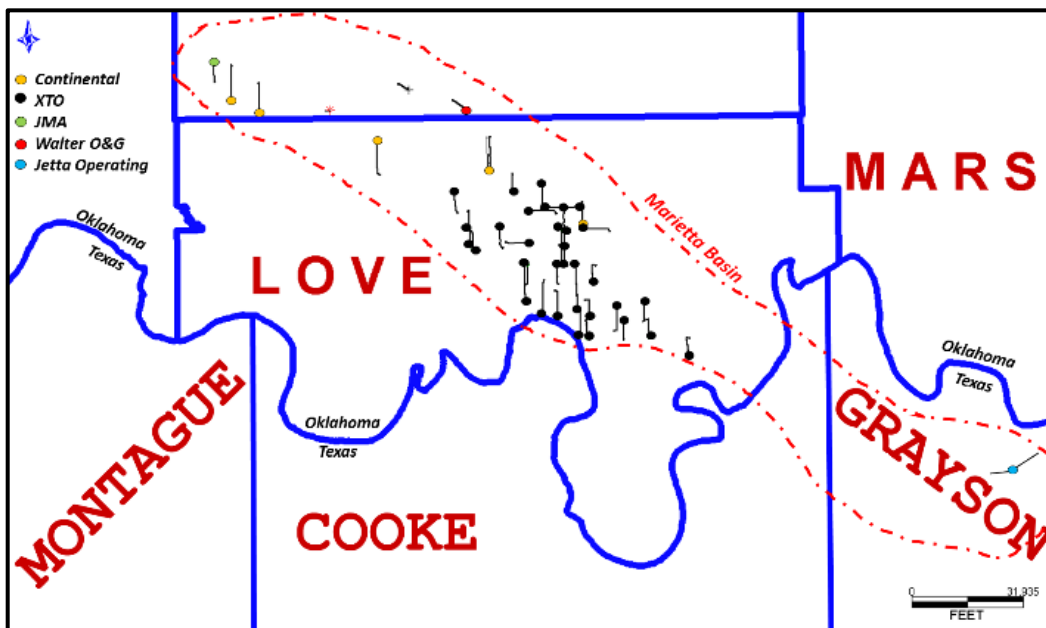


Figure 105 Map with the location of Woodford Shale horizontal wells in the Marietta Basin. They are color-coded by well operator (the legend is in the upper left). Dash line represents the Marietta Basin outline.

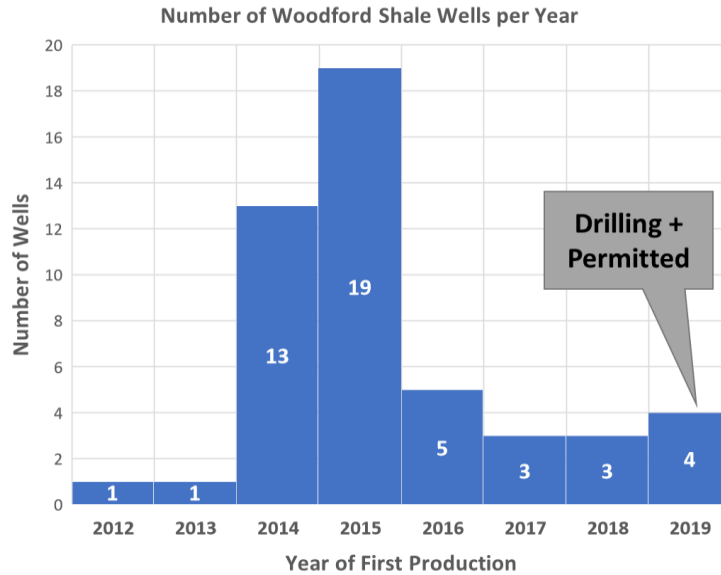


Figure 106 Histogram of Woodford Shale horizontal wells drilled and in production by year. 2019 number represents the number of Woodford wells with permits approved to drill. The peak of drilling activity was reached in 2015 with 19 wells.

For the Decline Curve Analyses (DCAs) and forecasting, this dissertation focuses on the "Core" area around of the Woodford Shale well activity around the Township Seven South (7S) and Range One East (1E) where most of the black wells are located in Figure 105. XTO Energy Inc. drilled most of these wells, and it is the only area in the Marietta Basin were the development of the play had advanced enough to analyze the play performance and EURs.

7.1 Decline Curve Analysis (DCA) Theory

Arps (1945 and 1956) defined the critical principles of Decline Curve Analysis (DCA) through a set of empirical equations that best represented the production performance of oil and gas wells over time. These equations are the Exponential, the Hyperbolic, and the Harmonic decline curves. Arps' technique is still the most common production forecasting methodology used in the petroleum industry for conventional and unconventional reservoirs around the world thanks to the simplicity of its application.

It is important to note that Arps' equations are not theoretically derived, but instead, they are empirical relationships based on observations of the production history of fields in development. In principle, Decline Curve Analysis consists of 1) fitting the past production of a well to a Decline model (or curve), and 2) extrapolating the production over time to a user-set economical rate that serves as the end of the forecast period to provide the Estimated Ultimate Recovery (EUR).

The basic principle or assumption of Decline Curve Analysis is the preservation of the status quo of the factors controlling a reservoir performance over time. In other words, the factors that controlled the production in the past will be the same in the future. This assumption comes with the limitation that any change in controls (new completions, new artificial fracturing, or similar) will create variations in the predictions of future production.

The theory behind Arps' decline models is the Decline Parameter Equation, the inverse of the Decline Parameter, which is the Loss Ratio and the Derivative of it. If the loss ratio stays equal over time, then the derivative of the production rate per unit of time will be proportional to the production rate; resulting in the Exponential Decline Model:

$$q = q_i e^{-dt}$$

where **q** is current production rate, **qi** is initial production rate (start of production), **dt** ($dt=d=di$) is the nominal decline rate (a constant), and **t** is the cumulative time since the start of production.

If the Loss Ratio does not stay equal in time but continually varies over time instead, then the derivative of loss ratio (also known as the "b factor" or "b constant") will be constant, and according to Arps (1945) can vary from zero to one ($0 > b > 1$). The representation relationship is Arps' Hyperbolic Decline Model:

Finally, if the "b factor" is equal to one, then the rate of production over time is defined by Arps' Harmonic Decline Model:

$$q = \frac{q_i}{(1 + b d_i t)^{\frac{1}{b}}}$$

where **q** is current production rate, **qi** is initial production rate (start of production), **di** is the initial nominal decline rate (at $t = 0$), **t** is the cumulative time since the start of production, and **b** is the hyperbolic decline constant ($0 < b < 1$).

It is important to notice that during the life of an oil and gas well, the flow initiates within the Transient Flow Domain (during the first days of production), and then it transitions to

Boundary-Dominated Flow Domain. It is during the Boundary-Dominated Flow that Arps' models work best, and it was demonstrated by Fetkovich (1980) when it could relate the decline model parameter defined by Arps to reservoir properties. In summary, the "b factor" in a hyperbolic curve should not be larger than one if the curve fitting includes only in the Boundary-Dominated Flow domain. If the curve fitting includes the Transient Flow Domain, then the "b factor" can and will yield values larger than one.

The last and least commonly used Arp's equation is the Harmonic Decline Model, and it is only used for specific cases of decline production:

$$q = \frac{q_i}{(1 + d_i t)}$$

Figure 107 shows the graphic representation of the three Arp's decline models. For unconventional shale resources like the Woodford Shale, the most widely used model is the Hyperbolic Decline Curve with b factor closer to 1. This model creates unrealistically high reserve estimates in longer times, and to mitigate this issue, the Hyperbolic curve is converted to Exponential at some point of time. Therefore, with that modification, Estimated Ultimate Recovery can be calculated.

Exponential, Hyperbolic and Harmonic Equations

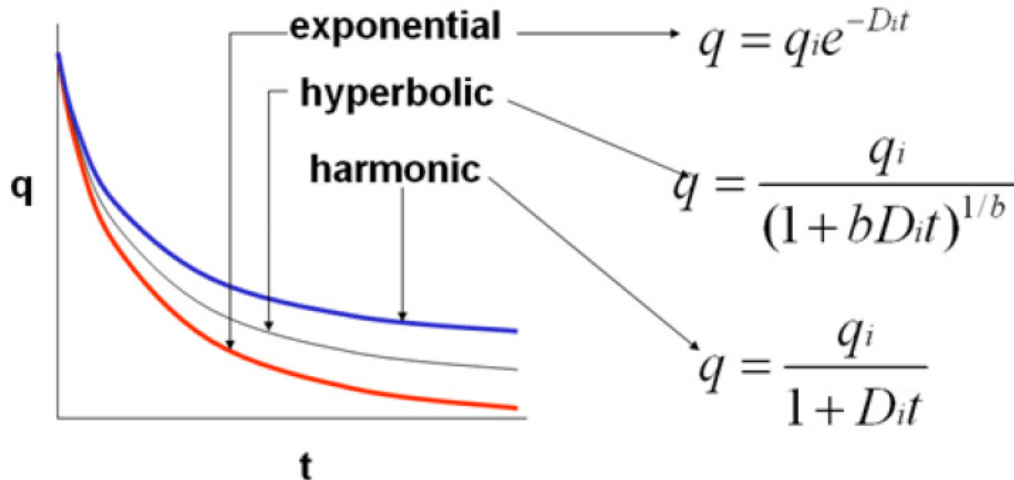


Figure 107 Graphic representation of Arp’s Decline Models. Hyperbolic curve varies between harmonic and exponential by changing the b factor value of the equation between 0 (exponential) and 1 (harmonic). Figure modified from Odagme (2016).

7.2 Data Available

Production data from Woodford Shale wells in the Marietta Basin are available through the Oklahoma Corporation Commission (OCC) webpage. The University of Oklahoma also has an academic subscription with DrillingInfo which provide additional searching and sorting capability when searching production data by operators and target formation.

This dataset includes 41 wells drilled with Woodford Shale Formation as the target reservoir with information on the location of the wells, operator name, directional survey, total depth, monthly oil production, monthly gas production, amount of proppant and fluids used during the completion jobs, and other miscellaneous data related to the wells.

7.3 Methods

Decline Curve Analysis (DCA) should be done well by well. Being consistent with the methodology applied to each well is critical. The production history in the play varies by well because some wells have better targets or different completion jobs.

Wells with longer production history usually have better decline curves because the production trends are better defined making it easier to fit the curve models to them; therefore, more accurate predictions of Estimated Ultimate Recovery (EUR).

Below is the step by step methodology followed to perform Decline Curve Analyses and forecasting in this dissertation:

1. Monthly production data of each well was downloaded from the Oklahoma Corporate Commission (OCC) website or the DrillingInfo Web Database.
2. The production database in Excel spreadsheets was built and organized to import data into the Decline Curve Analysis software PHDwin (graciously donated by Paisano Energy LLC).
3. Oil and Gas Production Rate (Y-axis) versus Time (X-axis) for each well was plotted. Y-axis was set in Logarithmic scale. Oil and Gas were plotted in different charts for simplicity and together for comparison depending on the case.

4. The starting point in time to apply the curve fitting process was chosen for each well. Usually, this point represents the changes from Transient flow to Boundary-Dominated flow and the decline rate by time increases. It was imperative to note any workover, addition of artificial lifting, gas lifting, or re-completion because any of this affects the decision of where to place the starting point.
5. Type curve was matched by choosing the Arps' Curve Model that best fit the decline curve for each well: Exponential, Hyperbolic, or Harmonic.
6. In the case of Hyperbolic fit, several "b factor" (also known as Curvature Factor) were tested to find which value would work best for the production history. Changes in the "b factor" increase or decrease the curvature of the line to the production trend. For conventional reservoir, the "b factor" could go from 0 to 1. In the case of low permeability formations (less than 1mD), the "b factor" could be higher than 1; as it is in the case of unconventional resource plays like the Woodford Shale if the interpreted curve is influenced by transient flow.
7. Production history was matched to the curve up to the last reported production date.
8. The production curve was projected into the future for each well. When the Hyperbolic Model is used, a specific point in time should be used to switch the model to Exponential Curve to prevent overestimation of EUR. For this analysis, the switch from Hyperbolic to Exponential Model was set at 6% decline rate because at this rate most of the curve has

flattened out and start projecting to infinity. After switching to Exponential, the curve did not go to infinity but instead went to zero at different times depending on the production history; which prevent overestimation of EUR projections.

9. Estimated Ultimate Recovery (EUR) was calculated for each well. There is an EUR for Gas production and an EUR for oil production. After total EUR's were calculated they were normalized to 1000 ft. so wells with different lengths could be compared one to one.

10. Statistics were run to observe the distribution of decline rates, EUR, and "b factor" between wells.

11. Normalized EUR data was plotted versus geologic maps to find correlations between well performance and reservoir thickness, target zone thickness, amount of proppant injected into the formation, and other geologic parameters.

7.4 Decline Curve Analysis (DCA) Results

The Decline Curve Analysis (DCA) of current Woodford Shale producing wells has several inputs and outputs like initial decline rate, b factor, and Estimated Ultimate Recovery (EUR). In this subchapter, we discuss these results and the statistics of each variables.

MCKAY 1-22H15 drilled by XTO Energy is the oldest Woodford horizontal well in the basin. It is a 6000-foot horizontal well. It had an Oil Initial Production Rate (Qi) of 9500 barrels and an Initial Decline Rate (Di) of 60%. The Gas Qi of this well was 826.05 Mcf and Gas Di of 52%.

Figure 108 shows the graphic DCA for the well.

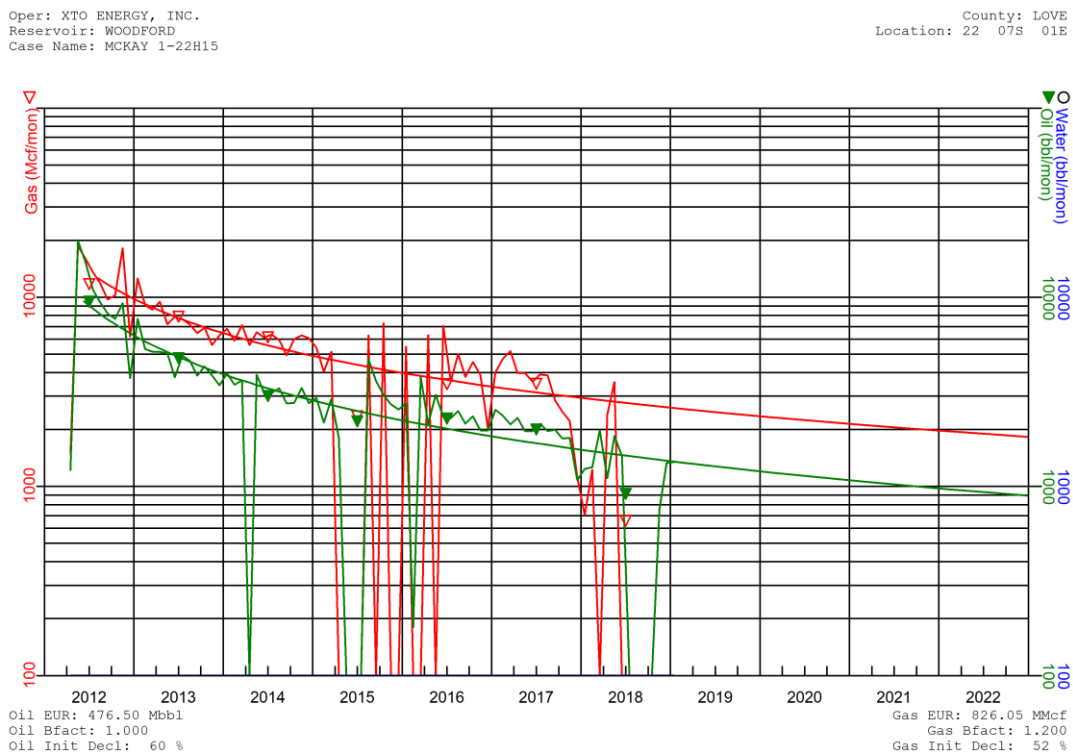


Figure 108 Decline Curve Analysis of the well XTO MCKAY 1-22H15. Green line represents oil. Red line represents gas. Hyperbolic Model was used with a “b” factor of 1.

The commercial EURs for this well are 476,000 barrels of oil and 0.8 Bcf. of Gas. If EUR is normalized to 1,000 feet, then the Oil EUR per 1,000 ft. would be 79,122 bbl., and Normalized EUR of 137Mcf. Commercial EUR has been defined when the well reached a 6% decline rate. In this case, the well will reach this decline rate (6%) in the year 2072. Half a million barrels of oil and nearly one billion cubic feet of gas, make this well an excellent well. However, not every Woodford well in the basin performed similar to the MCKAY 1-22H15, for example, the MANNING 1-3H (also drilled by XTO in 2014) shows oil EUR of only 109,660 barrels and 0.48 Bcf. of gas (**Figure 109**). If the values are normalized to 1,000 feet, so it can be

compared to the MCKAY, then the Oil EUR would be 25,503bbbls and 112Mcf. This well is going to reach the lifespan cutoff of 6% decline rate in the year 2068.

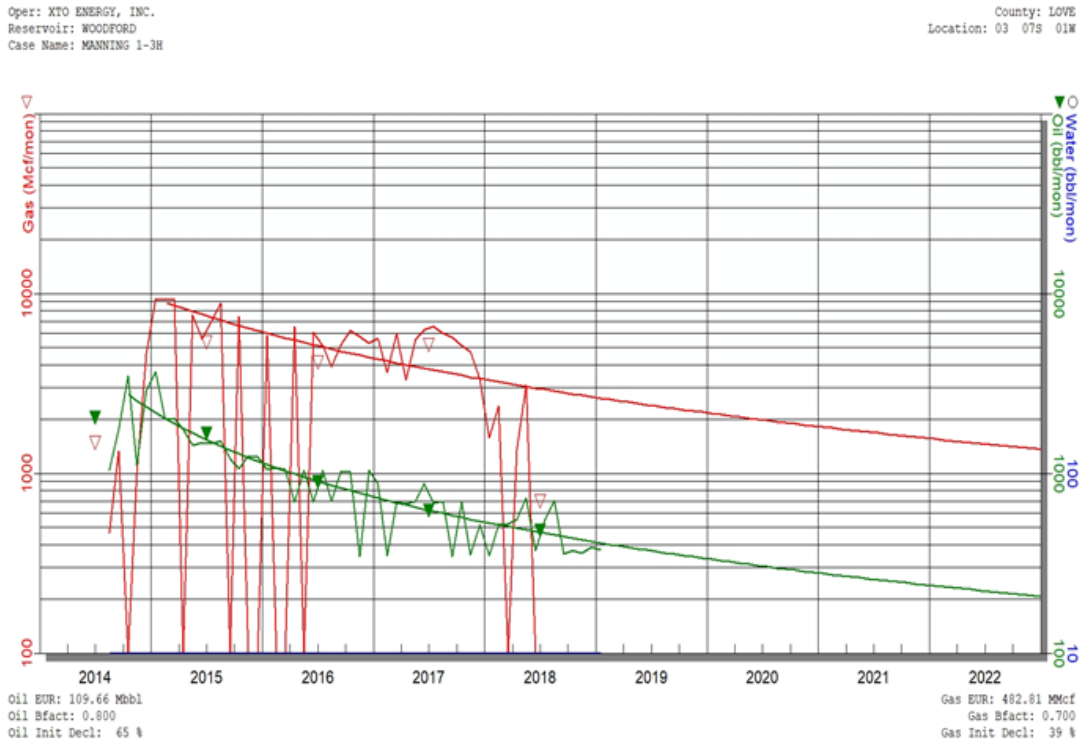


Figure 109 Decline Curve Analysis of the well XTO MANNING 1-3H. Green line represent soil. Red line represents gas. Hyperbolic Model was used with a “b” factor of 1.

The outlook of this well (XTO MANNING 1-3H) is not as promising as the MCKAY 1-22H15. The MANNING 1-3H has an equivalent gas EUR/1kft of 112Mcf versus the 137Mcf, but the oil EUR is just a third or less of the oil EUR of the MCKAY well (79,122 bbl. vs. 25,503 bbl.).

One of the best wells in terms of production performance and forecast is the ROBERTS 1-19H drilled by XTO in 2015 (**Figure 110**). It has a total economic EUR of 1.079 MMBO and 1.3 Bcf. of gas predicted for the year 2078. To compare to the previous two discussed wells, the EUR was normalized to 1000 feet lateral resulting in EUR/1kft of 214,667 bbl. of oil versus

79,122 bbl. for the MCKAY well and 25,503 for the MANNING well. For Gas, ROBERTS is 252Mcf vs. MCKAY 137Mcf and MANNING 137Mcf.

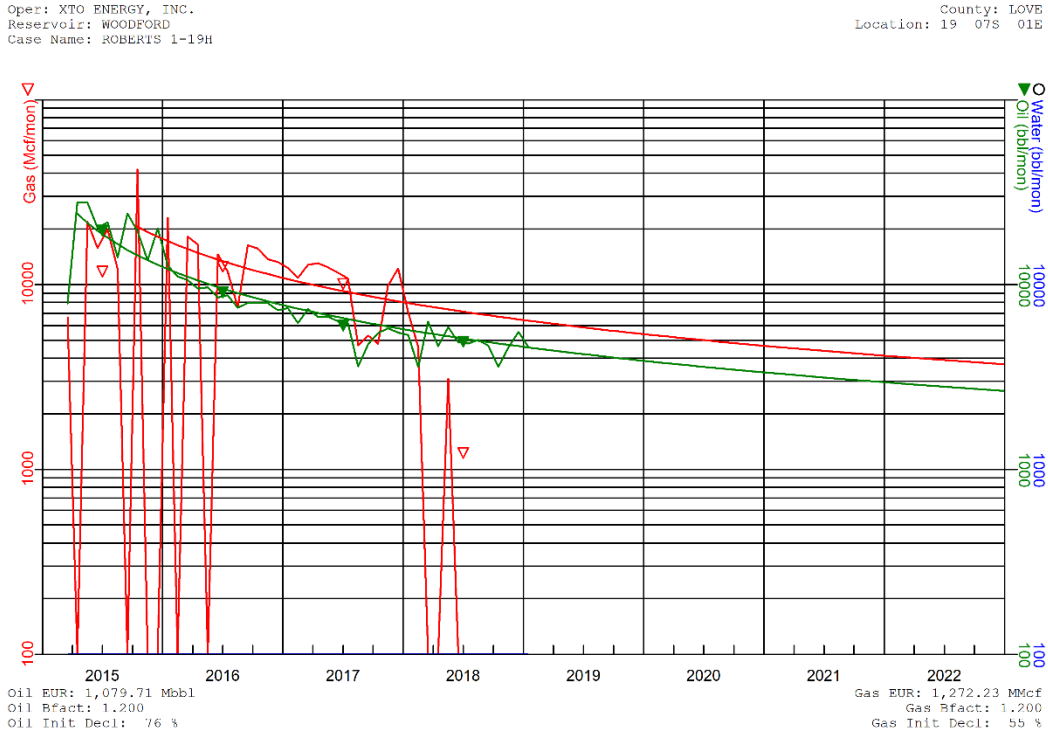


Figure 110 Decline Curve Analysis of the well XTO ROBERTS 1-19H.

Based on this production analysis and forecast, the well XTO ROBERTS 1-19H is an outstanding Woodford well producer. For comparison, a Woodford well in the SCOOP (South Central Oklahoma Oil Play) area has an initial production of 300 to 350 barrels per day, but this well (ROBERTS) initial production was around 800 barrels per day.

Instead of looking well per well, histograms for each variable was generated. The first observed variable is the Initial Production Rates (Q_i) which represents the performance of the well in the initial months of production. **Figure 111** represents the distribution of the initial production rate for oil and gas from all the analyzed Woodford wells represented in figure 7.4. The initial production rate of these wells ranges from 4000 to 24,000 bbl./month with an average

of 10,200 bbl./month. Gas initial production rate has a better-defined distribution ranging from 5000 Mcf to 50,000 Mcf/month, and an average of 17,700 Mcf/month.

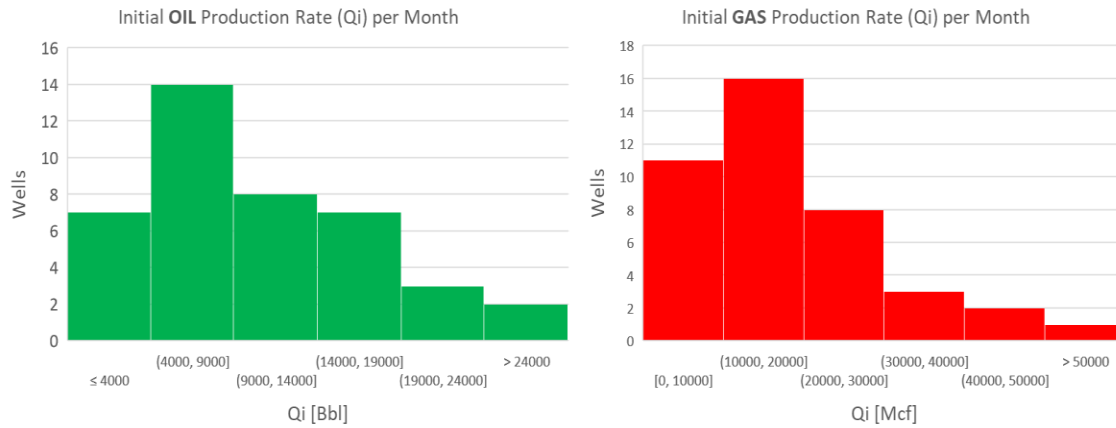


Figure 111 Initial Production Rates (Qi) per month for all the analyzed Woodford horizontal wells in the Marietta Basin. Green histogram represents oil, and red represents gas.

The distribution of Initial Decline Rates (Di) for each Woodford horizontal well in the Marietta Basin are shown in **Figure 112**. Oil Di ranges from 30 to 90% with a mean average of 58%. Gas Di ranges from 10% to 90% with an average of 48%.

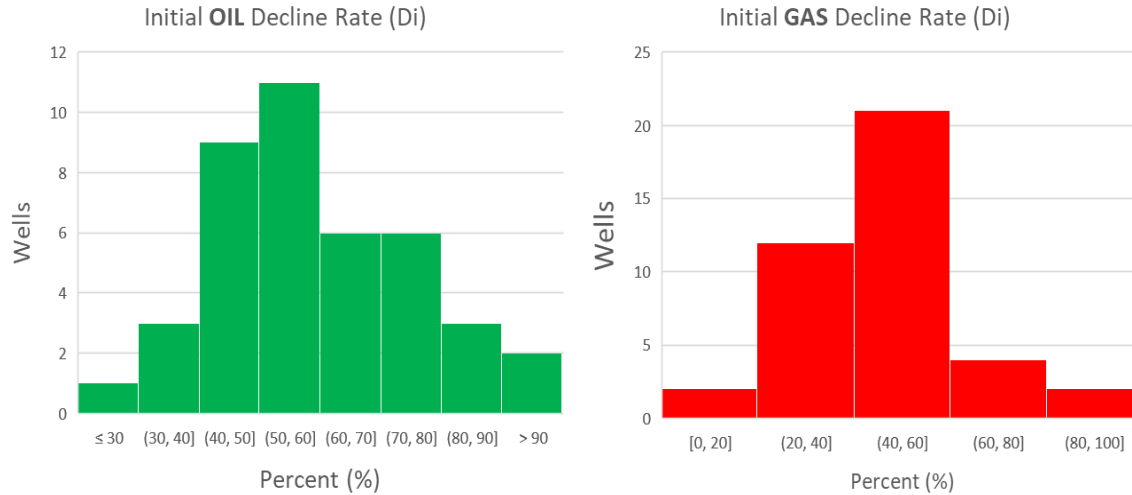


Figure 112 Initial Decline Rates (Di) per month for all the analyzed Woodford horizontal wells in the Marietta Basin. Green histogram represents oil, and red represents gas.

Finally, the distribution of Estimated Ultimate Recovery (Non-Normalized) (EUR) for each Woodford horizontal well in the Marietta Basin are shown in **Figure 113**. Oil EUR ranges from 98,446 bbl. to 1,078,00 bbl. with an average of 479,000 barrels of oil. Gas EUR ranges from 360 MMcf. to 2,624 MMcf. with an average of 966 MMcf. After normalizing those numbers for every 1000 feet of lateral well, the results (**Figure 114**) of Oil EUR range from 18,000 bbl./month to 241,419 bbl./month. Gas ranges from 48,031 Mcf to 606,147 Mcf.

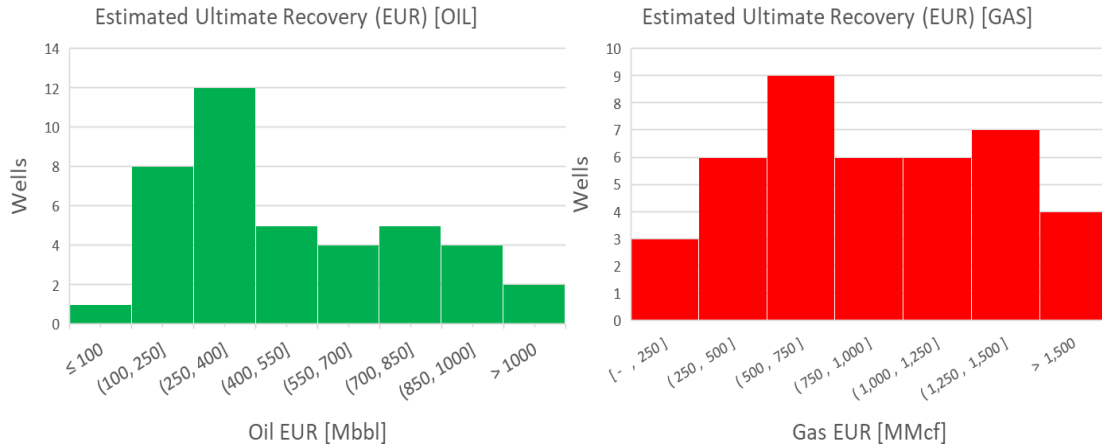


Figure 113 Histogram of the Estimated Ultimate Recovery (EUR) for all the analyzed Woodford horizontal wells in the Marietta Basin. Green histogram represents oil, and red represents gas.

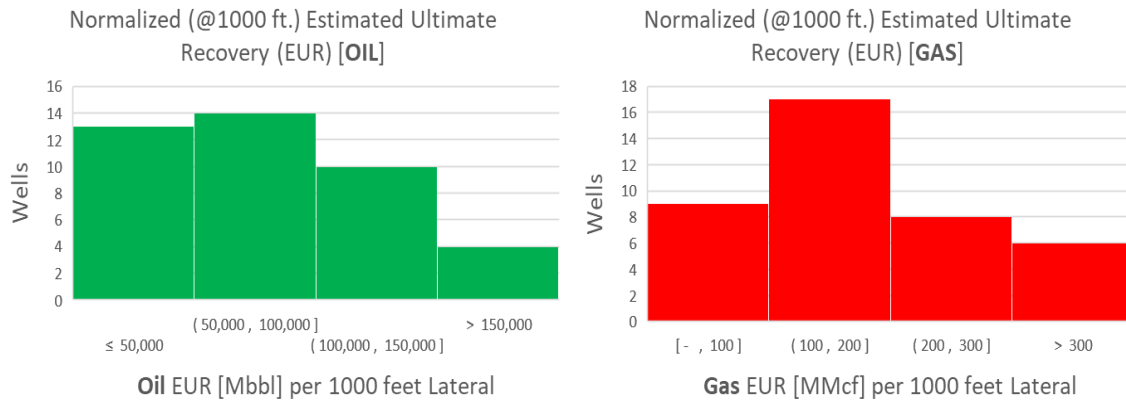


Figure 114 Histogram of the Estimated Ultimate Recovery (EUR) for all the analyzed Woodford horizontal wells in the Marietta Basin normalized per 1000 feet of the lateral well. Green histogram represents oil, and red represents gas.

7.5 Integration with Geology

The Estimated Ultimate Recovery (EUR) calculations made in the previous subchapter were plotted against the geologic maps, and completions maps of the Woodford Shale in the Marietta Basin shown in Chapter 6 (Subsurface Mapping). After testing several combinations, EUR values correlated the best with geology than variability in completion design. In other words, the size of the completion job (gallons of water and pounds of proppant) did not define the resulting EURs of these wells, but instead their location, depth, and thickness of the best target zone.

Figure 115 shows the structure map of the top of the Woodford Shale in the Marietta Basin with oil and gas EURs plotted on each well location. The size of the pie chart represents the total EUR of the well. The larger the circle, the larger the total EUR of the well. Notice that the larger EURs are in areas where the Woodford is deeper than 10,000 feet. This relationship is probably driven by the pressure profile of these wells in the basin. Even though there is no available information about reservoir pressure from these wells, the difference of True Vertical Depth (TVD) of the top of the formation between the less performing wells in the northern half of the basin and the better performing wells in the lower half of the basin, results in tangible differences between reservoir pressure. The deeper the formation, the deeper the well, the more pressure support for production, and the larger the EUR.

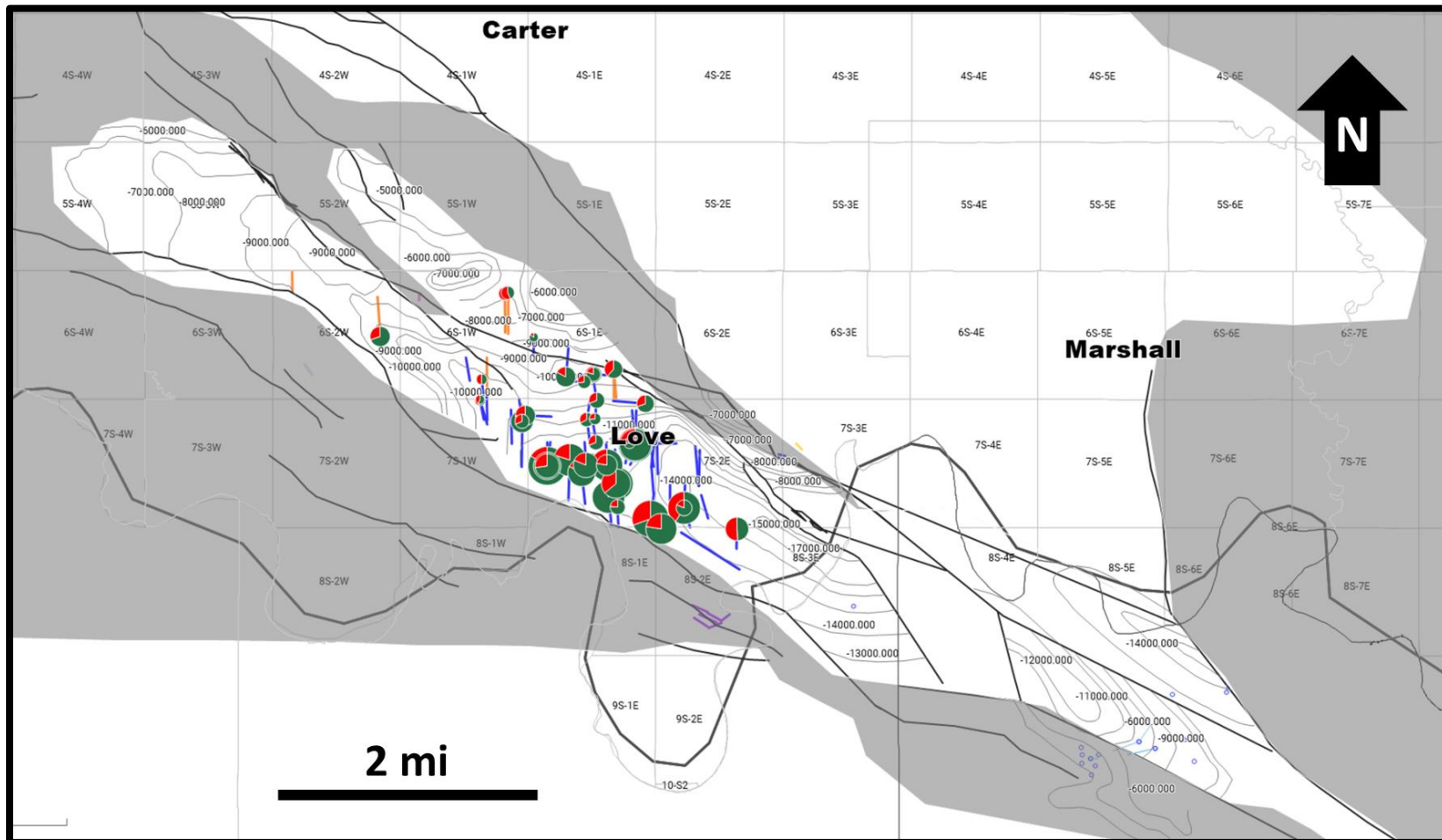


Figure 115 Woodford Shale-Top Structure Map (TVD). Contour Interval: 1000 feet. Pie chart size represents the Estimated Ultimate Recovery. Green represents oil and Red represents Gas. Larger EURs are located in deeper areas (>10,000 feet).

The thickness of the identified target zone (**Figure 116**) within the Woodford Shale Marietta Section between the maximum flooding surface (mfs) and the base of the Chert-dominated interval was mapped and is shown in **Figure 117**, cross-plotted with total economic EURs.

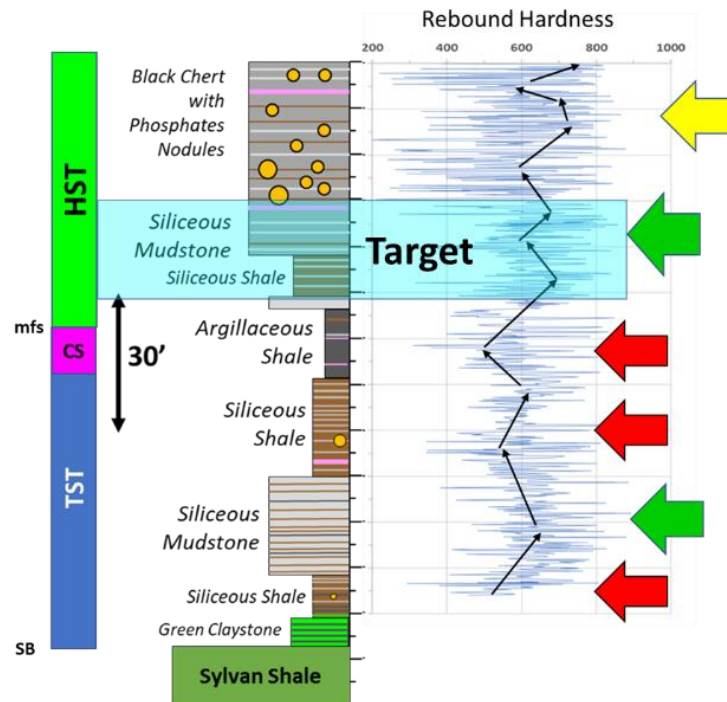


Figure 116 Target zone between mfs and base of the Chert beds with Phosphate Nodules

In conclusion, based on the production data of the Woodford Shale wells integrated with the thickness and structure maps of this formation in the basin, there is enough evidence to interpret that depth (and by relationship, the reservoir pressure) and the thickness of the target interval as the main drivers of the performance of these horizontal wells and the forecast of final EURs. Furthermore, it is not a surprise that XTO Energy has drilled first this area (with thick target interval and depth greater than 10,000 feet) to hold the acreage by production very early in the appraisal phase of the field and to later infill these sections with additional development wells.

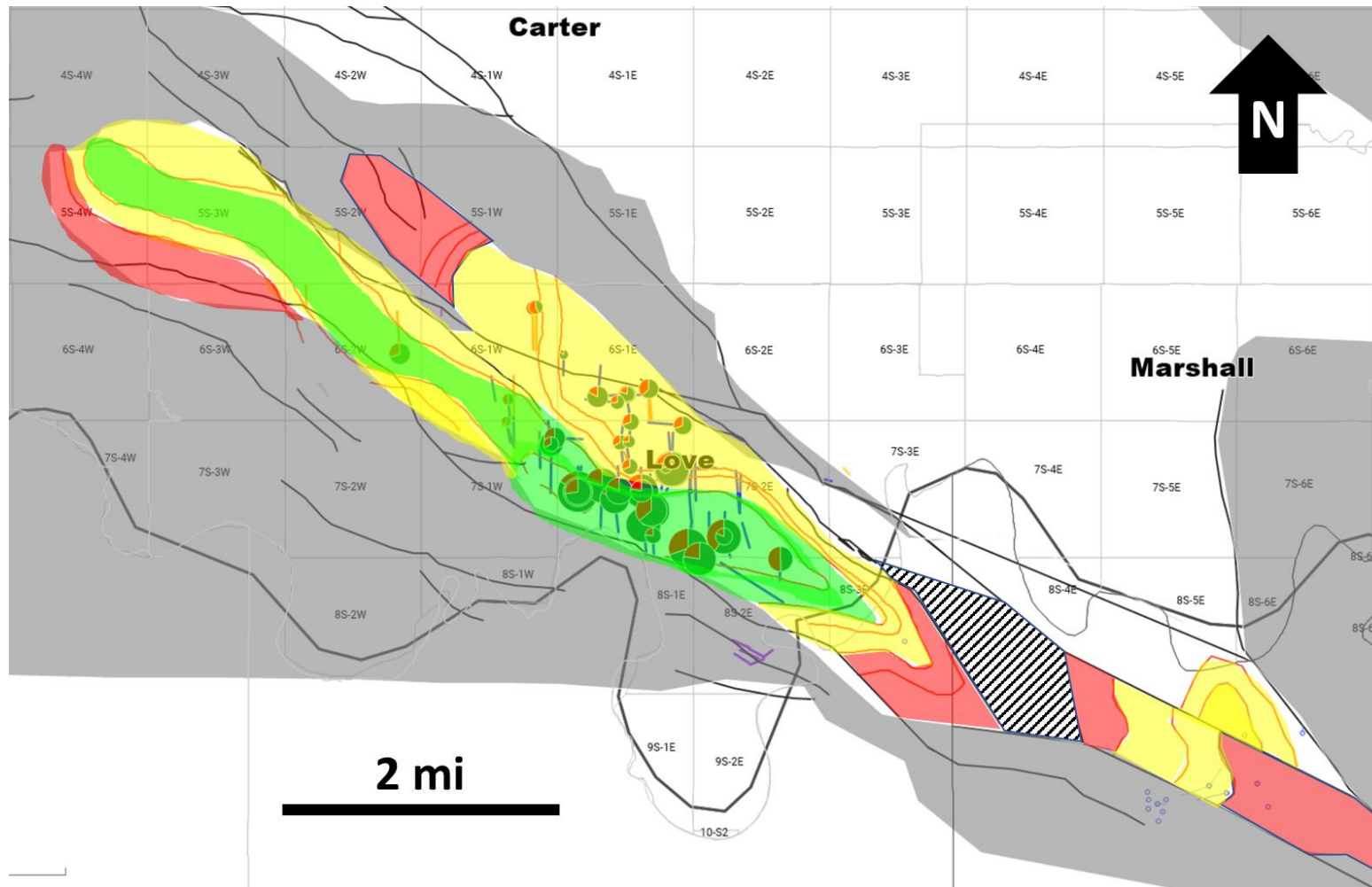


Figure 117 Thickness Map of the Target Interval (between mfs and base of the Chert section – See Figure 7.13). Green areas have a thickness larger than 100 feet. Yellow areas represent a thickness between 60 and 100 feet. Red areas have thickness lower than 60 feet. Notice that the wells with larger EURs correlate with areas with thicker target intervals (in green).

Chapter 8: Conclusions and Recommendations

The Marietta Basin is considered a frontier basin in Oklahoma and North Texas. Only one oil and gas operator has partially unlocked the Woodford Shale resources in the basin when many others have failed to do so. Log, core, and seismic data available to the public are limited. The primary goal of this dissertation was to generate a geologic characterization of the Woodford Shale formation in the Marietta Basin based on the methodology used in outcrops by our research group in the Institute of Reservoir Characterization (IRC). The structure and the significance of this dissertation are about answering a set of vital questions concerning the characteristics and resource potential of this formation in this lesser-known basin. Below are the outcomes to those questions based on the results of the research work done in each discipline (stratigraphy, diagenesis, geochemistry, geomechanics, subsurface mapping, and production analysis), as well as, a set of recommendations for future work.

Which facies and units/intervals of the Woodford Shale are present in the Marietta Basin compared to outcrop Woodford sections in southern Oklahoma?

Based on the description of the only available core from the Marietta basin and based in the facies described on Woodford Shale outcrops by our research group, there are six significant lithofacies present in this Woodford Shale section. These are Siliceous Mudstone (SM), Siliceous Shale (SS), Black Chert (BC), Argillaceous Shale (AS), Green Claystone (GC), and Dolomitic Mudstone (DM). The most common lithofacies in the Woodford section is the Siliceous Mudstone (SM) followed by the Siliceous Shale (SS) which differ in the amount of quartz and

lamination where shales have better-defined laminations than mudstones. Chert and Siliceous Mudstones have the highest quartz content in the section (>80%) and are poorly to moderately laminated. Argillaceous Shale and Siliceous Shale have higher clay content (>30%), lower quartz content (<80%) and are well laminated. Green Claystone facies has the highest clay content and is bioturbated giving a mottled texture. One limitation found in this dissertation when applying our outcrop facies classification was that many of the outcrop facies defining characteristics are based in weathering features like fissility and weathering color, which limited their applicability to core data. However, this dissertation adapted the outcrop methodology and was able to adapt it to core description.

Does the Woodford Shale in the Marietta basin have similar stratigraphy as the Woodford Shale in other locations in Oklahoma (such as outcrops)?

The Speake Ranch Shale Pit located in the southern limb of the Arbuckle Mountains studied by Galvis (2017) is the type section used in this dissertation. The Woodford Shale in the Marietta Basin correlates with the type section in the Arbuckle Mountains with equivalent facies description and assemblage in both sections. Using the facies associations from core description, combined with the core gamma-ray log response, and the X-Ray Fluorescence (XRF) profiles, I mapped a full second-order depositional sequence in the Marietta Basin. The Maximum Flooding Surface (MFS) of the cored section occurs at the top of the Argillaceous Shale (AS)-dominated interval and is the most correlative surface between the core and the type section. The MFS has the highest gamma-ray peak and is located at the top of the correlative condensed section dominated by Argillaceous Shales facies. Two primary sequence stratigraphic systems

tracts were identified in the Marietta Basin: The Transgressive Systems Tract (TST) in the lower and middle Woodford section and the Highstand Systems Tract (HST) in the upper Woodford section. These two system tracts have been identified in outcrops (Galvis, 2017), as well as in the subsurface of Central Oklahoma (McCullough, 2014; Turner, 2016)

What kind of diagenetic alterations are present in the Woodford Shale of the Marietta Basin?

Are there any similarities to the diagenesis of other locations?

Using Scanning Electron Microscope (SEM) imagery and Energy Dispersive X-Ray (EDX) Elemental Analysis in thin sections extracted from the Marietta Basin core, several diagenetic features were identified in this section of the Woodford Shale. The most significant diagenetic alterations are in and nearby the vertical mineralized fractures, the phosphate nodules, and the silica cementation in the Tasmanites and Radiolarians. The generation of phosphate nodules was an early diagenetic process probably when the sediments were very close to the water-sediment interface (2-5 feet). Horizontal fractures are present along laminations because they are planes of weakness and they probably were opened during the expulsion of hydrocarbons during the middle to late diagenesis. Mineralized vertical fractures are compacted implying they were created during or before compaction, and they are usually filled with dolomite, calcite, and pyrite. There is an unusually high presence of Magnesite (Magnesium Carbonate) that “flowers” out of fractures into the matrix. Magnesite altered the matrix probably when fluids moved through the fractures and filtered into the matrix. This effect is not unique of the Marietta Basin, but it was also identified by Roberts (2017) in Woodford cores from South-Central Oklahoma. Silica cementation occurred early in the diagenesis (even before compaction)

resulting in Tasmanites preserving their spherical shape. Finally, Pyrite is present in each facies within the fractures (middle to late diagenesis), and in the matrix (early diagenesis) as framboids.

How is the Woodford Shale geochemically and geomechanically characterized in the Marietta Basin?

In terms of Geochemistry, the Woodford Shale in the Marietta Basin is an excellent source rock; therefore, it has excellent Reservoir Quality (RQ). RockEval and TOC data from the core show the Woodford Shale at this location has excellent organic richness with TOC ranging from 2.93% to 9.75%. Kerogen type is interpreted to be dominated by Kerogen Type II Oil-Prone Marine. The average thermal maturity based on Vitrinite Reflectance is 0.79% V_{ro}, placing this section in the middle of the oil window.

As for the geomechanical characteristics of the Woodford Shale in the Marietta Basin, using rebound hardness data, it was found that high quartz content beds like Cherts and Siliceous Mudstones are harder rocks than the softer Argillaceous Shales and Siliceous Shales. This relationship is very similar to the results in the other sections of the Woodford Shale in Oklahoma including the Speake Ranch Shale Pit and the I-35s Roadcut in the Arbuckle Mountains (Becerra, 2017; Galvis, 2017). However, the most significant discovery during this research in terms of geomechanics was that vertical mineralized fractures were identified only in the brittle Siliceous Mudstone facies and Black Chert facies. These vertical fractures can be straight in the Black Chert beds, and compacted/convoluted in the Siliceous Mudstone beds. No other facies had mineralized vertical fractures. These mineralized vertical fractures are bed

bounded, and the data shows the clay content is the primary variable that drives the fracture distribution. In contrast, Horizontal fractures are mainly present in the Argillaceous Shale and Siliceous Shale facies. The Green Claystone facies and the Dolomite Mudstones only have a few minor horizontal fractures.

How laterally extensive is the Woodford Shale across the Marietta basin? How does its thickness vary laterally?

To answer this question, structure and thickness maps were generated correlating the available well log data in the basin. This well data is minimal with just a few sets of wells located in the shallow structures of the basin and a few others in the deeper areas. Because of these limitations, no previous attempt to map the Woodford Shale in the Marietta Basin has been done and published. This dissertation is the first publication of its type in the Marietta Basin. The result is the Woodford Shale is present only in the syncline axis of the basin, and it has been eroded at the edges of the basin probably due to several uplifts and orogenic events of the Wichita and the Ouachita Thrust Belts. Based on the structure maps, the True Vertical Depth (TVD) of the top of the Woodford Shale can be as shallow as 5000 feet in the NW, and as deep as 17000 feet in the SE of Love County (OK). The gross Woodford Shale thickness is on average 180 feet, and it ranges from 50 feet at the edges of the basin to 300 feet in the northwestern side of the basin along the syncline axis.

One key finding in this dissertation is the Woodford-Hunton relationship reported in other publications (McCullough, 2014; Infante et al. 2016) is not present in the Marietta Basin.

According to these authors, when the Hunton is thinner or eroded, the Woodford Shale tends to be thicker or the thickest in the area. However, in the Marietta Basin, the Woodford Shale thickness does not vary based on the Hunton Presence. Even in areas where the Hunton is absent (in the southeastern side of the Marietta Basin), the Woodford has the same relative thickness as in other areas. This dissertation proposes that the reason why the Woodford-Hunton thickness relationship is absent is because in the Marietta Basin the absence of the Hunton is not due to erosion but instead due to non-deposition of these carbonates. Core data at the contact between the Sylvan Shale and the Woodford Shale (where the Hunton is absent), show no sign of erosion, which validates the hypothesis stated above.

How do the Woodford Shale Horizontal wells perform in the Marietta Basin and what is the most significant variable that affects hydrocarbon production and EURs on those wells? Are the target zones on outcrops correlative to target zones in the subsurface and can outcrops even be used to evaluate subsurface equivalent strata?

The Decline Curve Analysis (DCA) of the current producing Woodford Shale horizontal wells in the Marietta Basin show average initial production rates of 10,000 bbl. per month per horizontal well (300 bbl. per day) and average initial decline rates of 60%. The average Estimated Ultimate Recovery (EUR) of these wells normalized by 1000 feet is 90,000 bbl.; therefore a 5000-foot lateral well (one section) will produce in average in its life 450,000 bbl. of oil and 1 Bcf of gas. These values are equivalent to Woodford wells in the SCOOP (South-Central Oklahoma Oil Play) play in Grady and McClain county and even better than the

Woodford Wells in the STACK play in Kingfisher and Canadian County due to the lower gas-oil ratios of the Marietta Basin production.

When combining the EURs of the current Woodford wells in the basin and normalizing them based on lateral length and completion jobs, the main variables driving EURs look to be the thickness of the Target Interval and reservoir depth. This “Target Interval” is located in the lower part of the Highstand Systems Tract (HST); between the Maximum Flooding Surface (MFS) and the base of the Black Chert-dominated section with phosphate nodules. The outcrop work done by Galvis (2017) identified a similar section with ideal characteristics in the Arbuckle Mountains which I have correlated 40 miles south to the Marietta Basin and the core location. This “Target Interval” based from outcrops and correlated to the Marietta Basin has an excellent combination of Reservoir Quality (RQ) and Completion Quality (CQ); forming an ideal brittle-ductile couplet. This target section is dominated by brittle siliceous mudstones interbedded by organic-rich siliceous shales. It does not suffer the adverse mechanical effect of the high clay content (>35%) from the argillaceous shale that reduces the efficiency of induced fractures, and it does not have the very high quartz content (>90%) from the black chert/phosphate nodules that reduce the rate of penetration (ROP) when drilled. This "Target Interval" section is thickest (>100 ft.) and deeper (>10,000 ft. TVD) in township T7S 1RE and T7S R2E where the EURs are the largest in the basin resulting in the best performing wells. The depth variable affects the reservoir pressure of the Woodford Shale. The deeper the formation is, the higher the supporting reservoir pressure is to drive hydrocarbons to the borehole. Probably the only operator that has found this relationship is XTO Energy, and that is why they chose this area to be the first location for the Woodford appraisal wells and hold the acreage early by production to infill with more

development wells later. Furthermore, these results show evidence that target intervals interpreted from outcrop sections (like Speake Ranch Woodford Outcrop) can be used effectively in the subsurface when drilling and completing Woodford wells. This should encourage additional correlations from outcrop to subsurface to better understand this Woodford Shale Unconventional Reservoir.

This dissertation provides the only published comprehensive study of the Woodford Shale in the Marietta Basin integrating many types of data like core, logs, and production to generate a vertical and lateral stratigraphic framework. Most of the questions established at the beginning of this dissertation book were completely or partially answered using the analysis of the data and interpretations through the chapters of this dissertation. There are many additional questions raised through this dissertation that can serve as the starting point for future research and listed in the Recommendation section below. However, it is essential to address that the main limitations for future work will always be the amount of data available for future research.

Recommendations

- Perform biomarker analysis to samples extracted from the Marietta basin Woodford Shale Core studied in this dissertation.
- Request oil samples from the current Woodford producing wells in the Marietta Basin and perform biomarker analysis to correlate the geochemical fingerprint extracted from the oils to the geochemical fingerprint extracted from core.
- Use the same methodology used in this dissertation to correlate target zones identified from Woodford Outcrops to other producing Woodford areas in the vicinity of the outcrops (like Ardmore Basin Play or the SCOOP play) because the Marietta Basin study shows correlating outcrop “Target Intervals” to the subsurface provides additional insight for future development of the play.
- If 3D seismic is available, extract 3D seismic attributes like Curvature or Coherence to identify areas that could be highly fractured closer to faults or folds. This approach is currently applied in another Woodford plays in Oklahoma like STACK and SCOOP.
- Because the core used in this studied is not oriented, it is difficult to correlate their relative orientation with the major Woodford fracture sets studied by Ghosh (2017) in outcrops. However, a deeper study of the mechanism of the formations of fractures present in the core should be done in-depth.
- Generate a chronostratigraphic framework for the Marietta Basin Woodford Core using palynology and conodonts identification. If a time framework for this Woodford Shale Section is created, it will increase the accuracy of correlation of this section with other

Woodford Sections in other basins (like the Anadarko and Arkoma basins) and outcrops in the uplift areas of the Arbuckle Mountains and Criner Hills.

- Identify additional rare minerals in the mineralized fractures to interpret if the Woodford Shale in the Marietta Basin was an open system or a closed system during early to late diagenesis. A similar work was done by Roberts and Elmore (2017) and can be replicated in this location.
- Calculate volumetric values for oil in place in the Woodford Shale Marietta Basin using the maps constructed as part of this dissertation. To do this, estimation of water saturation using petrophysics and formation volume factor should be used.
- Predict the effect of future infill wells in the current production and calculation of total EURs per section. In STACK and SCOOP, Woodford infill wells tend to affect negatively the production of the first well in the section. This could be done by modelling production by adding hypothetical wells to the area.

References

- Althoff, C., 2012, Characterization of depositional megacycles in the Woodford Through of Central Oklahoma: Master's thesis, University of Oklahoma, Norman, Oklahoma, 107 p.
- Arps, J. J., 1945, Analysis of decline curves: Transactions AIME, v. 160, no. 1, p. 228-247, doi 10.2118/945228.
- Arps, J. J., 1956, Estimation of primary oil reserves: Transactions AIME, v. 207, p. 182-191.
- Ataman, O., 2008, Natural fracture systems in the Woodford Shale, Arbuckle Mountains, Oklahoma: Master's thesis, University of Oklahoma, Norman, Oklahoma, 185 p.
- Badra, H., 2011, Field characterization and analog modeling of natural fractures in the Woodford Shale, southeast Oklahoma: Master's thesis, University of Oklahoma, Norman, Oklahoma, 156 p.
- Becerra, D., 2017, Integrated geological characterization at the bed scale of the Woodford Shale at the I-35 outcrop, southern Oklahoma: Master's thesis, University of Oklahoma, Norman, Oklahoma, 202 p.
- Becerra, D., H. Galvis, and R. Slatt, 2018, Characterizing the two principal rock types comprising the Woodford Shale resource play: application to shale geomechanics: Interpretation, v. 6, no. 1, p. SC67–SC84.
- Berryman, J., 2013, Timing and paragenesis of the calcite fracture fill in the Woodford Shale: Shale Shaker, v. 64, no. 1, p. 40-53.
- Blakey, R., 2012, Paleogeography and geologic evolution of North America: North American paleogeographic maps: <http://jan.ucc.nau.edu/~rcb7?nam.html>; (accessed, June 20, 2013).
- Bontempi, C. P., 2015, High resolution stratigraphy of thin bedded shales radiolarites, Woodford Shale, Arbuckle Wilderness area, Oklahoma: Master's thesis, University of Oklahoma, Norman, Oklahoma, 81 p.
- Bradfield, H. H., 1968, Stratigraphy and structure of the deeper Marietta Basin of Oklahoma and Texas: in W.J Stewart, ed., Basins of the southwest: North Texas Geological Society, v. 1, p. 54-70.
- Breyer, J. A., R. A. Denne, T. Kosanke, J. M. Spaw, J. Funk, P. Christianson, D. A. Bush, and R. A. Nelson, 2016, Facies, fractures, pressure, and production in the Eagle Ford Shale (Cretaceous) between the San Marcos arch and the Maverick Basin, Texas, U.S.A.: in J.A. Breyer, ed., The Eagle Ford Shale: a renaissance in U.S. oil production: AAPG Memoir 110, p. 363-384.
- Brito, R. J., 2017, The Woodford Shale in the Marietta Basin (North Texas): AAPG Search and Discovery Article #90292, AAPG Southwest Section, Midland, Texas, April 29 - May 2, 2017, p. 1.

- Caldwell, C., 2012, Rock types and lithostratigraphy of the Devonian Woodford Shale, Anadarko Basin, West-Central Oklahoma: AAPG Annual Convention and Exhibition, Long Beach, CA, p. 1.
- Cardona-Valencia, L. F., 2014, Integrated characterization of the Woodford Shale in the southern Cherokee Platform, Oklahoma: Master's thesis, University of Oklahoma, Norman, Oklahoma, 98 p.
- Cardott, B. J., W. J. Metcalf, and J. L. Ahern, 1990, Thermal maturation by vitrinite reflectance of Woodford Shale near the Washita Valley fault, Arbuckle Mountains, Oklahoma, in: Nuccio V. F. and C. E. Barker, eds., Applications of thermal maturity studies to energy exploration: SEPM, Rocky Mountain Section, p. 139-146.
- Cardott, B. J., 2009a, Woodford gas-shale plays of Oklahoma: Louisiana oil, gas symposium: Oklahoma Geological Survey: <http://www.ogs.ou.edu/fossilfuels/pdf/LAoilgas2009.pdf>; (accessed on October 4, 2009).
- Cardott B. J., 2009b, Application of vitrinite reflectance to the Woodford Gas-Shale play in Oklahoma: American Association of Petroleum Geologists Mid-continent Meeting, Books of Abstracts, Tulsa, Oklahoma.
- Cardott, B. J., 2012, Thermal maturity of Woodford Shale gas and oil plays, Oklahoma, USA: Journal of Coal Geology, v. 103, p. 109-119
- Cardott, B. J., 2014, Woodford Shale play update: expanded extent in the oil window: AAPG Search and Discovery Article #80409, 51 slides.
- Cardott, B. J., 2018, Bibliography of Marietta Basin: Oklahoma Geological Survey: <http://ou.edu/content/dam/ogs/documents/information/Bibliographiesbasins/Maritta-Basin.pdf>; (accessed May 11, 2019).
- Catuneanu, O. Galloway, W. E., Kendall, C.G.St.C., Miall, A. D., Posamentier, H. W., Strasser, A., and M. E. Tucker, 2011. Sequence stratigraphy: methodology and nomenclature: Newsletters on Stratigraphy, v. 44/3, p. 173-245.
- Chain, A. R., 2012, Stratigraphy and composition of the Woodford Shale in depositionally updip and downdip wells, Anadarko Basin, Oklahoma: Master's thesis, University of Oklahoma, Norman, Oklahoma, 236 p.
- Comer, J. B., and H. H. Hinch, 1987, Recognizing and quantifying expulsion of oil from the Woodford Formation and age-equivalent rocks in Oklahoma and Arkansas: AAPG Bulletin, v. 71, p. 844-858.
- Comer J. B., 1992, Organic geochemistry and paleogeography of Upper Devonian formations in Oklahoma and northwestern Arkansas: in K. S. Johnson and B. J. Cardott, eds., Source rocks in the southern Midcontinent: Oklahoma Geological Survey Circular 93, p. 70-93.

- Comer, J. B., 2005, Facies distribution and hydrocarbon production potential of Woodford Shale in the southern Midcontinent, in: B.J. Cardott, ed., Unconventional energy resources in the southern Midcontinent: Oklahoma Geological Survey Circular 110, p. 51-62.
- Comer, J. B., 2008, Woodford Shale in southern Midcontinent, USA-Transgressive system tract marine source rocks on an arid passive continental margin with persistent oceanic upwelling: AAPG Annual Convention, San Antonio, TX, poster, 3 panels.
- Comer, J. B., 2009, The forms of quartz and dolomite in Woodford Shale of the southern Midcontinent, USA: indicators of paleoclimate, paleogeography, paleoceanography, and depositional processes: American Association of Petroleum Geologists Mid-Continent Meeting, Book of Abstracts, Tulsa, Oklahoma, 30 p.
- Connock, G. T., 2015, Paleoenvironmental interpretation of the Woodford Shale, Wyche Farm shale pit, Pontotoc County, Arkoma Basin, Oklahoma with primary focus on water column structure: Master's thesis, University of Oklahoma, Norman, Oklahoma, 253 p.
- Cook, J., 2010, Stratigraphy depositional environments and reservoir description of the tussy (desmoinesian) sandstones, southeast joiner city Field, Love and Carter counties, Oklahoma: Master's thesis, University of Oklahoma, Norman, Oklahoma, 95 p.
- Curtis, M. E., B. J. Cardott, C. H. Sondergeld, and C.S. Rai, 2012, Development of organic porosity in the Woodford Shale with increasing thermal maturity: International Journal of Coal Geology, p. 26-31.
- EIA (U.S. Energy Information Administration)., 2016, Map of Lower 48 states shale plays, 20-Feb- 2016, <https://www.eia.gov/>.
- EIA (U.S. Energy Information Administration)., 2019, Monthly Production of Oil and Gas in the United States, 8- January-2019, <https://www.eia.gov/>.
- Ekwunife, I. C., 2017, High-resolution chemostratigraphy of The Woodford Shale in the McAlister Quarry, Ardmore Basin, Oklahoma: Master's thesis, University of Oklahoma, Norman, Oklahoma, 152 p.
- Elmore, R. D., G. W. Heij, and A. K. Wickard, 2016, Paragenesis of mineralized fractures and diagenesis of prominent North American shales: The Sedimentary Record: SEPM, 14, 4-10, doi: 10.2110/sedred.2016.4.
- Fetkovich, M. J., 1980, Decline curve analysis using type curves: JPT 32 (6), p. 1065-1077.
- Frederickson, E. A., and R. H. Redman, 1965, Geology and petroleum of Love County, Oklahoma, Part I, Geology of Love County: OGS Circular 63.
- Galvis, H. A., 2017, Detailed lithostratigraphic characterization and sequence stratigraphy of a complete Woodford Shale Outcrop Section in Southern Oklahoma: Master's thesis, University of Oklahoma, Norman, Oklahoma, 169 p.
- Galvis, H. A., D. Becerra, and R. Slatt, 2017, Lithofacies and stratigraphy of a complete Woodford Shale outcrop section in South Central Oklahoma: Geologic considerations for

- the evaluation of unconventional shale reservoirs: Interpretation, v. 6, no. 1, p. SC15–SC27.
- Gaswirth, S. B. and D. K. Higley, 2014, Geologic assessment of undiscovered oil and gas resources in the Cambrian–Devonian stratigraphy of the Anadarko Basin, Oklahoma, Kansas, Texas, and Colorado: U.S. Geological Survey Digital Data Series DDS–69–EE, 42 p.
- Ghosh, S., 2017, Integrated studies on Woodford Shale natural fracture attributes, origin, and their relation to hydraulic fracturing: Doctoral dissertation, University of Oklahoma, Norman, Oklahoma, 264 p.
- Ghosh, S., and S. Buset, 2017a, Prediction of hydraulic fracture damaged zone geometries in the Woodford Shale in Arkoma Basin using Discrete Fracture Network Model: Abstract presented at AAPG Southwest Section Meeting, Midland, Texas.
- Grotzinger, J. G., and T. H. Jordan, 2010, Understanding Earth: W. H. Freeman; Sixth Edition, 672 p.
- Ham, W. E., 1973, Regional geology of the Arbuckle Mountains, Oklahoma: Oklahoma Geological Survey Special Publication, v. 73-3, p. 61.
- Hass, W. H., and J. W. Huddle, 1965, Late Devonian and Early Mississippian age of the Woodford Shale in Oklahoma as determined by conodonts, in Geological Survey research: U.S. Geological Survey Professional Paper 525-D, p. 125-132.
- Hester, T. C., H. L. Sahl, and J. W. Schmoker, 1988, Cross sections based on gamma-ray, density, and resistivity logs showing stratigraphic units of the Woodford Shale, Anadarko Basin, Oklahoma: U.S. Geological Survey Miscellaneous Field Studies Map MF-2054, 2 sheets.
- Hester, T.C., J. W. Schmoker, and H. L. Sahl, 1990, Log-derived regional source-rock characteristics of the Woodford Shale, Anadarko basin, Oklahoma: U.S. Geological Survey Bulletin 1866-D, p. 38.
- Hoffman, P., J. F. Dewey, and K. Burke, 1974, Aulacogens and their genetic relation to geosynclines, with a Proterozoic example from Great Slave Lake, Canada, in modern and ancient geosynclinal sedimentation: SEPM Special Publication v. 19, p. 38-55.
- Infante-Paez, L., L. F. Cardona, B. McCullough, and R. Slatt, 2016, Seismic analysis of paleotopography and stratigraphic controls on total organic carbon: Rich sweet spot distribution in the Woodford Shale, Oklahoma, USA: Interpretation, v. 5-1, p. 33-47.
- Infante-Paez, L., L. F. Cardona, B. McCullough, and R. Slatt, 2017, Seismic analysis of paleotopography and stratigraphic controls on total organic carbon: Rich sweet spot distribution in the Woodford Shale, Oklahoma, USA: Interpretation, v. 5, p. T33-T47, doi: 10.1190/INT-2015-0151.1
- Jacob, H., 1989, Classification, structure, genesis and practical importance of natural solid oil bitumen (“migrabitumen”): International Journal of Coal Geology, v. 11, p. 65-79.

- Johnson K. S., T. W. Amsden, R. E. Denison, S. P. Dutton, A. G. Goldstein, B. Rascoe Jr., P. K. Sutherland., and D. M. Thompson, 1989, *Geology of the southern Midcontinent: Oklahoma Geological Survey Special Publication*, v. 89-2, p. 1-53.
- Johnson, K. S., and B. J. Cardott, 1992, *Geologic framework and hydrocarbon source rocks of Oklahoma*, in K.S. Johnson and B.J. Cardott, eds., *Source rocks in the southern Midcontinent, 1990 symposium: OGS Circular 93*, p. 21-37.
- Johnson, K. S., 2008, *Geologic History of Oklahoma*, Oklahoma Geologic Survey: Educational Publication, V. 9, p. 1-8.
- Jones, L. C., 2017, *An Integrated analysis of sequence stratigraphy, petroleum geochemistry, and the Hangenberg Crisis in the Woodford Shale, Oklahoma: Master's thesis*, University of Oklahoma, Norman, Oklahoma. 198 p.
- Jarvie, D. M, R. J. Hill, T. E. Ruble, and R.M. Pollastro, 2007, *Unconventional shale-gas systems: The Mississippian Barnett Shale of north-central Texas as one model for thermogenic shale-gas assessment: American Association of Petroleum Geologists Bulletin*, v. 91, p. 475-499.
- Keller, G. R., E. G. Lidiak, W. J. Hinze, and L. W. Braile, 1983, *The role of rifting in the tectonic development of the midcontinent, USA: Tectonophysics*, 94(1), p. 391-412.
- Kennedy, L., J. Beuthin, and J. Kostelnik, 2016, *Fracture stratigraphy: predicting fractures from small-scale lithologic and textural changes: The International Symposium of the Society of Core Analysts held in Snowmass, Colorado, USA*, p. 21-26.
- Killian, B. J., 2012, *Sequence stratigraphy of the Woodford Shale, Anadarko Basin, Oklahoma: implications on regional Woodford target correlation: Master's thesis*, University of Oklahoma, Norman, Oklahoma, 102 p.
- Kirkland, D. W., R. E. Denison, D. M. Summers, and J. R. Gormly, 1992, *Geology and organic geochemistry of the Woodford Shale in the Criner Hills and western Arbuckle Mountains, Oklahoma: in Johnson, K.S. & Cardott, B.J. (eds.) Source rocks in the southern mid-continent: 1990 Symposium: OGS Circular 93*, p. 38-69.
- Kuykendall, M., and Fritz, R., 2001, *Misener Sandstone of Oklahoma: AAPG Search and Discovery*, p. 117-134.
- Lambert, M. W., 1993, *Internal stratigraphy and organic facies of the Devonian Mississippian Chattanooga, Woodford Shale in Oklahoma and Kansas*, in B.J. Katz and L.M. Pratt, eds., *Source rocks in a sequence stratigraphic framework: AAPG Studies in Geology 37*, p. 163-176.
- McCullough, B. J., 2014, *Sequence stratigraphic framework and characterization of the Woodford Shale on the southern Cherokee Platform of central Oklahoma*, Master's thesis, University of Oklahoma, 211 p.

- McCullough, B. J., 2017, Sequence-Stratigraphic Framework of the Woodford Shale on the Southern Cherokee Platform of Central Oklahoma: *The Shale Shaker*, v. 68, no. 3, p. 112-138.
- Miceli-Romero, A. A., 2010, Geochemical characterization of the Woodford Shale, central and southeastern Oklahoma, Master's thesis, University of Oklahoma, Norman, Oklahoma, 133 p.
- Miceli-Romero, A. and R. P. Philp, 2012, Organic geochemistry of the Woodford Shale, southeastern Oklahoma; how variable can shales be?: *AAPG Bulletin*, v. 96, 493– 517, doi: 10.1306/08101110194.
- Miller, R., Young, R., 2007, Characterization of the Woodford Shale in outcrop and Subsurface in Pontotoc and Coal Counties, Oklahoma: Abstract presented at the AAPG Annual Convention, Long Beach, CA, 3 panels.
- Molinares, C., 2013, Stratigraphy and palynomorphs composition of the Woodford Shale in Wyche Farm Shale Pit, Pontotoc County, Oklahoma, Master's thesis, University of Oklahoma, Norman, Oklahoma, 90 p.
- Morgan, G. D., 1924, Geology of the Stonewall Quadrangle, Oklahoma: *Oklahoma Bureau of Geology Bulletin*, v. 2, 248 p.
- Northcutt R. A. and J. A. Campbell, 1995, Geologic Provinces of Oklahoma map. Oklahoma Geological Survey: http://www.ogs.ou.edu/geolmapping/Geologic_Provinces_OF5-95.pdf (Accessed: February 2017).
- O'Brien, N. R., and R. M. Slatt, 1990, *Argillaceous Rock Atlas*: New York, Springer-Verlag ed., 141 p.
- Odagme, B., 2016, MS Evaluation of the Methodologies of Analyzing Production and Pressure Data of Tight Gas Reservoir: Oral Presentation. SPE Nigeria Annual International Conference and Exhibition, Lagos, Nigeria.
- Paxton, S. T., A. M. Cruse, and A. M. Krystiniak, 2006, Fingerprints of global sea-level change revealed in Upper Devonian/Lower Mississippian Woodford Shale of south-central Oklahoma: *American Association of Petroleum Geologists Search and Discovery article* #4021.
- Paxton, S. T., and T. Olsen, C. Price, E. Gross, and S. Allison, 2015, Spectral gamma-ray profile of Woodford Shale - OHMEGCO Locality, Oklahoma. PowerPoint presentation prepared for Ardmore Geological Society, January, 108 slides.
- Peters, K.E., 1986. Guidelines for evaluating petroleum source rock using programmed pyrolysis. *AAPG bulletin*, 70(3), p. 318-329.
- Portas, R. M., 2009, Characterization and origin of fracture patterns in the Woodford Shale in southeastern Oklahoma for application to exploration and development: Master's thesis, University of Oklahoma, Norman, Oklahoma, 110 p.

- Roberts, J., 2017. A diagenetic and paleomagnetic study of the Woodford Shale, Oklahoma, USA. M.S. thesis, University of Oklahoma, Norman, Oklahoma, 63p.
- Roberts, J., R.D. Elmore, 2017, A diagenetic study of the Woodford Shale in the Anadarko Basin, Oklahoma, U.S.A.: Interpretation, v. 6, no. 1, p. SC1-SC13.
- Sanchez, J. D. A., 2012. Sequence stratigraphy and seismic interpretation of the Upper Devonian-Lower Mississippian Woodford Shale in the Cherokee Platform: a characterization approach for unconventional resources, Master's thesis, University of Oklahoma, Norman, Oklahoma, 109 p.
- Schieber, J., 1996, Early diagenetic silica deposition in algal cysts and spores: a source of sand in black shales?: Journal of Sedimentary Research, v. 66, p. 175-183.
- Serna-Bernal, A., 2013, Geological characterization of the Woodford Shale in the McAlister Cemetery Quarry, Criner Hills, Ardmore Basin, Oklahoma: Master's thesis, University of Oklahoma, Norman, Oklahoma, 165 p.
- Sierra, R., 2011, Integrated geomechanics and geological characterization of the Devonian-Mississippian Woodford Shale: Master's thesis, University of Oklahoma, Norman, Oklahoma, 110 p.
- Siy, S. E., 1988, Geochemical and petrographic study of phosphate nodules of the Woodford Shale (Upper Devonian-Lower Mississippian) of southern Oklahoma, Master's thesis, Texas Tech University, 172 p.
- Slatt, R. M., and N. R. O'Brien, 2011, Pore types in the Barnett and Woodford Gas Shales: contribution to understanding gas storage and migration pathways in fine-grained rocks: AAPG Bulletin, v. 95 (12), p. 2017-2030
- Slatt, R. M., 2011, Important geological properties of unconventional resource shales: Central European Journal of Geoscience, v. 3, no. 4, p. 435-448.
- Slatt, R. M., and Y. Abousleiman, 2011, Merging sequence stratigraphy and geomechanics for unconventional gas shales: The Leading Edge, v. 30-3, p. 274-282.
- Slatt, R. M., and N. D. Rodriguez, 2012, Comparative sequence stratigraphy and organic geochemistry of gas shales: commonality of coincidence?: Journal of Natural Gas Engineering and Science, vol. 8, p. 68-84.
- Slatt, R. M., 2013, Stratigraphic reservoir characterization for petroleum geologists, geophysicists, and engineers: Origin, recognition, initiation, and reservoir quality 2nd edition, Elsevier, Amsterdam, Netherlands, 478 p.
- Slatt, R. M., B. J. McCullough, C. E. Molinares-Blanco, and E. T. Baruch, 2016, Paleotopographic and depositional environmental control on "sweet spot" locations in some unconventional resource shales: The Houston Geological Society Bulletin, v. 58 (8), p. 37-39.

- Slatt, R. M., 2017, Outcrop and subsurface geology applied to drilling, sweet spot and target zone detection of resource shales: the Woodford example: SPE Luncheon, Oral presentation.
- Slatt, R. M., 2018, Outcrop and subsurface geology applied to drilling, sweet spot and target zone detection of resource shales: the Woodford example and beyond: The Houston Geological Society Bulletin, v. 60, no. 8, p. 11.
- Sullivan, K. L., 1985, Organic facies variation of the Woodford Shale in western Oklahoma: Shale Shaker, v. 35, p. 76-89.
- Suneson, N., 1996. The geology of the Ardmore Basin in the Lake Murray state park area, Oklahoma: prepared for the spring field meeting of the Oklahoma Academy of Science, 44 p.
- Taff, J.A., 1902, Description of the Atoka quadrangle: U.S. Geological Survey Geologic Atlas Folio 79, scale 1:125,000, 8 p.
- Tarr, R., 1955. Paleogeologic map at base of Woodford, and Hunton isopachous map of Oklahoma. AAPG, 2 p.
- Tissot B. P. and D. H. Welte, 1978, Petroleum formation and occurrence: Springer Verlag Berlin Heidelberg, Germany, 538 p.
- Torres, E.J., Slatt, R.M., Marfurt, K.J., Infante, L.E., & Castillo, L.A., 2017, Identification of Potencial Lacustrine Stratigraphic Intervals in the Woodford Shale, Oklahoma, Using Multi-Attribute 3-D Seismic Displays and a Supervised Neural Network: Unconventional Resources Technology Conference, Austin, Texas, p. 1, doi: 10.15530/urtec-2017-2692737
- Treanton, J. A., 2014, Outcrop-derived chemostratigraphy of the Woodford Shale, Murray County, Oklahoma, Master's thesis, The University of Oklahoma, Norman, Oklahoma, 83 p.
- Turner, B., J. Tréanton, and R. M. Slatt, 2016, The use of chemostratigraphy to refine ambiguous sequence stratigraphic correlations in marine mudrocks: An example from the Woodford Shale, Oklahoma, USA: Journal of the Geological Society, v. 173, p. 854-868, doi: 10.1144/jgs2015-125.
- Urban, J. B., 1960, Microfossils of the Woodford Shale (Devonian) of Oklahoma. Master's thesis, The University of Oklahoma, Norman, Oklahoma, 77 p.
- Verma, S., and K. Marfurt, 2014, A way of TOC characterization on Barnett and Woodford Shale: Abstract presented at AAPG Annual Convention and Exhibition, Pittsburgh, Pennsylvania.
- Von Almen, W. F., 1970, Palynomorphs of the Woodford Shale of south-central Oklahoma with observations on their significance in zonation and paleoecology: Doctoral dissertation, Michigan State University, East Lansing, Michigan, 179 p.

- Wang, F. P., and J. F. Gale, 2009, Screening criteria for shale-gas systems: The Gulf Coast Association of Geological Societies, 15 p.
- Wang, T., 2016, An organic geochemical study of Woodford Shale and Woodford Mississippian tight oil from Central Oklahoma: Doctoral dissertation, University of Oklahoma, Norman, Oklahoma, 299 p.
- Wang, T., and P. Phil, 2019, Oil families and inferred source rocks of the Woodford Mississippian tight oil play in North-Central Oklahoma: AAPG Bulletin, in press, DOI:10.1306/09181818049.
- Westheimer, J. M., 1965, Geology and petroleum of Love County, Oklahoma. Part II. Petroleum geology of Love County: OGS Circular 63, p. 48-77.
- Wickham, J., 1978, The Southern Oklahoma Aulacogen: Master's thesis, University of Oklahoma, Norman, Oklahoma, 41 p.